

MINISTÉRIO DO EQUIPAMENTO, DO PLANEAMENTO E DA ADMINISTRAÇÃO DO TERRITÓRIO

Laboratório Nacional de Engenharia Civil

NÃO CONFIDENCIAL

CENTRO DE ESTUDOS E EQUIPAMENTO DE ENGENHARIA SÍSMICA

Proc. 260/17/10956

Eng. António F. F.

CHARACTERIZATION OF THE NEW LNEC SHAKING TABLE

(HCM Contract ERBCHECT – 920010)

RELATÓRIO 148/96 — C3ES

Lisbon, March 1996

Study carried out within the Project ECOEST – European Consortium
on Earthquake Shaking Tables

— I&D —

ESTUDOS E EQUIPAMENTO DE ENGENHARIA SÍSMICA

CARACTERIZAÇÃO DO NOVO SIMULADOR SÍSMICO DO LNEC

RESUMO

Este relatório descreve o programa de ensaios efectuados no novo simulador sísmico do LNEC, constituindo uma das tarefas incluídas no projecto de cooperação europeia ECOEST. Apresenta-se uma caracterização detalhada das funções de resposta em frequência da plataforma sísmica, bem como uma avaliação da fidelidade do controlo da mesma. Esta informação servirá de base inicial à exequibilidade dos ensaios futuros a realizar nesta instalação.

Para além da descrição dos procedimentos e dos resultados obtidos durante os testes, foi também compilado bastante material relativo à instalação como um todo.

CARACTERISATION DE LA NOUVELLE TABLE VIBRANTE DU LNEC

RÉSUMÉE

Ce rapport décrit le programme des essais effectués avec la nouvelle table vibrante du LNEC dans le cadre du project de collaboration européenne ECOEST. Une caractérisation détaillée des fonctions de réponse en fréquence de la table ainsi qu'une évaluation de la qualité de son contrôle sont décrites. Ces informations serviront de base initiale à l'évaluation de la faisabilité des essais à effectuer.

La description des procédures et des résultats obtenus pendant ces essais de caractérisation est accompagnée d'une description de l'installation.

CHARACTERIZATION OF THE NEW LNEC SHAKING TABLE

ABSTRACT

As part of ECOEST European research activities, this report describes the experimental programme carried out at the new LNEC seismic simulator facility. It is reported a detailed characterization of the frequency response of the shaking table and the results from an assessment of its control fidelity. This information will act as a benchmark, against which the performance of future tests at this facility could be gauged.

Apart from the description of the procedures and results of the test programme carried out, it was also compiled descriptive material about the entire facility.

CHARACTERIZATION OF THE NEW LNEC SHAKING TABLE

LIST OF CONTENTS

1.0 INTRODUCTION.....	1
1.1 Background.....	1
1.2 Earthquake research using shaking tables.....	1
1.3 Recent experience in Earthquake Engineering at LNEC.....	2
1.4 Motivation for this research.....	3
1.5 Scope and structure of this report.....	3
2.0 DESCRIPTION OF THE LNEC SHAKING TABLE FACILITY.....	5
2.1 The Shaking table.....	5
2.2 LNEC facility characteristics.....	10
2.2.1 Summary of shaking table characteristics.....	10
2.2.2 Additional characteristics.....	13
2.3 The analytical model.....	14
2.3.1 General.....	14
2.3.2 Use of analytical models in earthquake engineering.....	14
2.3.3 Analytical model of the shaking table.....	15
2.4 Computer equipment and hardware.....	17
2.5 Safety and Maintenance.....	18
3.0 SHAKING TABLE SYSTEM OPERATION.....	19
3.1 General.....	19
3.2 Control laboratory (CTL Lab.).....	20
3.3 Observation laboratory (OBS Lab.).....	23
4.0 PERFORMANCE REVIEW.....	26
4.1 Aims and objectives of the review.....	26
4.2 Shaking table performance assessment.....	26
4.2.1 Assessment criteria.....	26
4.2.2 Instrumentation layout.....	27
4.2.3 Instrumentation error sensitivity.....	29
4.2.4 Test specimen.....	29
4.2.5 Definitions and Calculation Procedures.....	31
4.3 Frequency response tests.....	34
4.3.1 Definition of input motion and post-processing of data.....	34
4.3.2 Frequency Response Functions summary results.....	35
4.4 Control fidelity tests.....	37
4.4.1 Definition of input motions and post-processing of data.....	38
4.4.2 Control fidelity summary results.....	38
4.6 System performance analysis.....	40

5.0 CONCLUSIONS	44
5.1 Generalities.....	44
5.2 General of Dynamic characteristics of the shaking table.....	45
5.3 Overall performance of adaptative control system	46
REFERENCES.....	50

LIST OF APPENDIXES

APPENDIX I - Target Time Series: Random White Noise and Kalamata Earthquake
APPENDIX II - Test Measured Time Series: Random White Noise - Sample 5 and Kalamata Earthquake
APPENDIX III - Frequency Response Functions: Unadapted Test
APPENDIX IV - Frequency Response Functions: Adapted Test without Model
APPENDIX V - Frequency Response Functions: Adapted Test with Model
APPENDIX VI - Control Fidelity: Response Spectra of Target and Achieved Motion for Random White Noise
APPENDIX VII - Control Fidelity: Response Spectra of Target and Achieved Motion for Kalamata Earthquake
APPENDIX VIII - Analytical Model of LNEC Shaking Table: Mode Shapes

List of Figures

Figure 2.1 - General perspective of new LNEC shaking table.....	6
Figure 2.2 - Elevation of new LNEC shaking table (taken from Emilio et al. 1989).....	7
Figure 2.3 - Plan view of new LNEC shaking table (taken from Emilio et al. 1989).....	8
Figure 2.4- Longitudinal actuator and small torsion bar system during construction.....	9
Figure 2.5 - Main torsion bars and vertical rods during construction.....	9
Figure 2.6 - Shaking table performance limits in the transverse direction.....	11
Figure 2.7 - Shaking table performance limits in the vertical and longitudinal directions..	12
Figure 2.8 - Platform finite elements mesh.....	16
Figure 3.1 - Control instrumentation layout.....	22
Figure 3.2 - Block diagram of the dual channel FFT.....	24
Figure 4.1 - Acquisition instrumentation layout for the characterisation tests.....	28

List of Tables

Table 2.1 "Bare Table Actuator Characteristics".....	11
Table 4.1 - Instrumentation sensitivity.....	29
Table 4.2 - Test specimen dynamic characteristics related to its position on the LNEC platform.....	30
Table 4.3 Summary of results for frequency resonance and transmissibilities for uniaxial tests (bn corresponds to transmissibilities values considerable low).....	37
Table 4.4 Measured and computed six first natural frequencies.....	40
Table 4.5 - Analysis of results in terms of the measured platform rotational components; triaxial tests, conducted for Kalamata earthquake with and without model (PGD = peak ground displacements).....	41
Table 4.6 Summary of results on the correlation between target and achieved response spectra ordinates.....	42
Table 4.7 Summary of results on the normalised intensity error between target and achieved motions.....	42

1.0 INTRODUCTION

1.1 Background

Earthquake risks have been an important feature of the Portuguese way of life ever since the 1755 earthquake (estimated magnitude $M = 8.75$) which destroyed Lisbon and caused widespread damage in the south western part of the Iberian Peninsula. The rebuilding of Lisbon was the first instance of what can be called the use of applied science to improve urban life. In effect, new streets were drawn according to a gridiron configuration, prefabrication and standardisation of most building elements were implemented, and also a new structural system called "gaiola" was developed with the purpose of increasing the earthquake resistance of the buildings.

The Portuguese "National Laboratory for Civil Engineering" (LNEC) in Lisbon, first began studying earthquake engineering in 1960 with an electrodynamic shaker (15 kN, 5-5000 Hz) which was used mainly for testing dam models. Until recently the main experimental facilities comprised a uniaxial horizontal shaking table (3.26 x 2.26m, in operation since 1972) and a vertical shaking table (2.65 x 1.60m, in operation since 1977) powered by servo-actuators. In addition to these there are also testing rigs for beam column assemblages, masonry panels and dam models. These facilities have been used mainly in civil engineering studies and in certification studies of electrical equipment (e.g. control cabinets for nuclear power plants - *Vieira Pinto et al., 1987*).

1.2 Earthquake research using shaking tables

A shaking table is a device designed to test large structural models under a wide range of simulated ground motions. It usually consists of a large, rectangular platform that is supported and driven in up to six degrees of freedom by a number of servo-controlled hydraulic actuators, or 'servoactuators'. The test signal which drives the actuators can vary from a simple sine-wave to a recorded signal of a real earthquake. The test specimens are secured to the surface of the platform and shaken. The dynamic behaviour of the structure can be evaluated using transducers (most commonly accelerometers and displacement transducers) and data acquisition systems.

In the 60's and 70's shaking tables were originally developed to enable the study of dynamic behaviour of civil engineering structures, mainly involving the safety needs of the power industries (e.g. hydroelectric, thermal and nuclear). With the development of finite element methods over the last twenty years, analyses in the linear range became completely feasible using analytical methods. As a result of this, experimental facilities such as shaking tables and reaction walls are more dedicated today to the study of non-linear (hysteretic) behaviour of reinforced concrete, masonry and steel structures, where analytical models are still being validated by research programmes such as PREC8.

Typical shaking tables currently vary in size world-wide from about 0.5m x 0.5m to 8.0m x 8.0m (special shaking tables such as the 15m x 15m - 1000 tonne machine in

Japan not included), although larger tables are known to be under construction. While smaller tables are generally cheaper to build, their use often implies that tests have to be carried out on scale models due to limitations in size of the platform, headroom, payload limits, etc. It is important to note that the reliability of the results from reinforced concrete and masonry models increase significantly as the scale factor approaches unity. In addition to this other problems arise with scaling in non-linear behaviour analyses.

All shaking tables are unique in some aspects; they are not 'bought-off-the-shelf' facilities, but are developed from basic electro-mechanical-hydraulic components by their builders and operators. For example, the shaking table at Bristol University is unique in that it is the only platform in existence which has a stiffened aluminium platform (rather than steel or concrete) giving it a 5:1 ratio of payload to platform weight. The new triaxial (3D) LNEC shaking table comprises a unique feature in its torque tube system which eliminates the platform's rotational degrees of freedom, restricting its movement to the three translational directions.

Individuality of a facility may not depend solely on the characteristics of the shaking table. Another unique feature of the Bristol shaking table is that it has been developed to operate under a Quality Management System, certified by the UK Nuclear Installations Inspectorate for testing nuclear power station components to BS5750 and ISO 9001 standards. Another example of individuality at a research centre can be found in Bergamo (Italy) where they have three shaking tables in the same hall, therefore allowing testing of bridge structures with three different base inputs.

1.3 Recent experience in Earthquake Engineering at LNEC

The Centre for Special Studies in Earthquake Engineering (C3ES) at LNEC have recently completed the construction of a new triaxial shaking table (5.6m x 4.6m). This table differs from others in Europe in that it is designed specifically for the study of masonry and r/c structures in the dynamic non-linear range. An important aspect of this type of research is the testing of specimens close to collapse. The platform is generally larger than its contemporaries in order to be able to test full scale or near full scale prototypes, so as to limit the problems linked to scaling.

Whereas the majority of shaking tables in Europe set out to control all six degrees of freedom using an active control system, the new LNEC platform isolates the translational degrees of freedom (transversal, vertical and longitudinal) to be controlled, whilst reducing rotational effects mechanically. This results in a passive control system for the rotational DOFs where the principal difficulty is to quantify, not control, the rotational effects of the platform. Another aspect that deserves mentioning is the attempt to reduce "cross-coupling" between the three translational degrees of freedom by attaching the actuators to the platform using long rods. Details of these systems may be found in chapter 2.1.

So far, with the exception of trial tests, little research has been carried out at the LNEC

facility. With the completion of the characterisation tests the facility will be considered as fully operational, although it is intended that the systems will continue to be updated in the foreseeable future. Proposed staffing levels for the facility are: 2 principal researchers, 1 senior researcher, 2 auxiliary researchers and 4 assistant researchers. Also available to support the testing activities are LNEC researchers from other departments, specialised in mechanical and control systems.

1.4 Motivation for this research

Following the report by the Earthquake Engineering Study Panel to the European Commission's Advisory Committee (*European Commission - 1990*) and as a first step towards unification of European activities in this field, an European consortium was established, currently consisting of four of the principal European research centres: Earthquake Engineering Research Centre (EERC - Bristol, UK), Laboratory for Earthquake Engineering (LEE - Athens, Greece), Istituto Sperimentale Modelli e Strutture (ISMES - Bergamo, Italy) and Laboratório Nacional de Engenharia Civil (LNEC - Lisbon, Portugal). Their combined facilities cover almost the total spectrum of usual shaking table types, although a greater degree of co-operation between the different organisations is required to bring Europe up to the same level as the USA and Japan.

With the objective of promoting co-operation in mind, a programme of earthquake shaking table standardisations was instigated. Previously, each facility had acted independently and there was no guarantee that the same test carried out on two different platforms would give the same result. The programme had two principal aims: to compare results from different facilities so as to identify any individual characteristics and to provide a bench-mark at each facility from which future research could be validated. It is important to ensure that these 'benchmarks' from different shaking tables in Europe are all based on similar tests, such that comparisons can be made of the individual capacities and requirements.

The first tests were carried out jointly by EERC and LEE (EC contract ERBGEI*CT920042) at their respective centres, and the results published in 1994 (*Crewe, A.J. et al. - 1994*). It was shown that by conducting frank and open comparative test procedures, the idiosyncrasies of each facility can be determined and allowed for in future tests. The tests carried out at the LNEC facility formed part of EC contract ERBCHGECT920010.

1.5 Scope and structure of this report

The principal aim of this project was to produce a detailed characterisation of the frequency response function (FRF) and the control fidelity of the LNEC shaking table. One noticeable difference between this facility and others in Europe is the clear distinction at LNEC between the roles of 'Shaking table Control' and 'Data

Acquisition'. Because of this distinction there exists a dividing line between these two areas in matters of computer software/hardware and operations. Limitations and features of the LNEC shaking table performance experienced during these tests are analysed and reported.

This report has five main chapters: Introduction, Description of the shaking table, Shaking table systems operation, Performance review and Conclusions. Details of the test data can be found in the appendices.

Chapter 1 introduces the objectives of the research and its background. Chapter 2 describes in detail the physical aspects of the LNEC shaking table, and includes a summary of the facilities characteristics and a list of the equipment used. A section on analytical modelling of the shaking table is also included in this chapter. The third chapter is divided up into three sections: general, control and observation operation systems. Chapter 4 presents the characterisation tests, the analysis and the results. Information is given here concerning instrumentation used, test programmes and a summary of the main observations. The conclusions and suggestions for further research can be found in chapter 5.

2.0 DESCRIPTION OF THE LNEC SHAKING TABLE FACILITY

2.1 The Shaking table

LNEC studied and built a new type of earthquake shaking table, that was optimized for the study of masonry and reinforced concrete structures in the non-linear ranges. The platform was designed to work in a frequency range from zero up to 20Hz. As far as the collapse of structures is concerned, this includes almost all the energy related to surface waves to which strong seismic motions are related. For this reason the tests discussed in this report are designed for that frequency range.

In order to have a shaking table simulating only the horizontal and vertical motions, the rotational degrees of freedom of the 5.6 x 4.6m platform are eliminated by torque tube systems, one for each degree of freedom. Each system is composed of a torsionally very stiff torque tube which can rotate around its longitudinal axis and is supported at both ends by bearings. General views of the shaking table can be seen below in figures 2.1 to 2.5.

At each of its ends the torque tube is linked, by way of a crank, to a stiff connecting rod. This, in turn, is connected to the platform. The vertical connecting rods are pinned at both ends, such that horizontal motion of the platform is allowed. When the platform moves vertically, it either pulls or pushes the connecting rods, rotating both cranks by the same angular amount and torque tube likewise; thus, no forces whatsoever arise. If there is an overturning moment and the platform starts to rotate, then vertical movement in opposed directions appears at the upper end of the connecting rods, which in turn causes a small opposite rotating force in the cranks. This is resisted by a large reaction force generated through torsional deformation of the stiff torque tubes, resulting in only a very small platform rotation.

It should be mentioned that in the future it may be possible to insert a short stroke actuator (i.e. a very stiff actuator) in one connecting rod (or in the two connecting rods to preserve symmetry) to eliminate the flexibilities of the torque tube system. It is expected that the overall flexibility of a torque tube system is smaller than the flexibility of a pair of vertical actuators, unless the actuators have a small stroke and a large piston area. A small stroke poses obvious restrictions on displacement requirements, which are unacceptable in a shaking table for testing reinforced concrete structures up to collapse, and a large piston area implies huge oil flow, regarding velocity requirements, and thus a quite expensive hydraulic power supply.

Obviously, a torque tube system only eliminates rotations around an axis orthogonal to the torque tube axis and parallel to the cranks direction. Therefore, two horizontal torque tube systems (1200mm diameter and 20mm thick) with horizontal cranks are set under the platform, in mutually orthogonal directions, to eliminate rotations about horizontal axes. A third horizontal torque tube system, with vertical cranks, is located on the side of the platform to cope with rotations about the vertical axis. Since the

torsional moments are expected to be much smaller than the overturning moments this tube system is smaller than the other two (800mm diameter and 20mm thick).

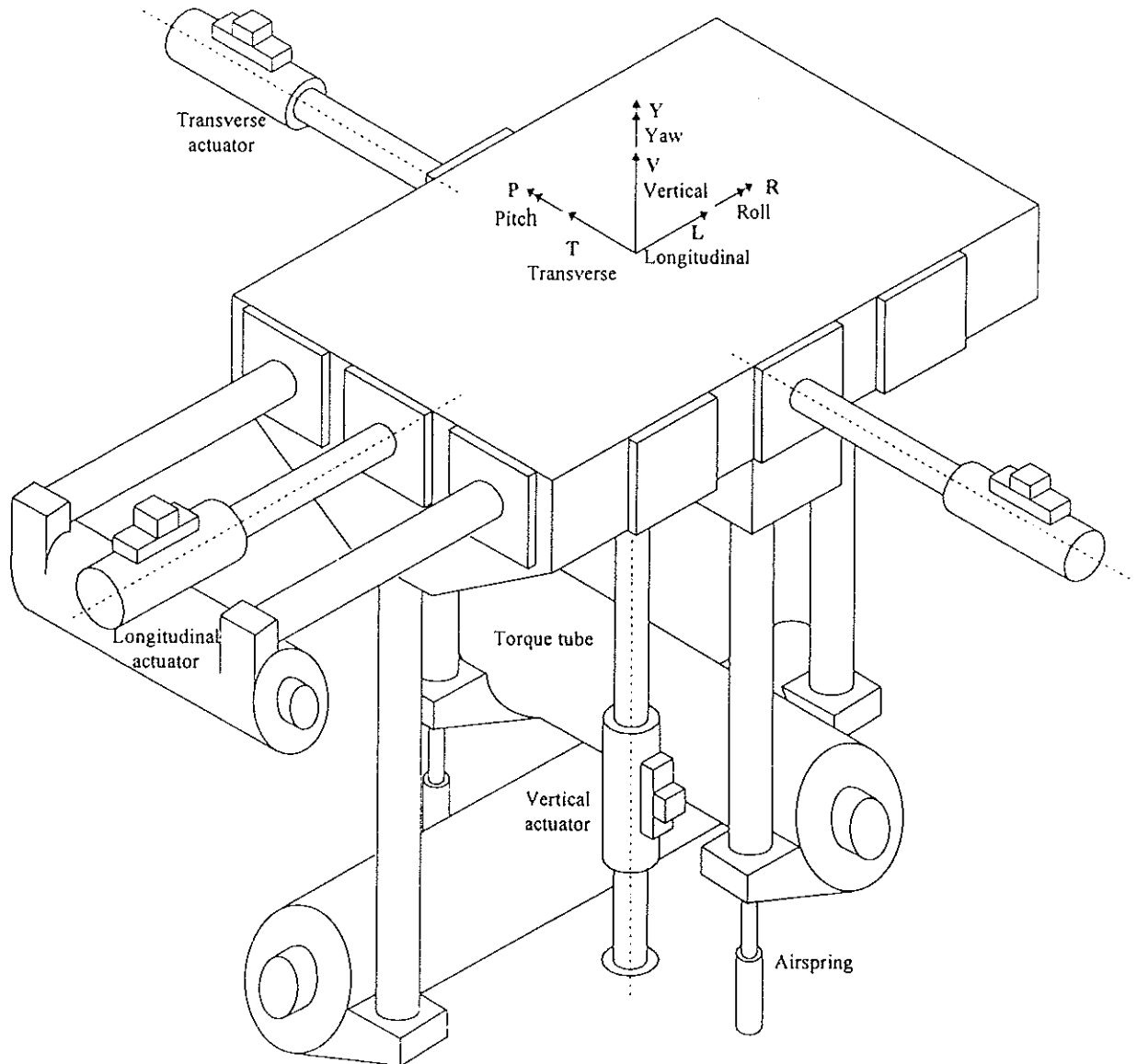


Figure 2.1 - General perspective of new LNEC shaking table

Between the underside of the horizontal cranks and the base are mounted passive gas actuators to cope with the dead-weight of the shaking table and the test specimen.. These can be replaced by rigid blocks which fasten the cranks to the base, thus significantly reducing vertical motion of the simulator and allowing the test of very heavy models in two horizontal directions.

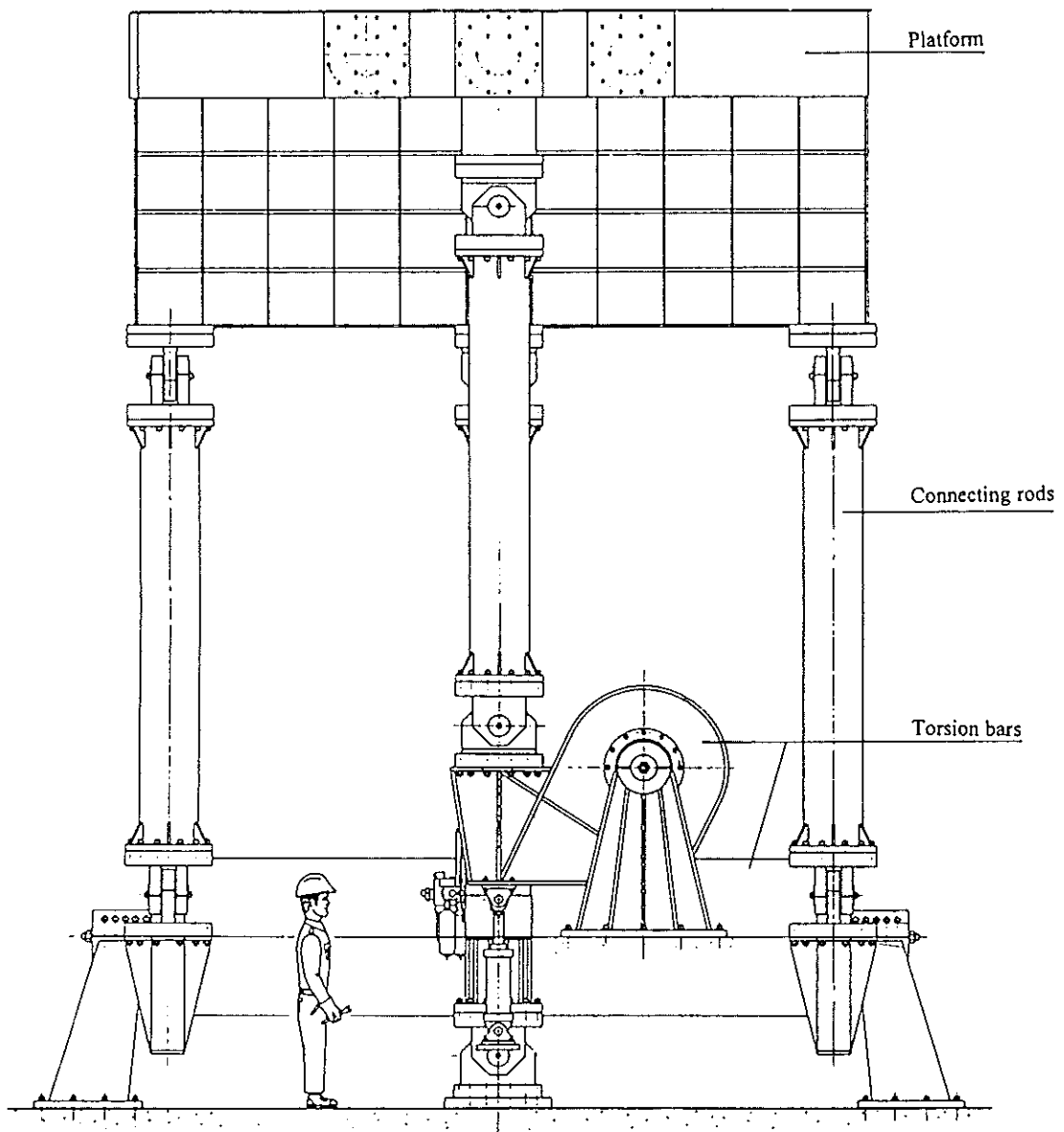


Figure 2.2 - Elevation of new LNEC shaking table (taken from Emilio et al. 1989)

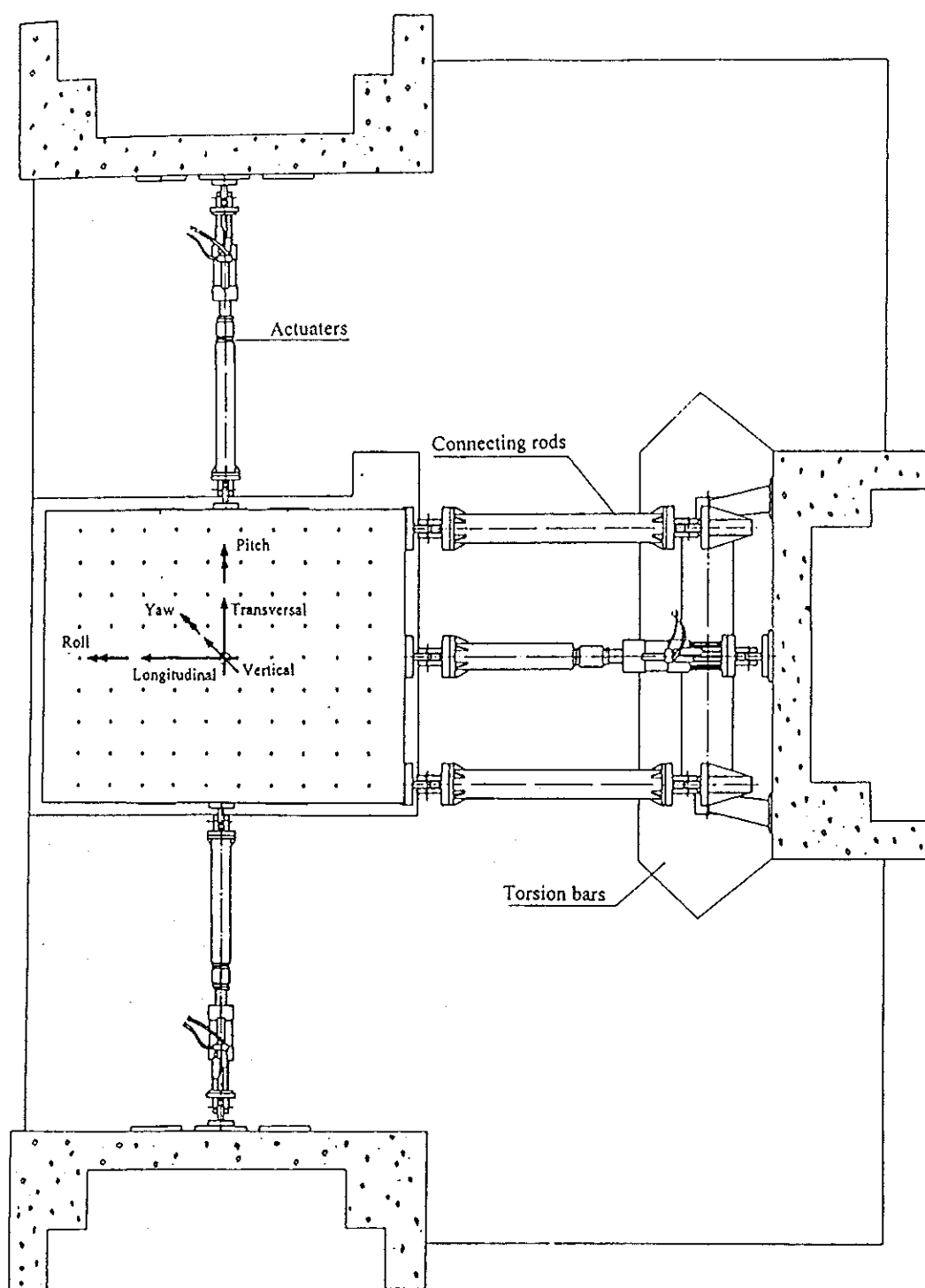


Figure 2.3 - Plan view of new LNEC shaking table (taken from Emilio et al. 1989)

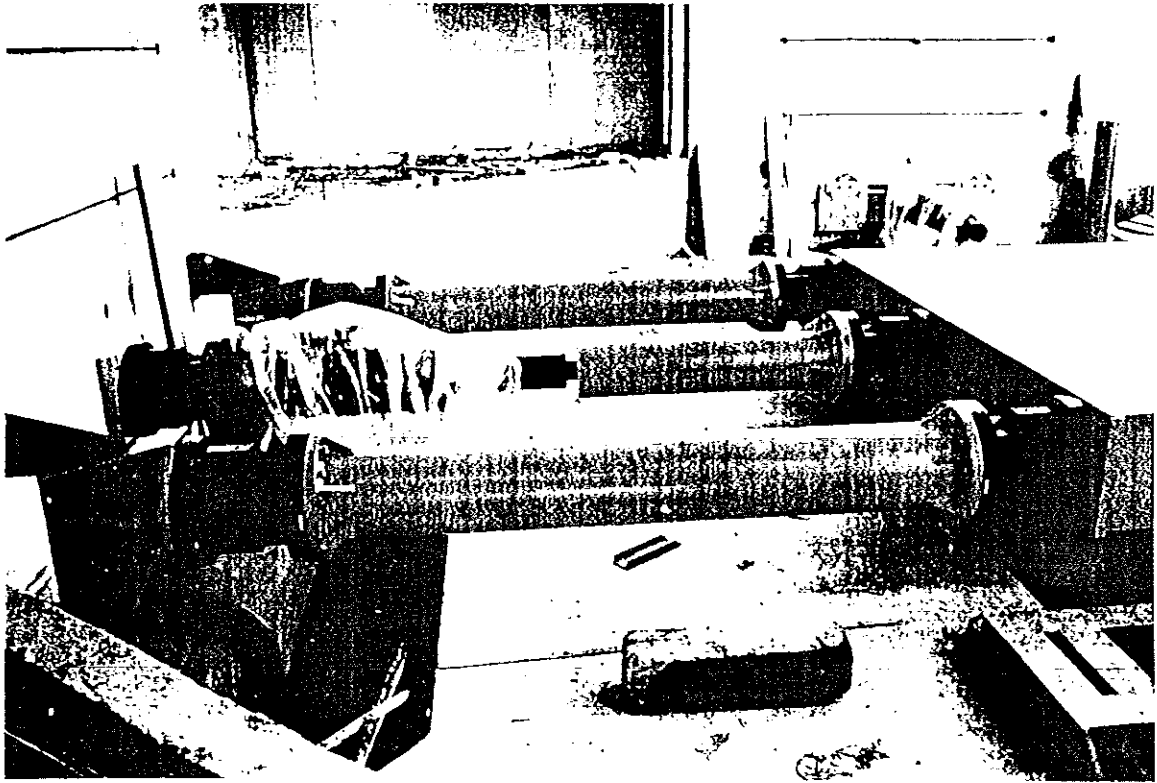


Figure 2-4- Longitudinal actuator and small torsion bar system during construction



Figure 2-5- Man working on the wall of the longitudinal actuator

The design approach behind this shaking table system was to try to balance out the relative component deformabilities, ensuring that no single concentrated deformation appears on the system operation, and resulting in an optimised system efficiency as a whole. This relies on careful design and in-depth analysis of the structure, as well as high levels of construction accuracy, taking into account the large dimensions involved in the simulator. An example of this is the accuracy taken in the construction of the attachment points for the actuators, where orthogonality and parallelism is crucial; errors below 0.1mm were specified.

One particular problem associated with shaking tables where the actuators are mounted perpendicular to the sides of the platform is the effect of 'cross-coupling' between the various degrees of freedom. An attempt to resolve this is made by connecting the actuators to the platform using long connecting rods such that any orthogonal movement of the platform relative to the axis of an actuator causes only minor mis-alignment. In this way the cross-coupling in the three orthogonal translational directions is reduced and the actuators are effectively decoupled.

An advantage of the 3D type of shaking table is the reduction in weight and cost associated with the installation of fewer actuators. Nevertheless there is still a considerable dynamic self weight of the platform (400 kN) and because of this an electro-hydraulic safety system was designed and installed at LNEC to ensure a safe stopping of the shaking table in the case of an hazard situation or an operator "error". This shaking table is controlled by a 3D digital system, acting on displacement and acceleration feedback signals, which is adjusted and controlled through a dedicated computer. More details of the control system may be found in section 2.3.2.

2.2 LNEC facility characteristics

2.2.1 Summary of shaking table characteristics

The general LNEC shaking table characteristics are summarised below. Table 2.1 shows the performance limits for a bare shaking table.

Platform	Size : 5.6m x 4.6m Mass : 400kN Max. payload (based on airspring capacity): 600kN
Controlled degrees of freedom	3
Translation	T, V, L
Rotation	N/A
Hydraulic system	Max. oil flow : 690 l/min Operating pressure : 210 bar

Axis	T (Transverse)	V (Vertical)	L (Longitudinal)
<u>SERVO-ACTUATORS</u>			
Quantity	2	1	1
Total force (kN)	600	300	1000
Max. displacement (cm)	20	20	20
Max. velocity (cm/s)	20	20	20
Max. acceleration	1,2g	0,6g	2,0g
<u>PASSIVE GAS ACTUATORS</u>			
Quantity	N/A	2	N/A
Total force (kN)	N/A	1000	N/A

Table 2.1 "Bare Table Actuator Characteristics"

More detailed information about the shaking table performance in the three translational axes is given in figures 2.6 to 2.7. These curves are deduced from INSTRON test values using a 300kN capacity actuator with applied dead loads varying between 0 - 600kN, for the actuator layout used at the LNEC facility. As far as the limit velocities are concerned, it was assumed that the platform motion is uniaxial; no consideration of shared oil flow between actuators was made for multi-axial test conditions.

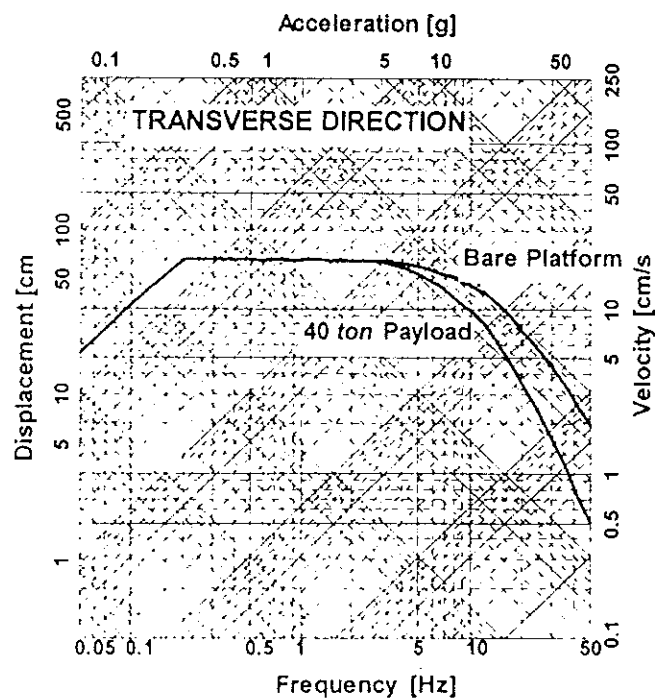


Figure 2.6 - shaking table performance limits in the transverse direction

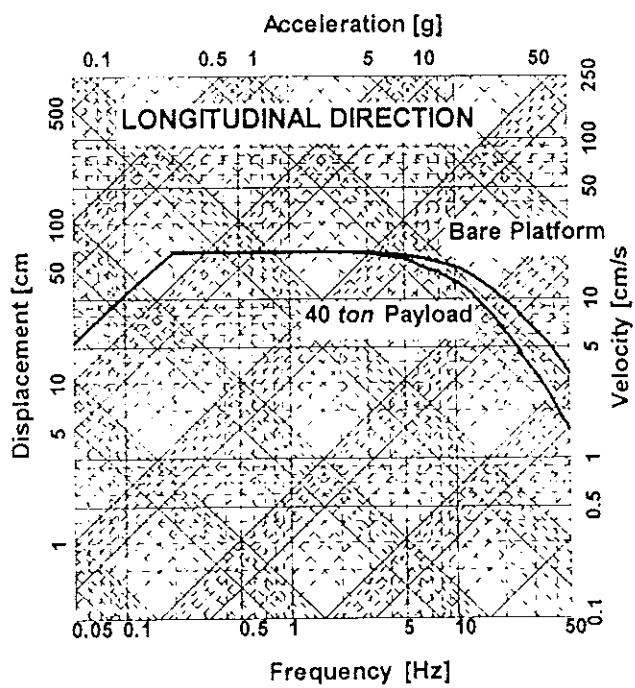
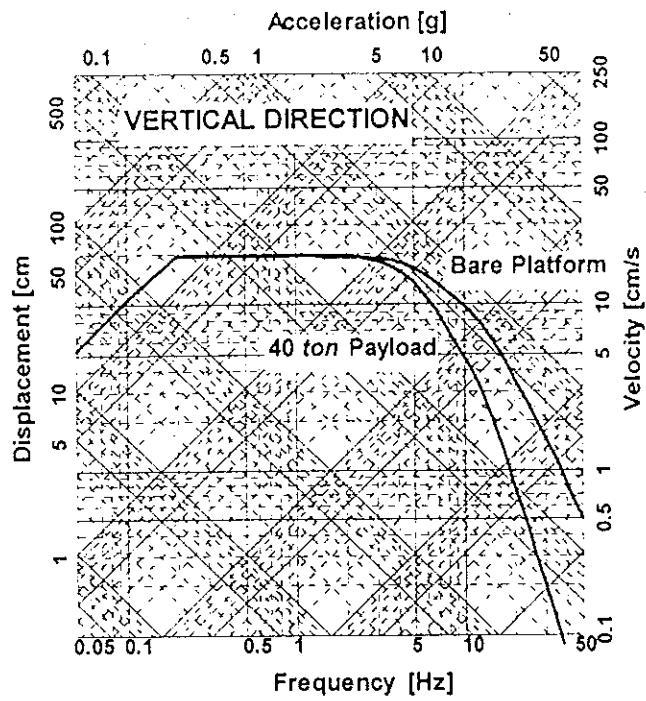


Figure 2.7 - shaking table performance limits in the vertical and longitudinal directions

It is worth mentioning that during the characterisation tests performed it was found that the velocity limits shown in figure 2.6 can be exceeded, even during multi-axial situations, if earthquake-like random signals are used in the place of the more demanding sweep-sine characterisation used by INSTRON. It appears that the oil accumulator capacity, currently limited to around 12 litres, provides sufficient flow for peak demands if it remains above 6 litres, at which point the system pressure drops below 120 bar and the system shuts down. These aspects have been confirmed by recent computer simulations taking into account the following variables: servoactuator oil flow demand (proportional to the actuator velocities), power station oil supply (limited to 690 l/min) and substation oil accumulator capacity (related to actuator displacement time histories). Further dedicated experimentation must be performed in order to properly characterise the complete power oil supply system, if, as is envisaged, an additional oil accumulator bank system is to be designed.

2.2.2 Additional characteristics

The effective capacities of an earthquake simulator do not depend only on the type of shaking table but are also dependent from the characteristics of the building where it is installed. In the case of the LNEC triaxial shaking table the building and the platform were conceived as a single integrated system to test up to collapse heavy models (200-400 kN). This system was designed to optimise the "test cycle" which comprises the construction of the model, its positioning over the shaking table and instrumentation, its vibration test and its removal.

The new building which houses the shaking table consists of a multi-cellular reinforced concrete structure. This comprises a 2m thick prestressed r/c. basement slab to support the vertical actuators and the two large torque tubes, and a prestressed concrete ring to support the horizontal actuators and the small torque tube system. On three sides of the shaking table there are mutually orthogonal reinforced concrete walls with a shallow U-section, situated above the prestressed ring, which are used as supports for measuring displacements. It is important to note that for the construction of these walls, as well as certain other specific elements of the facility, a high level of accuracy was used in the setting-out and construction methods, as required by the sensitive measurements involved in earthquake simulator testing.

The walls adjacent to the platform can also be used as "reaction walls" for small forces (up to 40 kN). They are connected over the roof by 3.3m deep x 0.6m thick beams which intersect over the shaking table. There are 8 fixation points on these beams, each with an individual capacity of 200 kN and a maximum total capacity of 800 kN per beam. From those fixation points will hang the suspending cables that will sustain the heavier elements of the model after the collapse.

The removal of a collapsed model from the shaking table is a critical phase of the testing cycle. By stationing the crane over the model during the test, a second set of suspending

cables can be connected to the heavy parts of the model; those cables will be looser than those going from the model to the roof beams. After the collapse of the model, the hoisting of the hooks will transfer the weight of the broken model from the roof suspending cables to the crane suspending cables. At that point, the roof cables will be disconnected from their fixation points; hence the special work platform on the crane. To protect the platform from the roof cables if the collapse of the model is associated to large horizontal displacements, twelve 200 kN fixation points are disposed on the three large walls and another four points are provided in the floor of the testing hall in the direction where there is no wall.

Some of the building characteristics are listed below:

Foundation	Non-isolated multi-reinforced concrete structure
Crane	4 Hooks (2 x 200 kN, 40 kN, 16 kN) Max. capacity = 400kN Minimum vertical velocity of 200kN hooks: 0.5 mm/s; Height of 200 kN hooks: 8.5 m

2.3 The analytical model

2.3.1 General

The control of shaking tables for tests where the model undergoes plastic deformation is a difficult task because the evaluation of the transfer functions between the target and achieved signals for the controlled degrees of freedom only takes into account the linear behaviour of the test specimen. The development of control software capable of following the changing dynamic characteristics of a system (e.g. platform and model) as the test progresses is currently the topic of a European research programme (CEASTADS).

2.3.2 Use of analytical models in earthquake engineering

Before carrying out experiments on a shaking table it is useful to be able to use analytical models (linear for the platform, non-linear for the model) to explore what is going to happen during a test in order to estimate the degree of error between achieved

and target imposed movements on the test platform. In the case of the LNEC shaking table this insight becomes more important since there is no active control of the rotational degrees of freedom.

Moreover, for the purpose of post-processing information gained from experimental tests it is also important to have analytical models and system-identification software packages working together. These allow a better identification of the test model and a calibration of the analytical model, which in turn provides a more accurate prediction of the next intensity level of testing. This process can be repeated until collapse of the test specimen, providing information about the intensity of earthquake action (energy input) versus the state of damage of the specimen.

Other reasons for using analytical models in conjunction with shaking table tests include the assessment of other state variables not measured during the tests (e.g. strain measurement of a particular element of the model) and pre-test numerical calculations to ensure that models used do not exceed the platform capacities.

This chapter describes the analytical model of the shaking table carried out previously and presents the results in terms of natural frequencies and mode shapes. A comparison of these results with the experimental FRFs can be found in chapter 5.

2.3.3 Analytical model of the shaking table

A dynamic analysis of the new shaking table was carried out at LNEC prior to its completion. (Emilio et al. - 1989). The shaking table natural frequencies were calculated, and the mode-shapes under self-weight were established.

For this purpose, use was made of a dynamic analysis program for three-dimensional structures (ADET), developed at LNEC, which provides for six degrees of freedom per node and considers bar and shell elements. The structure of the platform was modelled as 1764 triangular shell elements, the typical configuration being that of an isosceles right-angle triangle with 0.5 m cathetus, thus closely following the mesh (0.5m × 0.5m) of the steel plates that constitute the internal platform structure, Figure 2.8. Modelling of the other elements (actuators, torsion bars, cranks and connecting rods) was done using bar elements.

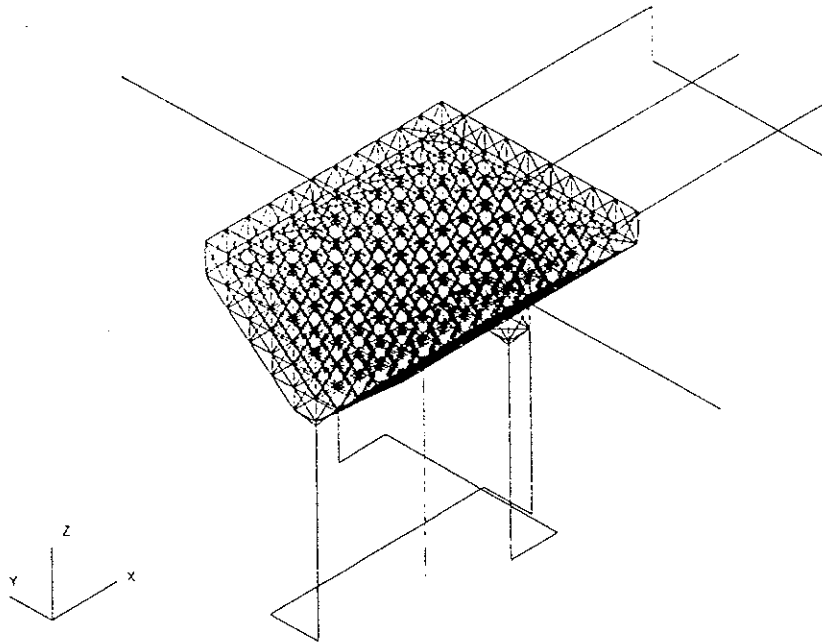


Figure 2.8 - Platform finite elements mesh

The numerical model of the unloaded shaking table includes 550 nodes which correspond to 3300 degrees of freedom.

After obtaining the natural modes of vibration of the unloaded platform, it was found, as it might well be expected, that the modes of the lowest frequencies correspond to the three rigid-body translations (due to the actuators deformability, with frequencies lying between 7 and 12 Hz according to the stiffness of the actuators involved. In the second mode (horizontal translation) a rotation component around a vertical axis was detected, this being explained by the asymmetry of distribution of masses (the actuators are not arranged symmetrically round the platform). The three following modes correspond to the flexibility of the torsion bar/crank/connecting rod systems, the fourth mode represents rotation around the vertical axis, or yaw, (15 Hz) and the fifth and sixth modes rotations around horizontal axes, roll and pitch, (but not parallel to the main axes of the platform), both lying in the range from 27 to 28 Hz. Modes higher than the sixth, which either involve deformation of the platform structure or are local modes of rods have their own frequencies between 50 and 90 Hz and are therefore not very significant.

In short, three classes of modes were found, corresponding to:

1. Six first modes, demonstrating rigid body platform motions (7Hz-27Hz).
2. Modes 7 to 21, corresponding to local deformation of guiding system (50.6Hz-89.3Hz)
3. Above the 21st mode, involving platform deformations (greater than 90.7Hz)

Mode shape drawings for the first seven modes can be seen in Appendix VIII.

2.4 Computer equipment and hardware

Below can be found a general list of the equipment used in the new shaking table facility during the characterisation tests described in this report:

Shaking table Components

- Power supply: 3 x 110 kW powerpack unit
- Oil pumps: Three units (each 230 l/min)
- Substations: three electrohydraulic (one per axis).
- Servo-valves: three two-stage MOOG72 servo-valves for the 300 kN actuators (transverse and vertical) and a three-stage MOOG79 for the 1000kN actuator (longitudinal).

Control Hardware from Control Laboratory (CTL Lab.)

- Inner servo position control loop system: INSTRON 8580 multi-axis digital control device
- PC-compatible computers: two 486 IBM-compatible computers

Acquisition hardware from Observation Laboratory (OBS Lab.)

- Acceleration transducers: 10 high frequency ENDEVCO® model 7290A (0 - 600 Hz) variable capacitance accelerometers
- Acceleration conditioners: 10 Piezoresistive Bridge Signal Conditioners, ENDEVCO® model 106, with pre-set 100Hz anti-aliasing 8-pole 'Butterworth' filters.
- Two power supplies for signal conditioner: ENDEVCO® model 109
- Displacement transducers: 4 x-y HAMAMATSU optical displacement transducers (comprising lens, sensor head and LED target)
- Displacement conditioners: HAMAMATSU conditioning device PSH Controller C2399
- Displacement anti-aliasing filtering: three analogue two-channel 'Butterworth' filters: Rockland model 1042F dual HI/LO filter and 'Krohn-Hite' model 3342 dual HI/LO filter.
- Data acquisition system: one 28-channel multiplexed Kaye-MDAS-7000 D/A unit
- Data acquisition buffering: one PC IBM-compatible 486 computer (66mhz, 16Mb)
- Data analysis: one PC IBM-compatible Pentium(133mhz, 32Mb)

2.5 Safety and Maintenance

The safety principles of the LNEC shaking table are to provide a safe working area, both for the trained operating personnel and any visitors/spectators. The new building which houses the shaking table facility is designed especially for this purpose, providing controlled laboratory conditions, as well as fire/security systems complying with modern standards. Access to the shaking table area is generally restricted to personnel involved in the current tests, while visitors may observe the tests from the safety of the laboratories. Larger groups of visitors may also be accepted into the facility, whereupon special security measures (e.g. safety barriers, warning alarms) may be employed.

From the operational point of view there are three built-in security systems that are able to shut down the system automatically in the event of a potentially hazardous situation:

- The system has special switches, attached directly to the actuators, that ensure displacements remain within desired limits (adjustable, usually set to $\pm 145\text{mm}$ in all axes).
- The oil pump power supply has built-in pressure switches that can shut down the shaking table system in the event of pressure loss. The cut-off pressure is adjustable, typically activated below 130 bars.
- There is a transducer for monitoring the temperature inside the oil tanks to avoid over heating, as well as special arrangements to avoid over-heating of the powerpack unit.
- Control software can also be used to provide actuator limits, typically set to $\pm 130\text{mm}$ in all axes.

The LNEC shaking table has only recently become operational. At present no maintenance procedure has been defined for the new shaking table, although experience gained so far, as well as that from other existing LNEC shaking tables, allows certain guidelines to be set:

- This new equipment should not be shut down for long periods of time. To do so can create problems with the equipment due to dust accumulation within bearings, oil filter blockages, and so on. These can be prevented if the system is a 'warmed-up' on a regular basis (e.g. weekly) with the same procedure as is done prior to a test ("warm-up procedure": slow, long motions of the platform, carried out for the three axes).
- The shaking table comprises a large number of pre-stressed bolted connections. These must be inspected regularly and, if necessary, adjustments must be made to ensure that the design pre-stresses are maintained.
- The system relies on passive gas actuators to cope with the dead-weight of the shaking table plus test specimen. The service pressure of this system must be maintained by recharging the specific accumulators to compensate for leakages within the system.
- The main swivel bearings of the system are provided with grease lubrication points allowing for periodic lubrication.

3.0 SHAKING TABLE SYSTEM OPERATION

3.1 General

This chapter presents the LNEC shaking table system operation, both from the point of view of the control (CTL) and observation (OBS) activities, and is therefore divided into two main sections. The first main section describes in detail the equipment and procedures used by the control laboratory. The nature of the activities carried out by the observation laboratory is such that equipment and procedures are constantly changing, and is dependant on the specimen being tested. The second main section therefore contains only general information regarding the tools used. More specific information concerning the procedures applied for the characterisation tests can be found in chapter 4.

The organisation of the shaking table facility is such that each group is based in a separate laboratory, using different equipment and training of personnel. The function of the control laboratory is to achieve a predefined shaking table motion on the three translational degrees of freedom, taking into account the driven mass (shaking table and model). The observation laboratory is more concerned with earthquake engineering problems, rather than the problems related to driving the shaking table. Its primary mission is to design the tests, acquire the data and analyse the results. Although they are separate areas, in-depth co-operation must exist between them, with both laboratories being involved in all phases of testing (planning, execution and analysis). This is essential to ensure the safe and efficient working of the facility.

Earthquake tests performed at this facility are intended to examine non-linear behaviour; problems related to the fidelity of control and reliability of the test model are anticipated as far as the limits of the shaking table are concerned. During non-linear behaviour testing the collapse of heavy models provides a potentially dangerous environment if not properly controlled. Therefore it is important to attempt to predict, from the point of view of earthquake engineering, what will happen during a test.

The separation of the control and observation laboratories presents certain advantages from an organisational point of view. However, a problem is also created: that of the exchange of data between the two laboratories. Currently, this only comprises a triggering system, representing the minimum essential link, although a computer network will shortly be installed to enable communication between the two laboratories. The current trigger system is necessary to avoid phase distortion problems between the separate data acquisition systems being used. The observation equipment is set up for a test and the data acquisition is triggered by the control system when the test begins. A warning light set-up allows each team to know the current status of the other.

A crucial part of earthquake simulation is the acquisition and processing of data retrieved from tests. To do this successfully relies on powerful modern computers and software. While the LNEC shaking table relies on standard computer hardware such as

IBM-compatible PCs, the software used includes both proprietary packages and software developed in-house at LNEC (see sections 3.2 and 3.3 for details).

Operation of this shaking table requires a full understanding of its characteristics and complete knowledge of the principles of signal analysis and control system theories, as well as all aspects of the mechanical, hydraulic and electronic systems.

3.2 Control laboratory (CTL Lab.)

The shaking table motion control is composed of four servoactuators, each linked to the INSTRON 8580 multi-axial digital control system. The platform is then controlled using two proprietary software packages. These two packages are installed on the two control computers that can share data by means of a local network. The main task of RSPlus control software is to drive signals and control the data acquisition system. The SPiDAR control software performs all the numerical analyses related to the outer loop phase of control. For further details about the shaking table system software refer to reference manuals.

- SPiDAR V2.1C (INSTRON)

Developed by INSTRON Ltd, SPiDAR is a general purpose software package for control, data analysis and display. It can produce multi-channel input signals for test rigs or machines which reproduce the conditions experienced under service conditions by a structure or component.

The version of SPiDAR used runs on PC-type computers with a 486 processor, running the UNIXTM based SCO Open DesktopTM version 3 system.

- RSPlus V2.95 (INSTRON)

RSPlus (1994) is a test rig command and communication software package, designed to carry out the different tasks necessary for dynamic testing. The principal functions are listed below:

1. Rig manager - configuration and control of the test rig
2. Instrumentation - transducers and data acquisition
3. Test manager - operation and design of a particular test
4. SPiDAR user - operation with SPiDAR iterative control software
5. Test operator - start/stop and maintenance of predefined tests

The RSPlus data format supports compatibility with a variety of other software packages for data analysis and presentation. (e.g. Lotus 123, Prosig Dats, nCode, Microcal Origin).

The outer loop control system used in the LNEC shaking table facility can be described as a multi-variable and adaptive "self-tuning" system, capable of evaluating non-square transfer function matrices between target/achieved signals. This means that it takes into consideration the effects of cross-talking between controlled variables, and employs

signal redundancy in order to better estimate the relationship between the three translational target motions and the achieved motions.

The control operation is an iterative process where in the first phase, known as rig characterisation, the whole system frequency response function is evaluated, inverted and then convolved with the target signal. The second phase (called iteration process) starts by injecting this first estimate of the most adequate driven signal into the system and a first achieved signal is then obtained. This signal, although close to the target, would still show some differences mainly due to the presence of non-linearities, and thus the control proceeds with the iteration process.

The second phase aims at fine tuning the input drive signal. The achieved signal is subtracted from the target to produce an error signal. This error, convolved with the previously estimated and accepted FRF, is added to the previous driving signal to produce a new drive signal which is input into the system. Once again the error signal can be obtained, and the process is then looped, until the error is reduced to acceptable levels.

During this phase, it is suggested that the operator applies a loop gain factor of less than 1.0 to the error. This is recommended because of the uncertainties in the evaluation of the FRF and non-linearities within the system. By limiting this factor to a value of less than unity the approach between target and achieved motions should be such that the magnitude of the error is decreased from step to step, therefore favouring system iteration stability (target values to be approached from below). The accuracy of the FRF estimate can be measured from the values of the partial coherence function matrix.

Performance of the iterative loop is very dependant on the specimen and test rig characteristics, as well as on the target response data. If the table-specimen system is linear, fairly simple, then the iterative loop will converge quickly (e.g. 4 loops) and a high loop gain factor can be used (e.g. 0.7). On the other hand, if the system is non-linear then a much lower loop gain may be required (e.g. 0.25).

The servo-position control system possesses its own data acquisition equipment. This consists of displacement transducers (LVDT) incorporated into the servoactuators, as well as accelerometers attached to the actuator heads. The signals from these transducers are acquired by specific data acquisition boards inside the INSTRON 8500 tower. This tower also has three control channels to drive signals to the servovalves. Figure 3.1 shows a simplified schematic of the control instrumentation layout.

In the adaptive outer loop, measurements of both accelerations and displacements can be used to control the translational DOFs (non-square matrix approach). This allows better estimates of the FRF to be made, as demonstrated by higher coherence function values in different frequency bands. This is achieved by taking into account the accuracy of each transducer type in any particular frequency band. For example, displacement transducers are more accurate for low frequencies, while accelerometers are better for high frequencies.

NEW TRIAXIAL EARTHQUAKE SIMULATOR

Simplified drawing of command and control

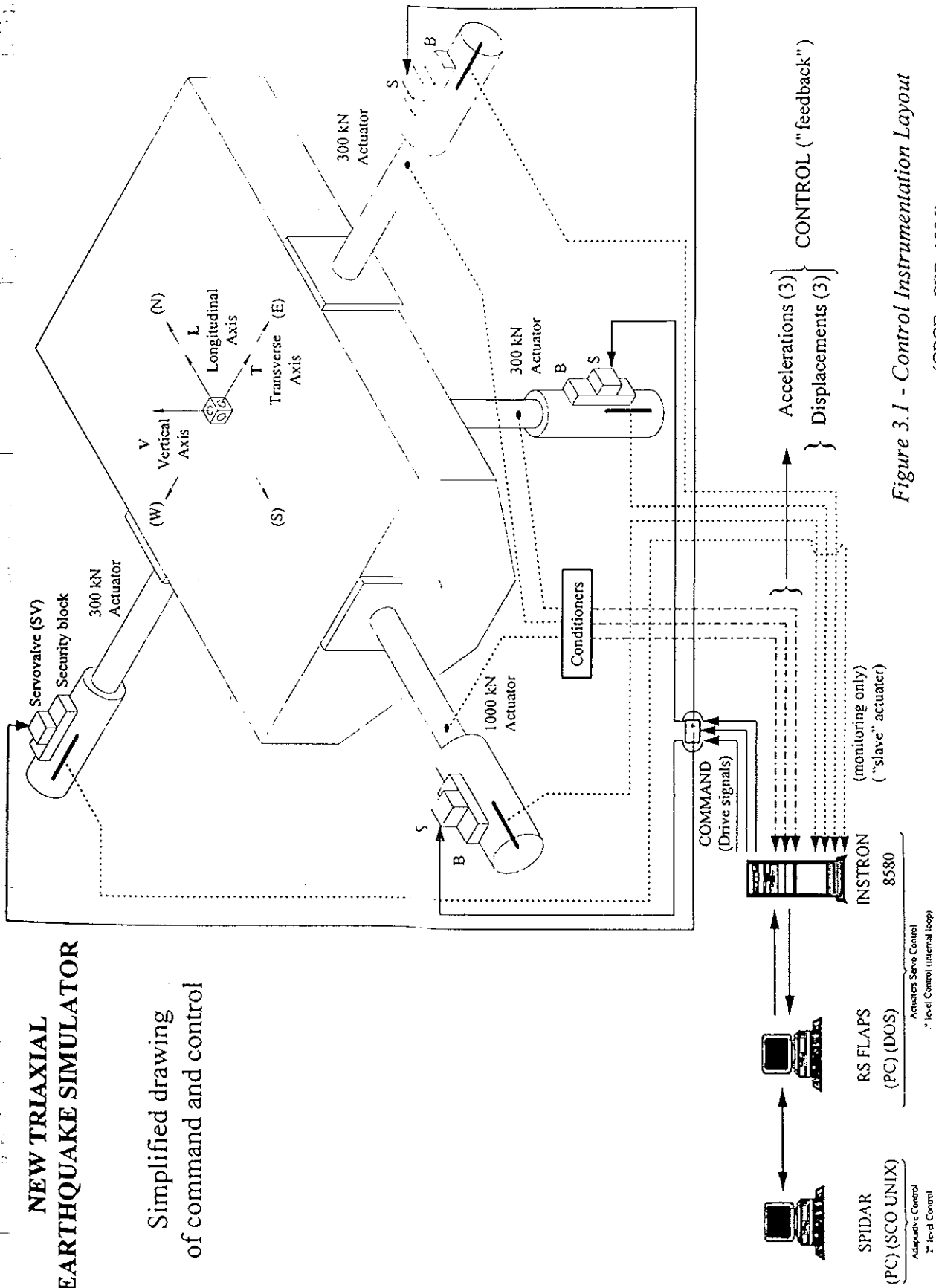


Figure 3.1 - Control Instrumentation Layout

(CPCE - FEB. 1996)

The location of the two types of transducers must be the same so as to provide measurements of similar motions. The actuators are purchased with instrumentation for measuring control displacements already incorporated and so their location is pre-defined. Hence, the control accelerometers must be positioned at the heads of the actuators, as shown above, and not directly on the platform. In order to be able to control the shaking table with accelerometers positioned on the platform it would be necessary to take into account the transfer function introduced by the 'stiff rods' situated between the heads of the actuators and the platform itself (see figure 4.1), and carry out an off-line compensation of the target displacements. Until this is done the effect of this transfer function will be to introduce errors into the control of the shaking table. These effects are discussed later in chapter 4.

3.3 Observation laboratory (OBS Lab.)

The principal equipment used in the OBS Lab. to perform the acquisition of data from the model is the MDAS 7000 data acquisition system. This system has a communication port of GPIB-type that enables its configuration and command from a PC, using software developed in LABVIEW (*mdas7000.lib*). The analysis of results is currently performed on a Pentium PC using in-house LNEC software (*fourier.lib*).

- *mdas7000.lib*

This is a general purpose command and display software package. It enables the OBS Lab. to specify within MDAS7000 the number of channels (up to 28) and the sampling rate, as well as the gain scale and offset for each channel respectively, and type of triggering system (manual, or from CTL Lab.). After the acquisition is complete the operator can display the time series of each channel and buffer the data onto the hard disk.

- *fourier.lib*

This software is a package of routines for signal analyses, developed in Fortran77, and compiled for 16-bit Windows™ environment. The modules within *fourier.lib* are compiled as Dynamic Link Libraries (dll), the principal ones of which are:

1. *twindow.dll* - Time windowing: Cosine taper, Kaiser-Bessel, Hanning and Flap-top.
2. *four.dll* - Fast Fourier Transforms (FFT), evaluation of direct and inverse discrete fourier transforms (DFT).
3. *fipro.dll* - Filtering (low-pass and high-pass) Integration, differentiation, double-integration and double-differentiation of time series.
4. *iwan.dll* - Computation of pseudo velocity response spectra (PSV) for either maximum relative displacement or maximum absolute accelerations responses.

The philosophy behind the development of this software package was to use the potential of the Windows™ graphic display and management environments. This allows the use of Win-based programmes (e.g. VISUAL BASIC, EXCEL) as front ends to input/output data, post-process and display results from the *dll* routines described above.

Dual Channel Spectrum Averaging

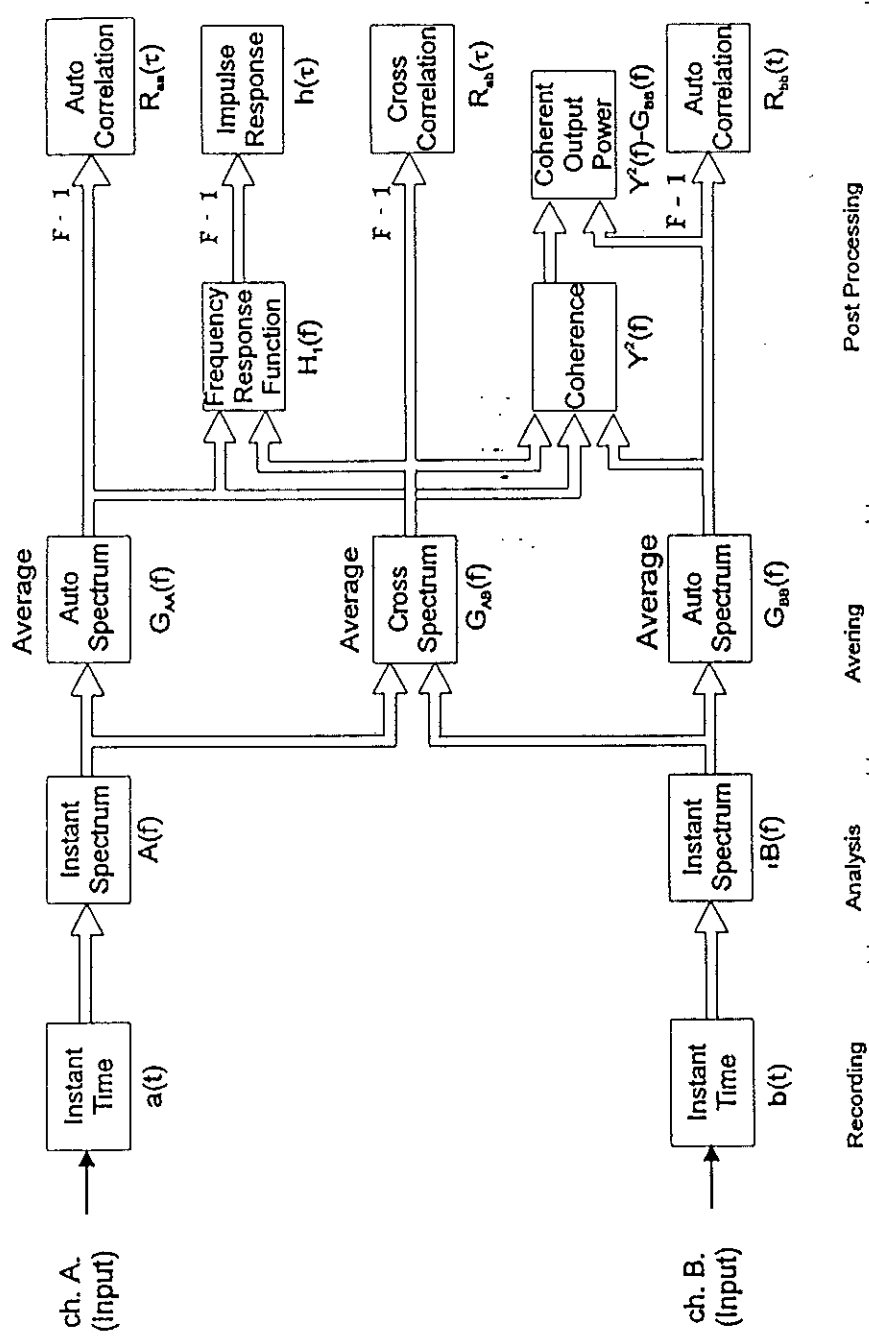


Figure 3.2 - Block diagram of the dual channel FFT

The software listed above is under continuous development and currently only caters for the individual processing of time-series, each limited to 4096 samples. For this reason, and for the purpose the characterisation tests, another FORTRAN77 program (*bare.for*) was developed at LNEC in the MS-DOS environment using the same routines as described above, but with the capability of performing dual-channel FFT analyses in spectrum averaging mode including the computation of:

1. Expected Frequency Response Functions (FRF).
2. Expected Phase Spectrum.
3. Coherence Function estimates.

This program reads and processes the output files from MDAS 7000 directly, although in its current format it is not very user-friendly; changes in the analysis to be performed require modifications in the main FORTRAN program. In the above figure 3.2 can be seen the block diagram of the dual channel FFT analyser in spectrum averaging mode implemented. For more details concerning the analysis performed by these software packages refer to Brüel & Kjaer or Bendat & Piersol (see references).

The test specimen motions are monitored using accelerometers and optical displacement transducers. These two groups of signals are each driven through different conditioning equipment, each with specific cabling furnished by respective companies. In the case of the accelerometers the conditioners have built-in low-pass filter option that activated filters out signal frequency components above 100Hz. The amplified displacement signals should be filtered separately using analogue filters in order to avoid aliasing. Both signals can then be converted digitally using the 16-bit MDAS 7000 data acquisition unit, which can supply a greater amplification by adjusting the gains with *mdas7000.lib*.

The acquisition instrumentation layout is specific to a particular test and hence no generalised layout drawing can be presented here. An example layout for the characterisation tests is shown in figure 4.1.

4.0 PERFORMANCE REVIEW

4.1 Aims and objectives of the review

This chapter describes the particular aspects of the test programme carried out, setting out the assessment criteria and instrumentation used, and highlighting the main observations made. One of the main goals of this project were to produce a detailed characterisation of the frequency response for the new LNEC shaking table and to assess its control accuracy, as part of an on-going European research programme.

It was originally intended to use a similar test programme as was used previously in Bristol and Athens. This comprised: Elcentro (single axis) & Kalamata (triaxial) earthquake signals, variable payload tests and random impulsive tests. However, due to current state of development of LNEC facility and its specific characteristics it was necessary to orient the original test programme to cope with a more in depth characterisation of the facility. It must be referred that the entire facility was thoroughly explored for the first time, including all equipment used in CTL and OBS Labs.

Because of these changes, and a strict test schedule, the Elcentro earthquake signal and the variable payload tests were not included in the current programme. However, tests with varying payload, up to the limits of the shaking table, are considered very important and are already foreseen in the near future.

4.2 Shaking table performance assessment

4.2.1 Assessment criteria

The performance of the facility is assessed using two criteria: FRF evaluation and control fidelity. The first criteria is concerned with the identification of the dynamic characteristics of the bare shaking table, assumed as a rigid body platform supported by the guiding system and actuators. Apart from the masses and the compliance of the guiding system (rods, torsion bars and cranks), these characteristics are also dependent on the flexibility of actuators/oil columns, which in turn are affected by the presence of the inner loop feedback control. The comparison of tests results with the modal analysis carried out using an analytical model, presented in section 2, allows a calibration of the model.

For shaking tables which actively control all six degrees of freedom the dynamic characterisation is less meaningful; theoretically, the outer loop control system could compensate all the resonance of the system. In the case of the LNEC shaking table, where the three rotational degrees of freedom are restricted mechanically, the dynamic characterisation tests are important because there are resonances which are only passively controlled (pitch, roll and yaw).

The assessment of the LNEC shaking table control fidelity is mainly concerned with the capacity of the overall control system (inner and outer loops) to accurately reproduce

specified earthquake motions at the base of test specimens attached on the platform. This capacity can be quantified by the differences between target and achieved platform motions, after completing the adapting procedures.

Two methods were used to assess the accuracy of the control system. The first one quantifies in what measure the relative amplitude of harmonic components of achieved and target signals follow the same trend, in the sense of the relative spectral description of the two signals (same peaks and valleys), independently of some bias error affecting the achieved signals. On the contrary, the second control accuracy measure identifies the existence of constant gain factor affecting the achieved signals in such a way that the intensity of both motions are not equal.

In particular, with the first type of error one is able to make a judgement about the ability of the control system to reproduce a given target signal. Typically this error will become larger if covariance between target and achieved signals is low or, in other words, if the global coherence of the two motions is low and the general trend of the spectral description of target signals is not reproduced in the platform.

With the second type of error it will be possible to conclude about intensity of achieved platform motions in relation to the intensity of the respective targets. This error will increase if mechanical and/or electrohydraulic resonances that were not properly compensated by the outer loop control procedures subsist. Those resonances could introduce an amplification on the achieved signals in a given frequency band, although the relative spectral description of target motions are globally reproduced on the platform.

For each of the tests performed, the accelerations and displacement time histories were recorded, both for a bare platform and with the test specimen. The tests were carried out for each single axis with pseudo random excitation, producing a frequency response function database for adapted and non-adapted situations. Additionally, one triaxial test was also conducted with motions taken from a real earthquake. As mentioned before, the design frequency range of the LNEC earthquake simulator is 0-20Hz. For this reason the tests discussed in this report are designed for that frequency range.

4.2.2 Instrumentation layout

In order to measure the motions of the platform a total of 15 channels were used, providing orthogonal measurements of the platform motions at several points using optical displacement transducers and accelerometers. Position transducers side by side at points A, B and C as shown in figure 4.1 allows the assessment of the three orthogonal translations and the rotations of the platform. The reference axes for these measurements are defined as being at the centre of the rigid body platform as shown in the same figure.

In general, both the Control and Acquisition laboratories utilise their own instrumentation to measure the platform motions. The only exception to this are an

additional three accelerometers positioned at the head of the actuators (*act_Lon*, *act_Tra* and *act_Ver* as shown in figure 4.1) which provide signals to both laboratories. It should be noted that the generalised six DOFs of the platform were computed by post-processing the signals coming from the transducers mounted on the sides of the platform (positions A, B and C in figure 4.1) and not those positioned on the actuators. From the point of view of control fidelity this difference poses some problems that are discussed later.

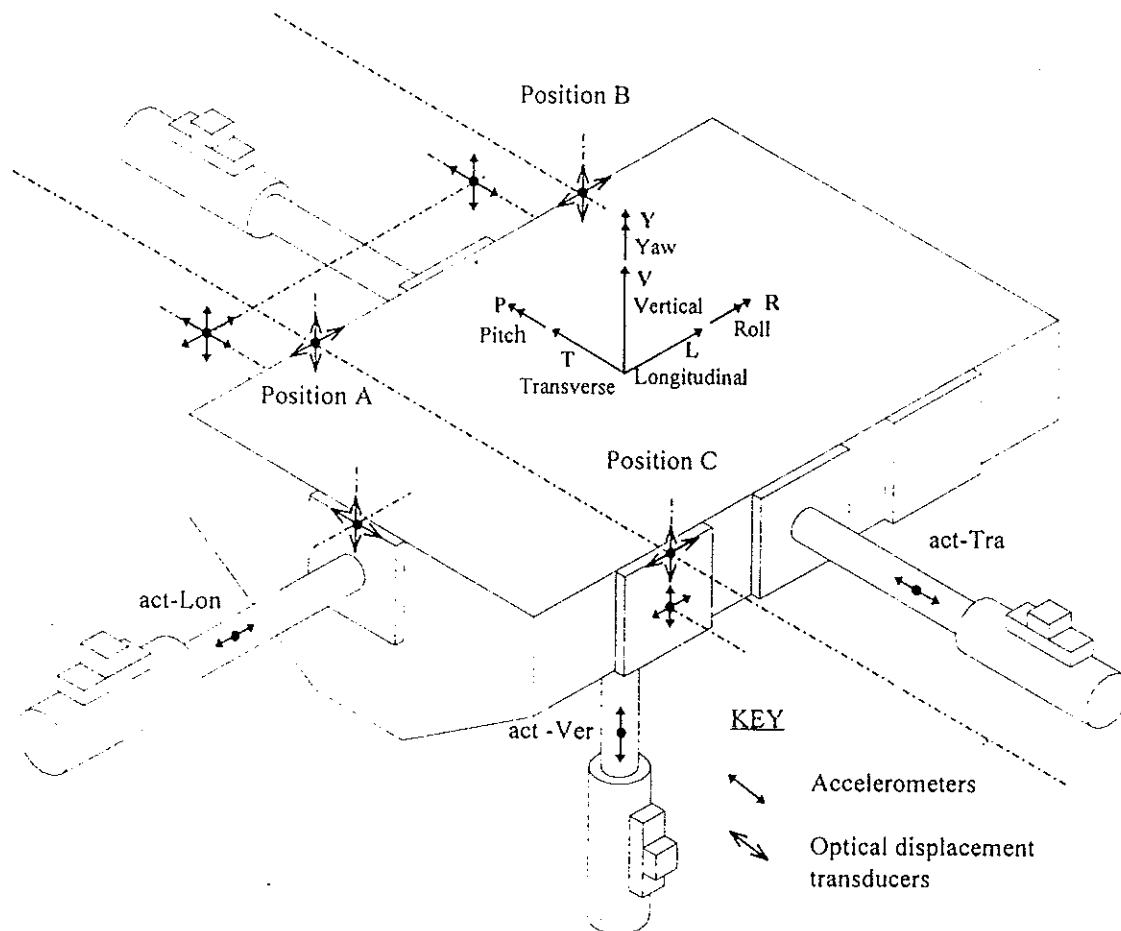


Figure 4.1 - Acquisition instrumentation layout for the characterisation tests

It is important to note that this was the first time that the measurement equipment was used; verification of the accuracy of the measurements and the efficacy of the data acquisition system was carried out by using more acceleration and displacement transducers than required, allowing cross-checking of the results.

As far as the instrumentation of the test model is concerned two orthogonal accelerometers were positioned on the underside of the lowest steel mass, enabling measurements of the longitudinal and transverse motions of the structure.

Acquired data is stored directly onto a computer hard disk, with a backup copy created and stored on floppy disks at the end of the test. Detailed information concerning the system measurement equipment used is provided in section 2.4.

4.2.3 Instrumentation error sensitivity

The optical displacement transducers comprise a position sensor and an infrared LED target. In the transverse direction these two components are separated by roughly 4.5m (the distance of the platform from the side wall). This distancing of the components allows measurements of up to $\pm 500\text{mm}$ of the absolute platform displacements. However, the error in the sensitivity of this equipment at this distance is 5mm, corresponding to 1% of the full scale measurement. Taking into account the distance between the neighbouring transducers (see figure 4.1; 2000mm between points A and B, and 4660mm between points A and C), this corresponds to the instrumentation errors in the sensitivities presented in table 4.1 below.

The error in the sensitivity of the accelerometers, measured at the frequency of 100Hz, is 0.05g. In the table below the minimum values that can be considered for each axis and for each component of motion are displayed.

Transducers	T	V	L	ROLL	PITCH	YAW
displacement	5mm	5mm	5mm	$2.1 \cdot 10^{-3} \text{ rad}$	$5 \cdot 10^{-3} \text{ rad}$	$2.1 \cdot 10^{-3} \text{ rad}$
accelerometers	0.05g	0.05g	0.05g	0.10 rad/s ²	0.24 rad/s ²	0.10 rad/s ²

Table 4.1 - Instrumentation sensitivity

The analysis of the error sensitivities indicated in table 4.1 shows that the errors in displacements measurements are considerable, taking into account the purposes of the tests that were carried out. However, previous experience with these transducers has shown that, under certain conditions, a 50% increase in accuracy can be obtained. As far as the frequency range of both type of transducer is concerned, the displacement transducers are designed to work from DC up to 156Hz, while the accelerometers are supposed to work between DC and 500Hz.

During the tests it was observed that the displacement transducer layout used was not sensitive enough to accurately measure the platform rotations. Therefore these measurements were based on the accelerometer layout only. It should be noted that the sensitivity of the acceleration measurements was not jeopardised by the being attached to the sides of the platform, since the special attachment points were used. At these points, special care was taken during the construction of the platform to ensure parallelism and orthogonality of the attachment plates relative to each other. Moreover, during the connection of the accelerometers to the platform attachment points special attention was paid to the levelling procedures in order to reduce all the possible cross-talking between components.

4.2.4 Test specimen

For the purposes of these tests one of the two model specimens used in the 'Athens/Bristol Shaking Table Assessment (ABSTA) Project' standardisation tests was transported to LNEC. The specimen was designed by EERC and constructed in the UK.

Two identical specimens exist: one which remains in Bristol while the other has been used by LEE (Athens) and ISMES (Bergamo) and is currently at LNEC (Lisbon).

Although this model is considered to be relatively small for the capacities of the LNEC shaking table it was decided to use one of the existing models, rather than build a new one, mainly to provide a reference datum. More details about the design of this model can be found in *Crewe, A.J. et al. - 1994*.

The specimen was conceived to represent a single degree of freedom structure. It consists of a two tonne steel frame onto which additional one tonne masses can be added. The total weight of the specimen used during the tests was 8 tonnes.

Both the Bristol (3m x 3m) and the Athens (4m x 4m) shaking tables have a 300mm square grid of 20mm diameter holes on the surface of the platform to bolt specimens for testing. The Lisbon shaking table (4.6m x 5.6m) has 30mm diameter holes set out on a 500mm square grid, and so it was therefore necessary to modify the base of the model. It was anticipated that these alterations will have an insignificant effect on the behaviour of the model during testing. The test model dynamic characteristics, as verified prior to the tests by assessing the impulsive response, are listed below in table 4.2.

	First natural frequency	Damping ratio
Transverse	5.76 Hz	1.9%
Longitudinal	7.13 Hz	4.1%

Table 4.2 - Test model dynamic characteristics related to its position on the LNEC platform.

It is important to note that despite the models being the same, the individual capacities of the earthquake simulators raises the question of suitability of one model to properly test a variety of different shaking tables.

For the tests carried out in Bristol the specimen was considered to provide a good test of shaking table performance. In Athens the same model was able to test the performance of the shaking table almost to its limits, due to its lower payload capacity. For both of these tests the model had a mass of up to 5 tonnes while the payload capacities of the shaking tables are 15 tonnes and 10 tonnes respectively. The shaking table in Lisbon has a much higher payload capacity of 40 tonnes. For the LNEC characterisation tests an 8 tonne specimen was used (all the available masses) in an attempt to reduce the structural frequencies and increase the overturning moments and shear forces to within limits more in line with this facility.

The purpose of the test programme carried out by ABSTA had originally been to examine test specimens in the linear and non-linear ranges. However, their programme was reduced to linear tests only, due to a limit of funding (*Crewe, A.J. et al. - 1994*). The ISMES and LNEC tests were based on this reduced programme. The LNEC characterisation test programme is well suited to the state of development of the facility, currently in a characterisation phase, although future tests should be performed with

larger models and higher payloads, looking specifically at the problems related to the non-linear behaviour of specimens, and limits of the earthquake simulator.

4.2.5 Definitions and Calculation Procedures

As already mentioned the shaking table performance was assessed in terms of the frequency response functions (FRF) between input or target motions and output or achieved six DOFs platform motions. Those FRFs were evaluated before and after the adaptation procedures carried out by of the outer loop control; unadapted and adapted tests.

The comparison between those two FRFs allow a qualitative assessment to the performance of the control system. Additionally the differences in pseudo velocity response spectral ordinates, between target and achieved motions, allows the quantification of control fidelity. Next paragraphs present the analytical post-processing procedures used for these purposes.

The FRF evaluation comprises estimates of the frequency response gain $|H(f_k)|$ and phase $\theta(f_k)$ spectra, as well as the coherence function $\gamma^2(f_k)$. As outlined by the block diagram in figure 3.2, the estimates used in the FRF evaluation are performed taking into account the following approach.

Sequences of data sampled in a time resolution h , are divided into q frames of n points with the total duration of the sequence given by $(n-1) \cdot h \cdot q$. These frames must then be padded to N points, corresponding to a power of two, and a cosine-taper window (generally 10% of total duration at the beginning and end of each frame) is then applied.

With the FFT procedure, estimates of one-sided power spectral density functions (psdf) for the input, output and cross-spectral can be evaluated using the following expressions:

$$\tilde{G}_{k,i}^x = \frac{2 \cdot h}{N} \cdot |X_{k,i}|^2 \quad \text{for the input psdf}$$

$$\tilde{G}_{k,i}^y = \frac{2 \cdot h}{N} \cdot |Y_{k,i}|^2 \quad \text{for the output psdf}$$

$$\tilde{G}_{k,i}^{x,y} = \frac{2 \cdot h}{N} \cdot |X_{k,i}^* \cdot Y_{k,i}| \quad \text{for the cross psdf between input and output}$$

where $|X_{k,i}|^2$ and $|Y_{k,i}|^2$ is the squared modulus of FFT components, at frequency f_k , for the input and output respectively and for frame i . The complex conjugate of $X_{k,i}$ is expressed by $X_{k,i}^*$.

Taking into account the averaging process over all the q frames, the expected power spectra estimates, at frequency f_k , for the total duration of the sequences are evaluated by:

$$\hat{G}_k^x = \frac{1}{q} \cdot [\tilde{G}_{1,1}^x + \tilde{G}_{1,2}^x + \dots + \tilde{G}_{1,q}^x]$$

$$\hat{G}_k^y = \frac{1}{q} \cdot [\tilde{G}_{1,1}^y + \tilde{G}_{1,2}^y + \dots + \tilde{G}_{1,q}^y]$$

$$\hat{G}_k^{x,y} = \frac{1}{q} \cdot [\tilde{G}_{1,1}^{x,y} + \tilde{G}_{1,2}^{x,y} + \dots + \tilde{G}_{1,q}^{x,y}]$$

The gain factor and the phase factor of the FRF between input x and output y can now be carried out using:

$$|H(f_k)| = \frac{|\hat{G}_k^{x,y}|}{\hat{G}_k^x} \quad \theta(f_k) = \tan^{-1} \left(\frac{\text{Im}(\hat{G}_k^{x,y})}{\text{Re}(\hat{G}_k^{x,y})} \right)$$

Finally, coherence estimates are evaluated by:

$$\gamma^2(f_k) = \frac{|\hat{G}_k^{x,y}|^2}{\hat{G}_k^x \cdot \hat{G}_k^y}$$

One possible definition of pseudo velocity response spectral ordinate $PSV_{k,\zeta}$ at frequency f_k and relative damping ζ for a given acceleration time series $\ddot{y}(\cdot)$, is expressed by:

$$PSV_{k,\zeta} = (2\pi \cdot f_k) \cdot \max_{0 \leq t \leq T} \left| \int_0^t h_{k,\zeta}(t-\tau) \cdot \ddot{y}(\tau) \cdot d\tau \right|$$

where $h_k(t-\tau)$ represents unit impulsive response of a single degree of freedom oscillator with natural frequency f_k and relative viscous damping ζ . The convolution integral gives the relative displacements time history response of that single DOF oscillator to input $\ddot{y}(t)$. The implemented computer algorithm used in the present work follows the exact analytic definition given above.

As already mentioned two types of errors were used in order to quantify the control fidelity. In particular, the first type of error quantifies the ability of control system to reproduce the relative frequency content of a given target signal. For that purpose it was used the statistical concept of correlation coefficient which, in the present case, reflects the degree of relationship between target and achieved response spectral ordinates.

To compute those correlation coefficients the response spectra of target and achieved motions are evaluated for 74 geometrically spaced spectral frequencies, ranging from 50

to 0.5 Hz (or 0.2 to 20 sec). For uni-axial tests each spectral ordinate is equal to the mean value of 10 time histories, whereas for the tri-axial test only one sample is available (Kalamata earthquake).

Taking those spectral ordinates, of target (t) and achieved (a) motions, those coefficients are given by:

$$\rho_{t,a} = \frac{COV_{t,a}}{\sigma_t \cdot \sigma_a} \quad \text{with} \quad COV_{t,a} = \sum_{n=1}^{74} (PSV_n^t - \mu_t) \cdot (PSV_n^a - \mu_a)$$

where PSV_n^t and PSV_n^a represent pseudo velocities response spectral ordinates at frequency n ; σ_t , σ_a , μ_t and μ_a are the mean and standard deviation of the $PSVs$ for target t and achieved a motions. Values of $\rho_{t,a}$ close zero are obtained when spectral ordinates of achieved signals are uncorrelated with the respective targets while values of $\rho_{t,a}$ close to one means a perfect correlation.

It must be stressed that the above defined coefficient is a measure of the linear relationship between two ranges of data; it only measures if spectral ordinates are associated or, more precisely, whether target and achieved spectral ordinates move together along the frequency band, independently of a constant bias affecting the achieved motions.

For the other component of inaccuracy of the control system (bias error) it seems more appropriate to establish a relationship between mean squared values of target and achieved signals given by the following expression:

$$e_{t,a} = \frac{\int_0^T [x(t)]^2 \cdot dt}{\int_0^T [y(t)]^2 \cdot dt} \approx \frac{\int_0^{2\pi f_{Ny}} G^a(\omega) \cdot d\omega}{\int_0^{2\pi f_{Ny}} G^t(\omega) \cdot d\omega}$$

where $G^a(\cdot)$ and $G^t(\cdot)$ are the psdfs of achieved $x(\cdot)$ and target motions; f_{Ny} is the Nyquist frequency. Values of $e_{t,a}$ can vary from approximately zero (for relatively low intensity of achieved signals) to high values (for relatively high intensity achieved signals); values of $e_{t,a}$ close to one means perfect match in terms of energy content of target and achieved motions.

For computing values of $e_{t,a}$, it was used the displacement (and not acceleration) motion components, promoting the low frequency, instead of high frequency, non compensated resonances. This option is in agreement with working frequency range of the shaking table (0-20 Hz), and the general characteristics of earthquake strong ground motions (decreasing energy above 5 Hz).

4.3 Frequency response tests

The evaluation of the frequency response functions is carried out assuming a single input linear system with multi-output state variables; all these tests are uniaxial, meaning that there is one single theoretical input (driving signal), while there are six physical outputs (generalised six DOFs). More specifically, the evaluation of the following frequency response functions were considered:

1. FRFs between drive and achieved platform motion for each direction individually, taking into account the input displacement and output measured platform accelerations.
2. FRFs between measured platform accelerations, in each direction of excitation, and measured accelerations in all other five DOFs.

The diagonal terms of the FRFs (see 1.0 above) were analysed taking into account different state variables than the non-diagonal terms (displacement/acceleration instead of acceleration/acceleration) because, by doing so, resonances within the system become more evident.

4.3.1 Definition of input motion and post-processing of data

The signal used in these tests has the following characteristics:

- frequency range between 0.5 Hz to 22 Hz
- 163.84 seconds duration, (0.005 seconds time interval, 32768 samples)
- peak amplitude of the signals are, ± 1 cm in the transverse and longitudinal and ± 5 cm in the vertical direction.

The frequency distribution of the displacement input signals can be globally characterised as pink noise modulated by the axis transfer function, thus exhibiting a decrease in certain frequency bands (due to system resonances) and an increase in higher frequency regions (due to system attenuation).

More precisely, the above drive signals have been achieved in an adaptive control fashion aimed at settling for an input signal that will produce an actual pink noise on the platform. This is done mainly because it has been found experimentally to lead to better coherences between output and input signals, thus allowing better estimates of the system transfer function.

Because of the initial signal ramp used by the CTL Lab. to cope with the possible initial transient effects, a triggering delay of about 2.5 seconds is created. This, combined with the limits in the buffering of MDAS7000 (32767 samples), causes the acquired time signals in the OBS Lab. to observe an initial phase distortion between input and measured signals. This phase distortion must be corrected which is done by simply removing the initial 494 points.

The sequence of data input and output is divided into eight frames of 4034 points each (padded to 4096 samples). A cosine-taper window (10% of total duration at the beginning and end) is then applied to all frames.

As mentioned above, the FRF evaluation comprises estimates of the gain $|H(f_k)|$, the phase $\theta(f_k)$ and the coherence spectra $\gamma^2(f_k)$. In what concerns the error of the estimates presented by the procedure outlined in section 4.2.5 it should be stated that the normalised error of the gain of the FRF estimates, for values of coherence equal to $\gamma^2 = 0.9, 0.8$ and 0.6 , are roughly 8%, 11% and 20% respectively.

4.3.2 Frequency Response Functions summary results

The test results of the procedures outlined in section 4.2.5 can be found in Appendix III. The analysis of these results, for the frequency band under consideration (0-22Hz) and regarding the characterisation of the FRFs of the non-adapted tests, is shown below. The FRF gains are expressed in g/g for the translation components and rad/s^2 per g for the rotational components.

Specifically for the excitation in the transverse direction, the following particular aspects were observed:

1. The cross-coupling between transverse and vertical directions are between 2%-8%, showing only coherence values greater than 0.8 in the frequency band between 16-18Hz, where the transmissibility reaches the higher limit.
2. Cross-coupling between transverse and longitudinal directions is apparent within the frequency range. Peak resonance values of 30% and 9%, at frequencies of 11Hz and 15.5Hz respectively, were found. For these resonances the corresponding coherence values are above 0.95.
3. The cross-coupling between transverse and pitch is about $0.1 rad/sec^2$ per g throughout the frequency range, exhibiting relatively low coherence values (≈ 0.7).
4. The cross-coupling between transverse and roll shows a peak value of $6 rad/sec^2$ per g , at 18 Hz, with high coherence (>0.9 in the frequency band of 8-20 Hz). The damping of this resonance is relatively high, as demonstrated by the slow phase changing (estimated as 9%).
5. The cross-coupling between transverse and yaw shows a clear peak value of $7 rad/sec^2$ per g , at 11Hz, with high coherence (>0.9 in the frequency band of 5-20Hz). Damping at this frequency is also relatively high, although exhibiting faster phase changing than previously (estimated as 7% of critical).

For the excitation in the vertical direction, the following particular aspects were observed:

1. Transmissibility between vertical and longitudinal directions is 2% in the frequency range 0-10Hz, but with a coherence lower than 0.7. Thereafter, the coherence increases up to 0.9 and the transmissibility peaks to about 30% at 21Hz.

2. Cross-coupling between vertical and pitch shows resonance (2 rad/sec^2 per g) and anti-resonance (0.1 rad/sec^2 per g) at frequencies of 21Hz and 8.5Hz respectively. The corresponding coherences are above 0.9 at the resonance and below 0.6 at the anti-resonance.
3. Cross-coupling between vertical and roll is relatively low (0.2 rad/sec^2 per g). The coherence is generally 0.65, rising to a peak value of 0.9 at 18.5Hz .
4. Transmissibility between vertical and yaw is also relatively low, about 0.1 rad/sec^2 per g , in the frequency range of interest. Mean coherence achieved for these measurements is about 0.65.

For the excitation in the longitudinal direction, the following particular aspects were observed:

1. The cross-coupling between longitudinal and pitch is evident in the frequency range between 10Hz - 22Hz . The slow phase-change in this range demonstrates that resonance occurs, reaching a peak of 6 rad/sec^2 per g at 18 Hz . The coherencies in this range are maintained above 0.9.
2. No evidence of cross-coupling was found between longitudinal and roll, where the mean coherence values are about 0.65.
3. The cross-coupling between longitudinal and yaw shows a clear peak value of 0.8 rad/sec^2 per g at 11Hz , with good coherence (>0.95), followed immediately by anti-resonance at 13Hz , where the coherence drops below 0.6.

The FRFs (gain factors, phase factors and coherence), taking into account the target displacements (mm) and the achieved accelerations ($\%g$), are shown also in Appendix III. Of these, the last three figures, correspond to the three uniaxial excitations. The following points must be stressed:

- The three translation natural frequencies of the system under analysis are close to 13.5Hz , 8.5Hz and 11Hz for the transverse, vertical and longitudinal directions respectively.
- In the transverse direction, there also exists some anti-resonance at a frequency of 11Hz .
- For the transverse and vertical direction, the coherence functions for these motions shows values of 0.95 in frequencies ranges outside the resonances frequencies. However, for the longitudinal direction, the frequency range where the values of coherence show a decreasing values seems to be larger than in the previous directions.

Table 4.3 provides a summary of the transmissibilities and gains listed above. As already mentioned, the diagonal terms (T/T, V/V and L/L) correspond to different transmissibility measurements.

DOFs	Excitation Direction		
	Transverse	Vertical	Longitudinal
Transverse	13.5Hz - 22.5%g/mm		
Vertical	bn	8.5Hz - 22.5% g/mm	
Longitudinal	11Hz - 0.3g/g	21Hz - 0.3g/g	11Hz - 90% g/mm
Pitch	bn	21Hz - 10 rad/s ² /g	18Hz - 6 rad/s ² /g
Roll	18Hz - 6 rad/s ² /g	bn	bn
Yaw	11Hz - 7 rad/s ² /g	bn	11Hz - 0.8 rad/s ² /g

Table 4.3 Summary of results for frequency resonance and transmissibilities for uniaxial tests (bn corresponds to transmissibilities values considerably low).

Although no reference to the upper off-diagonal terms of the FRF matrix has been made above (i.e. vert/trans, long/trans and long/vert), these relationships were briefly analysed and showed, as expected, anti-resonance slopes in the frequencies where their symmetrical terms exhibit resonance.

4.4 Control fidelity tests

The control response fidelity looks at the ability of the earthquake simulator to accurately reproduce the target motions in the three directions (T, V and L). More specifically, this section concerns the performance of the outer loop control to cope with the resonances and anti-resonances found during the evaluation of the FRFs, examined in last section. The outer loop control will attempt to flatten the global frequency response function and improve the coherence between target and achieved motions for the actively controlled DOFs (transverse, vertical and longitudinal).

Concerning the passively-controlled DOFs (pitch, roll and yaw) it is anticipated that the outer loop control will only have a minor influence. For this reason, few references to the cross-coupling involving the platform rotations have been made in this section. This aspect are confirmed by the results shown in Appendices IV and V.

The evaluation of the control response fidelity is carried out first assuming a single random white noise acceleration input signal with multi-output state variables, and then an earthquake-like multi input and output situation (i.e. Kalamata). All these tests are performed with bare shaking table and with the test model. The evaluation of the following frequency response functions were considered:

1. FRFs between target and achieved platform motion for each direction individually, taking into account the target and achieved accelerations.
2. Mean response spectra of target and achieved platform accelerations, for each DOF individually.

The results in terms of response spectra are presented in Appendix VI, for random white noise acceleration uni-axial tests and in Appendix VII for Kalamata earthquake.

It must be stressed that for single random white noise tests the control procedures were carried out for each translation DOF independently, meaning that the other translation

DOFs were only controlled by the inner loop; no zero input target signals were imposed on these DOFs in order to verify if the outer loop could cope with. Only in tests performed with Kalamata earthquake the performance of the outer loop control system was appreciated for the three translations.

4.4.1 Definition of input motions and post-processing of data

For the purpose of assessing the control fidelity two types of target motions were used. The first one consisted of ten sample time histories with the following characteristics:

- frequency range between 0.1 Hz and 20 Hz
- 20.48 seconds duration, (0.005 seconds time interval, 4096 samples)
- amplitude of the signals - all calibrated to have the same peak velocity: 10cm/s

The frequency distribution of these acceleration target signals can be characterised as white noise. The target signals have been artificially generated taking into account a constant amplitude Fourier spectrum in the above frequency range and with randomly distributed phases.

For the purposes of multi-axial excitation tests, three pre-processed components of a strong-motion record of the Kalamata earthquake were used (Crewe, A.J. et al. - 1994). This earthquake signal had been filtered to eliminate high and low frequency components, with most of its energy concentrated below 4 Hz. The LNEC shaking table was designed for testing at these frequency ranges and so the Kalamata earthquake was particularly appropriate for testing this facility.

The anti-aliasing filters currently used by OBS Lab. have a fixed cut-off frequency of 100Hz. Therefore, to provide a sampling rate compatible with the Nyquist frequency, the original signal of the Kalamata earthquake was interpolated to a new sampling rate of 200Hz using spline techniques.

The frequency resolution of the target time signals is about 0.05Hz. As before, the correction of the phase distortion was done by removing the initial 494 points.

4.4.2 Control fidelity summary results

The test results of the procedures outlined in section 4.2.5 can be found in appendices IV and V showing frequency response functions from the adapted tests, with and without the specimen respectively.

The FRF gains are expressed in g/g for the translation components and rad/s² per g for the rotational components. The following particular aspects were observed:

1. A significant reduction in the amplitude of the system resonances was observed in all the three axis in the frequency range of target motions, especially for the transverse direction.

2. However, for vertical direction, some amplification (≈ 1.7) at 8.5 Hz still remains and a resonance frequency of 16.7 Hz with a critical damping of 10% is clearly evident.
3. More reduced system amplification than before can also be found for the uniaxial tests in longitudinal direction. It is also apparent the same resonance frequency at approximately 16.7 Hz , although associated with an higher value of critical damping ($\approx 20\%$).
4. For the tests without specimen no significant change occurred in the magnitude, phase and coherence of the cross-coupling between axes, before and after the adaptation process took place.
5. The presence of the specimen had an apparent minimal effect on the controlled DOFs. However, in the other DOFs the effect was more pronounced at the resonant frequencies of the specimen (5.76 and 7.13 Hz transverse and longitudinal respectively).

The results in terms of response spectra for uniaxial tests, with and without model, are shown in Appendix VI. These results are shown for mean values and mean values plus and minus one standard deviation for achieved and target motions for each controlled translation degree of freedom. Additionally, the response spectra of measured motions in the other non-controlled translation DOFs, allowing an assessment of the global cross-coupling between components, are also presented. In Appendix VII the six response spectra corresponding to the tri-axial Kalamata earthquake tests, with and without specimen, are presented.

Globally, those response spectra exhibit what could be expected from the adapted FRFs analysed previously. More precisely, in what concerns the response spectra of target and achieved motions for the uni-axial tests, the following comments are due:

1. In the transverse direction, a perfect match between target and achieved response spectra was observed in all the frequency range. A maximum amplification error (achieved/target) around 1.5 was observed at 20 Hz .
2. In the vertical direction, a good match between target and achieved response spectra was only observed below 5 Hz . Above that frequency, the maximum amplification error of 4.2 at 16.7 Hz was found.
3. In the longitudinal direction, a not so good match was found as in the other two directions. Nevertheless, at same frequency of 16.7 Hz an amplification error of 2.7 was observed.
4. Concerning the cross-coupling between axes it was found that, for a frequency range of 0.1 Hz to 10 Hz (excluding the resonances frequencies reported above) response spectra ordinates in non-controlled DOFs are in general one order of magnitude below the controlled DOFs. However, this effect is clearly large for the longitudinal axe and for the case of vertical excitation.

5. As before, the presence of the specimen only affected the non controlled DOFs, more significantly at the resonant frequencies of the specimen. For the controlled DOFs the values of amplification referred above are similar and at the same frequencies.

For the tri-axial test conducted with the Kalamata earthquake, it was found that:

1. A not so perfect match between target and achieved motion as in the uni-axial tests. In fact a more involved situation of the resonances and cross-coupling between axes pointed above are apparent for this test.
2. In general the match was better in the range of the constant velocity of the response spectra (between 5 Hz and 0.5 Hz) where most of the energy of Kalamata earthquake is concentrated.
3. For frequencies above 5 Hz (0.2 sec) and frequencies below 0.5 Hz (2 sec) the achieved response spectra were above the respective targets with an amplification factor of about 2.0.
4. In what concerns the influence of the specimen in the match of the response spectra it must be said that the presence of the specimen promoted some differences between target and achieved. However, this fact can not be considered negative or positive in terms of the evaluation of control fidelity.
5. The peak values of Pitch, Roll and Yaw for the Kalamata tri-axial test without specimen are 0.43, 0.28 and 0.39 rad/s^2 , respectively.
6. The peak values of Pitch, Roll and Yaw for the Kalamata tri-axial test with model are 1.23, 0.52 and 0.39 rad/s^2 , respectively.

4.6 System performance analysis

Taking into account the test results shown in appendices III to VII, for which the principal observations were summarised in the last two sections, it is possible to analyse the main facts concerning the characteristics of the new LNEC shaking table.

The analysis of the results obtained during the tests and the six first natural frequencies obtained with the analytical model are presented in table 4.4. Those values clearly show that some corrections should be implemented in the analytical model in order to obtain better match of the six first natural frequencies of the system.

DOFs	Measured f_m (Hz)	Computed f_c (Hz)	Error ($f_c - f_m$)/ f_m
Transverse	13.5	10.3	-24%
Vertical	8.5	7.0	-18%
Longitudinal	11	12.1	10%
Pitch	18	27.6	51%
Roll	18	27.2	51%
Yaw	11	15.1	37%

Table 4.4 Measured and computed six first natural frequencies.

In particular, for the transverse and vertical directions, an increase on the rigidity of the bar elements used to simulate the actuators/oil columns while, for the longitudinal direction, that rigidity should be decreased. An increase on the rigidity of the transverse and vertical elements could be justified by a better performance of the inner-loop than assumed in the model. On the other hand, for the longitudinal direction, the different actuator (1000 kN) and servo-valve (three stages) could imply a decrease in that rigidity (worst performance of the inner-loop).

In what concerns the three natural modes of vibration with platform rotations predominance, it was found that either an higher stiffness of rotation restraining systems (torsion bars/cranks/connecting rods and swivels) or a lower rotational inertia mass were considered in the model when compared to the real situation. In fact, this justifies the higher frequencies obtained with the analytical model.

It was observed that the rotational resonances are all associated with relatively high damping values (>7% critical), compared to what might be expected for a steel structural system. It was also noted that higher damping occurred for the roll and pitch resonant frequencies than for the yaw component, indicating that these effects are likely to be related to the swivels at the end of the long rods. It is therefore assumed that a portion of the dead load of the platform imposes higher friction in the swivels for the yaw component than for the pitch and roll.

The influence of those resonance frequencies on the peak values of platform rotations can be estimated by a more detailed result analysis from Kalamata triaxial tests, with and without the influence of the overturning moments produced by the test specimen; rotational components of the platform centre can be used to assess the induced displacement differences at platform edges (roughly at $\pm 2.5 m$ from the centre). Naturally, pitch and roll are expressed as differences in vertical edged displacements, while the yaw is associated to the differences in horizontal motions at the same points.

Therefore, the rotations reported on points 5 and 6 in section 4.4.2, produce positives and negatives platform edge displacements shown in the first two rows of table 4.5. In the table, it is also presented the percentages of those values, related to the peak displacements of Kalamata earthquake in the respective direction (vertical, for pitch and roll and, longitudinal and transverse for yaw).

	PITCH	ROLL	YAW
Bare Platform	< 0.05 mm	0.5 mm	0.75 mm
Test Specimen	1.5 mm	1.0 mm	0.75 mm
Kalamata PGD	12 mm (V)	12 mm (V)	67 mm (L); 43 mm (T)
Bare Table - % of Kalamata PGD	< 0.4%	4%	1% (L); 2% (T)
Test Specimen-% of Kalamata PGD	13%	8%	1% (L); 2% (T)

Table 4.5 - Analysis of results in terms of the measured platform rotational components; triaxial tests, conducted for Kalamata earthquake with and without model (PGD = peak ground displacements)

From the analysis of the values presented on table 4.5 the following aspects deserve to be mentioned. It is evident that the peak rotations cannot be considered high. However, the relatively low frequencies for platform rotational resonances can decrease considerably when testing specimens with masses near the capacities of the platform. It should also be mentioned that the estimated overturning moments during Kalamata earthquake test, induced by the presence of the model, is below 140 kNm and therefore not considered too large.

By applying the control performance indicators developed in section 4.2.5 it is possible to quantify, in more general terms, the fidelity of the overall control system implemented at LNEC facility. Table 4.6 and 4.7 provides the values of correlation coefficient $\rho_{t,a}$ and normalised intensity spectral error $e_{t,a}$ respectively.

$\rho_{t,a}$	UNIAXIAL INPUT			TRIAXIAL INPUT
	<i>RWA Transverse</i>	<i>RWA Vertical</i>	<i>RWA Longitudinal</i>	<i>Kalamata</i>
Trans. without model	1.00	-	-	1.00
Vert. without model	-	0.83	-	0.96
Long. without model	-	-	0.92	0.98
Trans. with model	1.00	-	-	0.97
Vert. with model	-	0.76	-	0.90
Long. with model	-	-	0.94	0.98

Table 4.6 Summary of results on the correlation between target and achieved response spectra ordinates.

$e_{t,a}$	UNIAXIAL INPUT			TRIAXIAL INPUT
	<i>RWA Transverse</i>	<i>RWA Vertical</i>	<i>RWA Longitudinal</i>	<i>Kalamata</i>
Trans. without model	0.97	0	0	1.19
Vert. without model	0.01	0.98	0.04	1.43
Long. without model	0	0	0.77	0.96
Trans. with model	0.96	0	0	1.01
Vert. with model	0.01	0.99	0.03	1.21
Long. with model	0	0	0.79	0.87

Table 4.7 Summary of results on the normalised intensity error between target and achieved motions.

When considering uniaxial input to the platform, values in table 4.6 and 4.7 above show that a reasonable good match was observed for all the tests and for the three directions. In particular, an almost perfect platform reproduction of target motions in the transverse direction was achieved. For other two directions the match was not so perfect specially

in what concerns the frequency distribution of spectral ordinates of vertical signals and the intensity of longitudinal motions. Generally, cross coupling was considered to be low for these tests: the largest value of 4% of the input intensity was observed for bare platform in vertical direction while exciting the platform in the longitudinal direction.

From the triaxial Kalamata earthquake tests it is apparent that, although the perfect frequency description is maintained in all three translation axes, the intensities of the motions reproduced in the platform are generally higher than the respective targets. The largest intensity gain factor of 1.43 was observed for vertical motions. The presence of the test specimen had only a slight effect on the results as can be seen in both tables.

Globally, the outer loop control performance attained fairly good fidelity, at least for the frequency range of interest (0 - 20 Hz) and considering target and achieved platform displacements. This, in fact is shown by the good performance indices presented on tables 4.6 and 4.7 (values of around 1). However resonances in the range of 16 to 17 Hz, in vertical and longitudinal directions, could not be compensated by the outer loop control for the reasons presented in the following paragraphs.

The outer loop control procedures takes into account the displacements and accelerations of the actuator pistons and not the translation motions of the shaking table directly, since these transducers are positioned away from the platform. This control layout is a result of the non-squared characteristic of the algorithms and the predefined positioning of displacement measurements within the actuator pistons. This means that some differences could arise between different DOFs because there exists a mechanical system between them comprising a steel rod, a cylindrical wedge (to fasten the actuator pistons to the steel rods) and a swivel (attaching the rods to the platform).

The transfer functions between controlled accelerations (i.e. actuator pistons) and the three translation DOFs of the platform were analysed in order to inspect if flexibility of the rods/swivels/wedges system could justify those resonances. This confirmed that the differences between target and achieved platform motions are justified by that.

A relative low resonances frequencies (16 to 17 Hz), associated to high damping was also observed for transfer functions of those elements. That can be justified by the presence of the swivels and/or the cylindrical wedges. Again, in vertical direction, a compression stress state on those elements, due to dead load, could justify a lower damping value than for the other directions.

The measured cross coupling between translation DOFs, for adapted and non adapted tests, is not considered high. Typically, in terms of displacements components, for an excitation in a given direction, the output translation intensities observed in the other directions are below 4% of the input. However, considering acceleration components for the same motions, intensities of cross coupling between axes is increased a lot. In fact, response spectra and FRFs of achieved motions clearly show that the resonances of rods/swivels/wedges systems, already mentioned, constitute also the main source of cross coupling between axes.

5.0 CONCLUSIONS

5.1 Generalities

One of the principal aims of this project was to produce a detailed characterisation of the frequency response for the new LNEC shaking table and to assess its control fidelity, as part of an on-going European research programme. This would then act as a benchmark against which the performance of future tests at this facility could be gauged.

Apart from the description of the procedures and results of the tests which have been carried out, in its first part this report compiles a lot of descriptive material about the entire facility. More precisely, it can be found information regarding:

- Main characteristics of the building where the shaking table was constructed.
- Structural description of shaking table and its analytic modal analysis.
- Control laboratory (CTL Lab., from where the shaking table is driven) and observation laboratory (OBS Lab. from where the behaviour of models are observed), as well as report of the existing equipment, computer algorithms and main procedures used in both Labs.
- Characteristics of the equipment used to drive the table; actuators and power supply unit, and references to the safety operation measures.
- Experimental modal analysis of bare shaking table carried out with the dynamic characterisation tests.
- Assessment of the accuracy of computer control codes and procedures performed with control fidelity tests.

Due to current state of development of LNEC facility it was necessary to include a description of its specific characteristics; it must be referred that the entire facility was thoroughly explored for the first time, including all equipment used in CTL and OBS Labs.. It was necessary to orient the original test programme to cope with a in depth modal identification of the shaking table.

In what concerns the characteristics of the building it is evident that the entire facility was planed in all details to assure an adequate laboratory environment where experiments of full scale reinforced concrete and masonry structures are deemed to reach damage states near collapse.

For instance, during the tests herein reported, the clear physical separation between two different laboratories to conduct the experiments has revealed as a perfect option. Although the same type of equipment (i.e. transducers, data acquisition systems and computers) are used during a test, the distinct purpose of driving the platform and observe the behaviour of a tested specimen, requires complete different pre- and post-data processing. In fact, tests to be performed in non-linear range are generally carried out in several stages; a lot of data should be analysed at the end of each stage in order to proceed to the next stage.

In what concerns the security measures two distinct situations deserve mention. In relation to the protection against damage of equipment and safety of personal due to an hazardous operation of the shaking table sufficient features where foreseen and are

already effective. However, some minor aspects, also considered in the design, related to the full security of visiting public near the platform and personal working on the facility are not yet implemented.

5.2 General of dynamic characteristics of the shaking table

The new LNEC shaking table was designed to accomplish a main requirement: full scale earthquake test of reinforced concrete and masonry structures near collapse. That purpose poses the problem of controlling platform motions where heavy test specimens are changing constantly the dynamic characteristics due to non-linear hysteretic behaviour; any prior dynamic characterisation of the entire system (shaking table and model) in order to control the platform motions could be useless on those circumstances. Of course, that will depend mainly on the extent of the non-linear hysteretic behaviour and on relation between induced reaction forces of test specimen on the platform and the limit capacities of the driving actuators.

To minimise that issue two design options were assumed: reduction of the three platform rotations by passive control and, reduce the coupling of the three actuators motions. Ideally, the concept was to build a platform with only three translation degrees of freedom driven by three complete independent motions. This could allow future straightforward implementation of real time control algorithms. Naturally, it was not possible to construct such an ideal system; it is not feasible to construct infinite rigid torsion restraining systems or infinite long rigid arms (to impose the three independent translation motions to the platform) that could even nullify the need for geometric compensations.

Consequently the design options were materialised by constructing a special rigid torsion guiding systems (passive control of platform rotations) and rod systems, connecting the actuators to the platform (decoupling of actuators translation movements). However, those systems includes a lot of bearings and swivels whose dynamic behaviour are difficult to predict by analytic modelling. Moreover problems related to constructive misalignments due to the large proportions of the platform and guiding systems could jeopardise the initial goal.

It was therefore meaningful to conduct an experimental modal analysis to characterise the dynamic behaviour of the new LNEC shaking table. In particular, the identification of the three natural frequencies, with modal components predominance in the direction of platform rotations was important; those resonances cannot be compensated by the outer loop control procedures.

From those tests it was possible to conclude the following main points:

1. Natural frequencies of the shaking table, with predominant translation modal components along the transverse, vertical and longitudinal axis of the platform are 13.5 Hz, 8.5 Hz and 11 Hz respectively. Values found for transverse and vertical directions are denoting a better inner loop performance than expected. On the contrary, for longitudinal direction the three stage servo-valve and large capacity actuator, imposing the longitudinal motions to the platform, was pointed as the possible reason for obtaining an experimental frequency resonance value smaller than the one given by the analytical model.

2. Natural frequencies of the shaking table with predominant rotation modal components along the transverse - pitch -, vertical - yaw - and longitudinal - roll - axes of the platform are 18 Hz, 11 Hz and 18 Hz respectively. These platform rotational resonancies are exhibiting amplification factors in pitch and roll of $6 \text{ rad/s}^2/g$ and $7 \text{ rad/s}^2/g$ for yaw. Those gains are associated to motions imposed in transverse, longitudinal and transverse directions respectively, denoting relatively high damping values (above 7% critical damping).

Although values of peak rotations, for the specific tests presented in this report, were not considered high, the importance of those rotations components should be also appreciated in the individual context of tests foreseen for the shaking table. It is worth mentioning that, for heavier and higher test specimens, the resonance frequencies above reported may decrease to values within the frequency band of input earthquake motions and natural frequencies of the model.

Moreover, analytical values of natural frequencies of modes associated with platform rotations, were about 50% greater than the above reported experimental values. A possible reason for those discrepancies could be a flexibility, higher than expected, of swivels and/or cranks which, together with the torsion bars, are the main components of rotational restraining systems. Consequently, further tests are deemed important, with the specific purpose of checking those systems flexibility.

5.3 Overall performance of adaptive control system

As said, the other purpose of this report was to verify the capacity of new LNEC shaking table to reproduce predefined target motions on the platform; that was the purpose of control fidelity assessment experiments.

Although the new LNEC facility has an inner and outer loop control feedback systems, working together for adapting the three translation driving signals in an attempt to minimise the differences between target and achieved motions, the objective of the tests presented in this report were concerned with the capacity of the outer control algorithms and procedures to compensate all resonances appearing in the system in the three translation degrees of freedom of the platform, with or without test specimen.

Therefore an unique adaptation of the inner loop control was carried out by adjusting the PIDs values for each axis, prior to all tests. Afterwards, for each test the iterative operational procedure with the outer loop control computer algorithms were carried out taking into account actuator pistons acceleration and displacements components of motion. Finally, when it was considered that it was not possible to achieve a better control, the acquisition of platform motions was performed by the OBS Lab.. For that it was used different transducers and equipment. In the report it was briefly described the procedures used during the adaptive operation by the CTL Lab. carried out with the outer loop control computer algorithms as well as the equipment layout and sensitivity used by the OBS Lab..

Two types of tests were performed with two different target motions for bare platform. The first type comprises, three series of ten tests performed in each direction individually considering ten time histories of target motions (accelerations and displacements) with constant acceleration spectral distribution between 0.5 Hz and 20 Hz (randomly uniform phase distribution) and characterised by the same peak

velocity of 10 *cm/s*. The second type of test was carried out with an earthquake like triaxial target signal (Kalamata strong motion record sample) with energy concentrated below 4 *Hz*. All those tests were then repeated with a test specimen attached to the platform. That specimen weighed 8.5 *ton* and exhibited first natural frequencies of 5.76 *Hz* in transverse and 7.13 *Hz* in longitudinal directions.

It was also developed two types of control accuracy measures to assess the control fidelity. The first quantifies the fidelity of control procedures in terms of the relative frequency descriptions of target and achieved signals, independently of some bias intensity affecting achieved platform motions. The second one is more appropriate to detect if there is differences on intensities of the two motions. Basically, the last one is the relation between the first moment of power spectral densities functions of achieved displacements and target displacements, while the first one implicitly reproduces the relations of the second moments of those spectral descriptions.

From the tests and the analysis of the results obtained for the fidelity indices it was possible to conclude:

1. Globally, the outer loop control performance attained fairly good fidelity, at least for the frequency range of interest (0 - 20 *Hz*) and considering target and achieved platform displacements. This, in fact was evidenced by the good performance indices achieved. However resonances in the range of 16 to 17 *Hz*, in vertical and longitudinal directions, could not be compensated by the outer loop control, inducing not so good performance when target and achieved platform accelerations are confronted.
2. The cross coupling between axis is relatively low with a larger intensity value of transmissibility 4% appearing in the non controlled vertical direction with a longitudinal controlled excitation (uniaxial tests). As before, the frequency contents of those cross motions are in the range of 16 to 17 *Hz*.
3. The presence of the transfer functions between controlled motions (i.e. actuator pistons) formed by the rods/swivels/wedges systems and the three translation degrees of freedom of the platform motions justifies those resonances frequencies mentioned above.
4. As expected the control procedures did not change the transfer functions between each of the translation degree of freedom and the three rotations of the platform already presented. However the influence of those rotational resonances (pitch and roll) on the platform vertical edge differential displacements were appreciated by analysing the experimental results obtained with an earthquake like triaxial signal input (Kalamata strong motion record sample). This analysis were carried out for bare shaking table and for platform with a test specimen. For bare platform it was concluded that those values correspond to less than 4% the vertical maximum displacement of peak vertical component of Kalamata earthquake whereas, for platform with test specimen, inducing pitch and roll peak moments on platform of about 140 *kNm*, those relations increased to a maximum of 13% due to pitch.

From information presented in this report it is anticipated that a substantial increase on the fidelity of control system could be attained if the outer loop algorithm operates with degrees of freedom associated with platform translation motions. In doing so, the

control procedures could adapt the driving signals in order to compensate those mechanical resonances; better translation achieved signals and a reduction of the cross coupling are anticipated.

That can be implemented by moving the control transducers (accelerations and displacements), attached at the moment on actuators pistons, to the platform centre. However, if for the absolute acceleration components this solution doesn't create any difficulty, measurements of absolute displacements at that point are not so easy perform due to the lack of a fixed reference. A simpler solution could be implemented by moving only the control acceleration transducers to platform points close to the swivels on the extreme of the rods. That will oblige to a prior off line compensation of the target acceleration motions which couldn't be straightforward; that compensation implies an identification of the transmissibility frequencies for each specific load situation of the platform.

Finally it must be referred that tests, already foreseen, with payloads up to the limit capacity of the platform (400 kN) should be carried out not only to check the importance of some of the conclusions presented in this report but also to provide the necessary information for the design of an accumulator oil bank that will allow to reproduce strong motion earthquake signals with larger intensities.

Acknowledgements

The authors would like to take this opportunity to thank the European Commission for funding the project ECOEST.

We extend our gratitude to Dr F. Carvalhal, Dr T. Emilio and Dr A. Garrett from CPCE, who were always available throughout the development programme. Completion of the work carried out would not have been possible without their contributions.

Many thanks to the technician personnel from C3ES and CPCE, in particular to Senior Experimental Technician Fernando Coelho, for his vital role during the tests.

We also thank our colleagues in C3ES for their contributions, in particular Dr R. Bairrão and Civ. Eng. B. Lobo. And finally, thanks to A.Crewe (Ceng), from Bristol University, for his help during the tests.

Lisbon, National Laboratory for Civil Engineering, March 1996

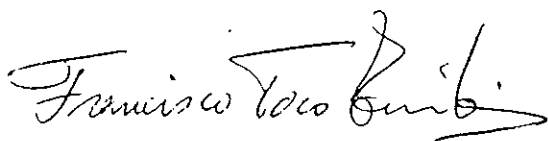
VISAS

C3ES

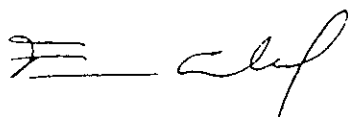


E. Cansado Carvalho
Principal Research Officer
C3ES Head

CPCE

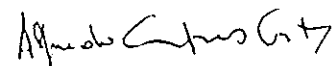


Francisco Toco Emilio
Principal Research Officer
GEM/CPCE Head



Francisco J. Carvalho
Principal Research Officer
CPCE Head

AUTHORS



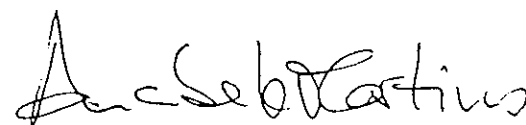
Alfredo Campos Costa
Research Officer



Paulo Jorge Gil de Morais
Assistant Research Officer



Barnaby Denys Wainwright
Bristol University,
Visiting Assistant Research Officer



Anabela Martins
Experimental Technician

REFERENCES

1. Commission of the European Communities. *Large Installations Plan (1989-1992) - Final Report of the Study Panel on Earthquake Engineering*. December 1990
2. Crewe, A.J.; Taylor, C.A., 1994, *Athens/Bristol Shaking table Assessment Project - Final technical report*, Earthquake Engineering Research Centre (EERC), University of Bristol, Bristol, UK.
3. Emilio, F.T.; Duarte, R.T.; Carvalhal F.J.; Oliveira-Costa, C.; Vaz, C.T.; Ritto Corrêa, M., 1989, *The new LNEC shaking table for earthquake resistance testing*, Memories N.º 757, LNEC, Lisbon, ISSN 0369-1179.
4. Vieira Pinto, A.; Gil Saraiva, J.A.; Duarte, R.T., 1987, *Seismic Tests on Physical Models*, 9th International Conference on Structural Mechanics in Reactor Technology, Lausanne, Aug. 1987.
5. Bendat, J.S.; Piersol A.G.; 1976, *Random data: analysis and measurement procedures*, Wiley Interscience, ISBN 0-471-06470-X, USA.
6. Carvalhal, F.J.; Costa, C. O.; Schiappa de Azevedo, F.; 1992, *Elementos de Sistemas e de Análise e Processamento de Sinais*, Curso LNEC, Lisboa.
7. Brüel & Kjaer, 1987, *Frequency analysis: 3rd Ed.* ISBN 87 87355 07 8. Denmark
8. INSTRON, 1994, *RSPlus V2.95 user manual - Test rig control software*, Catalogue No. 2490-790
9. INSTRON, *SPiDAR v2.1c user manual*,

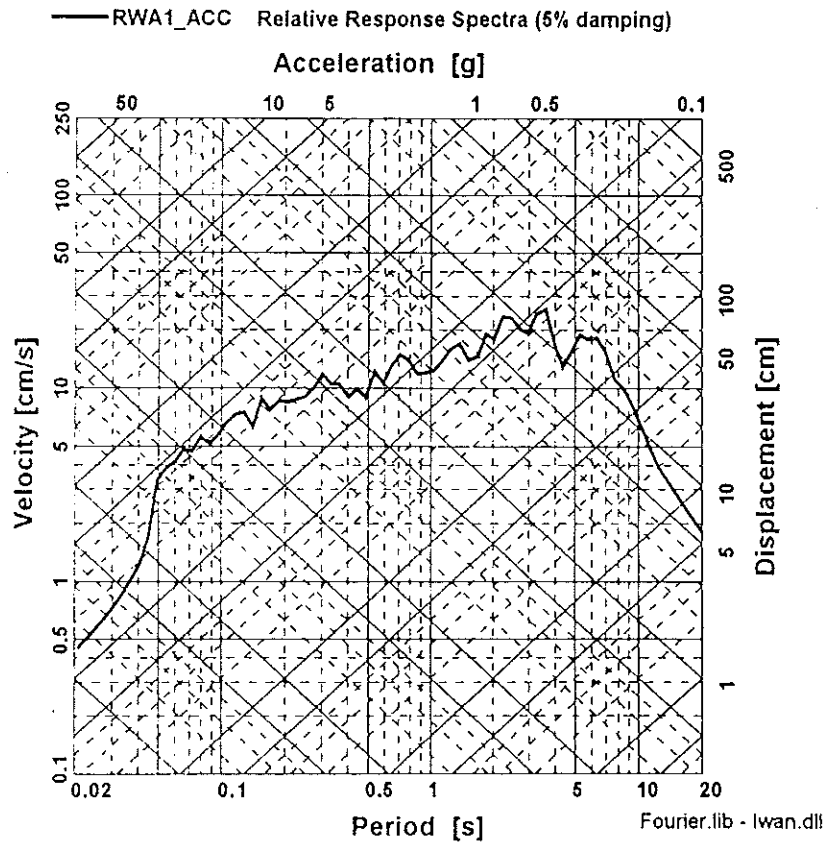
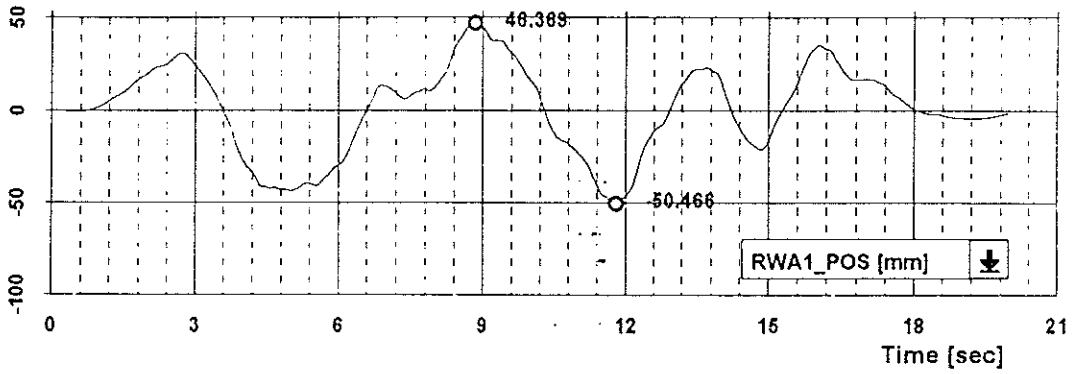
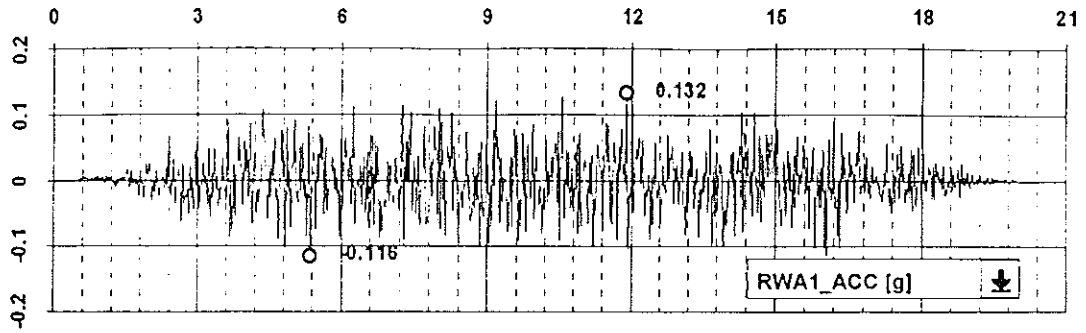
APPENDIX I

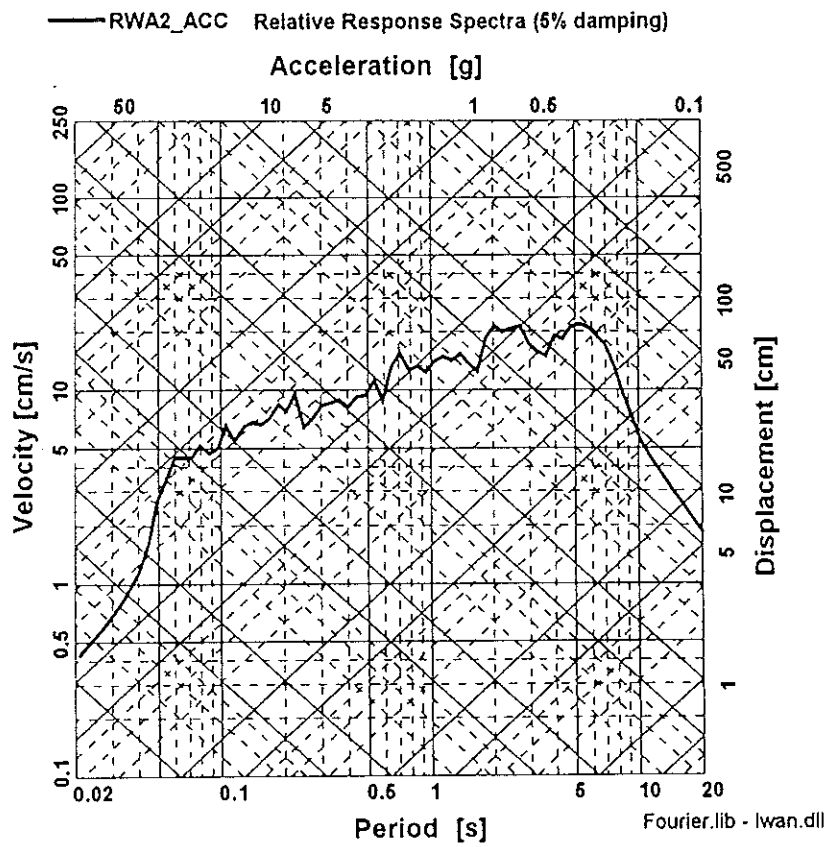
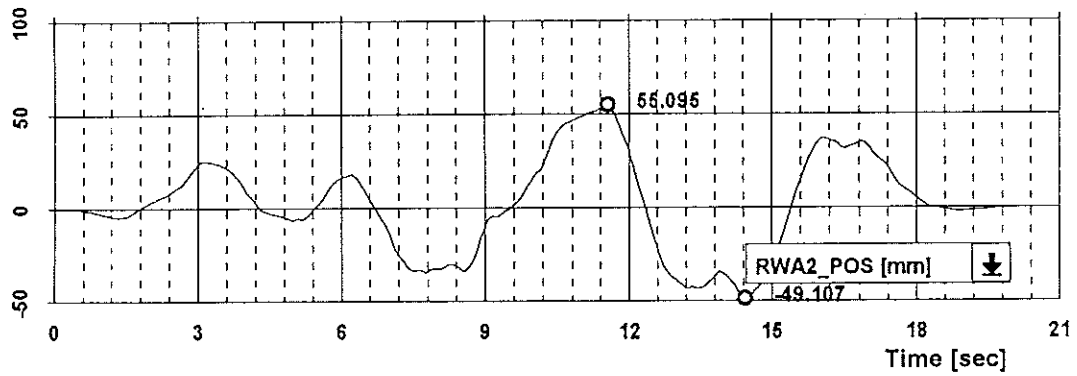
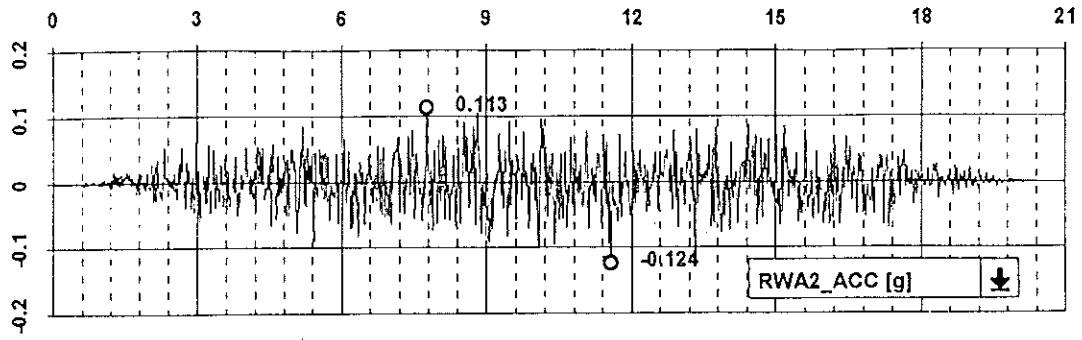
TARGET TIME SERIES

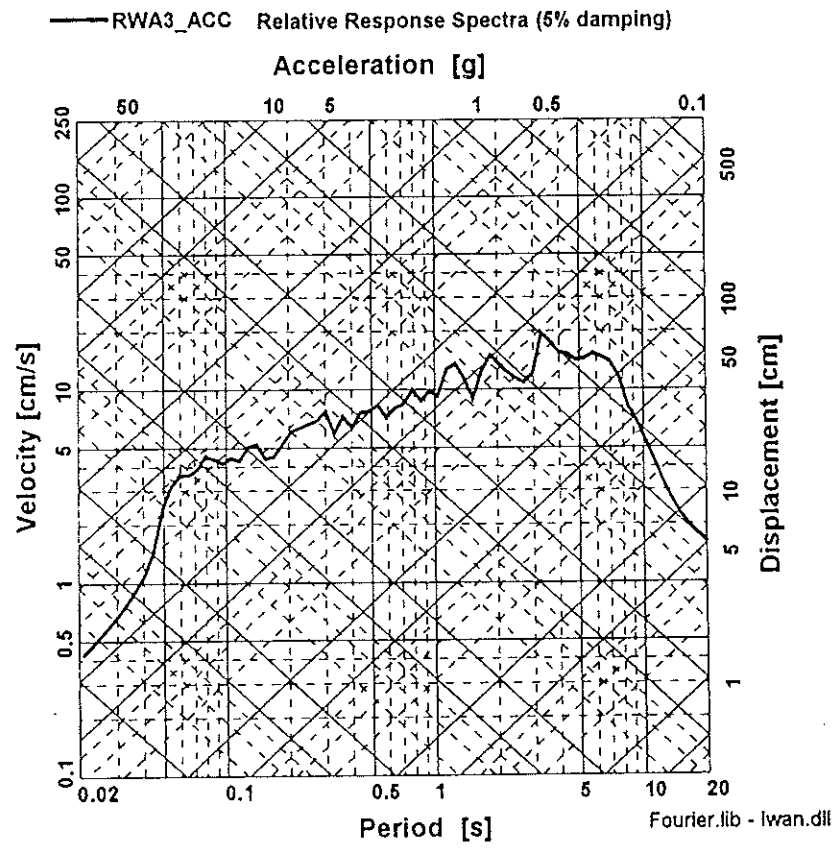
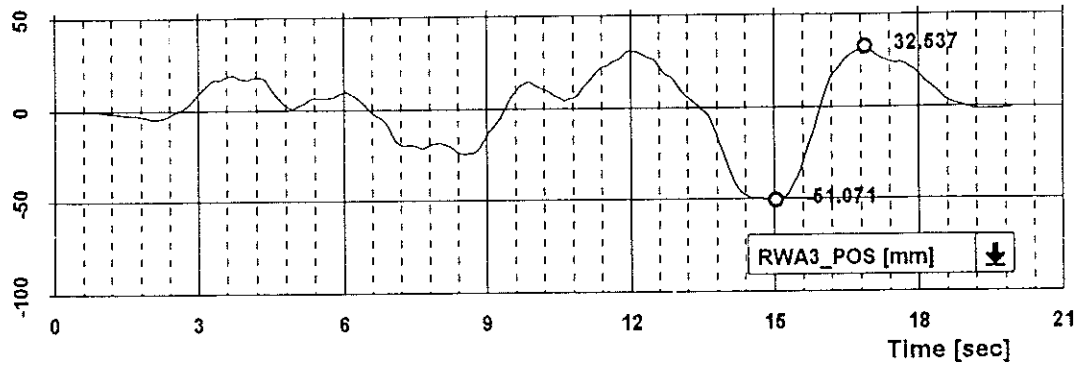
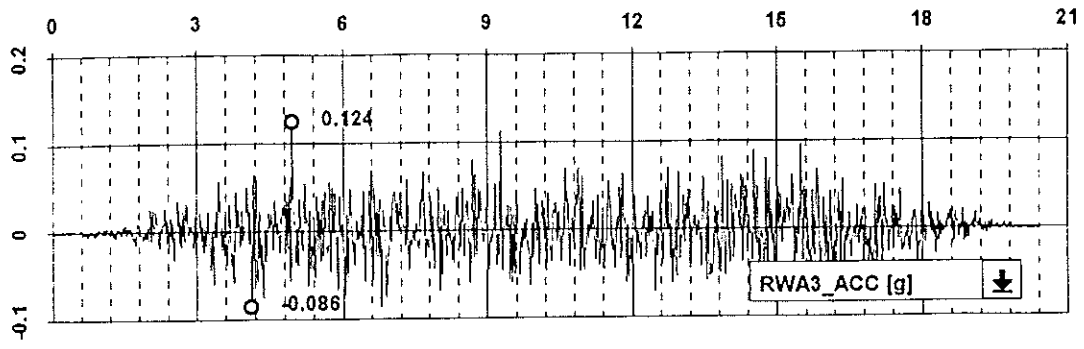
RANDOM WHITE NOISE AND
KALAMATA EARTHQUAKE

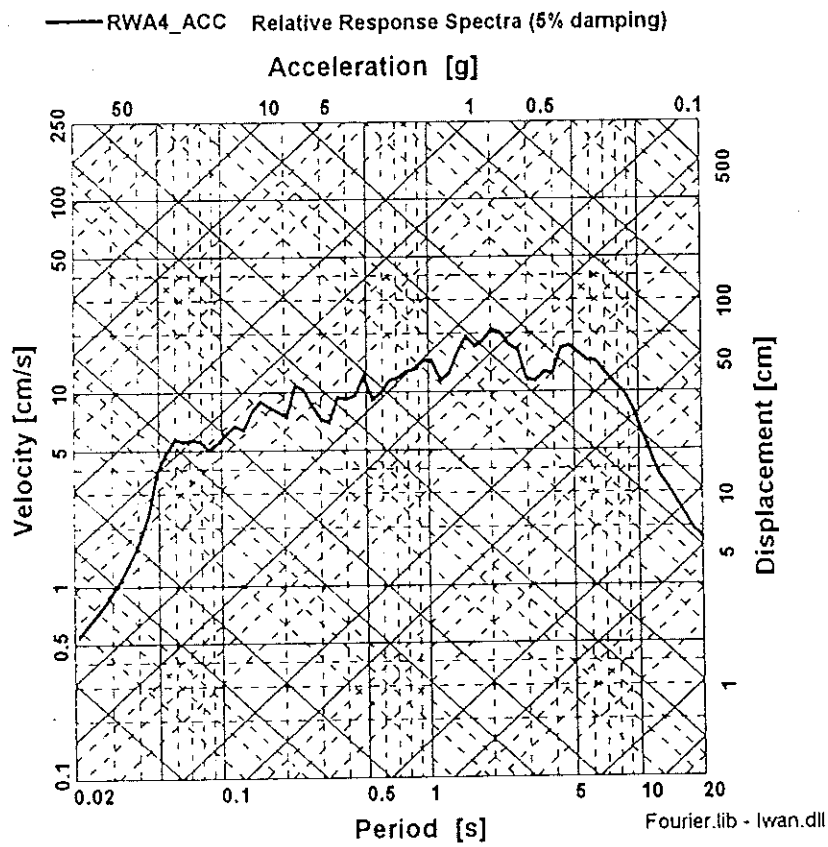
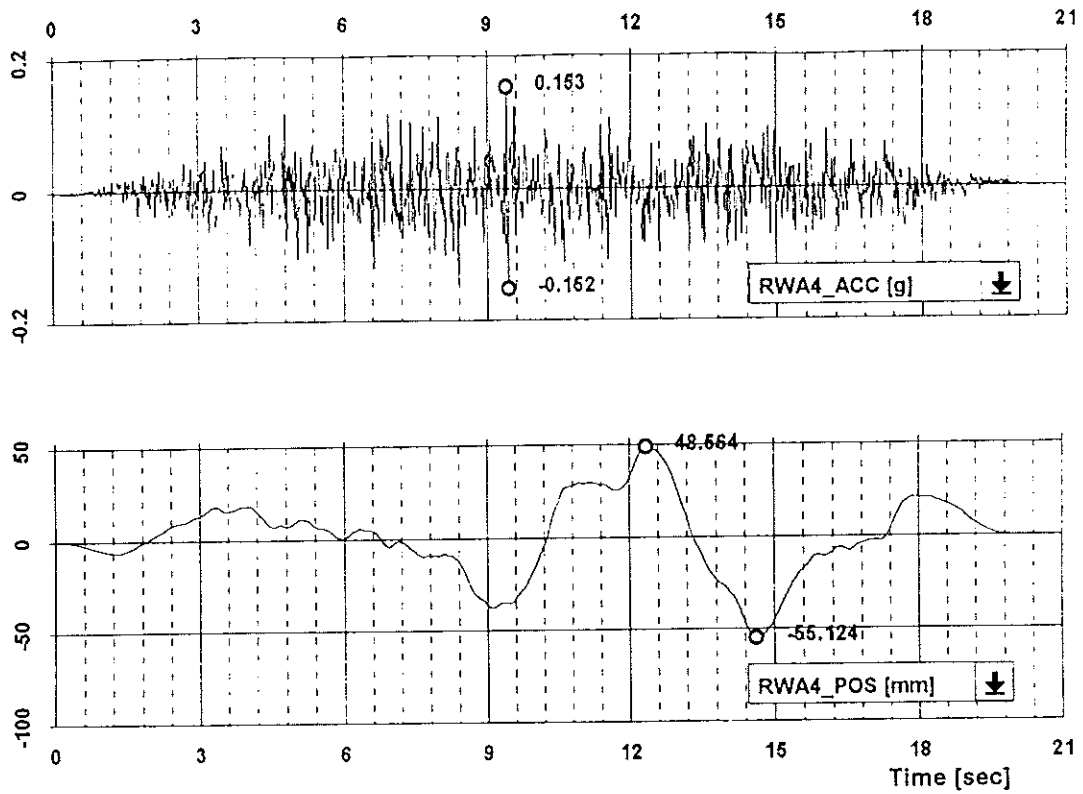
List of Figures

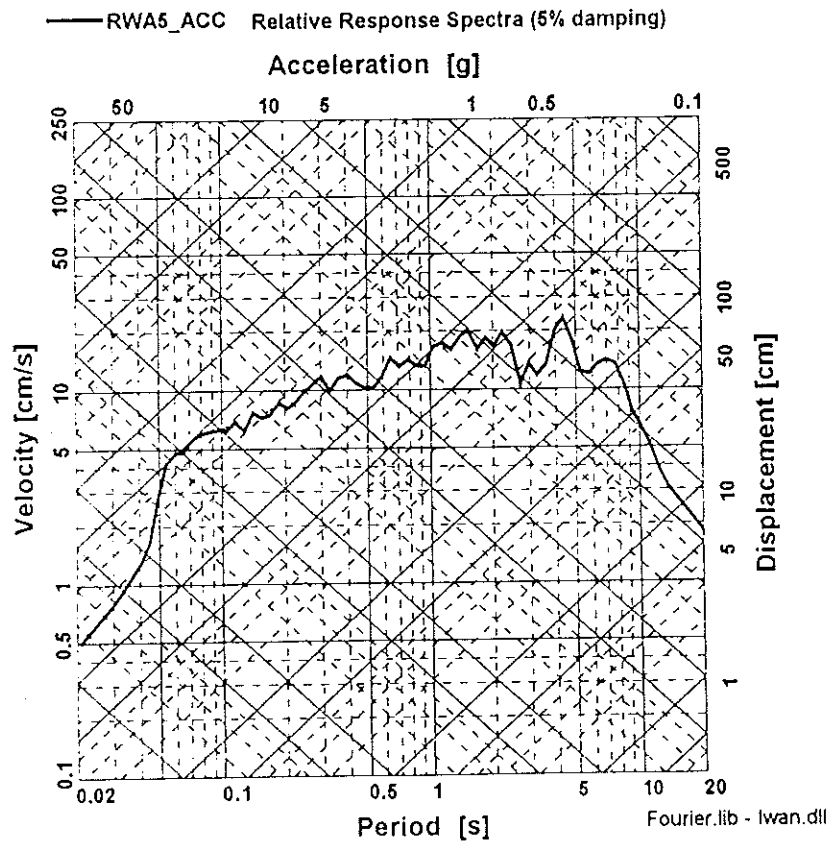
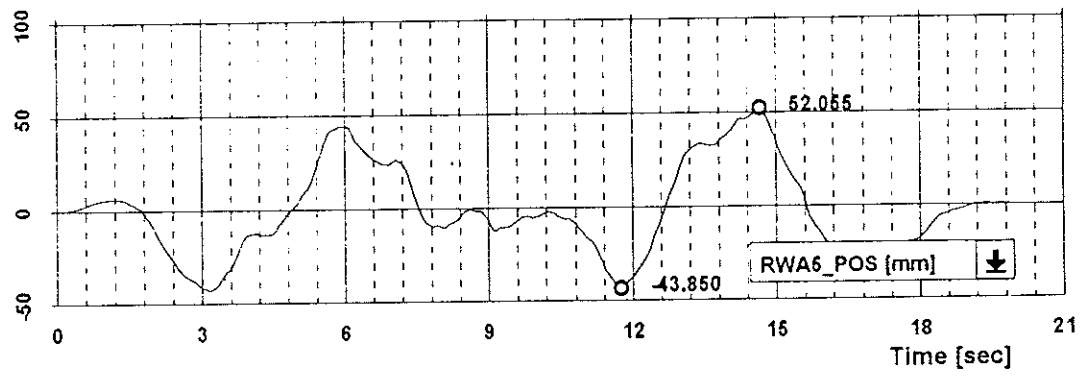
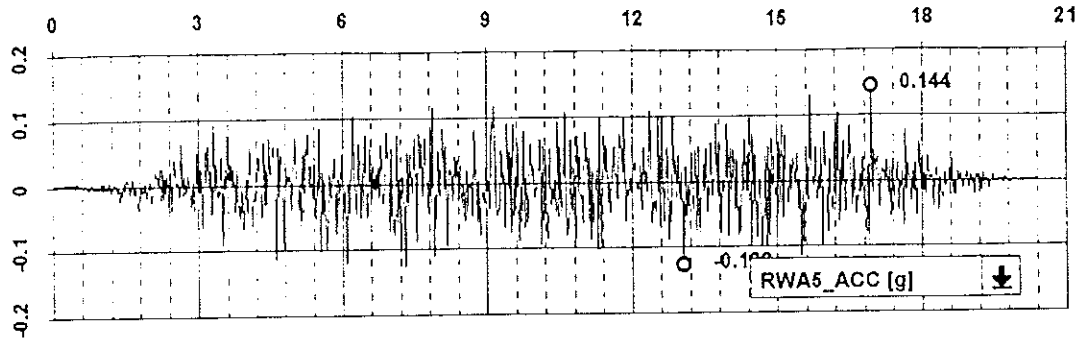
- AI.1 - Random white noise: 01 time serie acceleration, displacement and relative displacement response spectra
- AI.2 - Random white noise: 02 time serie acceleration, displacement and relative displacement response spectra
- AI.3 - Random white noise: 03 time serie acceleration, displacement and relative displacement response spectra
- AI.4 - Random white noise: 04 time serie acceleration, displacement and relative displacement response spectra
- AI.5 - Random white noise: 05 time serie acceleration, displacement and relative displacement response spectra
- AI.6 - Random white noise: 06 time serie acceleration, displacement and relative displacement response spectra
- AI.7 - Random white noise: 07 time serie acceleration, displacement and relative displacement response spectra
- AI.8 - Random white noise: 08 time serie acceleration, displacement and relative displacement response spectra
- AI.9 - Random white noise: 09 time serie acceleration, displacement and relative displacement response spectra
- AI.10 - Random white noise: 10 time serie acceleration, displacement and relative displacement response spectra
- AI.11 - Kalamata earthquake: time serie acceleration, displacement and relative displacement response spectra for the longitudinal direction
- AI.12 - Kalamata earthquake: time serie acceleration, displacement and relative displacement response spectra for the transversal direction
- AI.13 - Kalamata earthquake: time serie acceleration, displacement and relative displacement response spectra for the vertical direction

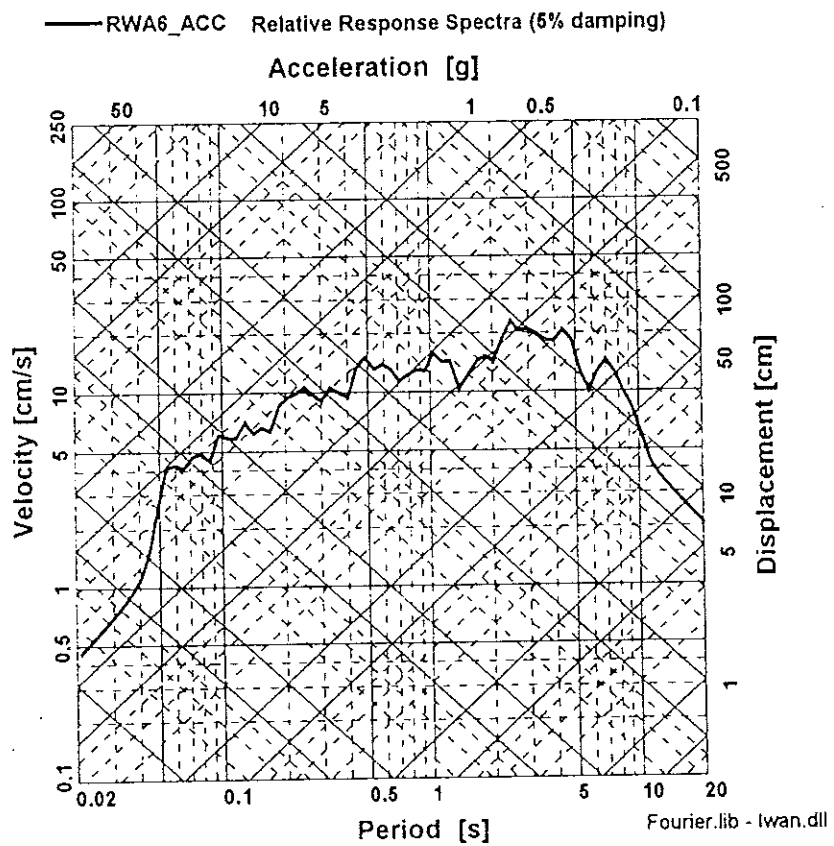
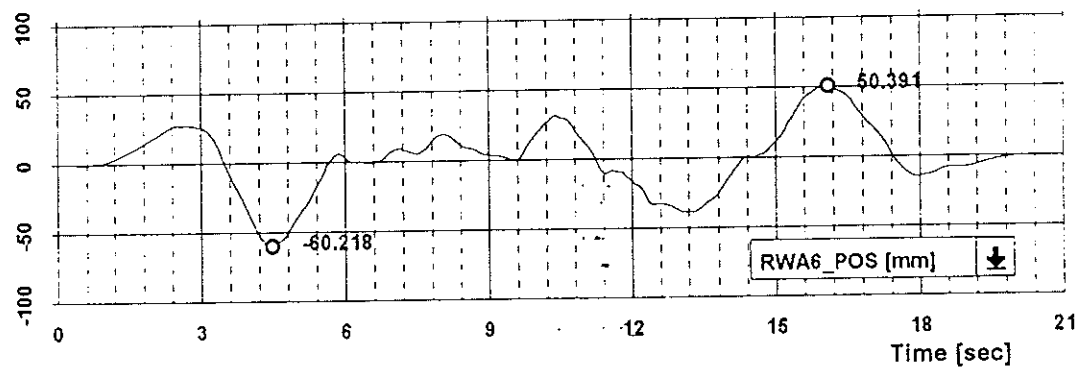
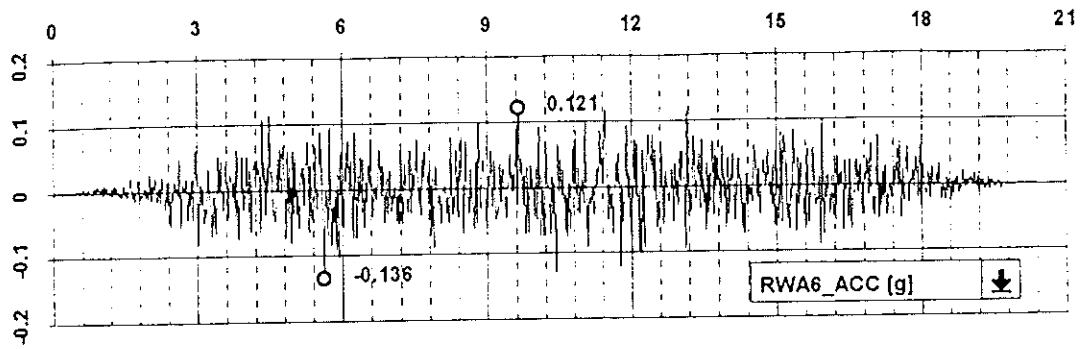


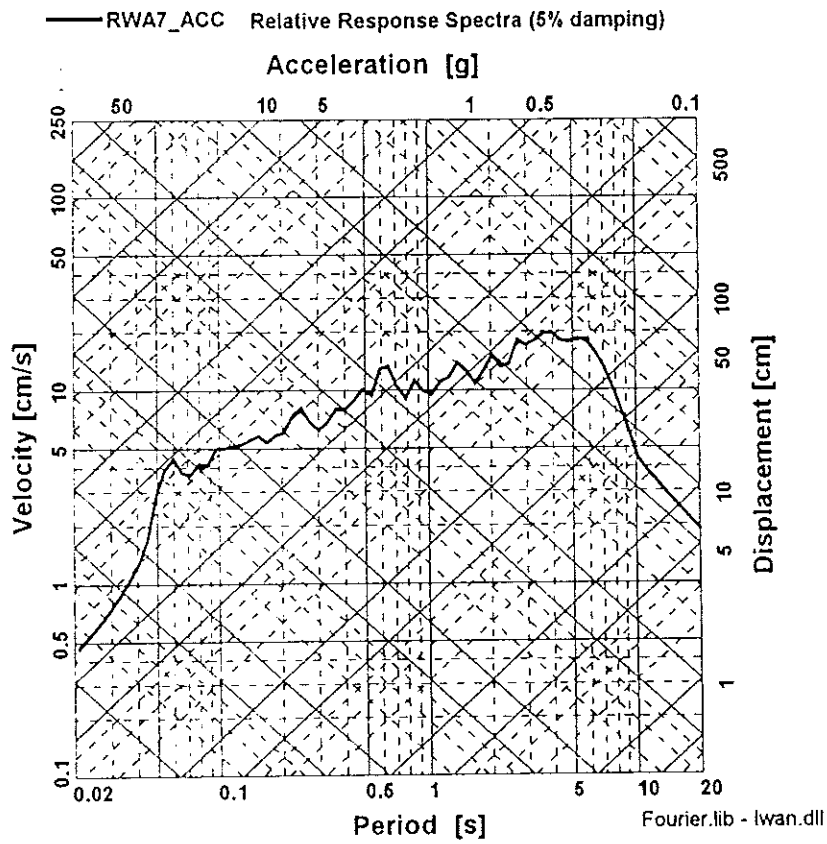
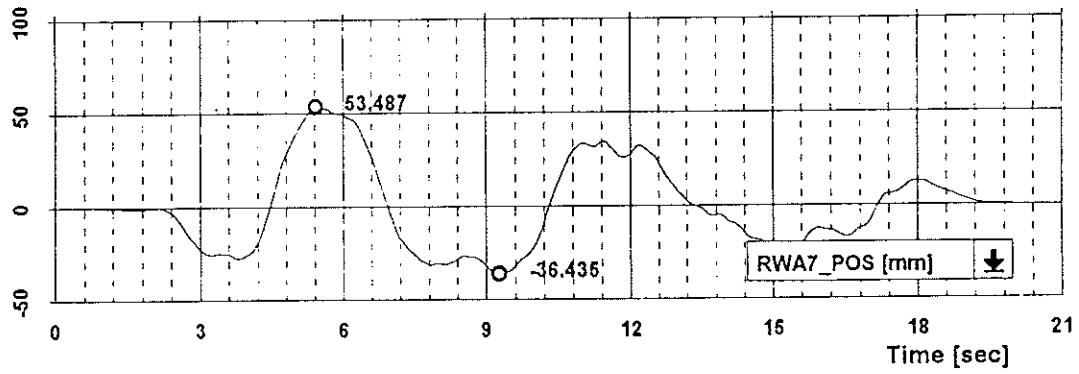
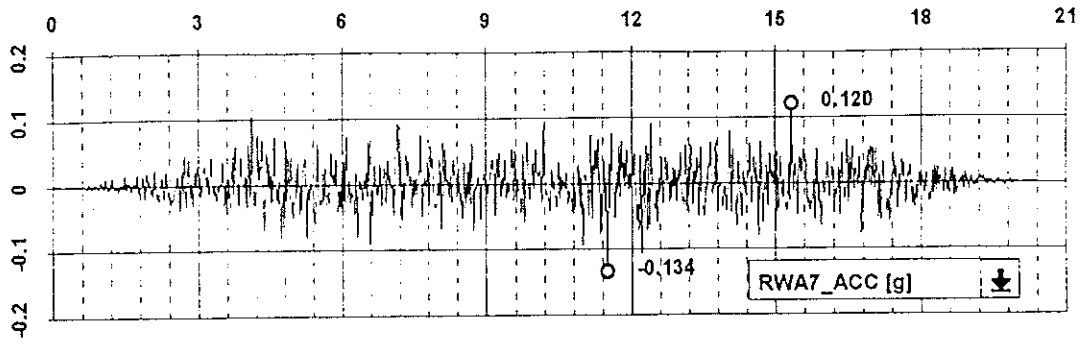


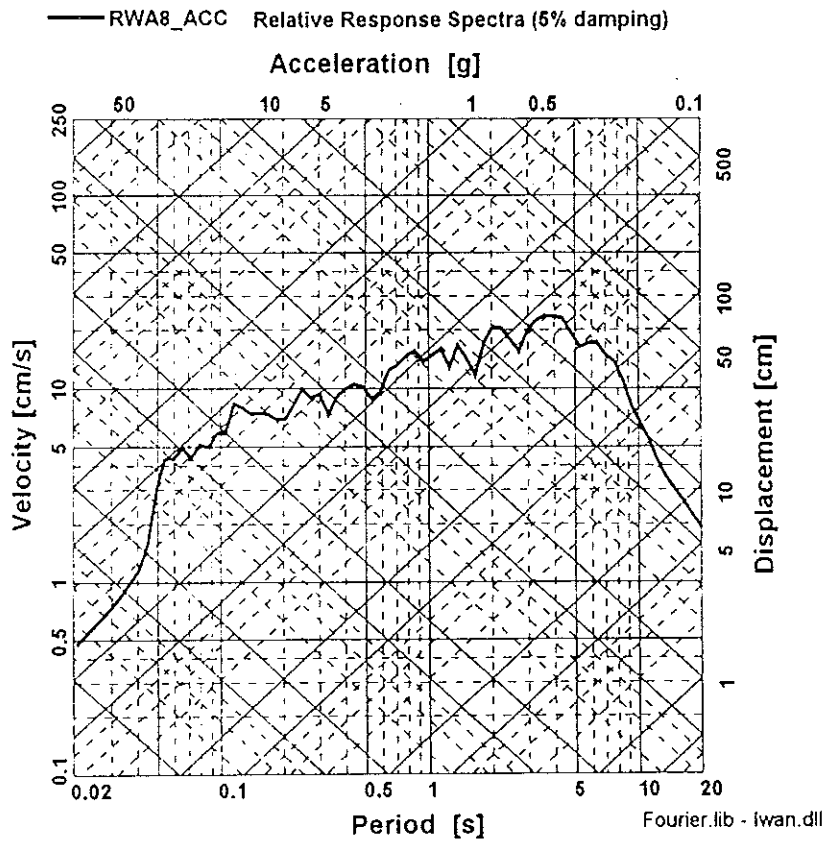
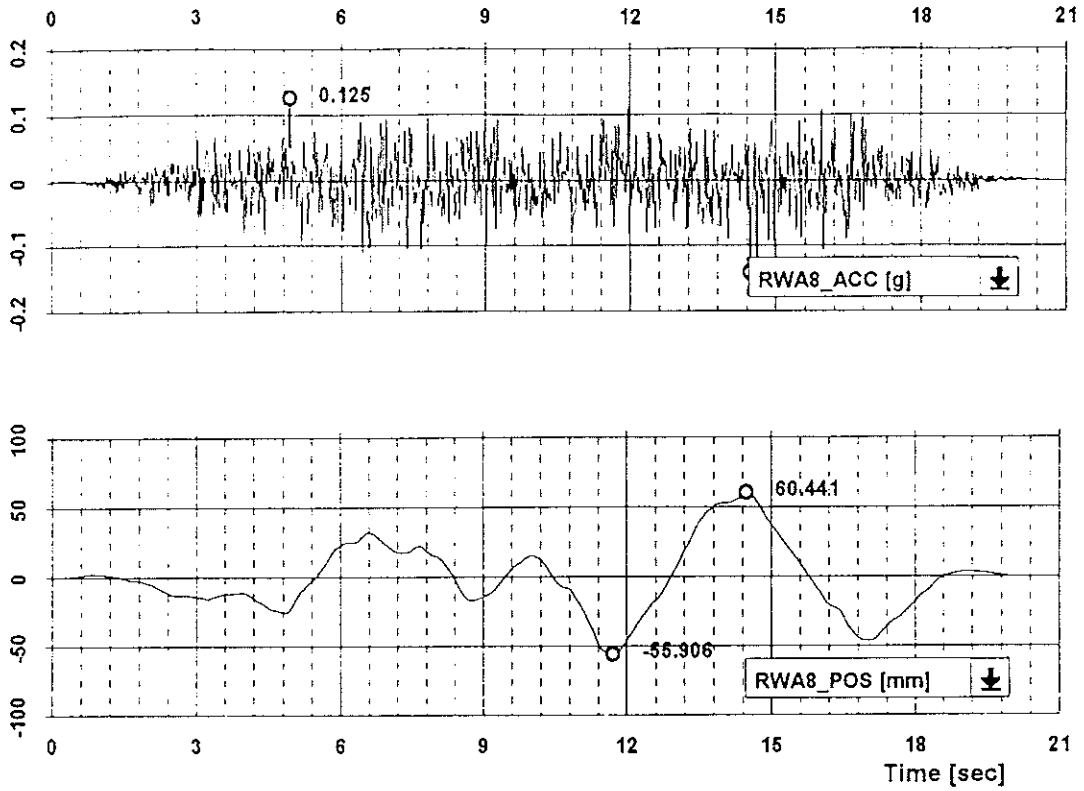


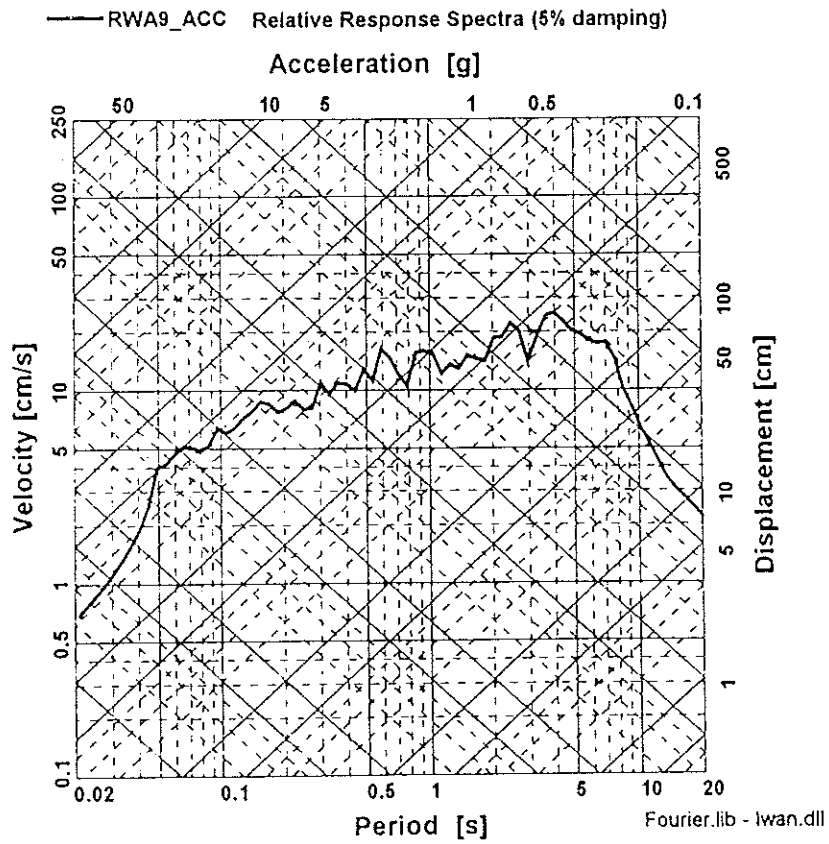
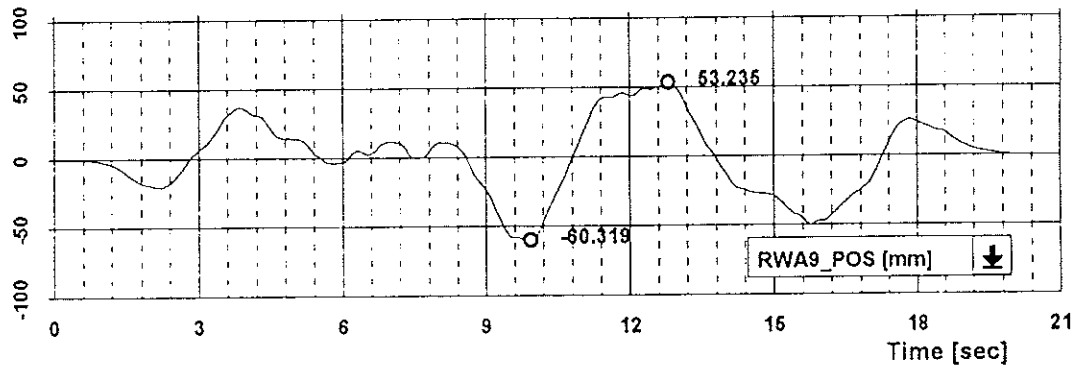
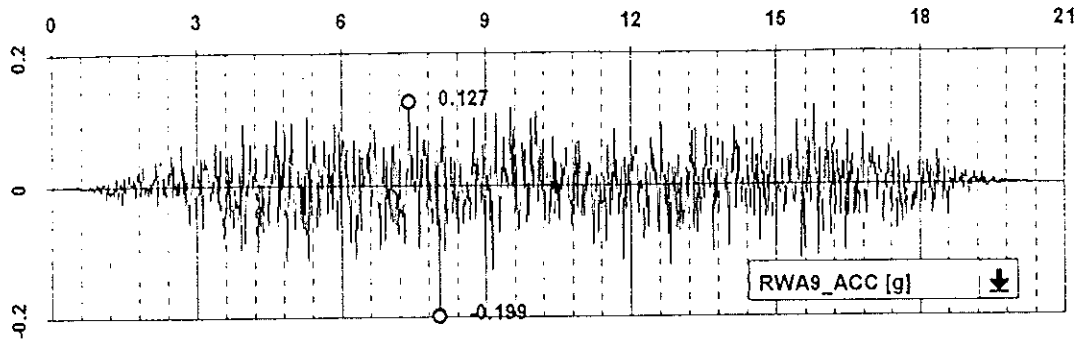


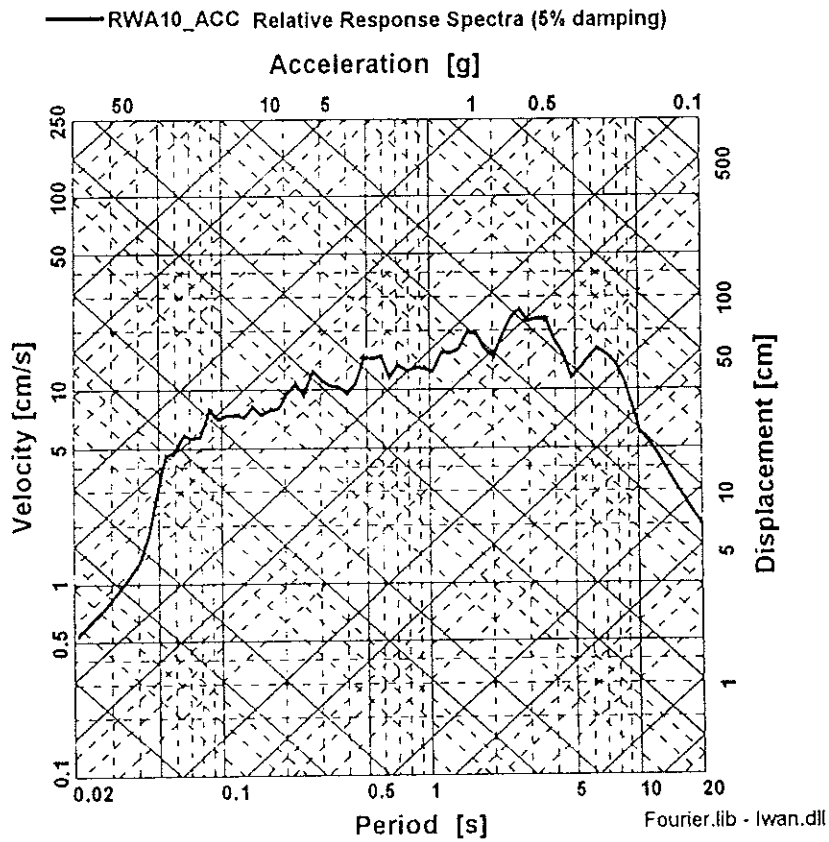
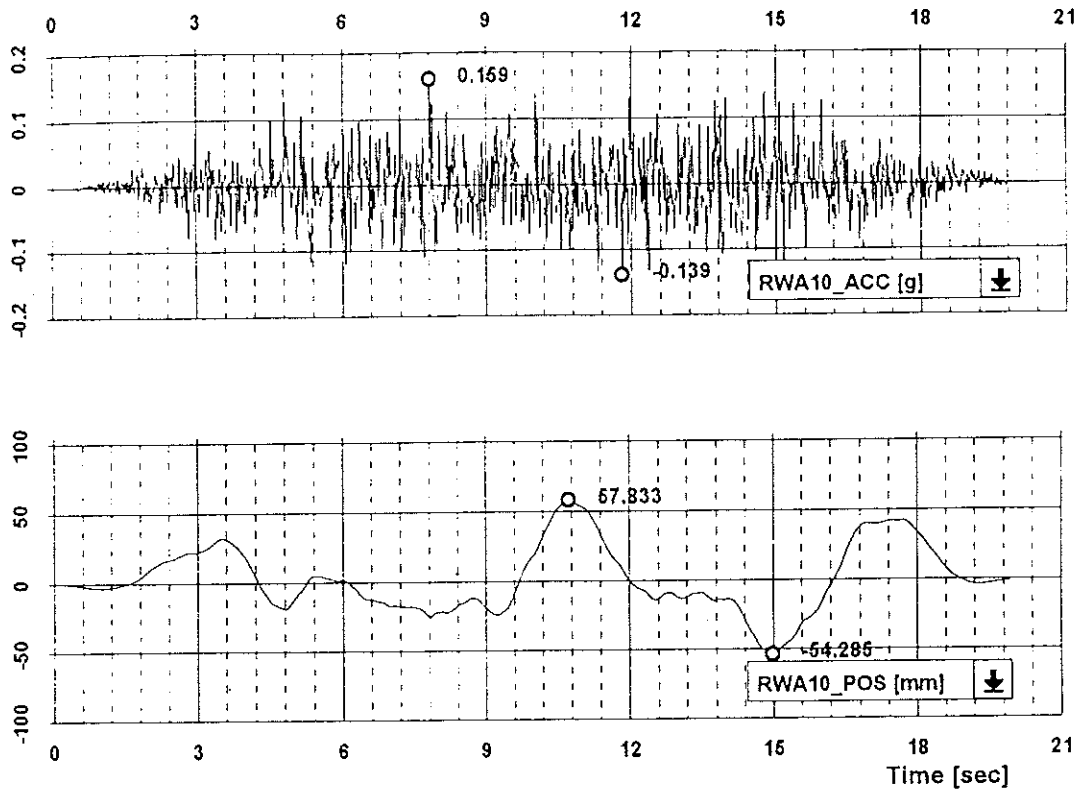


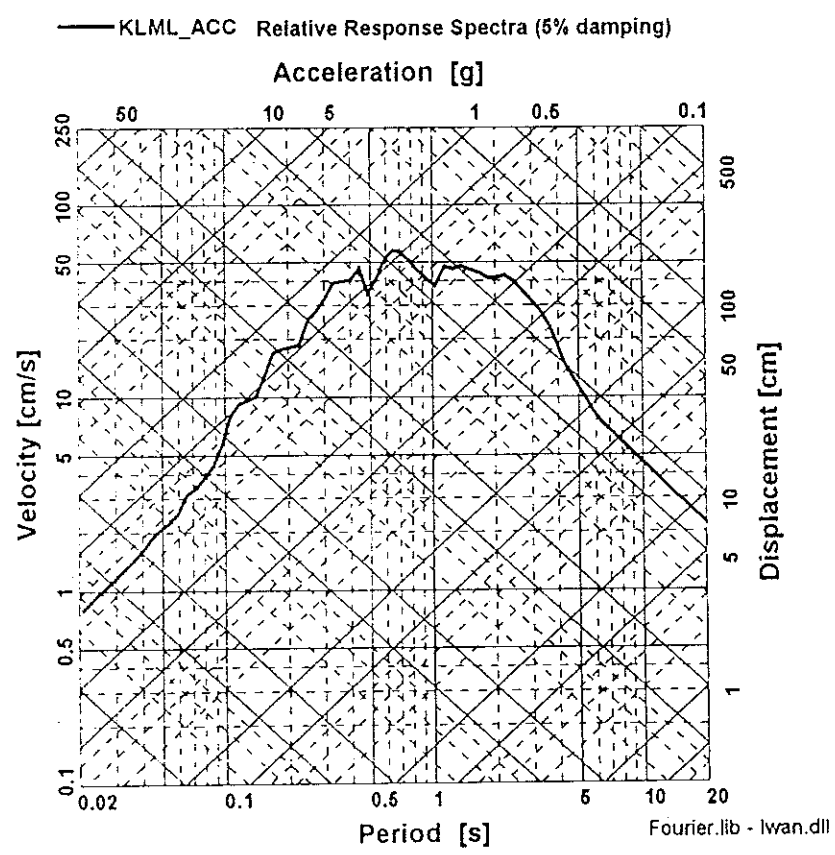
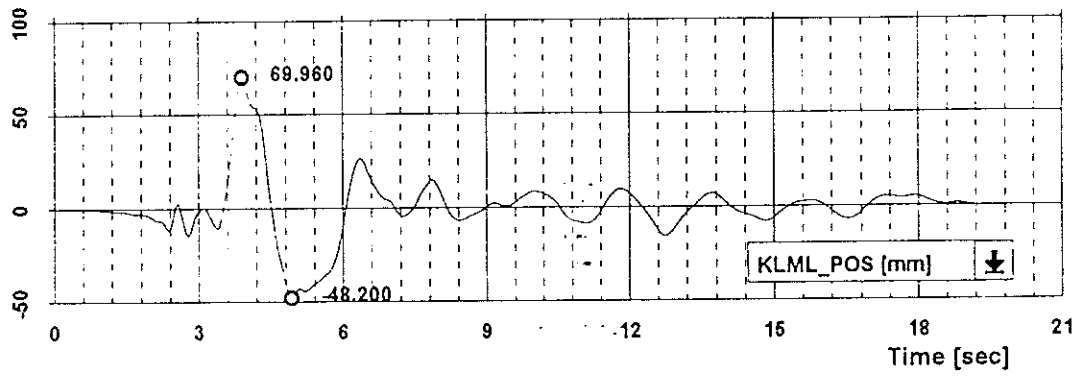
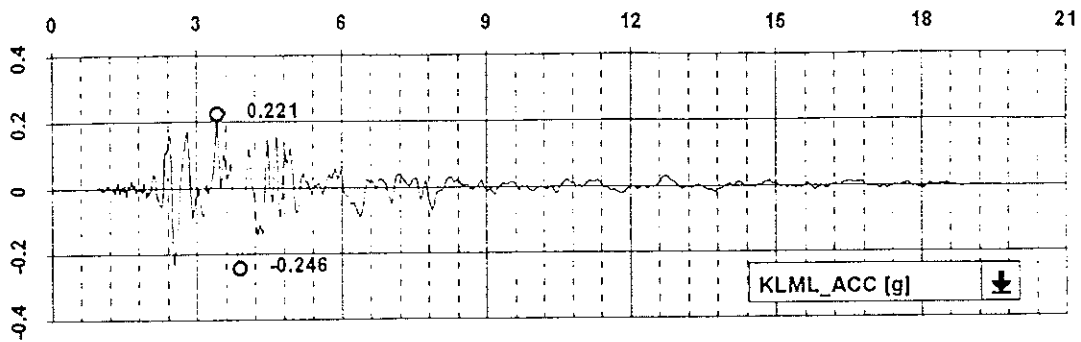


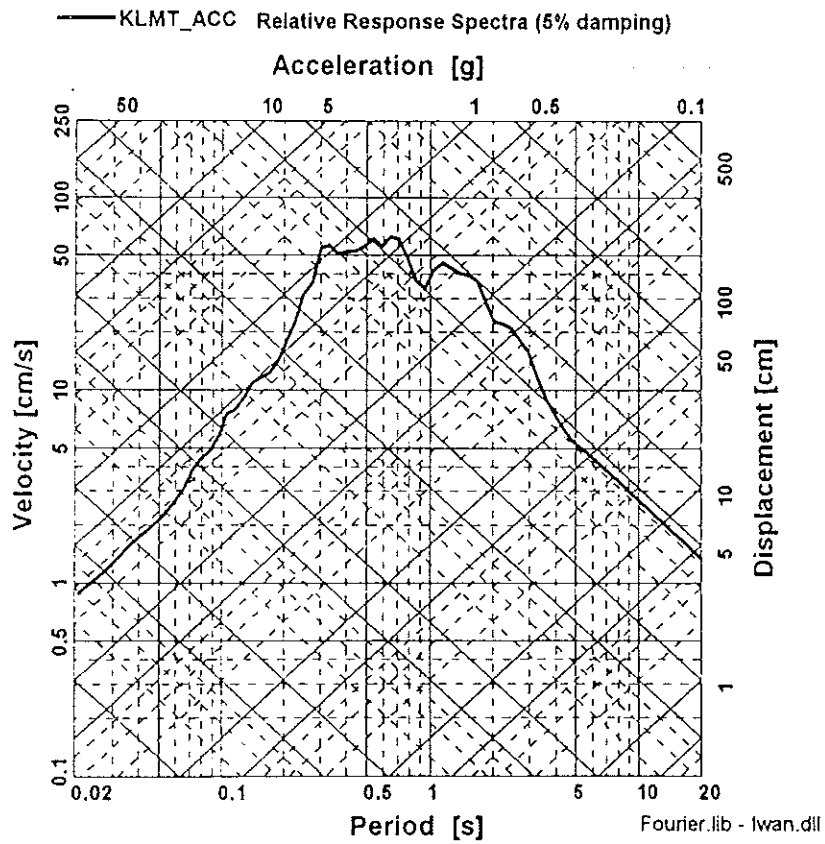
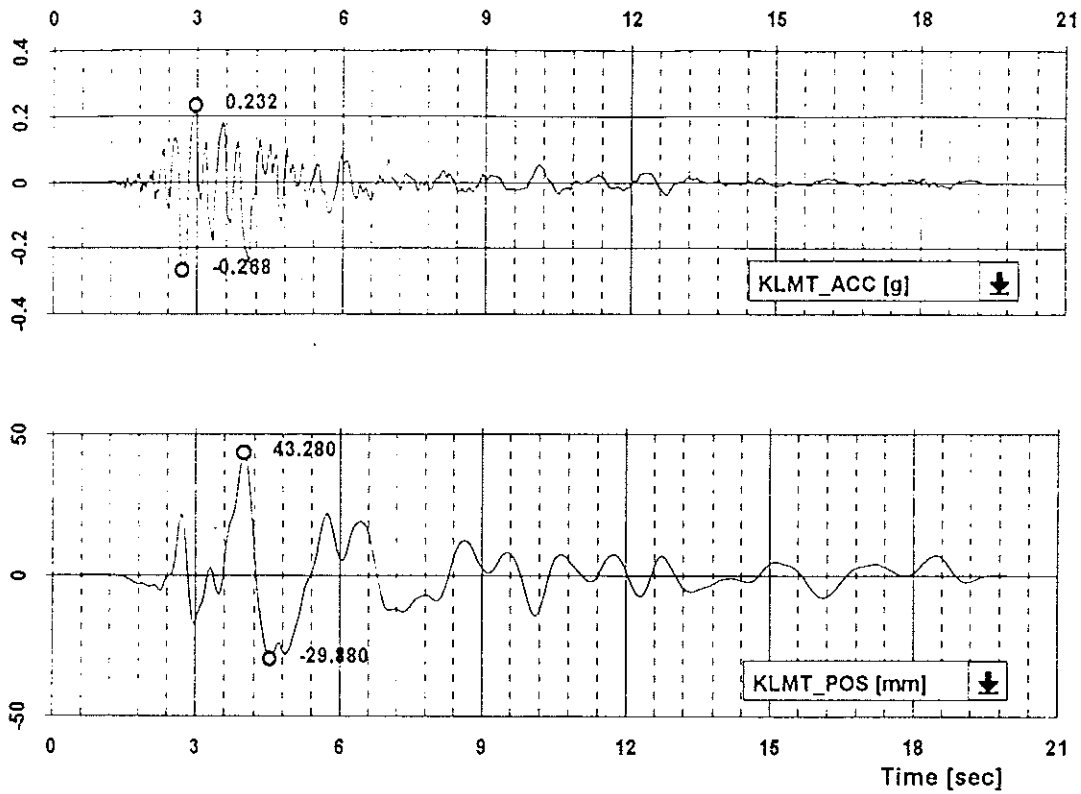


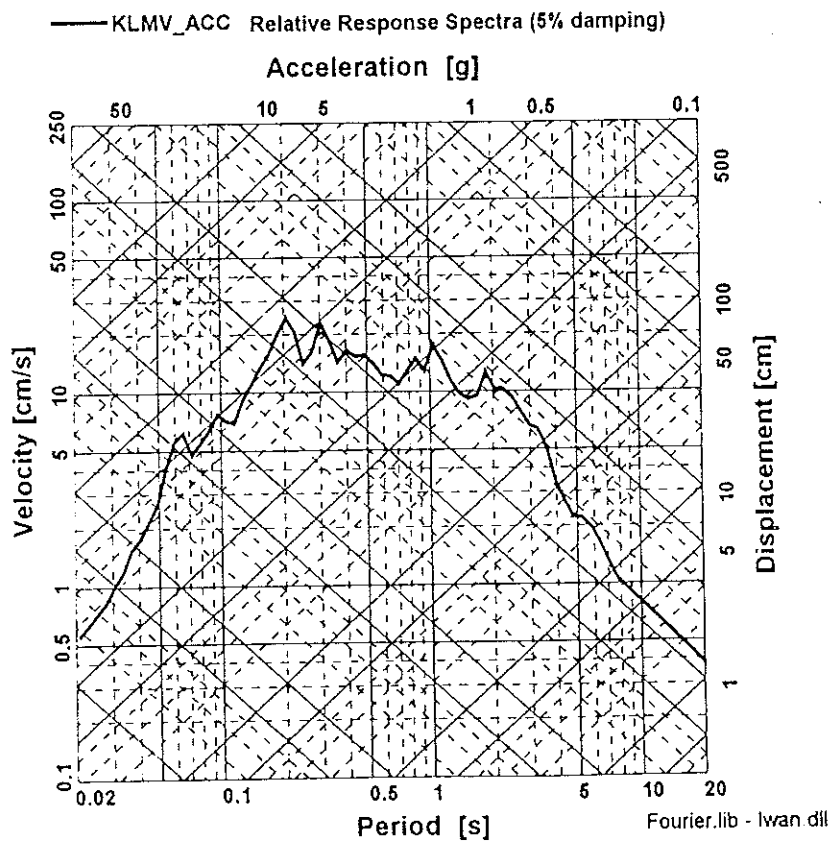
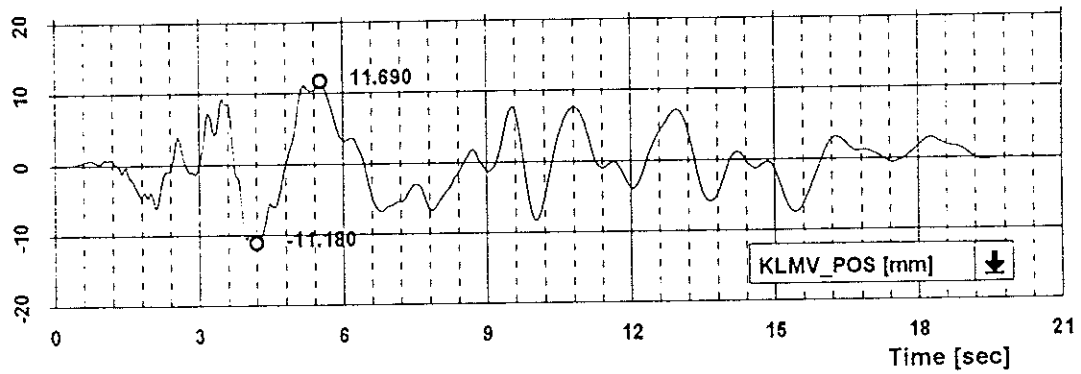
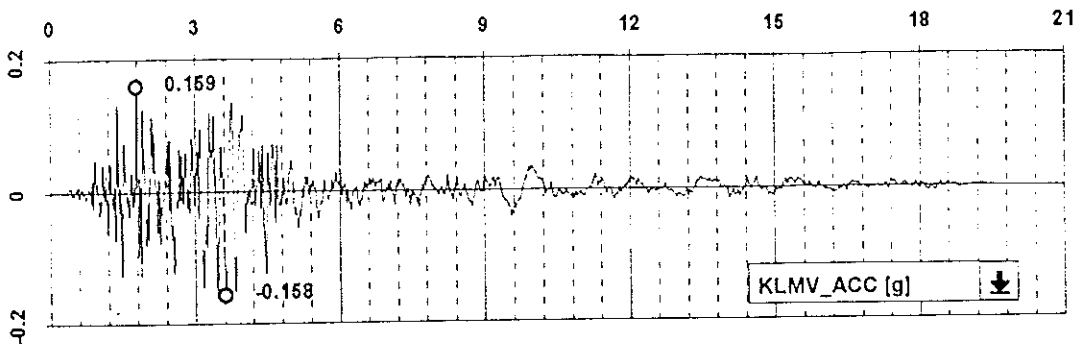












APPENDIX II

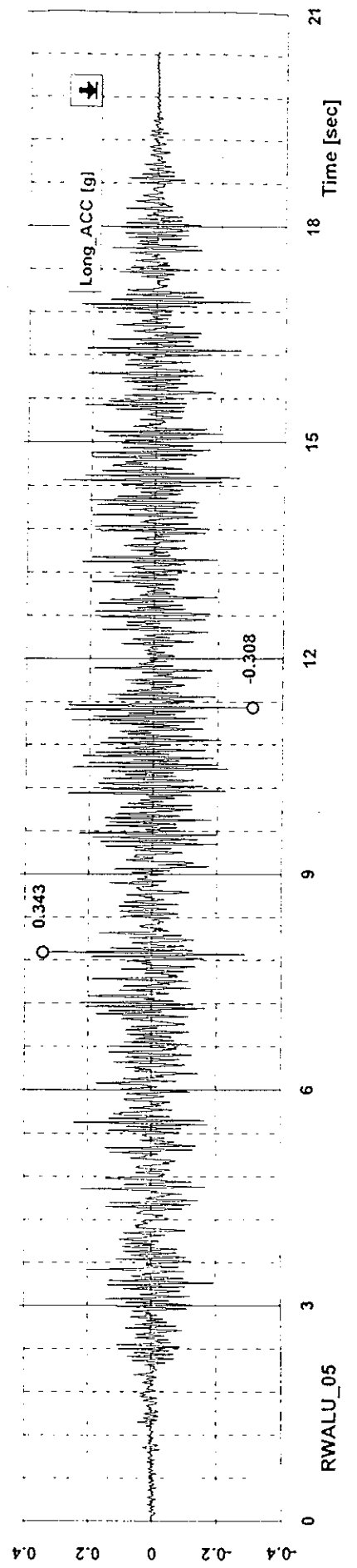
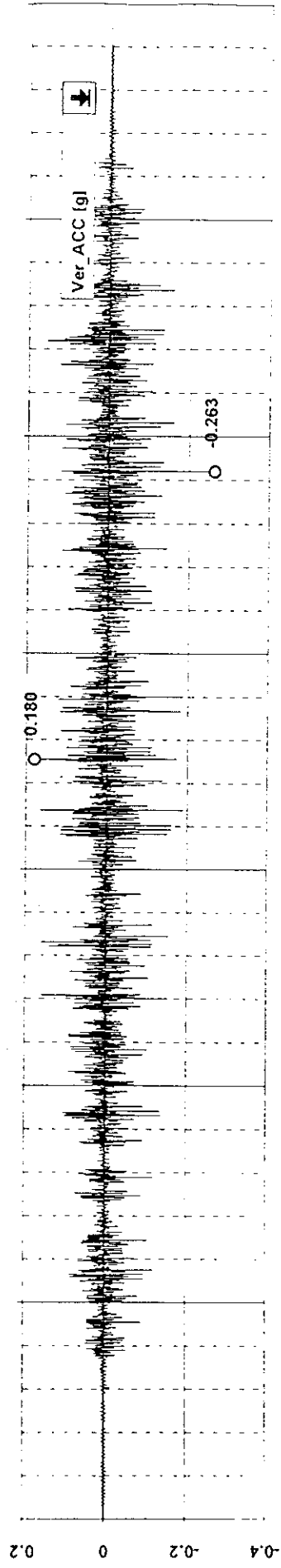
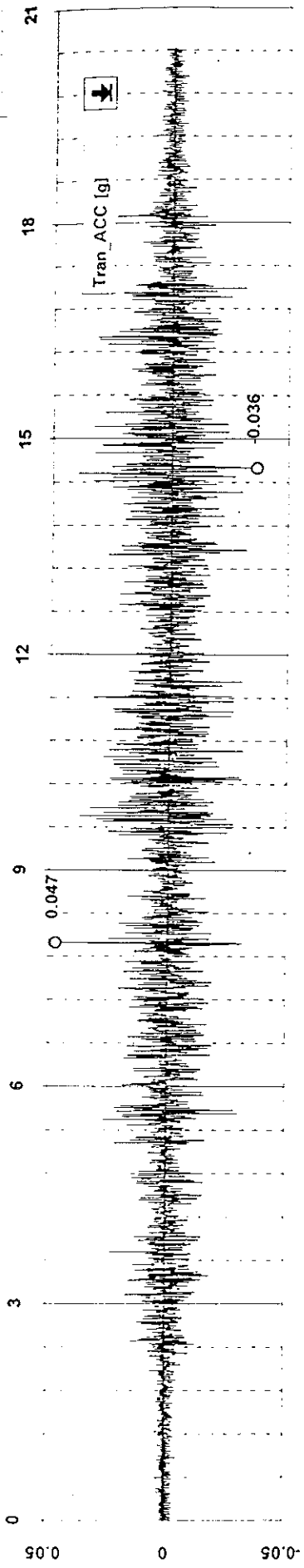
TEST MEASURED TIME SERIES

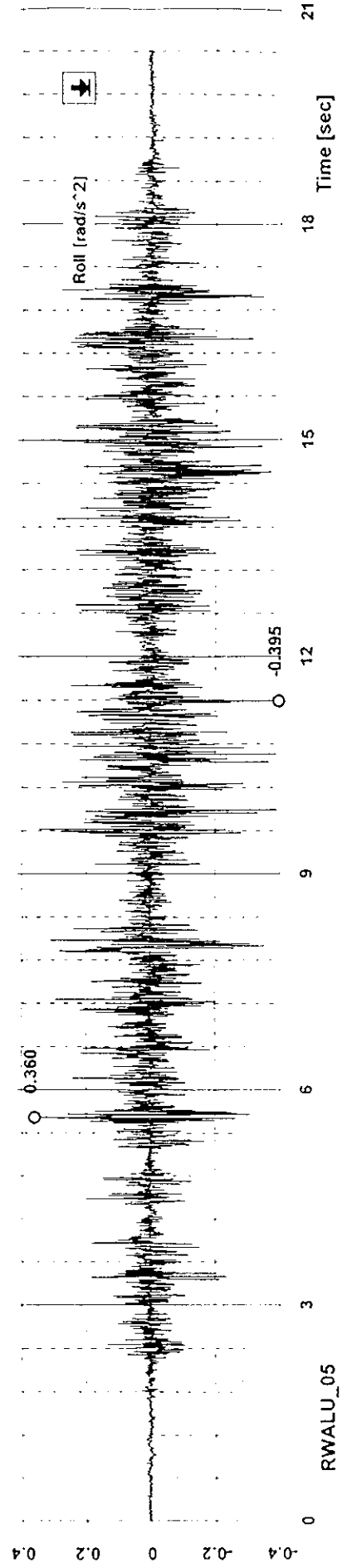
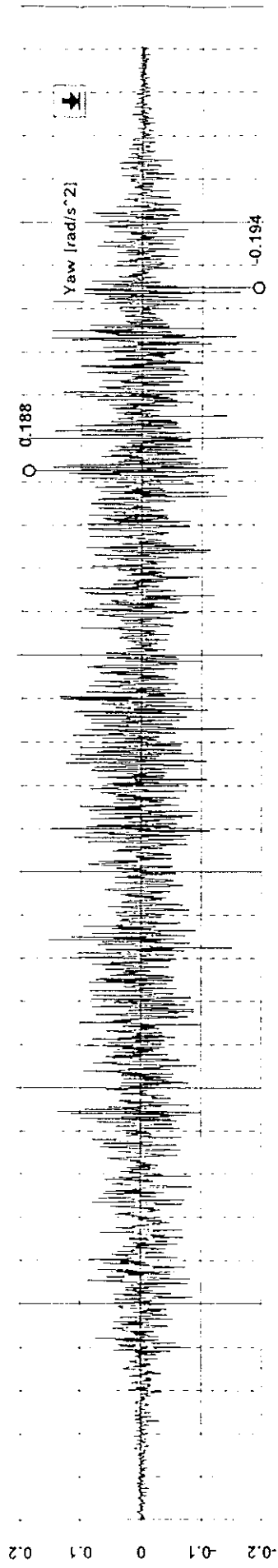
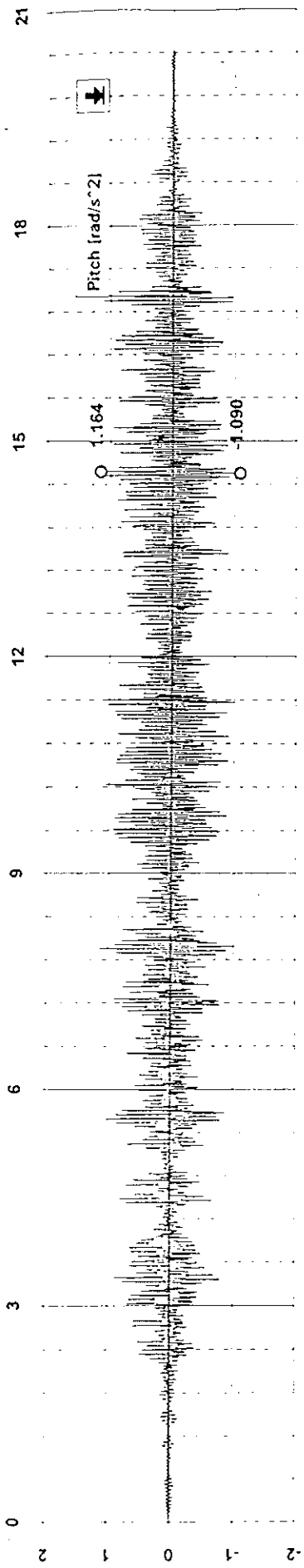
RANDOM WHITE NOISE - SAMPLE 5
KALAMATA EARTHQUAKE

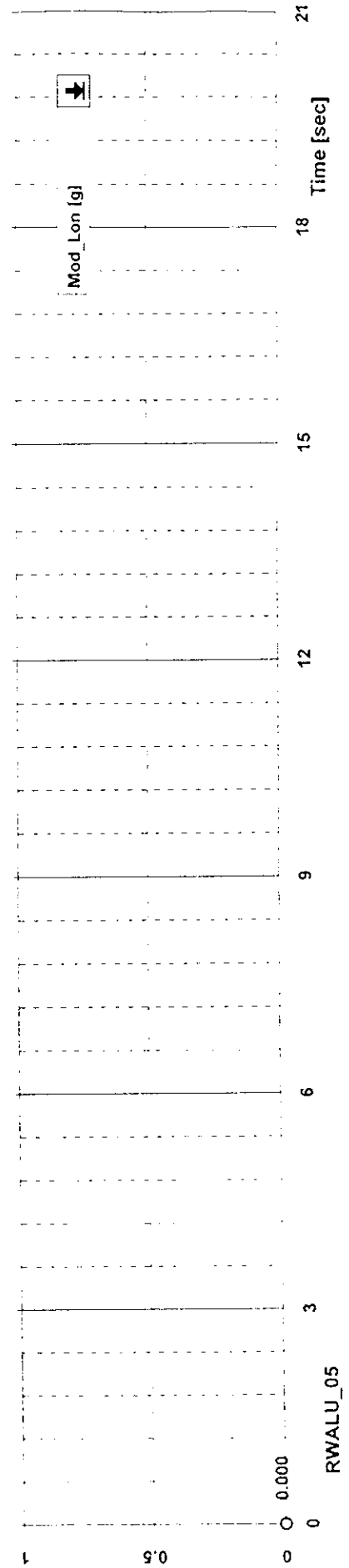
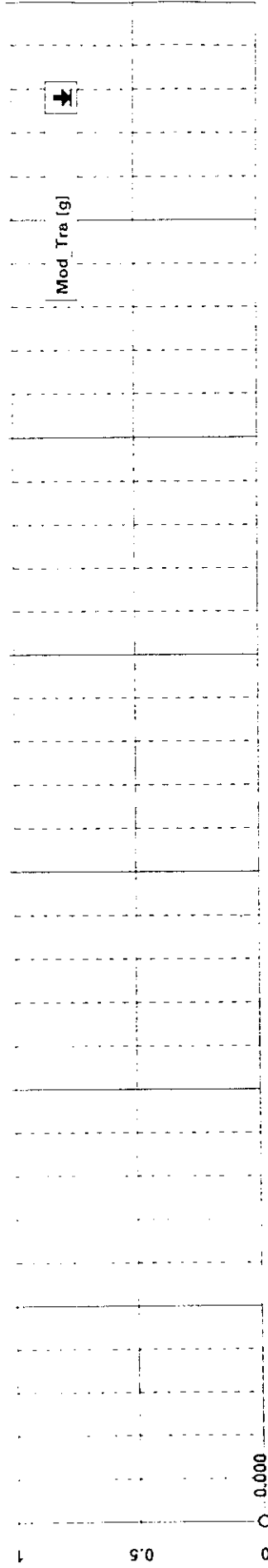
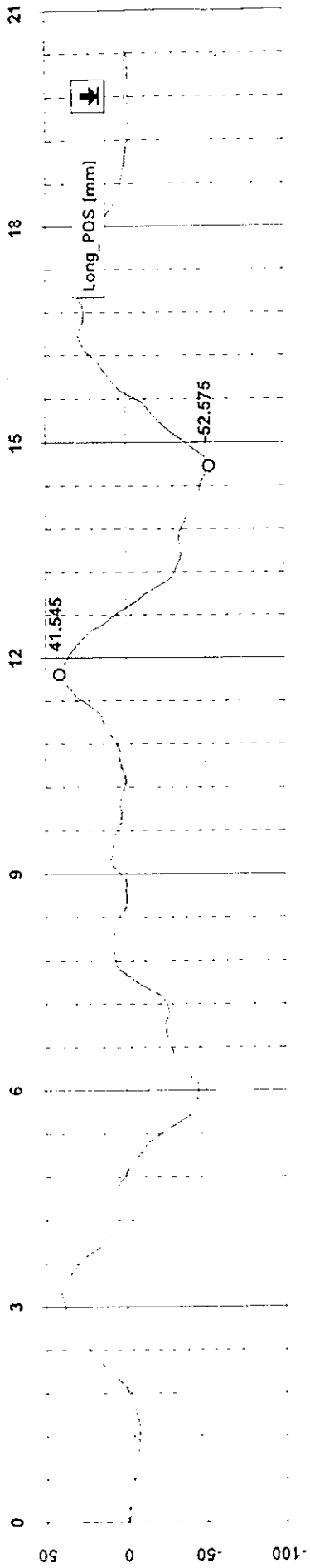
List of Figures

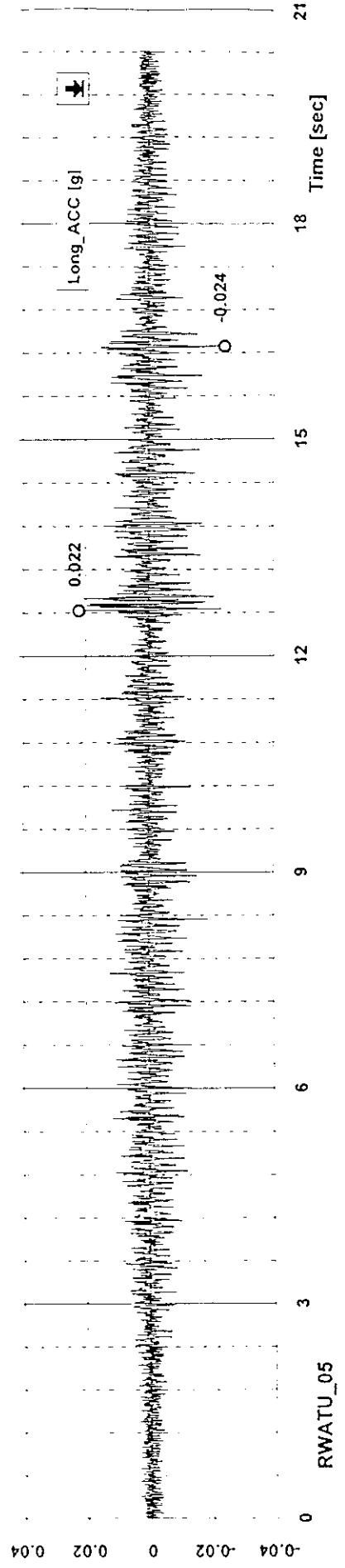
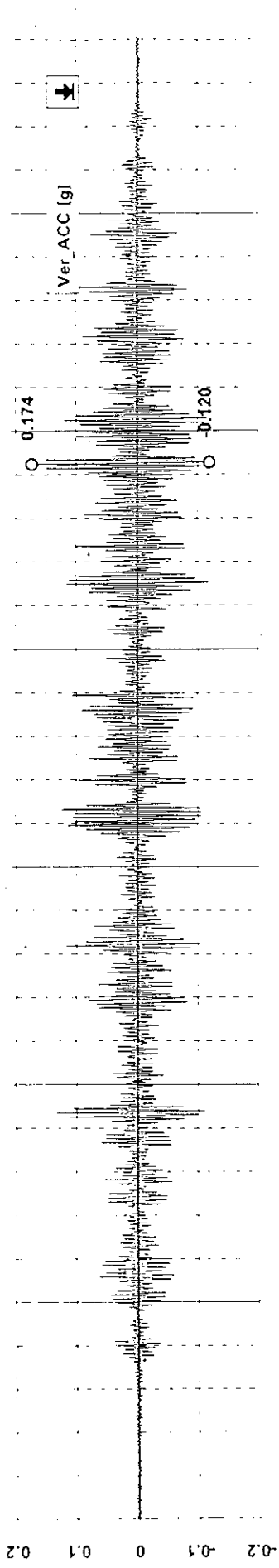
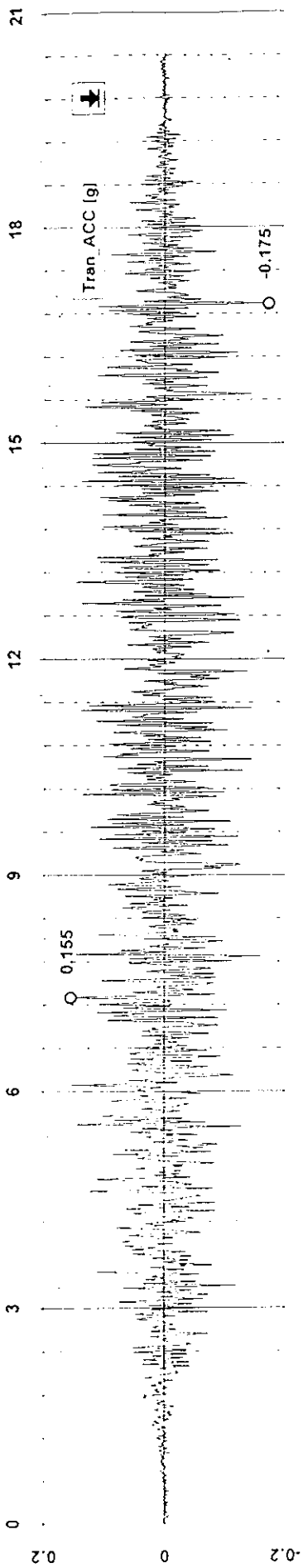
- AII.1 - Time series acceleration for the three orthogonal translations for a *Random White Noise (RWA) input, without model; uniaxial longitudinal excitation* (sample 5)
- AII.2 - Time series acceleration for the three orthogonal rotations for a *Random White Noise (RWA) input, without model; uniaxial longitudinal excitation* (sample 5)
- AII.3 - Time serie displacement for a *Random White Noise (RWA) input, without model; uniaxial longitudinal excitation* (sample 5)
- AII.4 - Time series acceleration for the three orthogonal translations for a *Random White Noise (RWA) input, without model; uniaxial transverse excitation* (sample 5)
- AII.5 - Time series acceleration for the three orthogonal rotations for a *Random White Noise (RWA) input without model; uniaxial transverse excitation* (sample 5)
- AII.6 - Time serie displacement for a *Random White Noise (RWA) input, without model; uniaxial transverse excitation* (sample 5)
- AII.7 - Time series acceleration for the three orthogonal translations for a *Random White Noise (RWA) input, without model; uniaxial vertical excitation* (sample 5)
- AII.8 - Time series acceleration for the three orthogonal rotations for a *Random White Noise (RWA) input, without model; uniaxial vertical excitation* (sample 5)
- AII.9 - Time serie displacement for a *Random White Noise (RWA) input, without model; uniaxial vertical excitation* (sample 5)
- AII.10 - Time series acceleration for the three orthogonal translations for a *Random White Noise (RWA) input, with model; uniaxial longitudinal excitation* (sample 5)
- AII.11 - Time series acceleration for the three orthogonal rotations for a *Random White Noise (RWA) input, with model; uniaxial longitudinal excitation* (sample 5)
- AII.12 - Time serie displacement for a *Random White Noise (RWA) input, with model; uniaxial longitudinal excitation* (sample 5) and time series acceleration for the model transducers
- AII.13 - Time series acceleration for the three orthogonal translations for a *Random White Noise (RWA) input, with model; uniaxial transverse excitation* (sample 5)
- AII.14 - Time series acceleration for the three orthogonal rotations for a *Random White Noise (RWA) input, with model; uniaxial transverse excitation* (sample 5)
- AII.15 - Time serie displacement for a *Random White Noise (RWA) input, with model; uniaxial transverse excitation* (sample 5) and time series acceleration for the model transducers
- AII.16 - Time series acceleration for the three orthogonal for a *Random White Noise (RWA) input, with model; uniaxial vertical excitation* (sample 5)
- AII.17 - Time series acceleration for the three orthogonal rotations orthogonal for a *Random White Noise (RWA) input, with model; uniaxial vertical excitation* (sample 5)

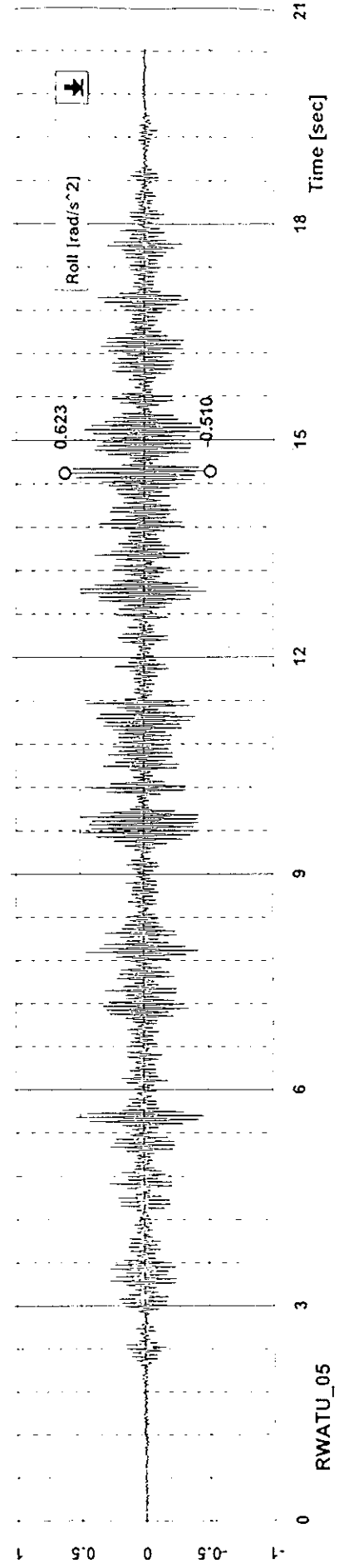
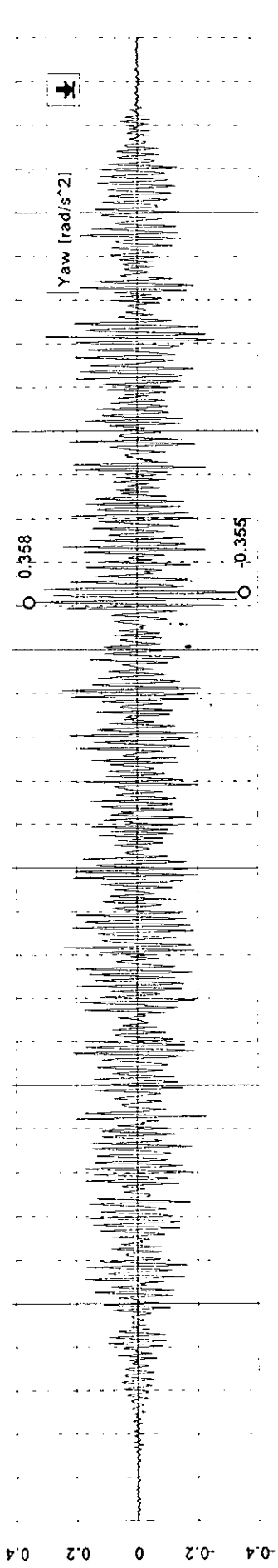
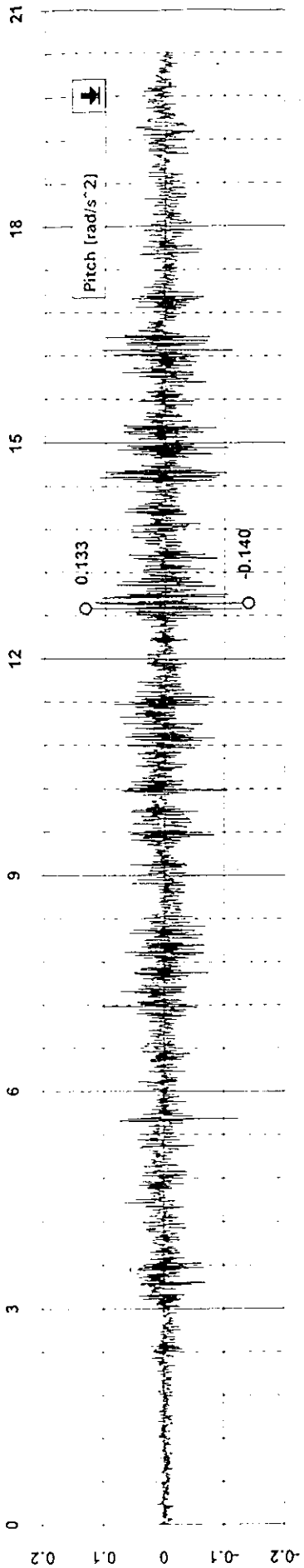
- AII.18 - Time serie displacement for a *Random White Noise (RWA)* input, with model; uniaxial vertical excitation (sample 5) and time series acceleration for the model transducers
- AII.19 - Time series acceleration for the three orthogonal translations for a *Kalamata earthquake (KLM)* input without model; triaxial excitation
- AII.20 - Time series acceleration for the three orthogonal rotations for *Kalamata earthquake (KLM)* input without model; triaxial excitation
- AII.21 - Time series displacement for *Kalamata earthquake (KLM)* input without model; triaxial excitation
- AII.22 - Time series acceleration for the three orthogonal translations for a *Kalamata earthquake (KLM)* input with model; triaxial excitation
- AII.23 - Time series acceleration for the three orthogonal rotations for *Kalamata earthquake (KLM)* input with model; triaxial excitation
- AII.24 - Time series displacement for *Kalamata earthquake (KLM)* input with model; triaxial excitation
- AII.25 - Time series acceleration for the model transducers for *Kalamata earthquake (KLM)* input with model; triaxial excitation

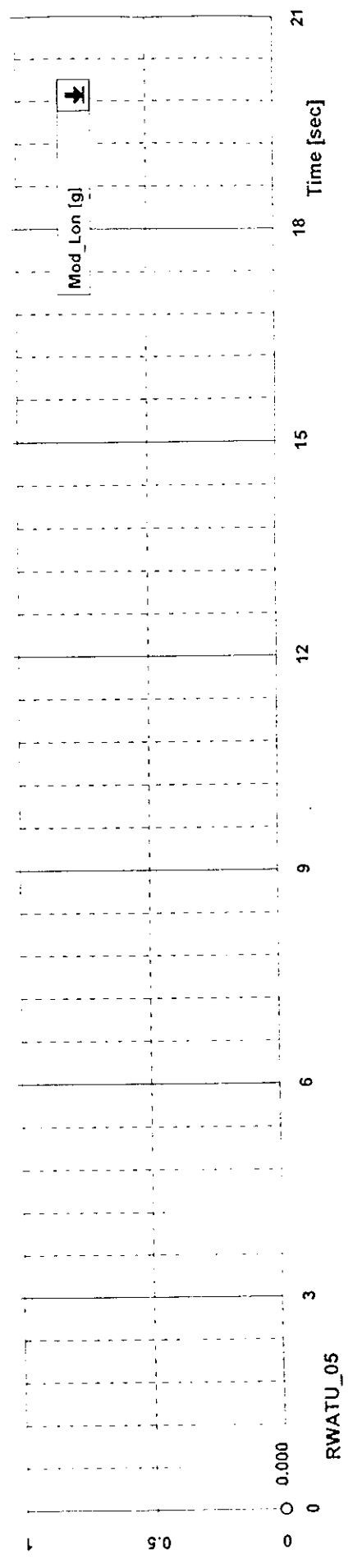
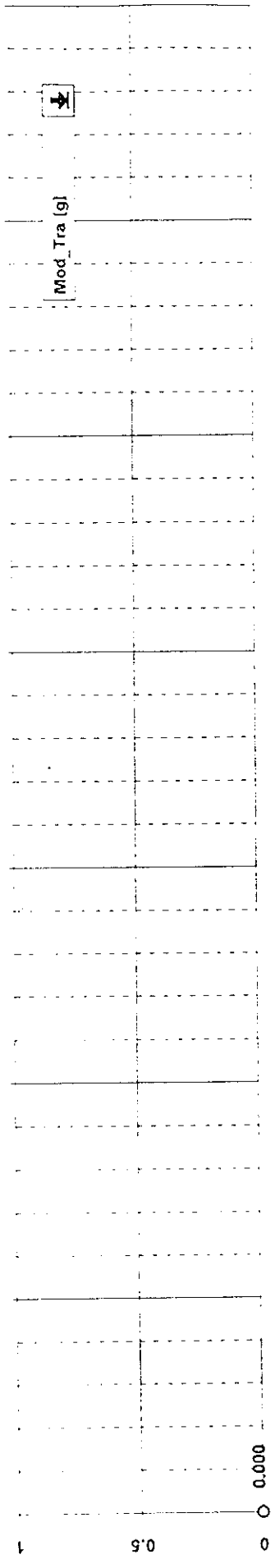
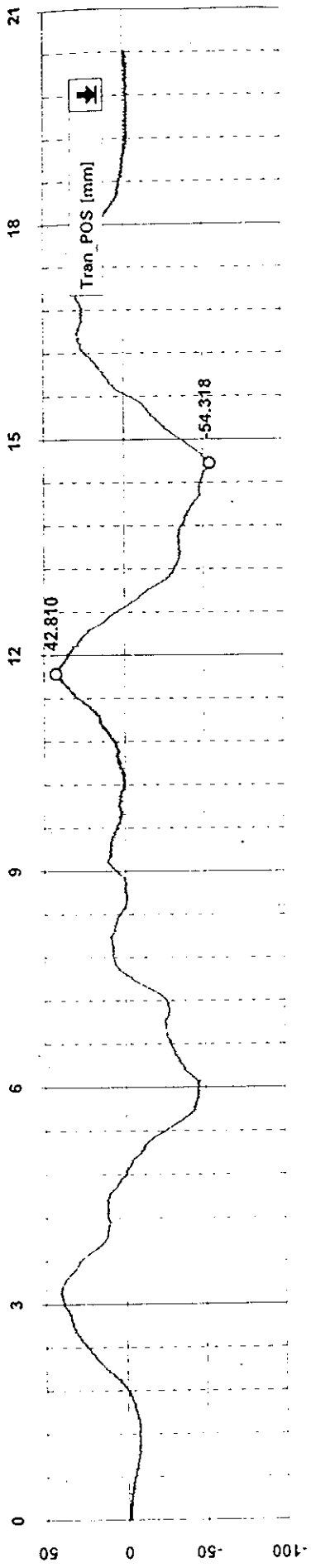


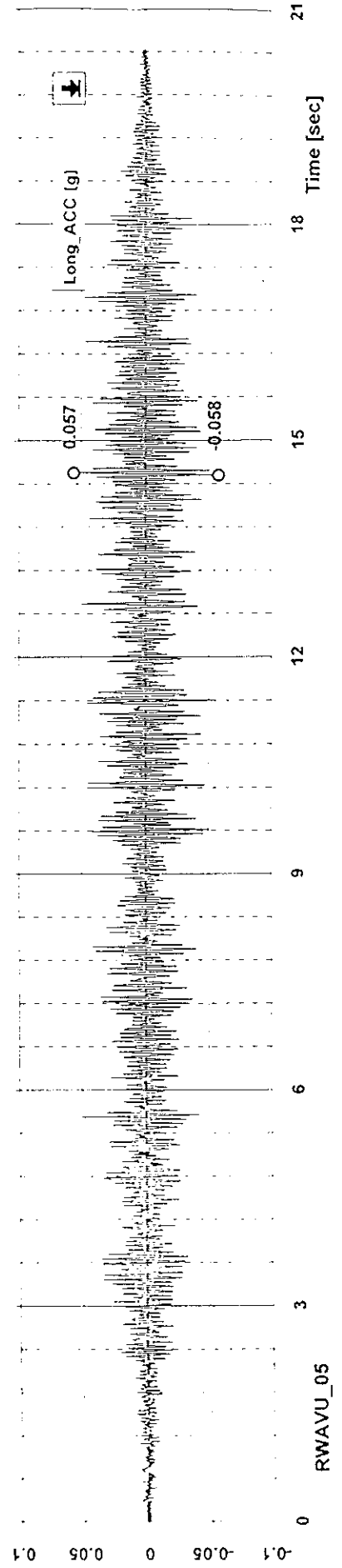
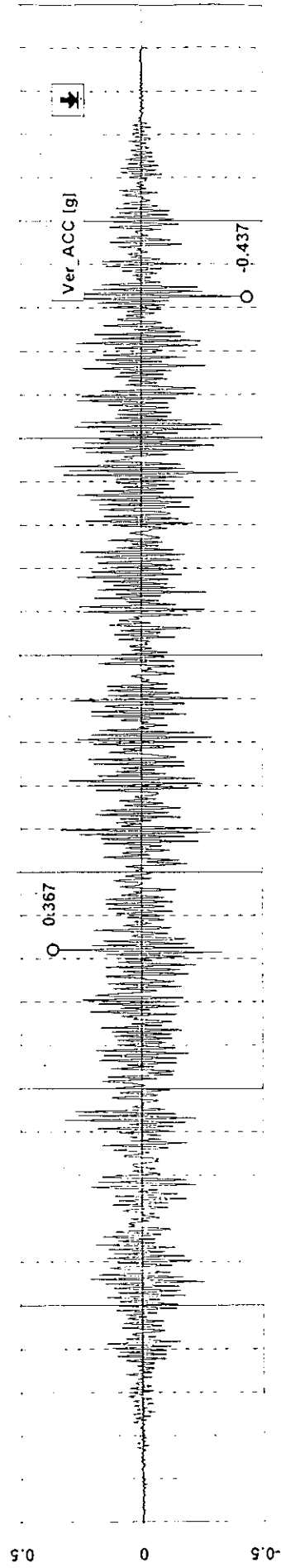
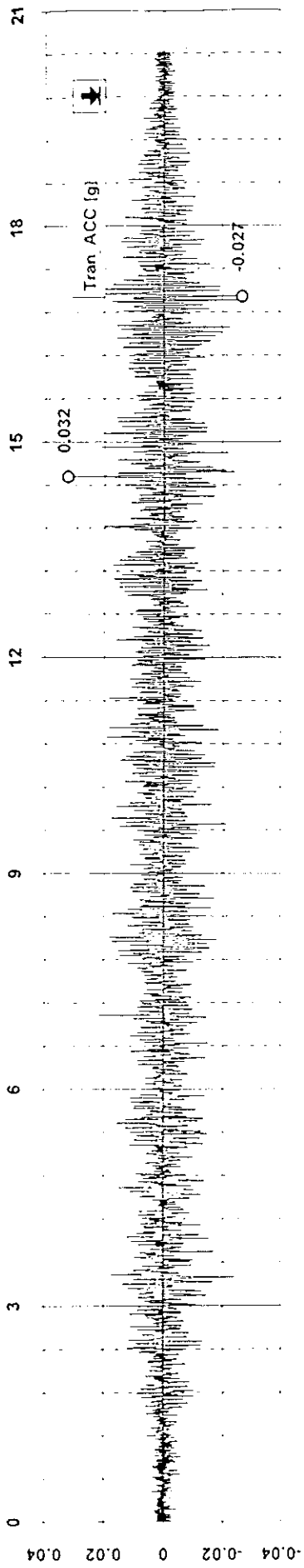


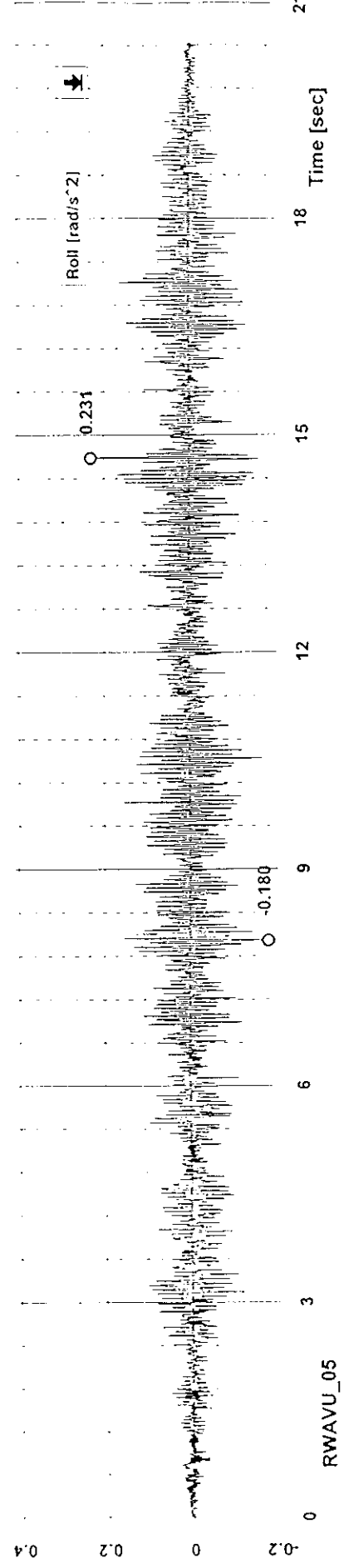
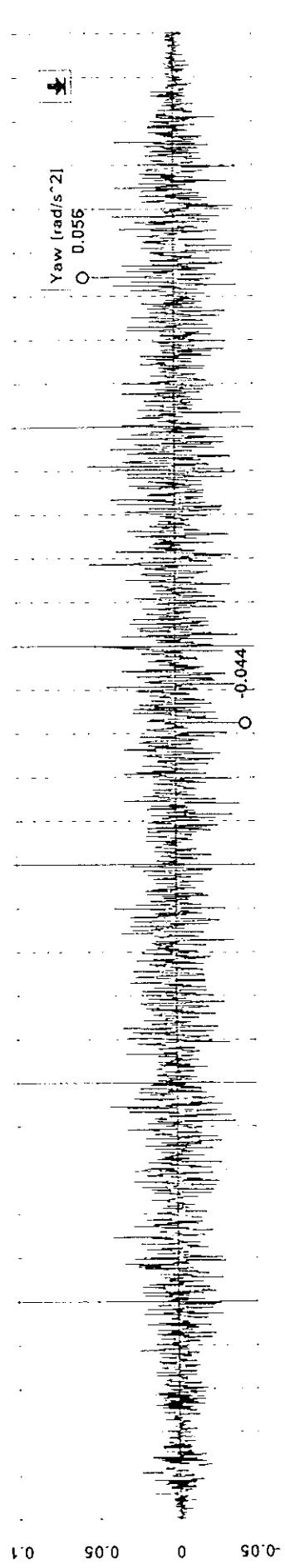
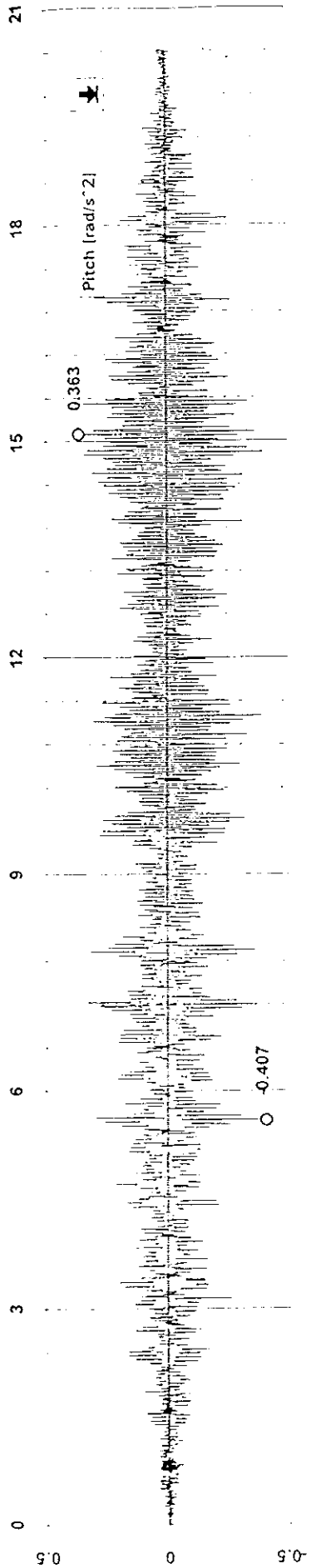


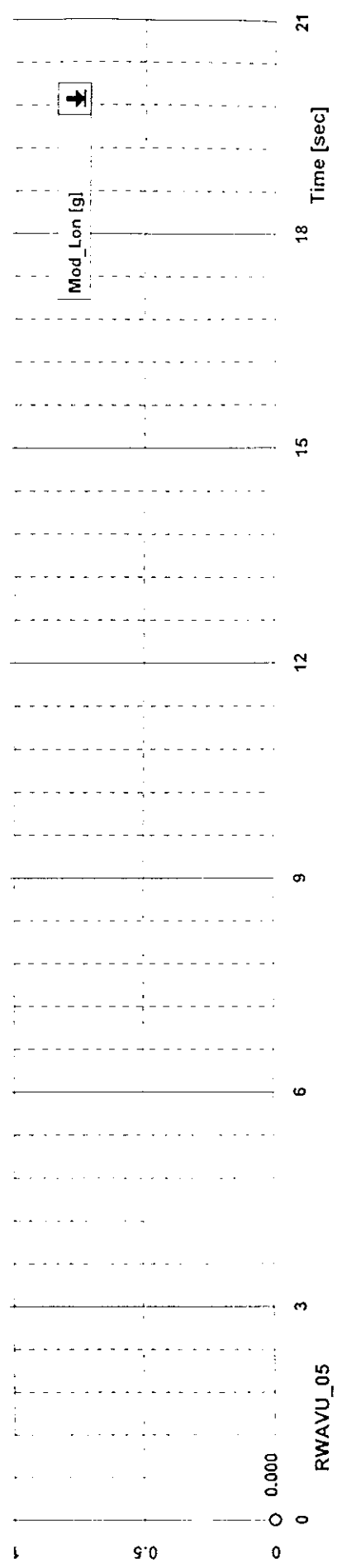
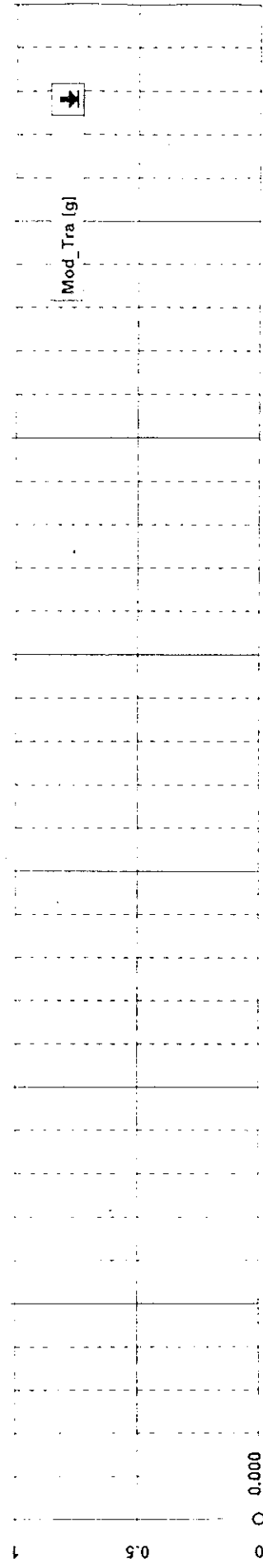
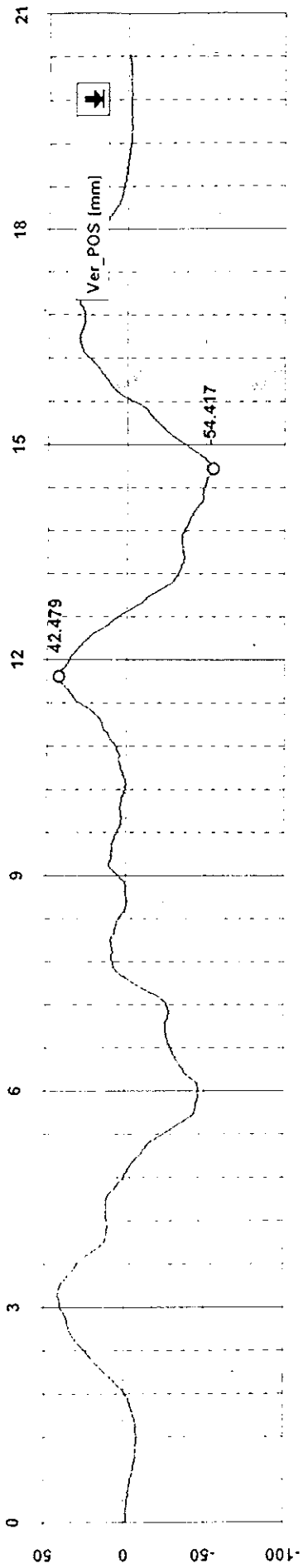


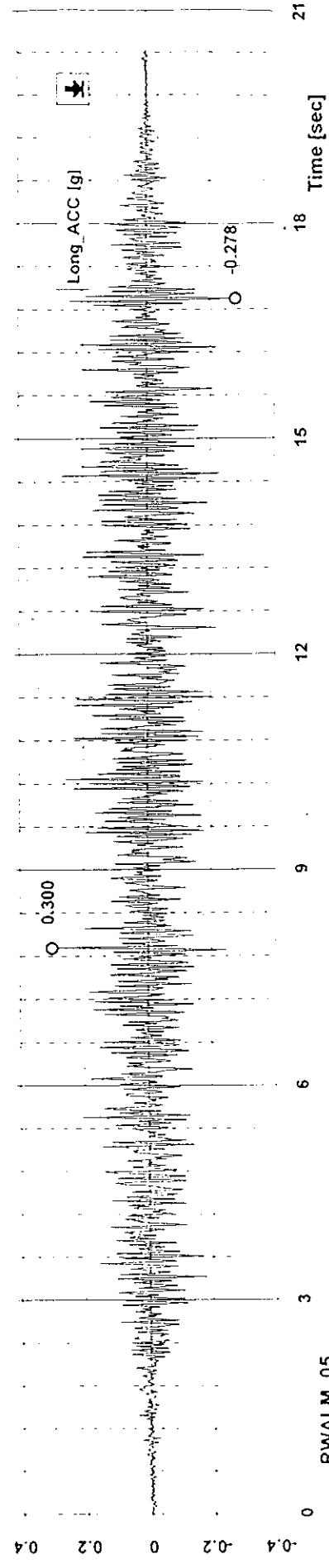
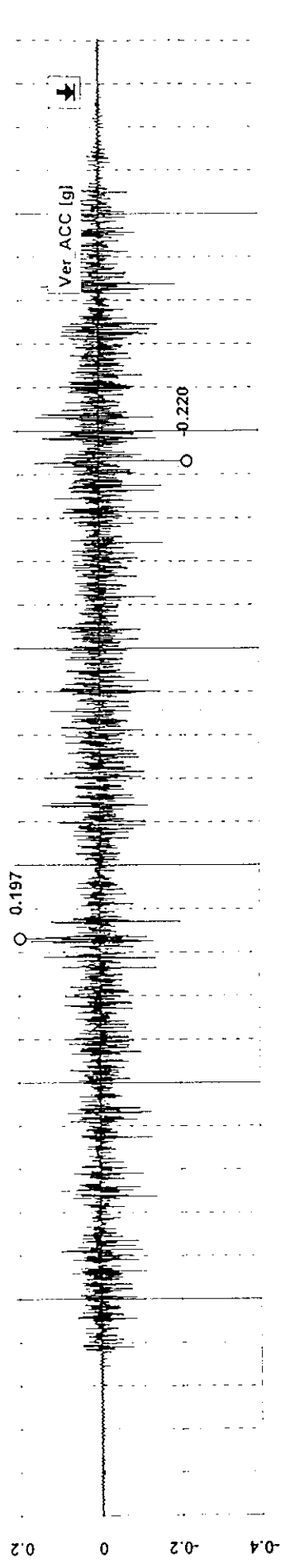
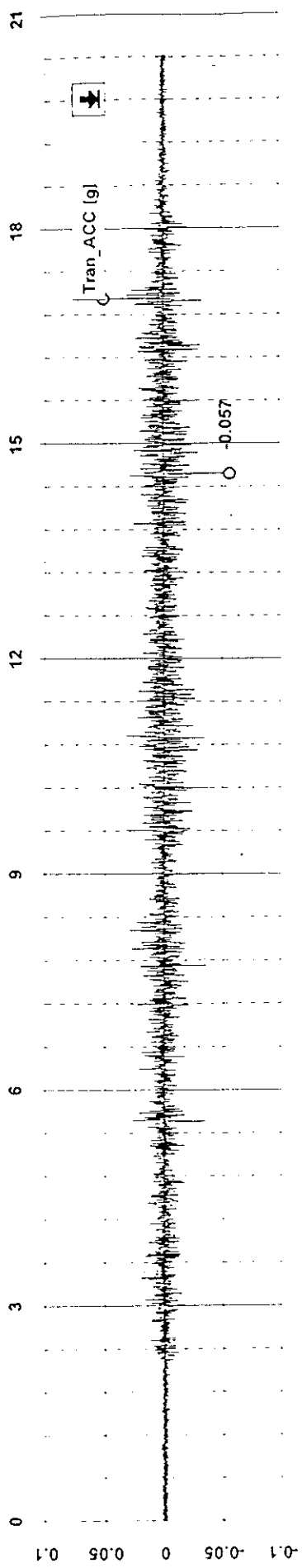


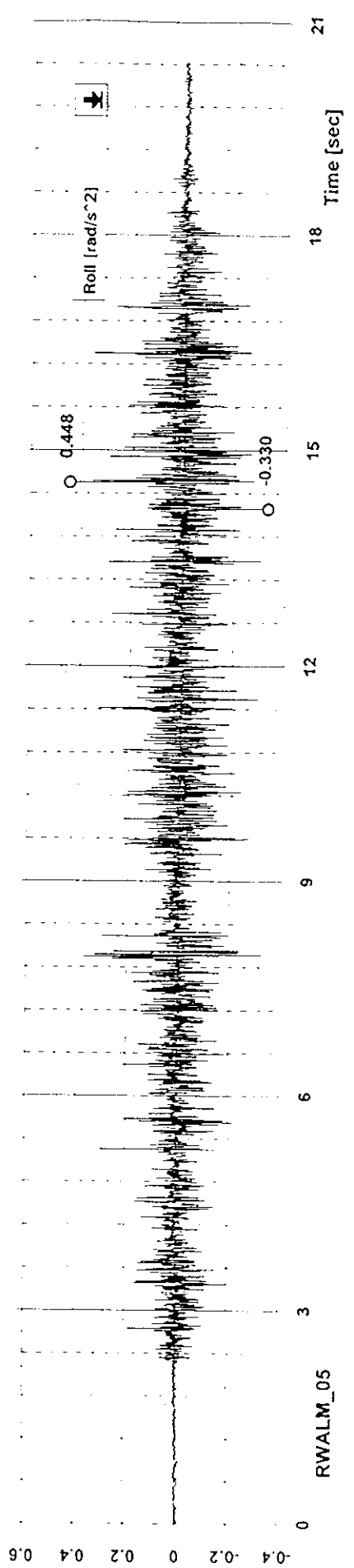
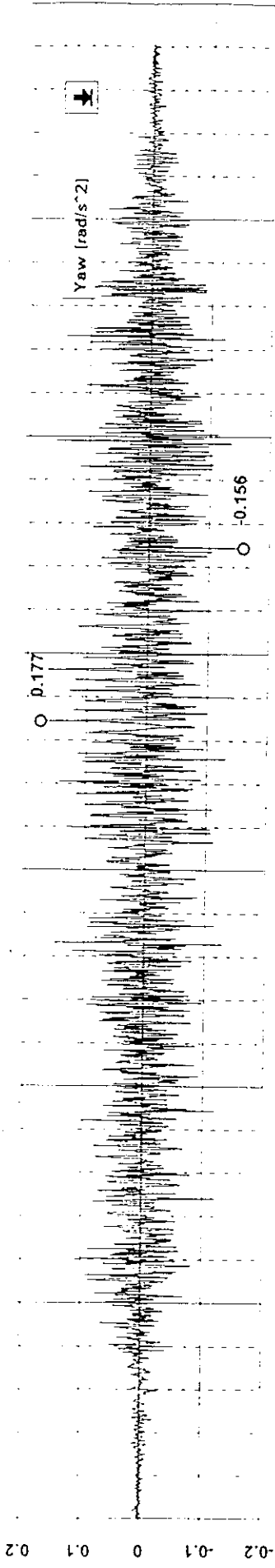
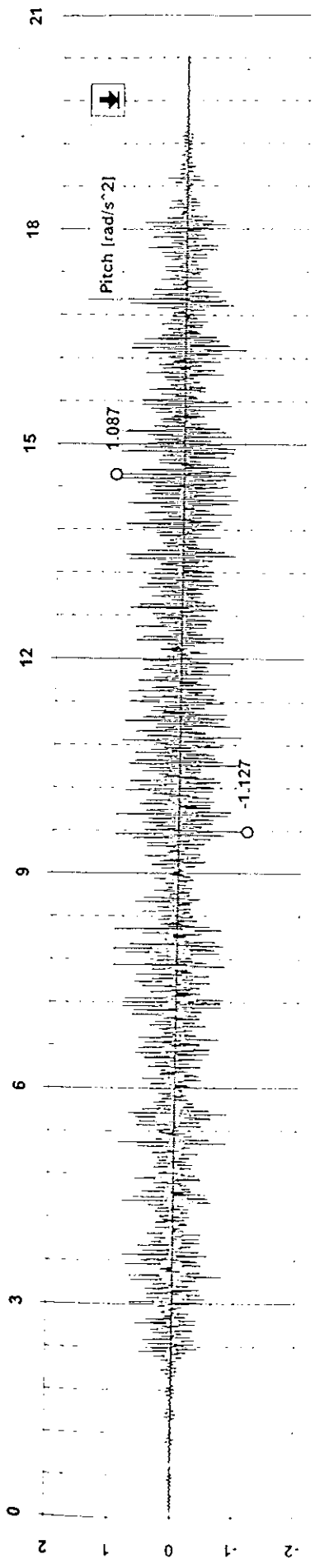




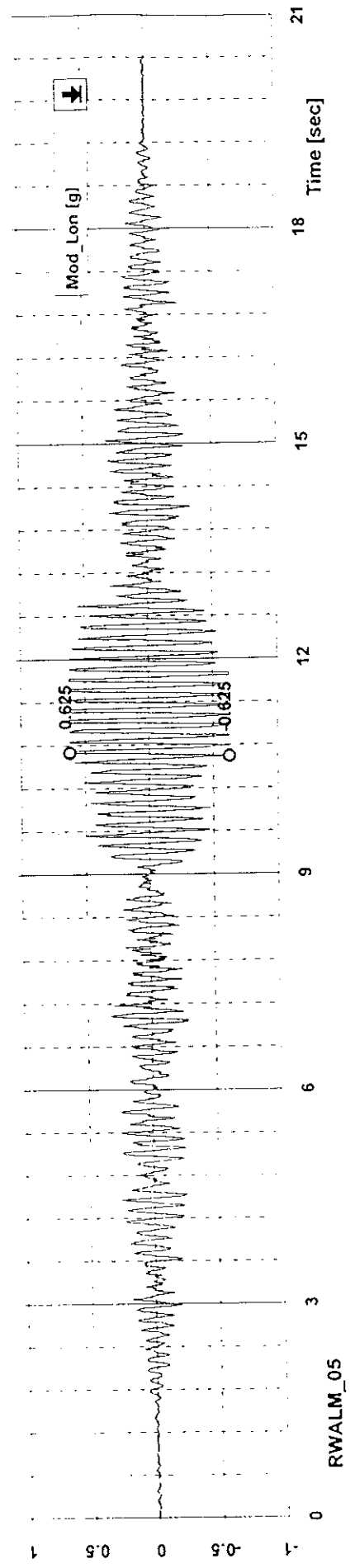
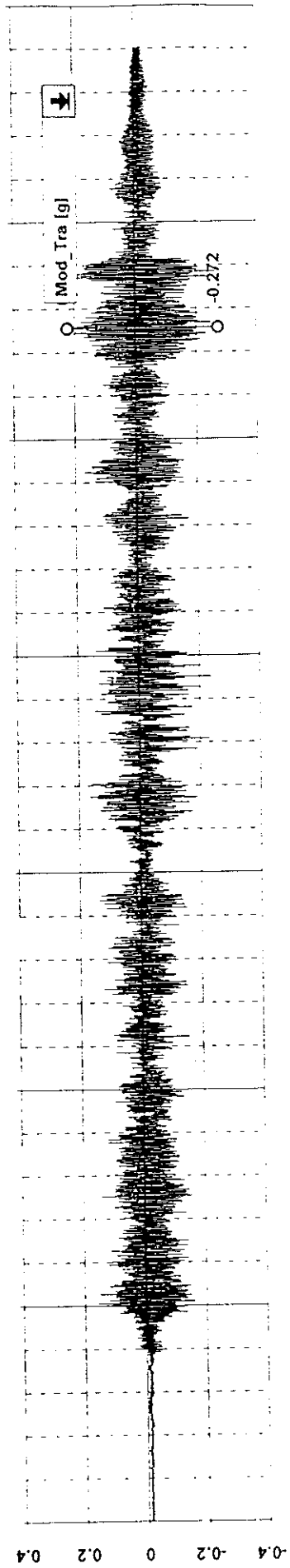
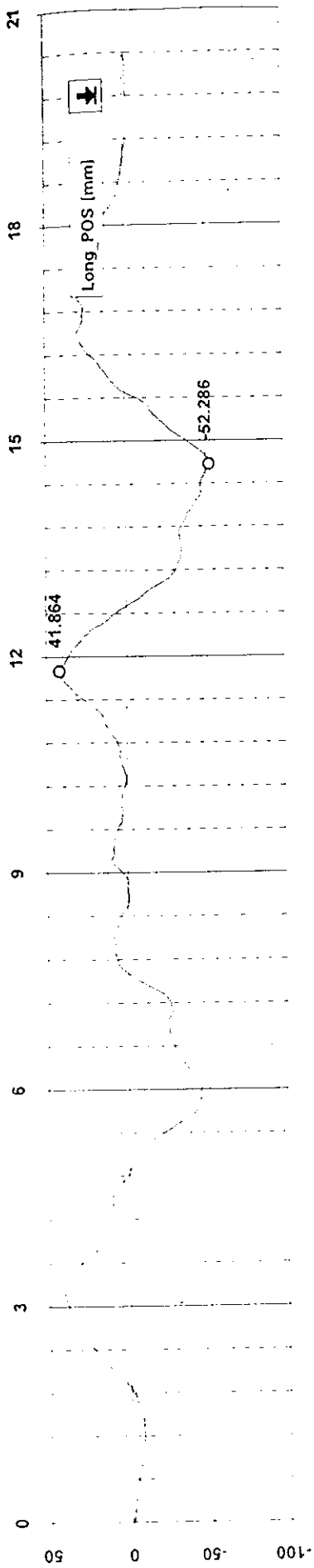


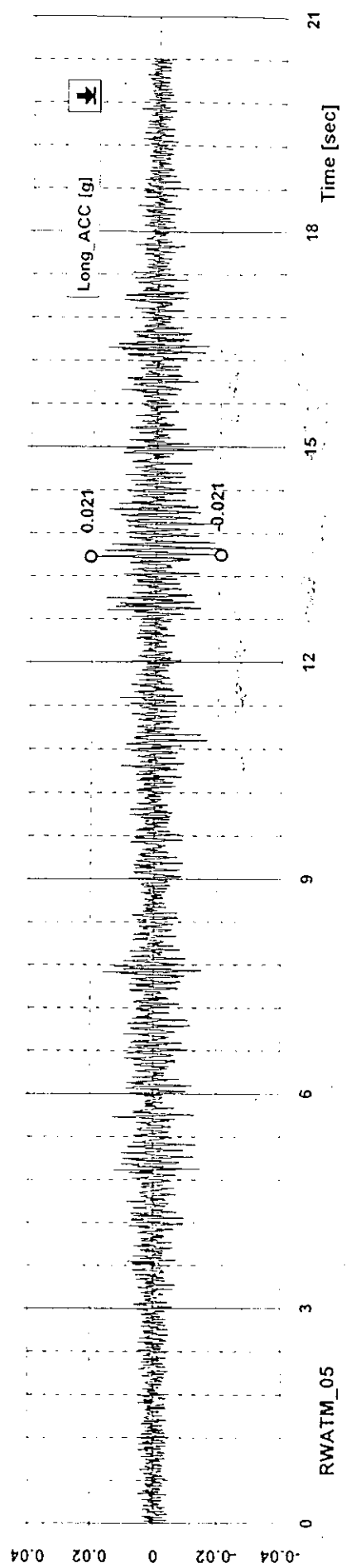
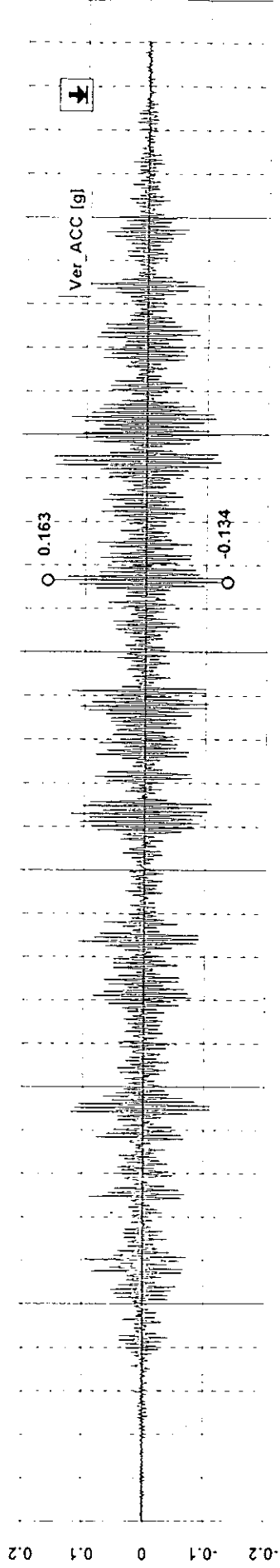
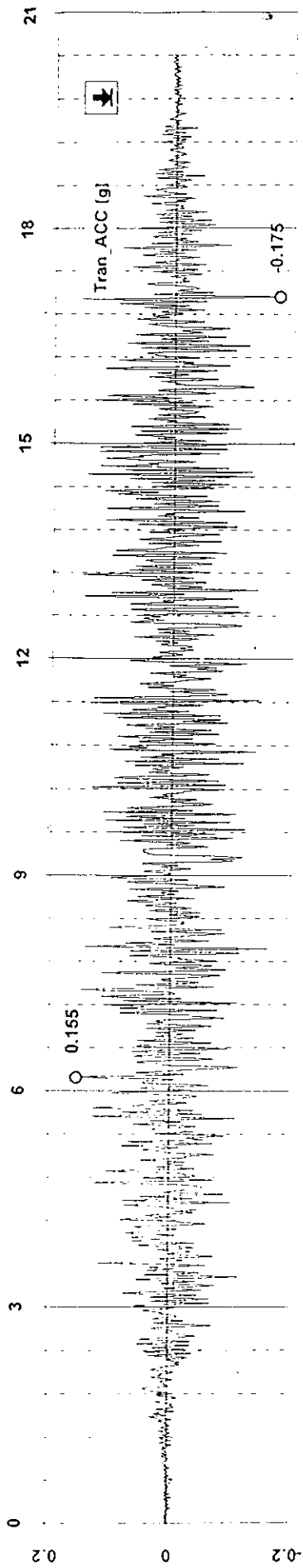


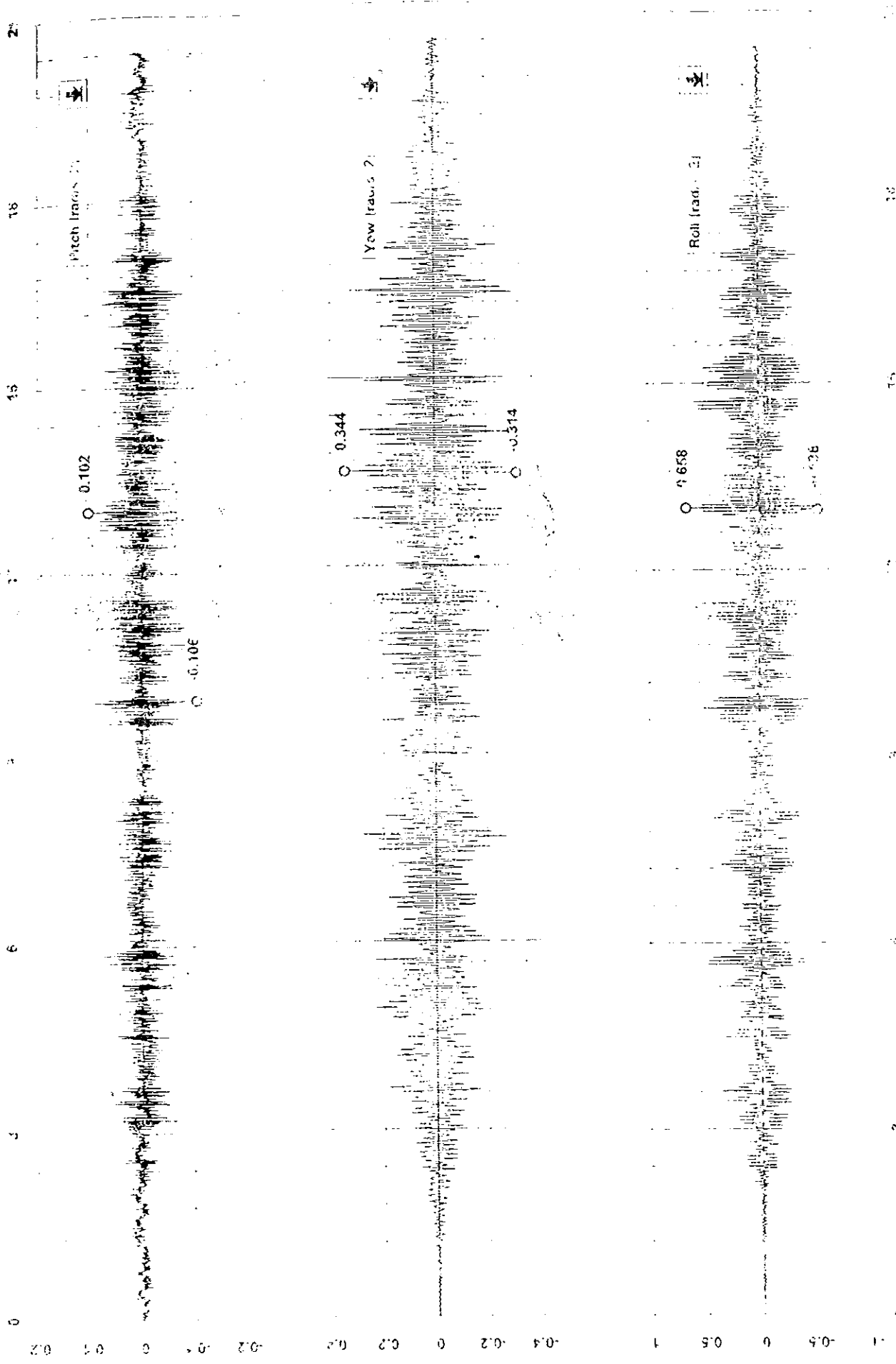


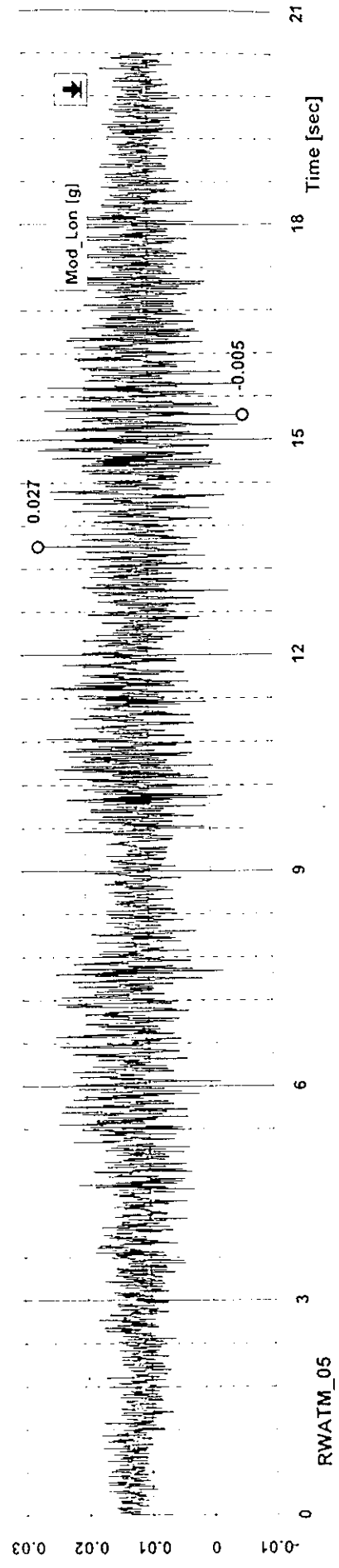
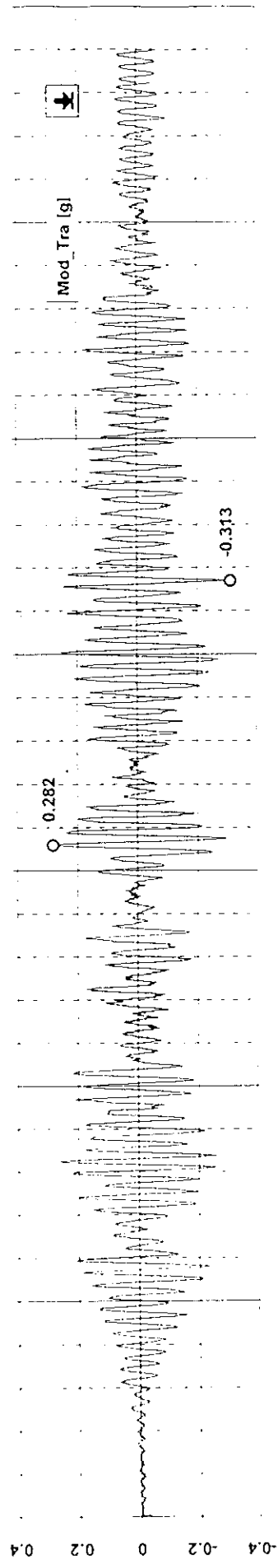
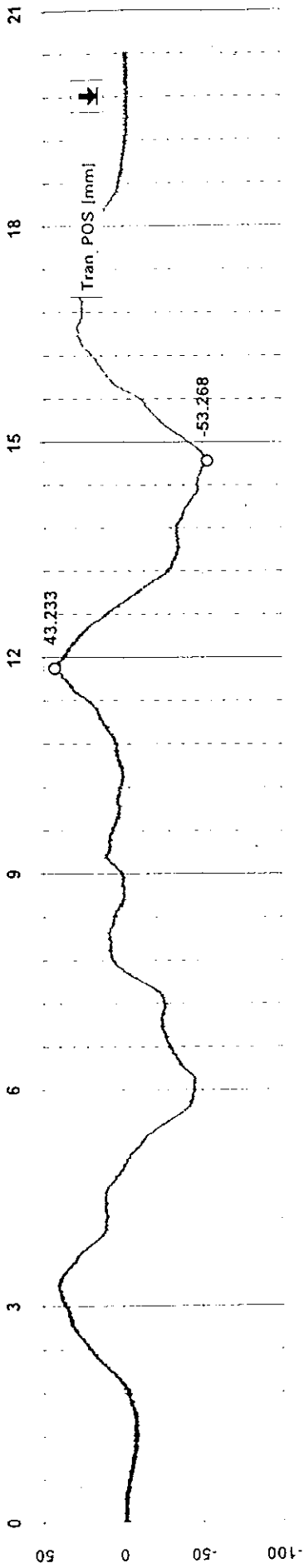


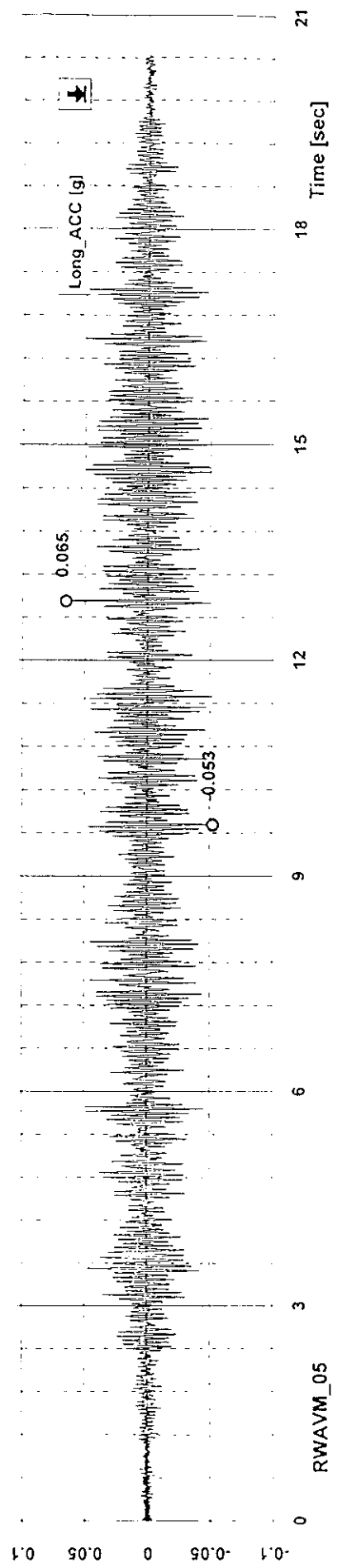
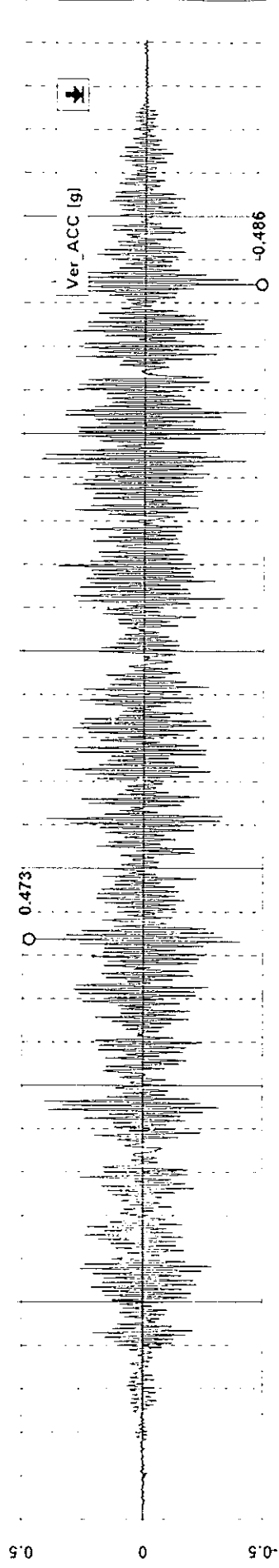
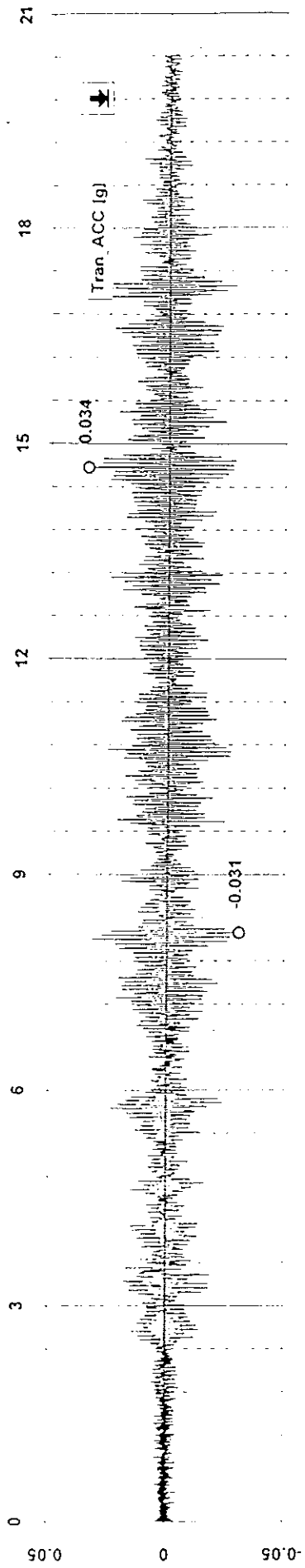
RWALM_05

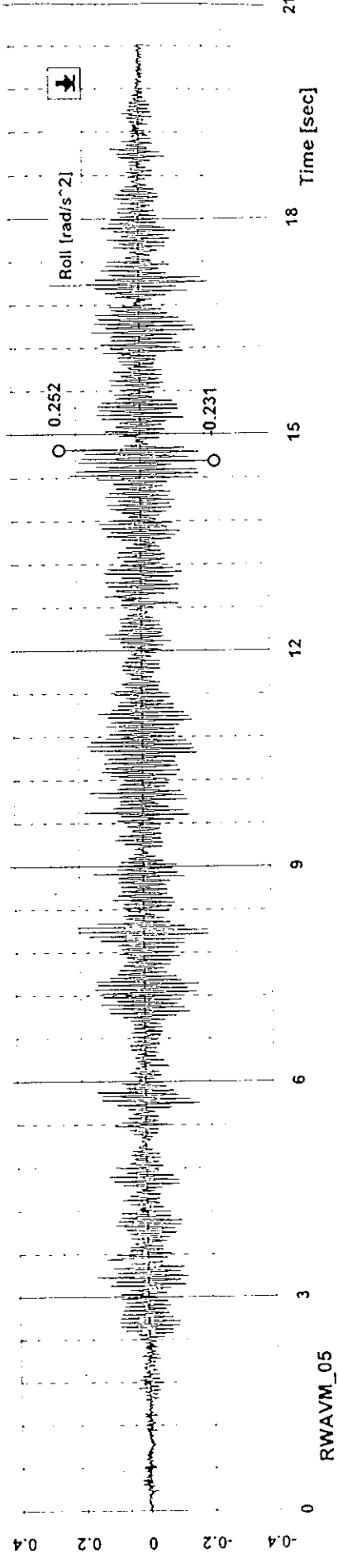
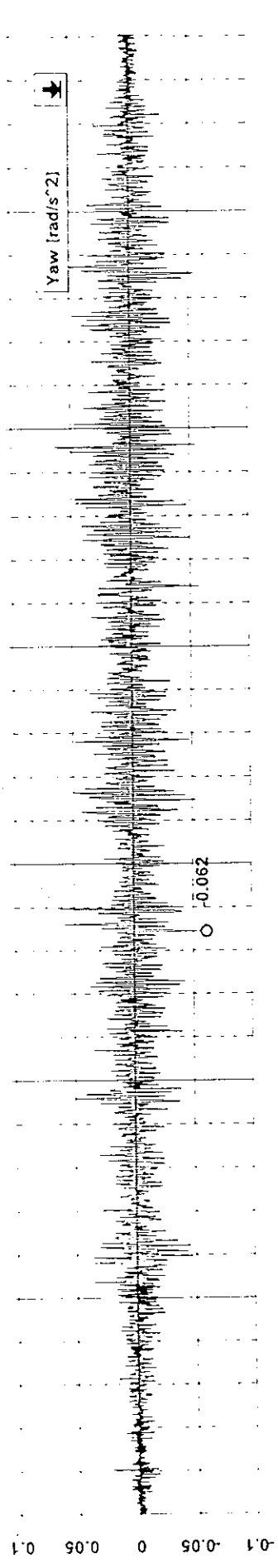
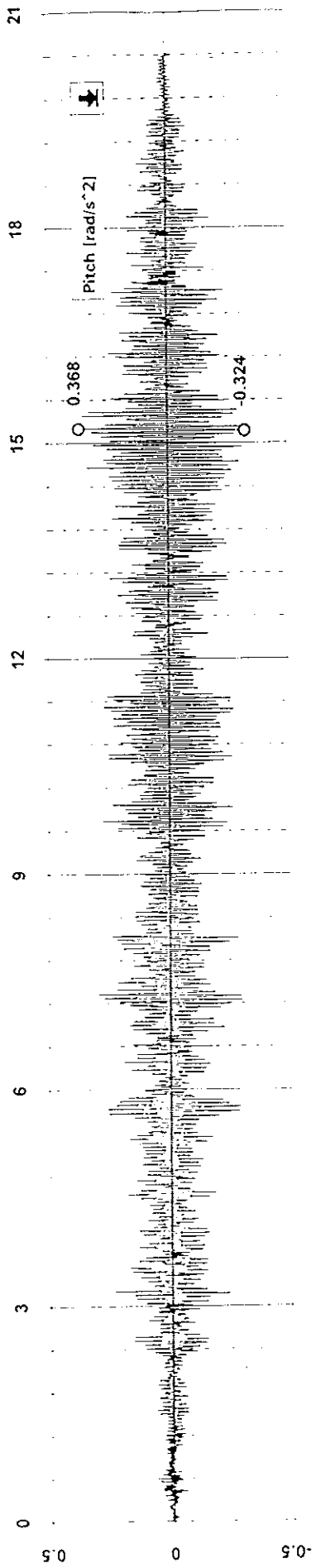


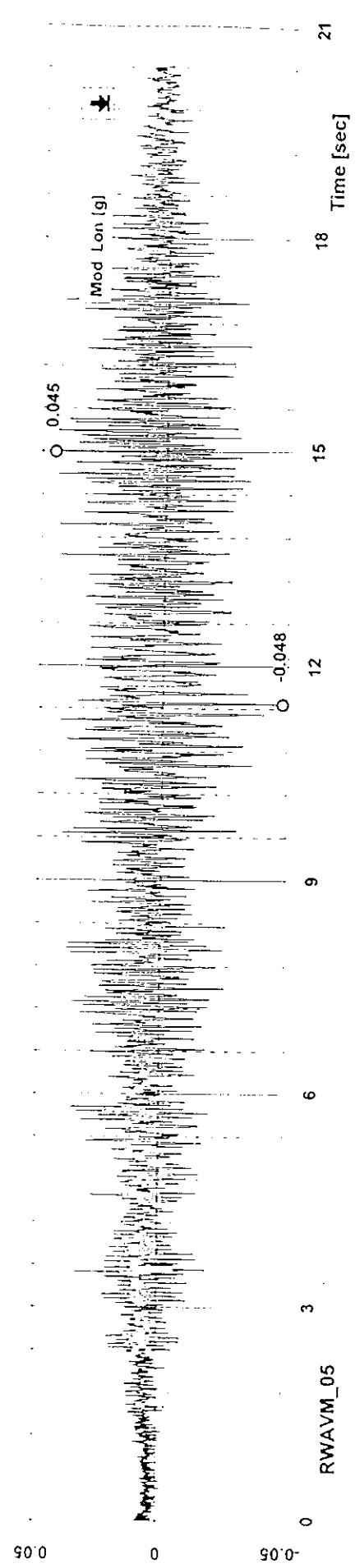
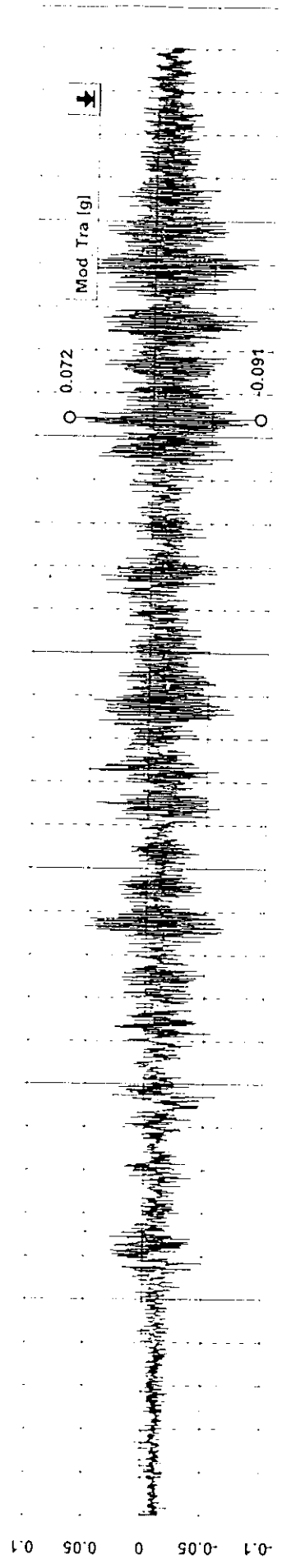
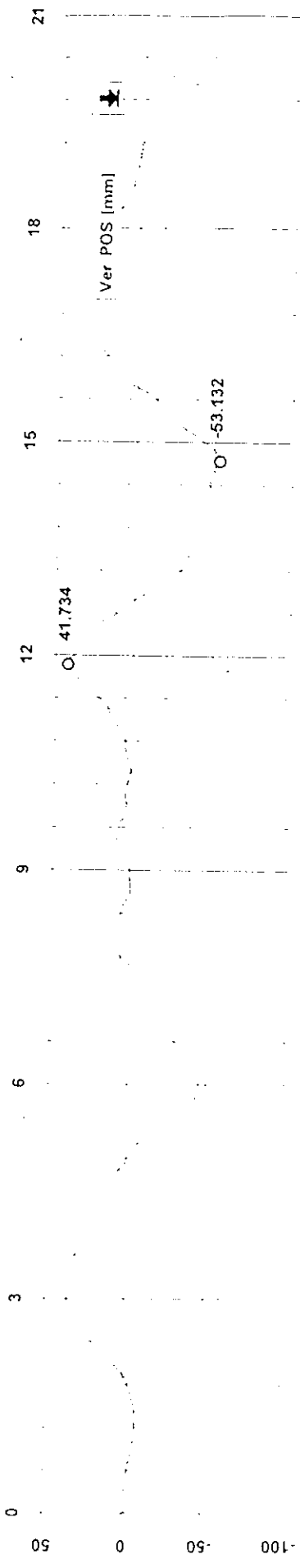


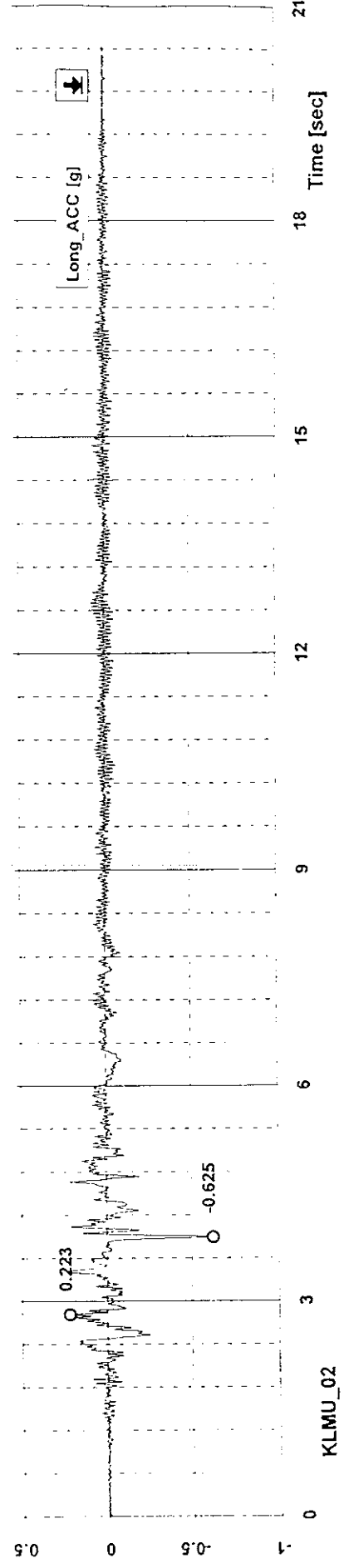
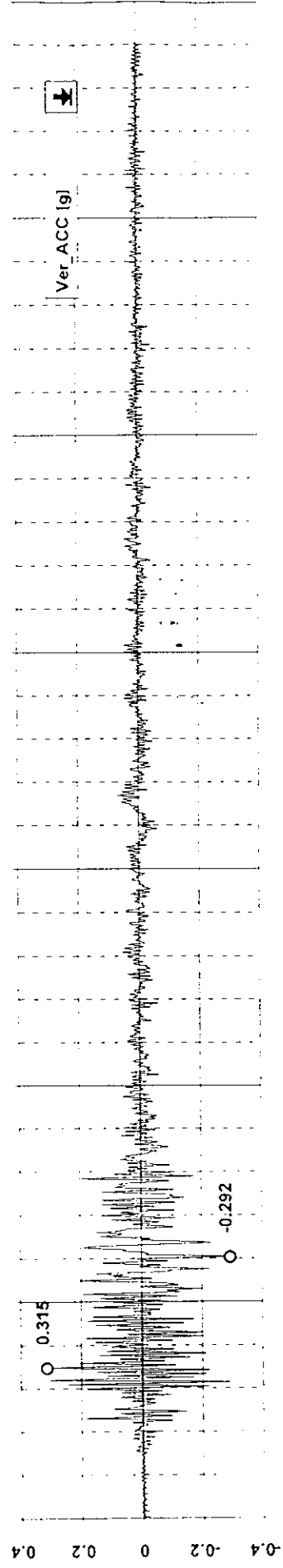
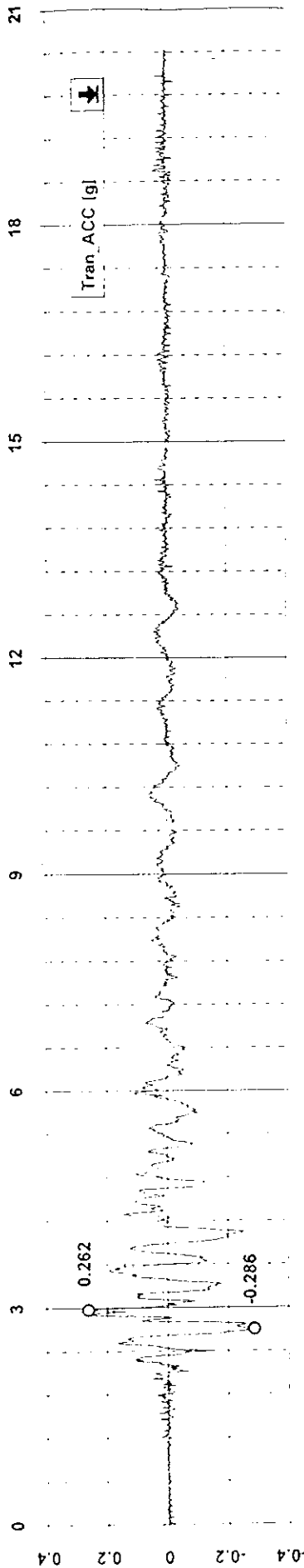


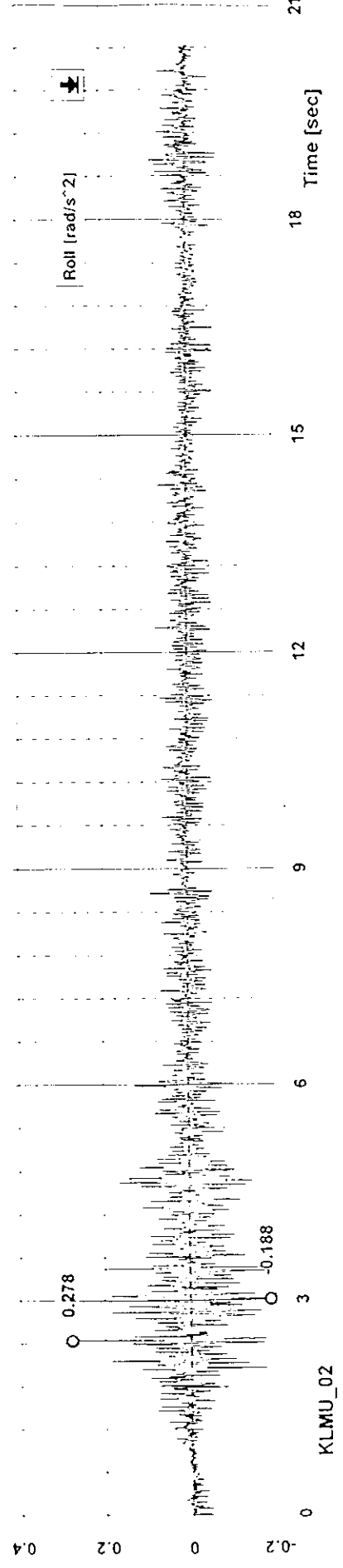
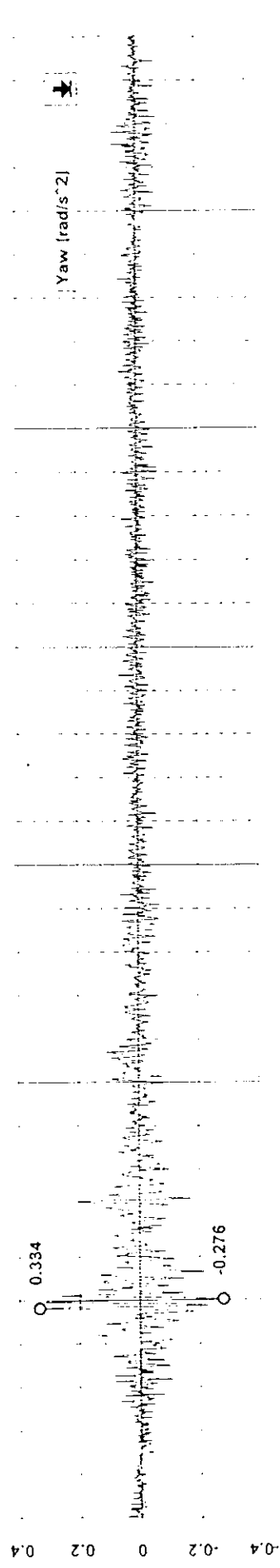
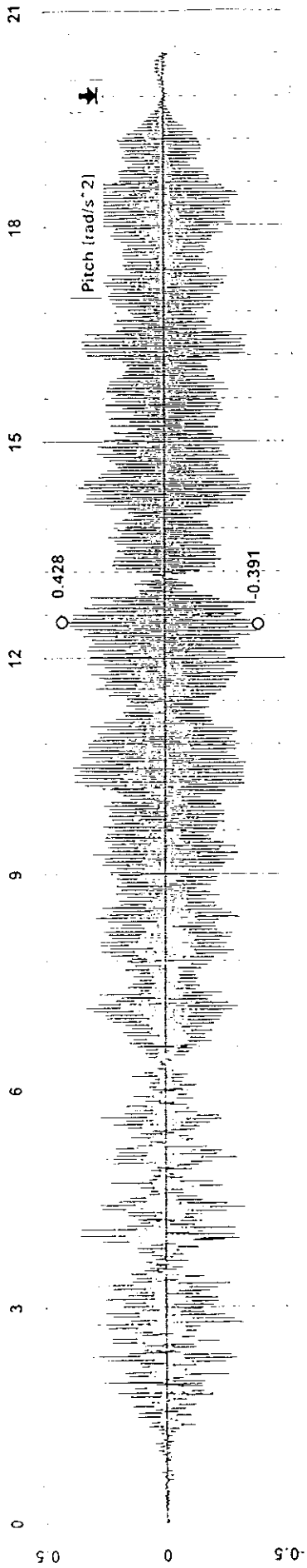


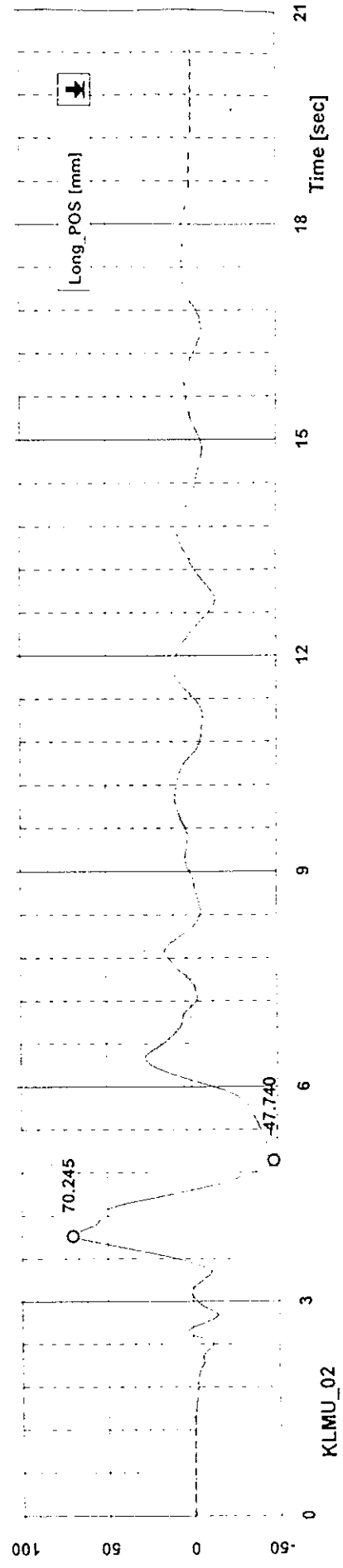
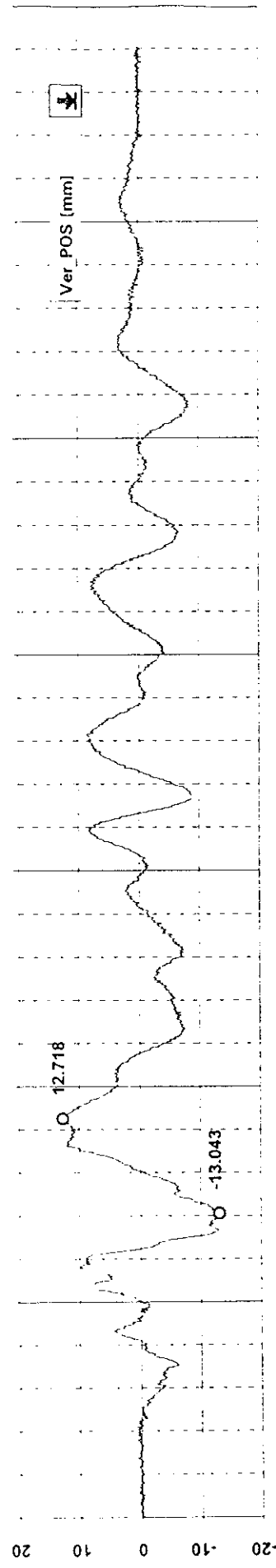
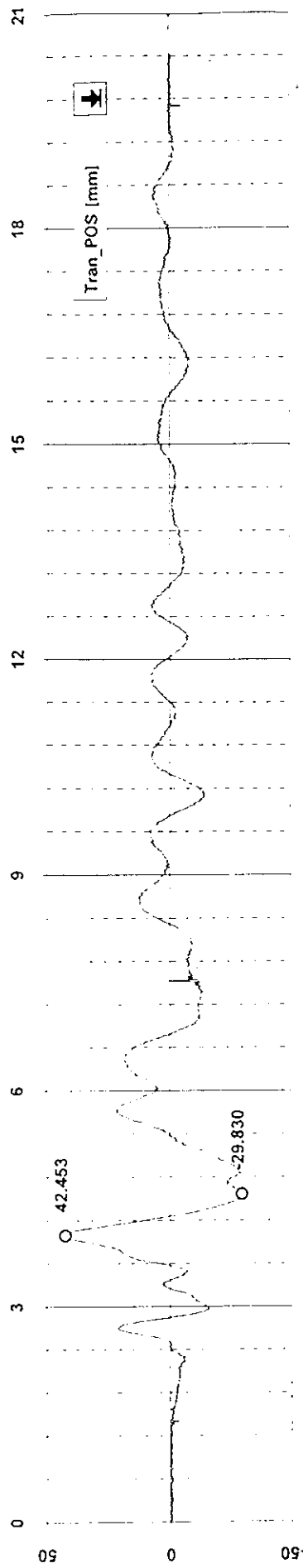


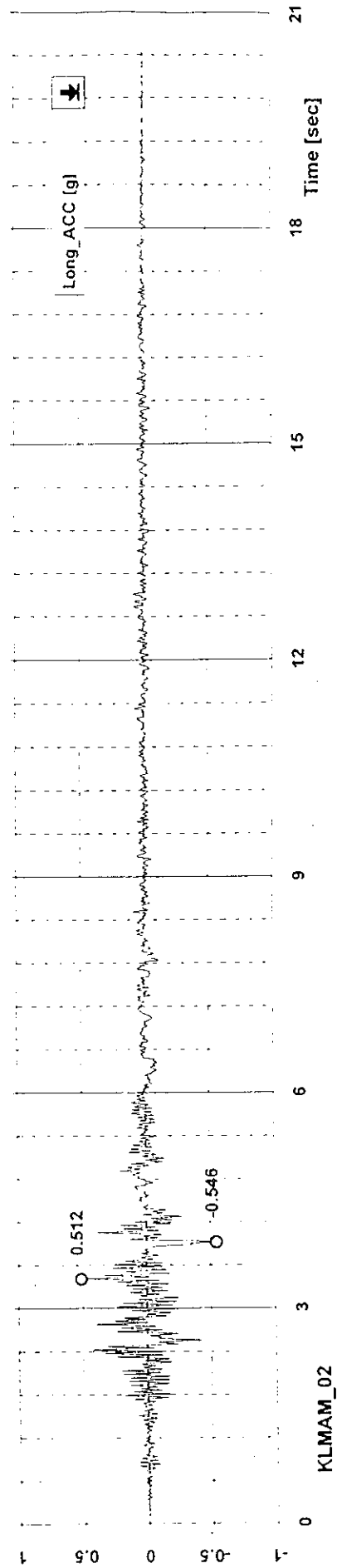
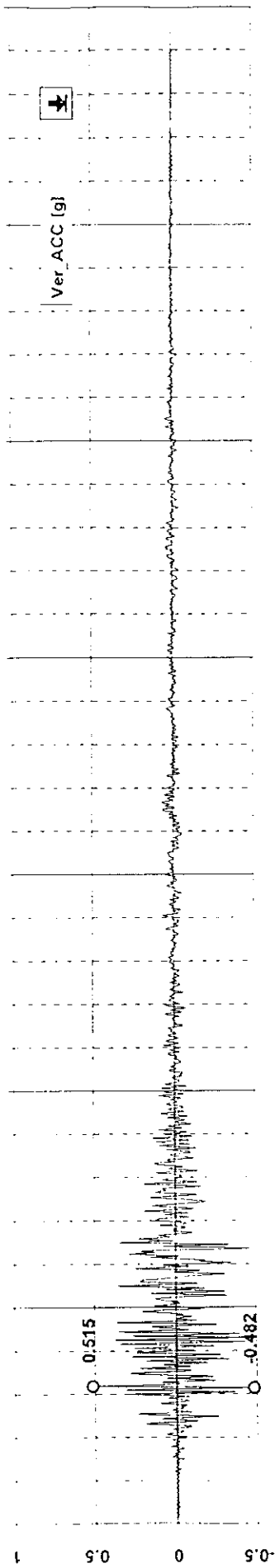
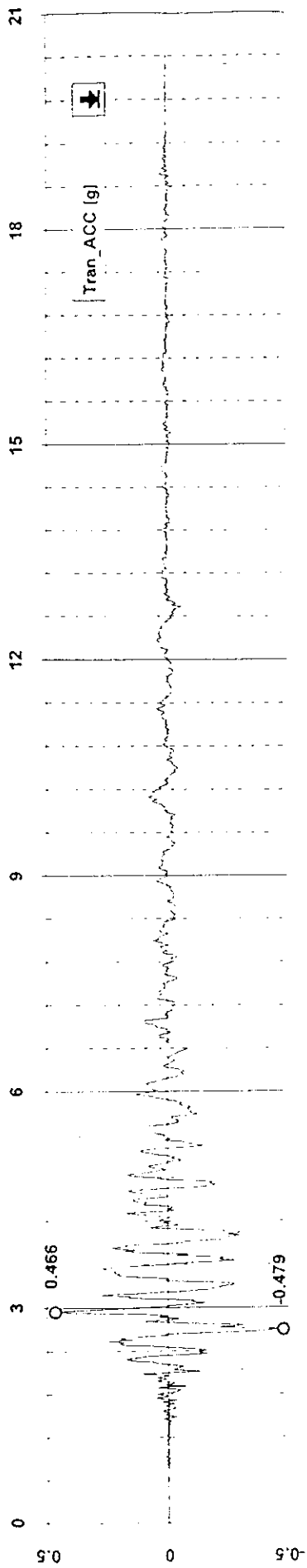


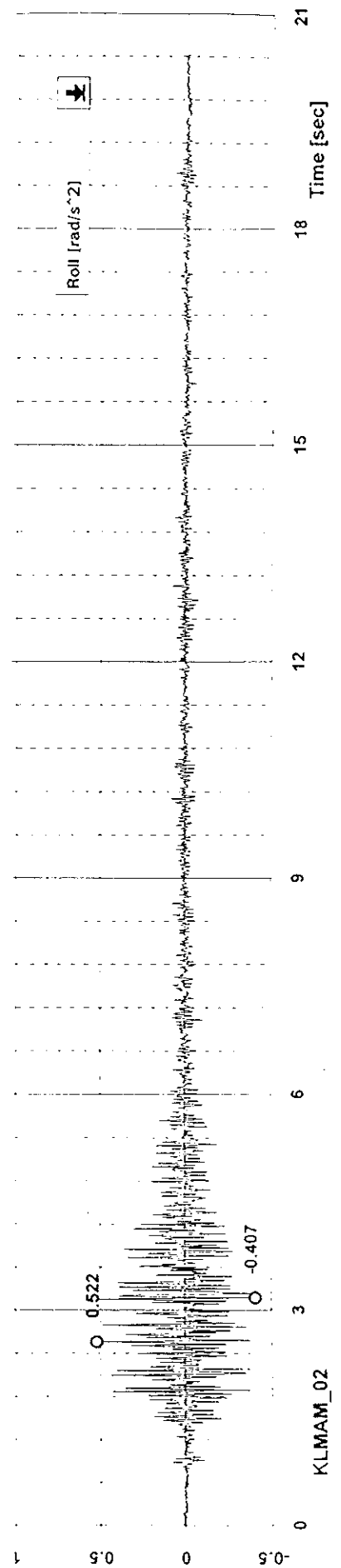
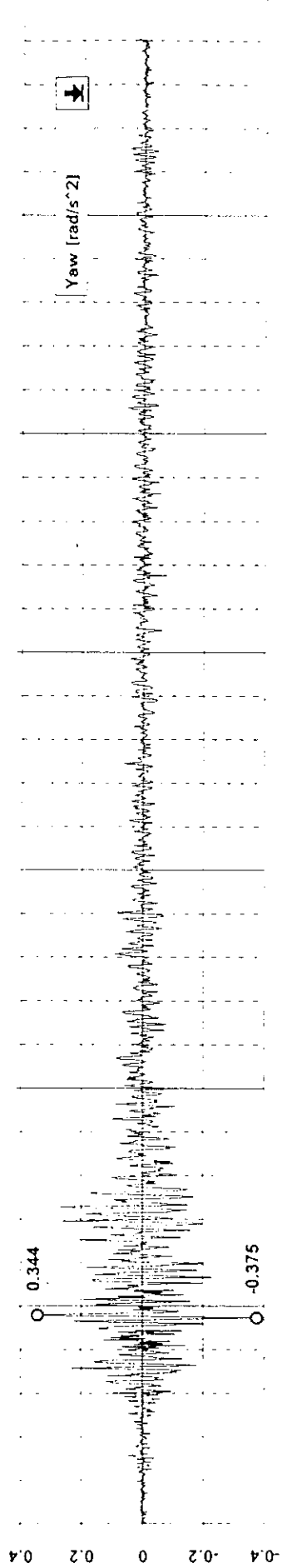
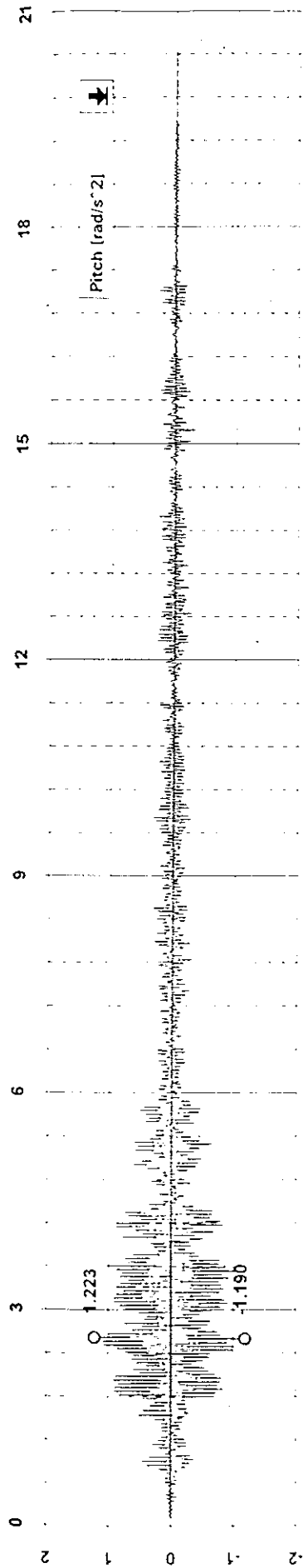


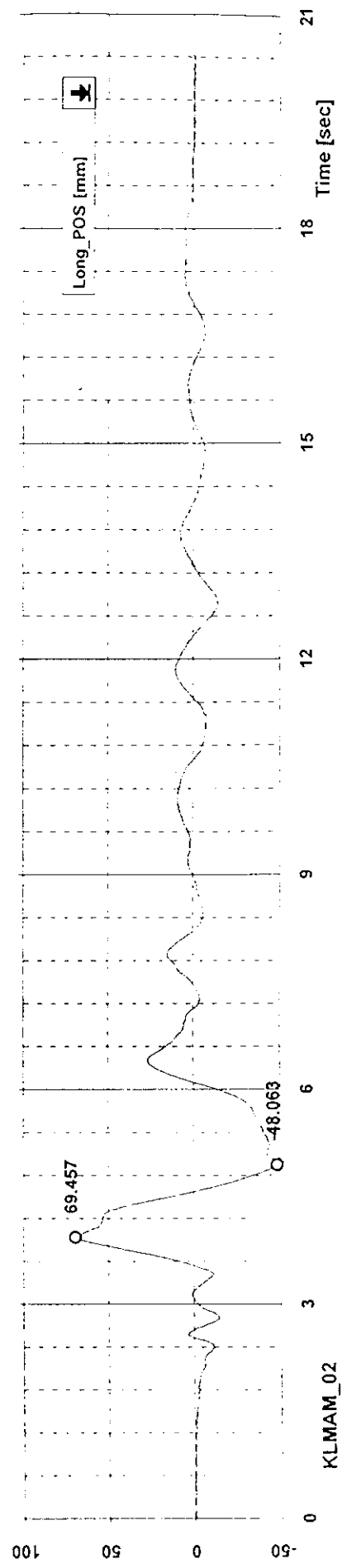
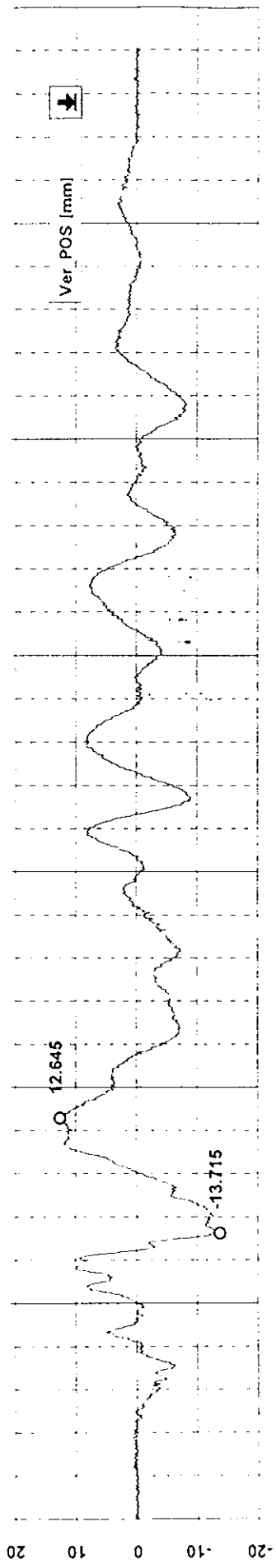
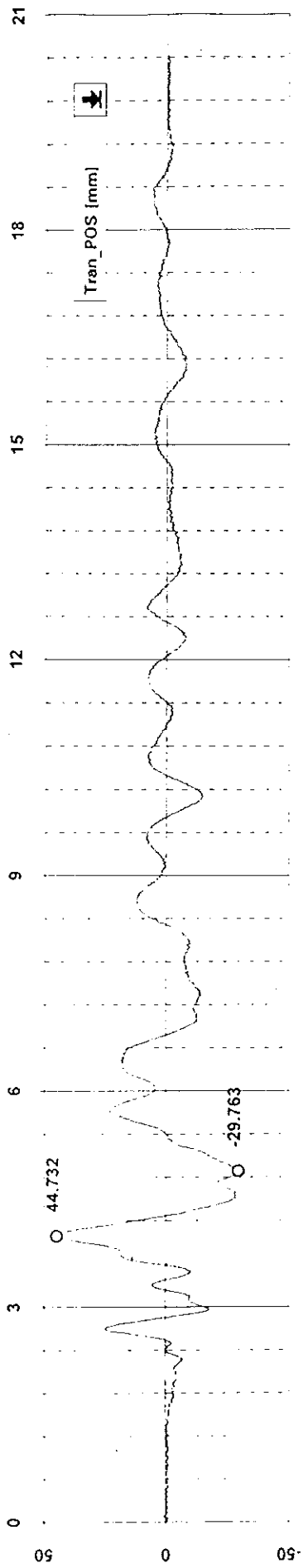


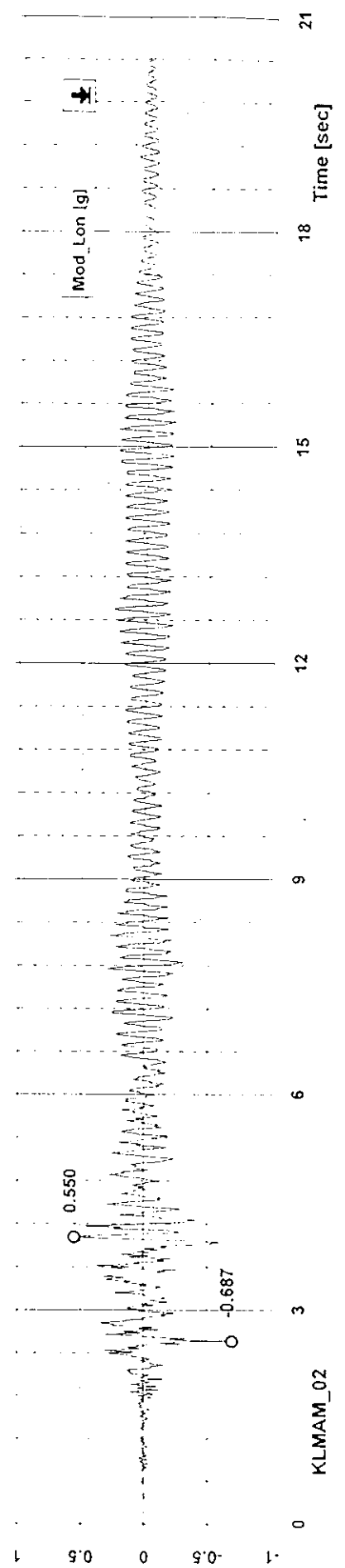
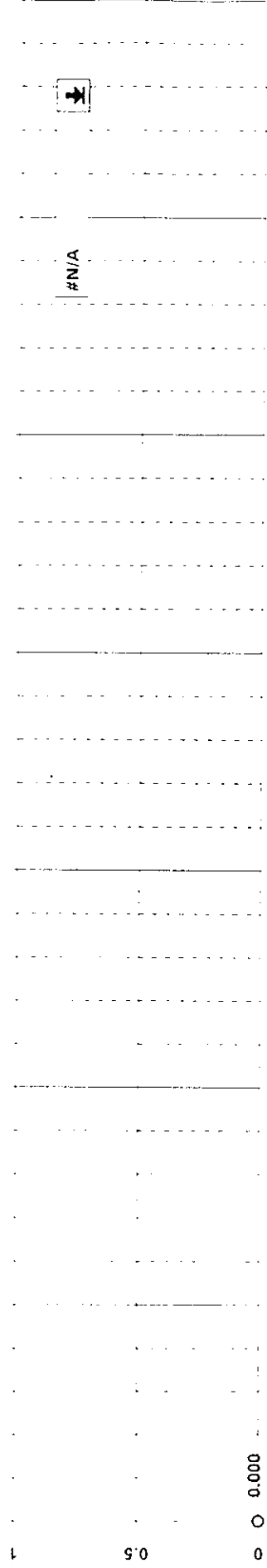
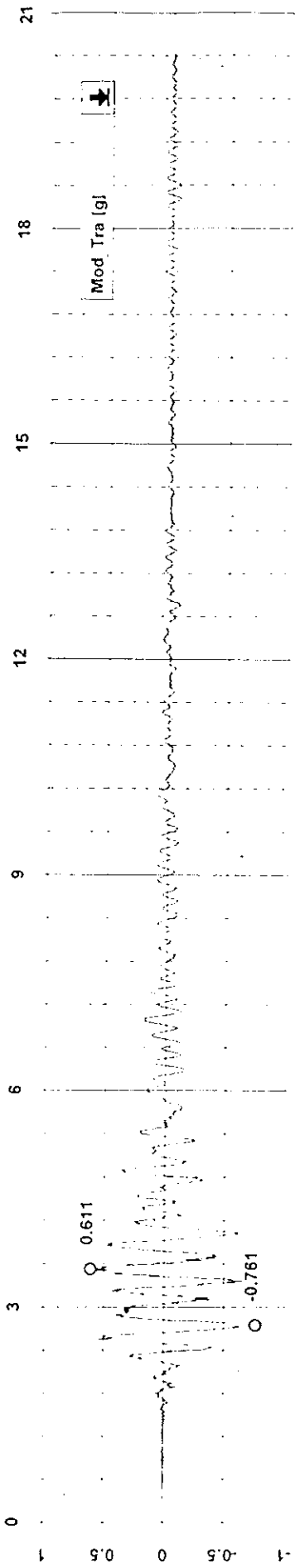












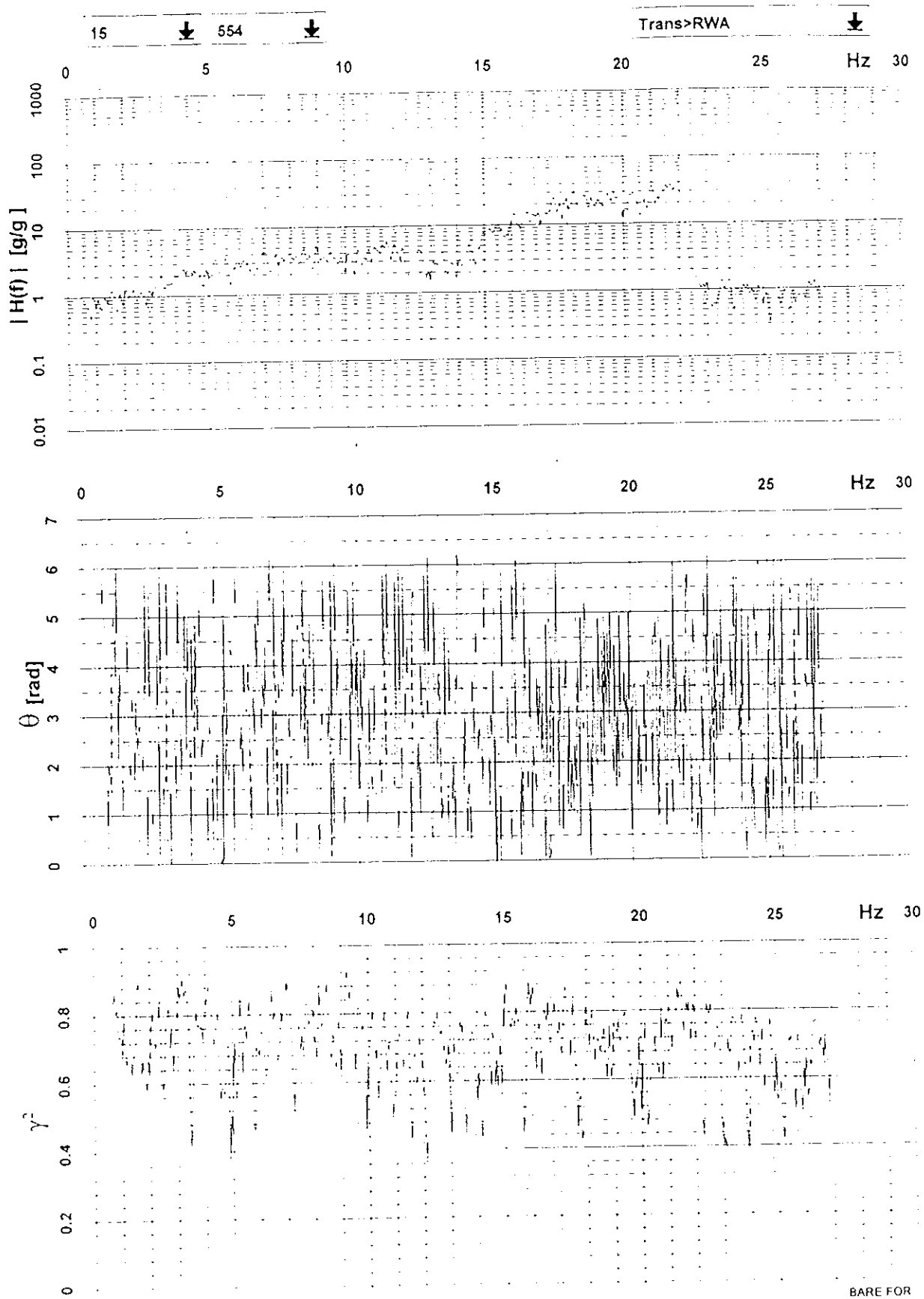
APPENDIX III

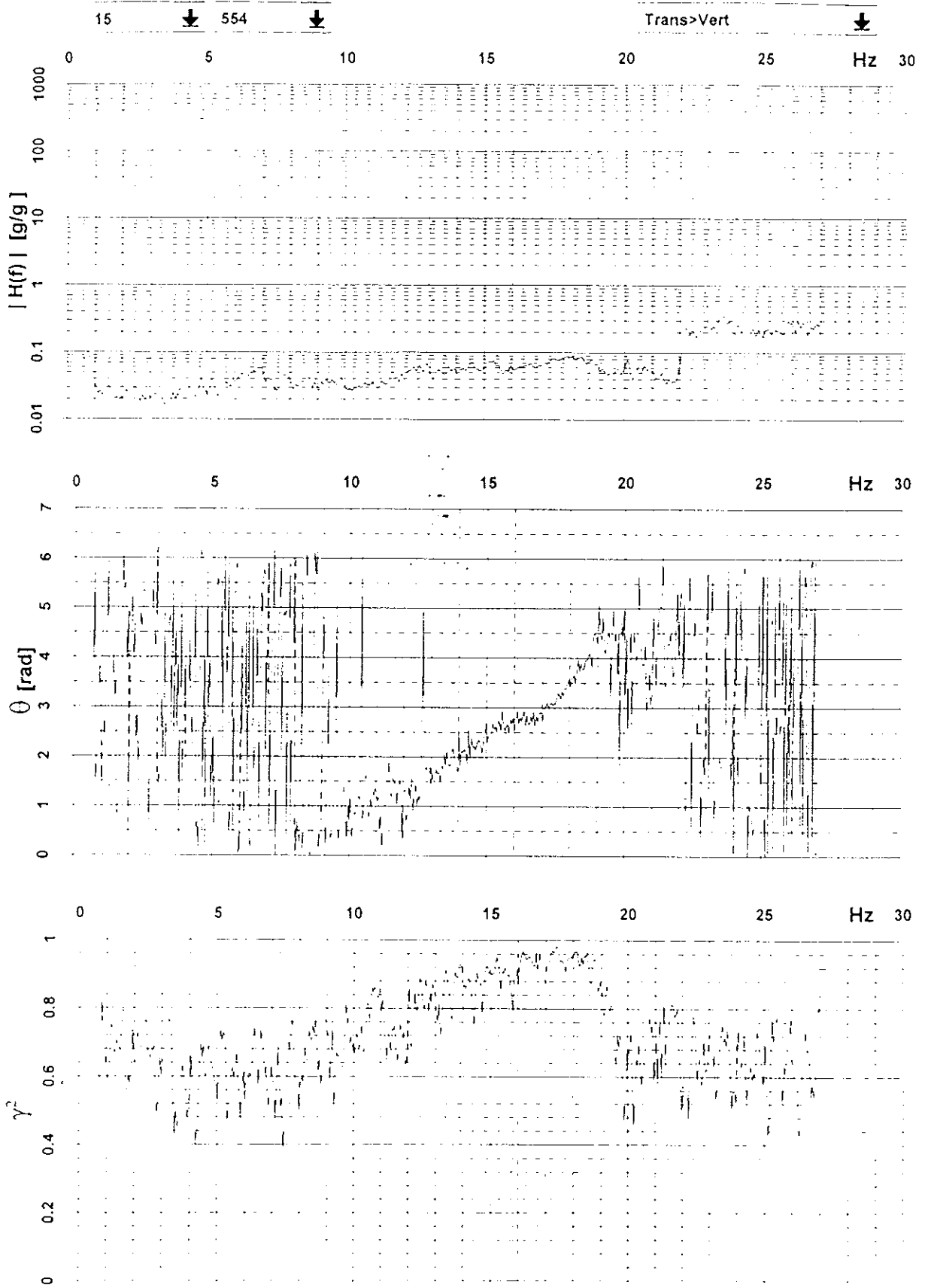
FREQUENCY RESPONSE FUNCTIONS

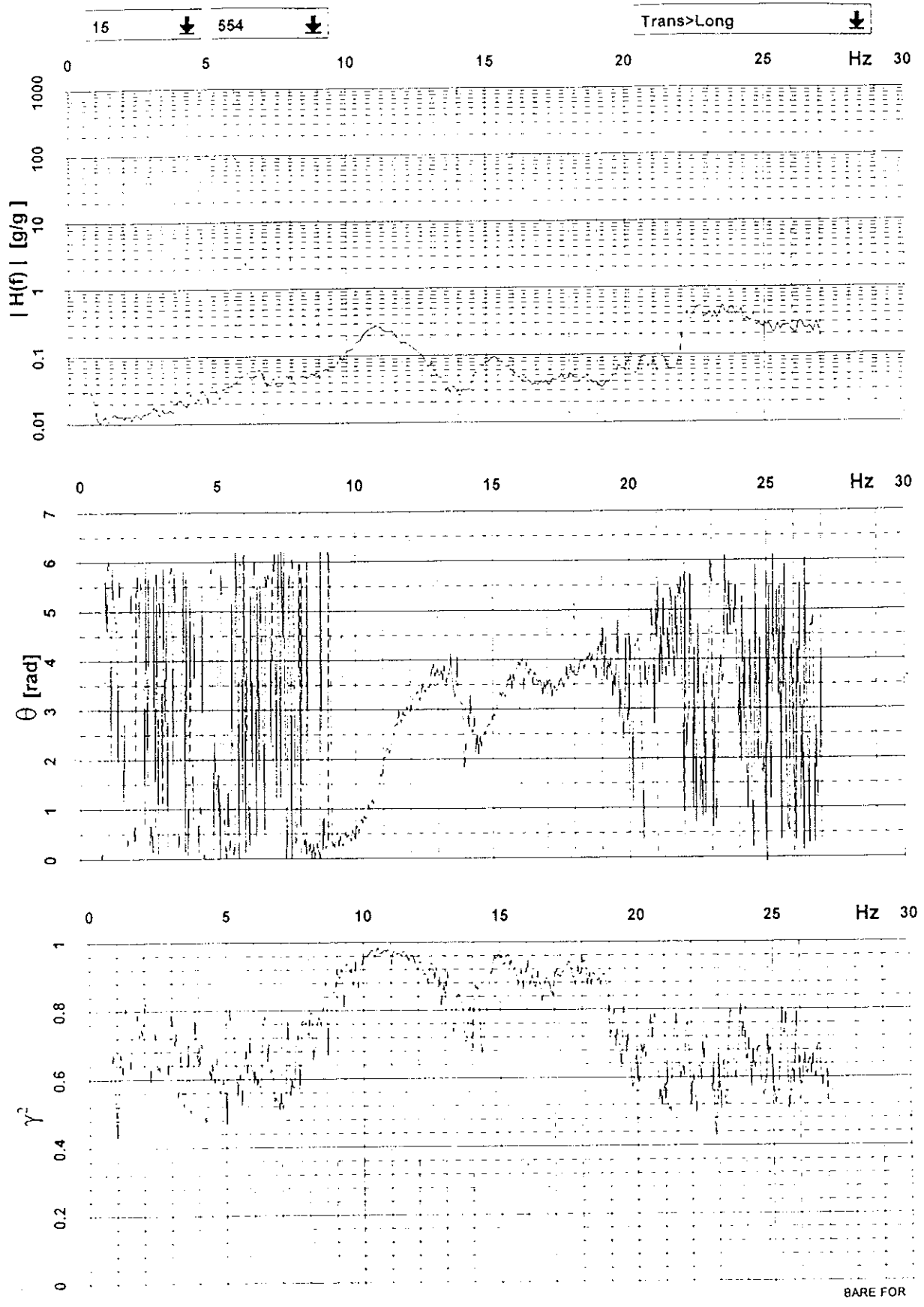
UNADAPTED TEST

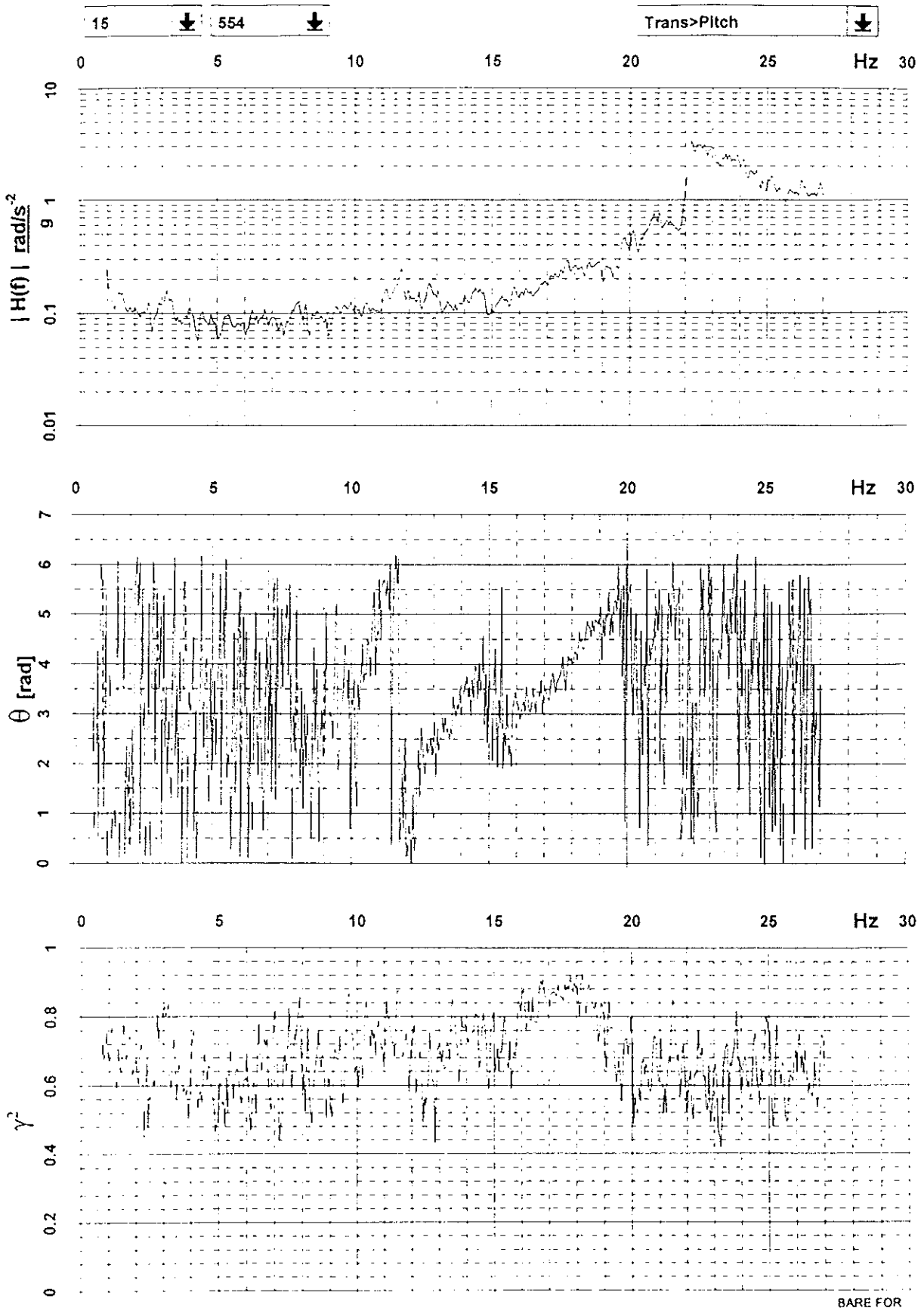
List of Figures

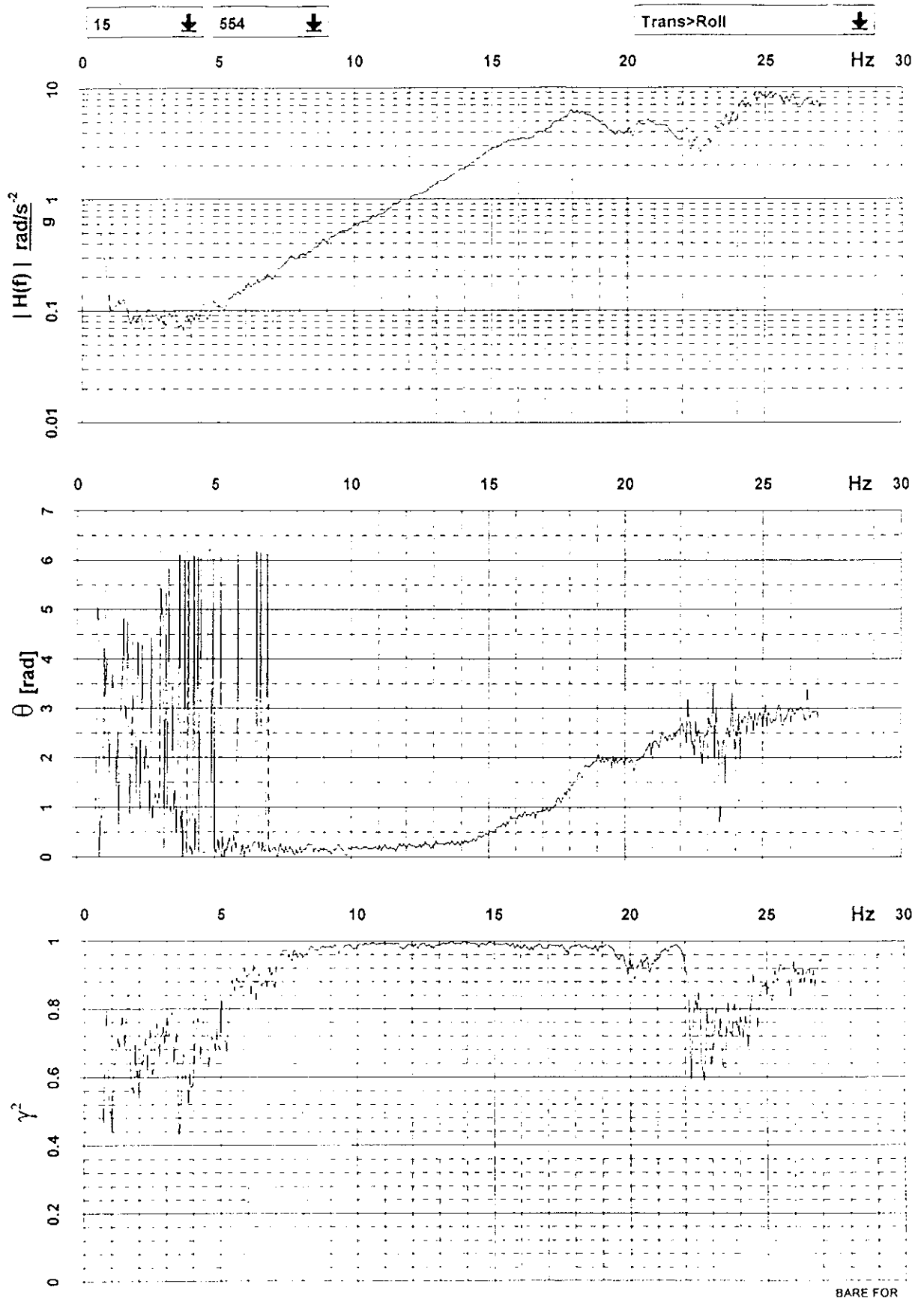
- AIII.1 - Modulus, Phase and Coherence of FRF; input Transverse output Driving Signal
- AIII.2 - Modulus, Phase and Coherence of FRF; input Transverse output Vertical
- AIII.3 - Modulus, Phase and Coherence of FRF; input Transverse output Longitudinal
- AIII.4 - Modulus, Phase and Coherence of FRF; input Transverse output Pitch
- AIII.5 - Modulus, Phase and Coherence of FRF; input Transverse output Roll
- AIII.6 - Modulus, Phase and Coherence of FRF; input Transverse output Yaw
- AIII.7 - Modulus, Phase and Coherence of FRF; input Vertical output Driving Signal
- AIII.8 - Modulus, Phase and Coherence of FRF; input Vertical output Transverse
- AIII.9 - Modulus, Phase and Coherence of FRF; input Vertical output Longitudinal
- AIII.10 - Modulus, Phase and Coherence of FRF; input Vertical output Pitch
- AIII.11 - Modulus, Phase and Coherence of FRF; input Vertical output Roll
- AIII.12 - Modulus, Phase and Coherence of FRF; input Vertical output Yaw
- AIII.13 - Modulus, Phase and Coherence of FRF; input Longitudinal output Driving Signal
- AIII.14 - Modulus, Phase and Coherence of FRF; input Longitudinal output Transverse
- AIII.15 - Modulus, Phase and Coherence of FRF; input Longitudinal output Vertical
- AIII.16 - Modulus, Phase and Coherence of FRF; input Longitudinal output Pitch
- AIII.17 - Modulus, Phase and Coherence of FRF; input Longitudinal output Roll
- AIII.18 - Modulus, Phase and Coherence of FRF; input Longitudinal output Yaw
- AIII.19 - Modulus, Phase and Coherence of FRF; input Transverse output Driving Signal in displacements
- AIII.20 - Modulus, Phase and Coherence of FRF; input Vertical output Driving Signal in displacements
- AIII.21 - Modulus, Phase and Coherence of FRF; input Longitudinal output Driving Signal in displacements

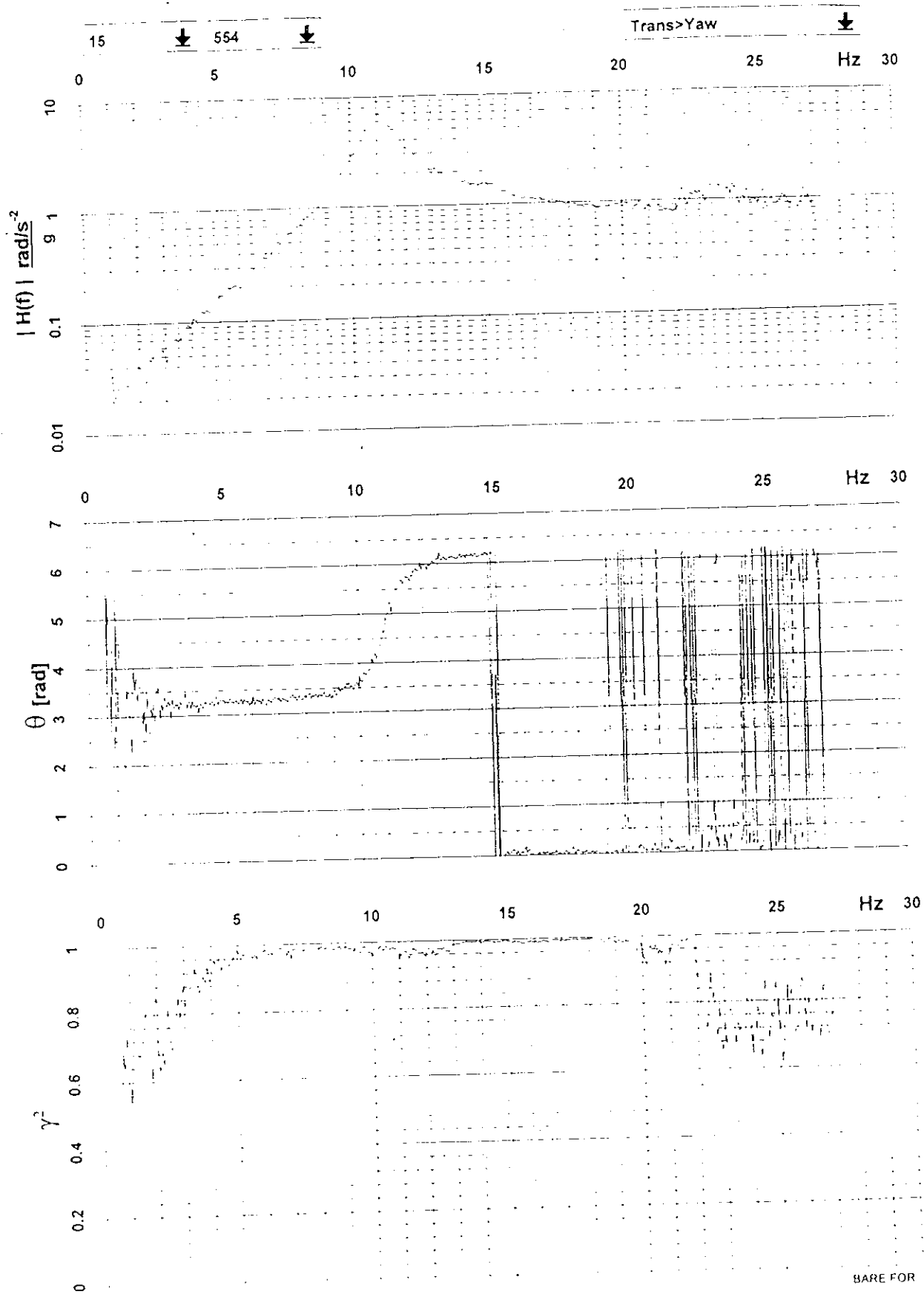




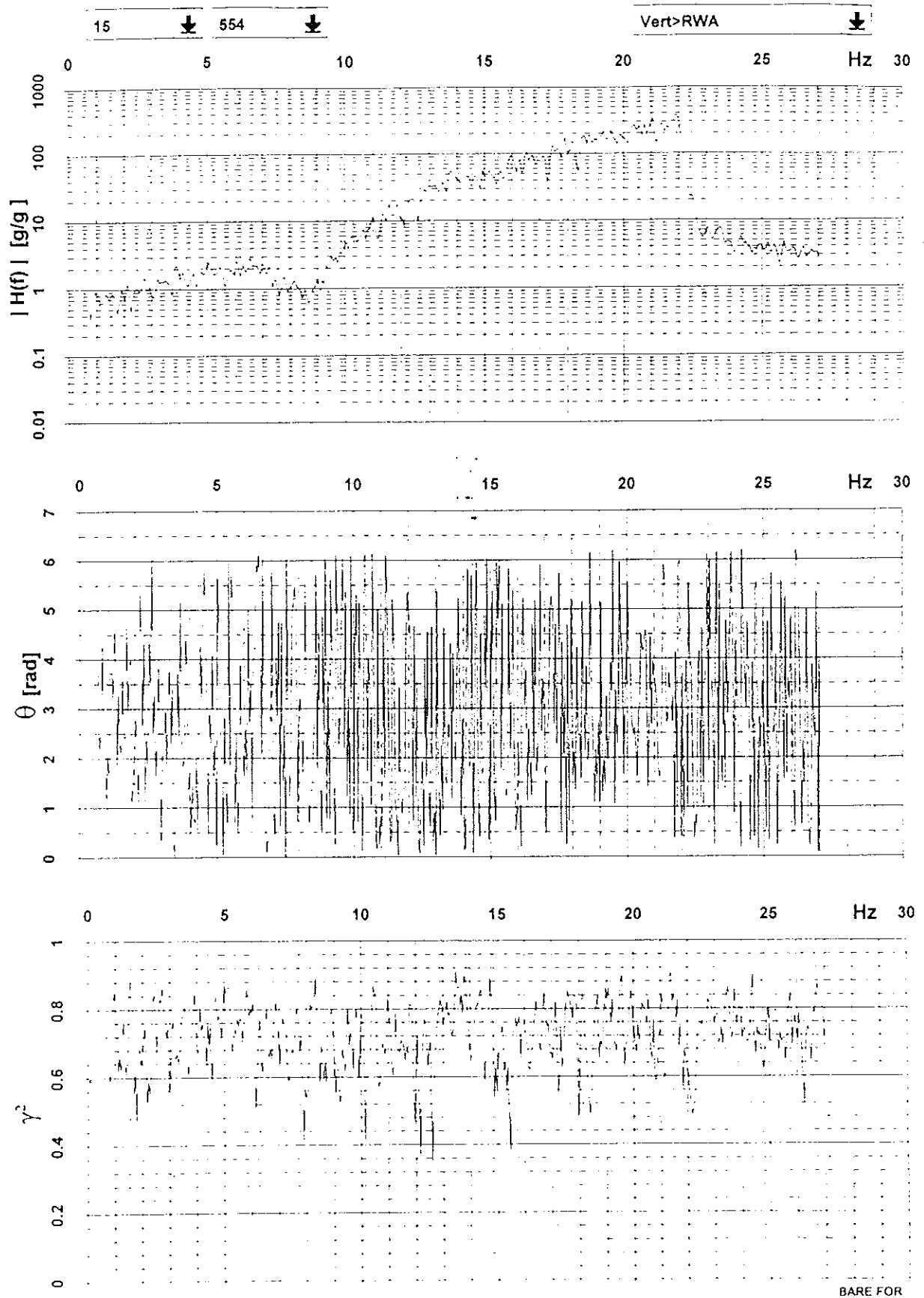


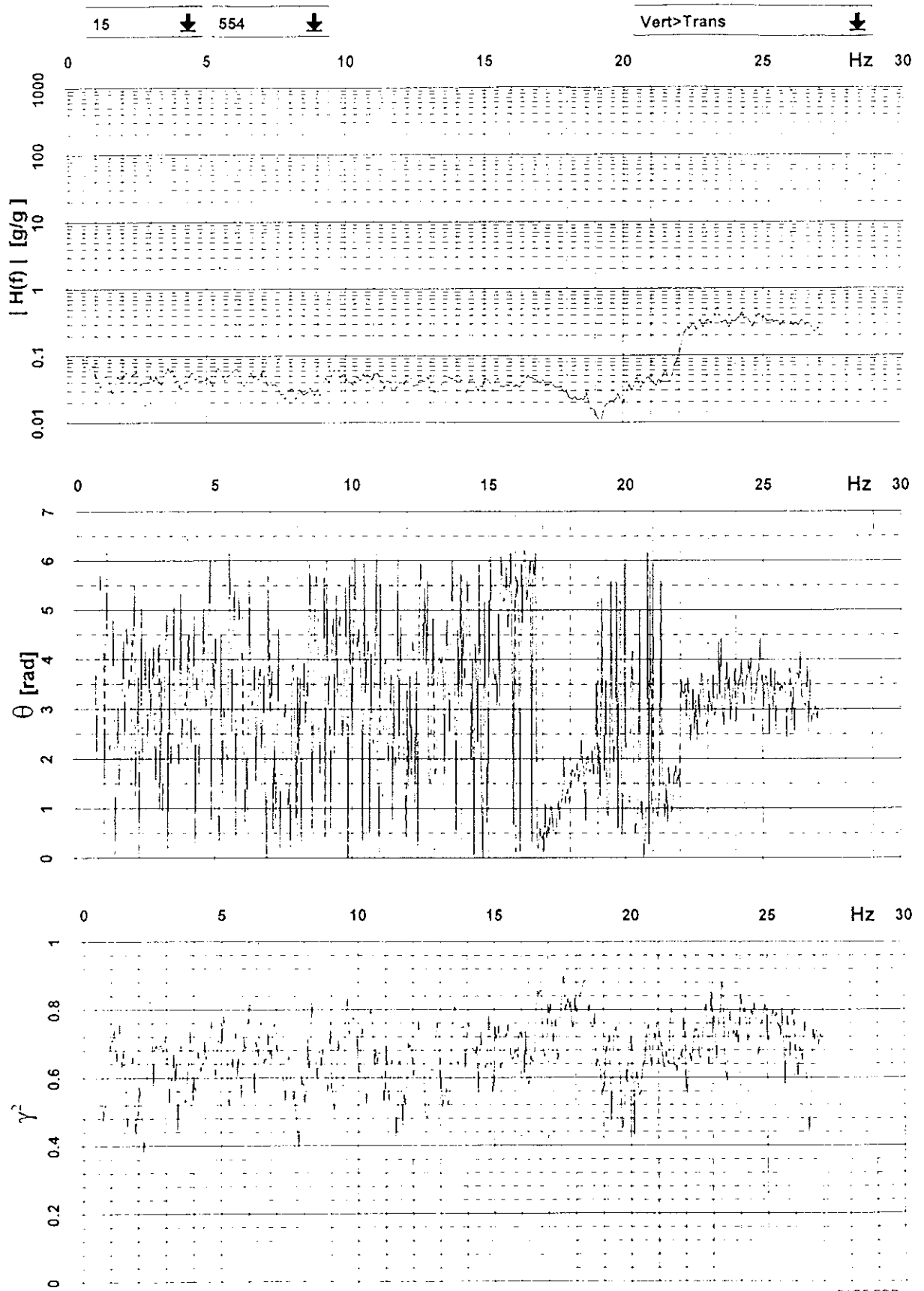


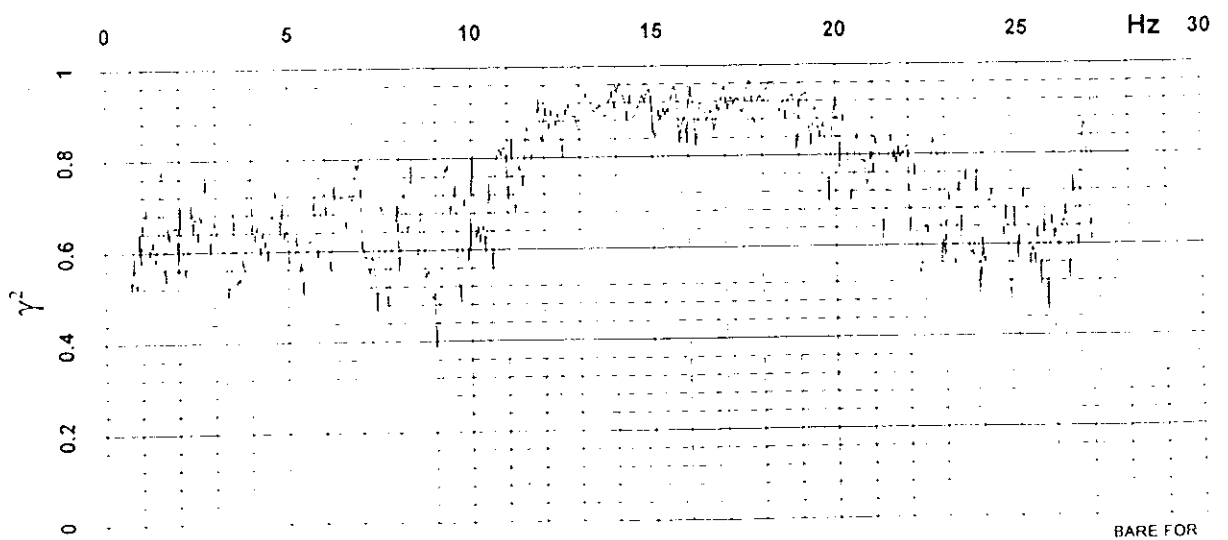
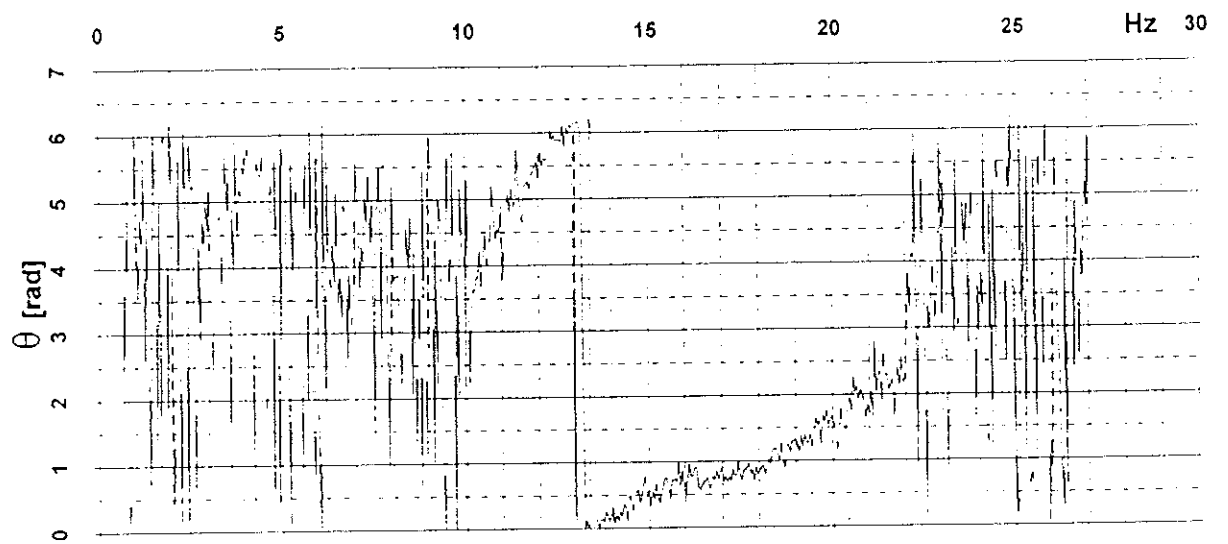
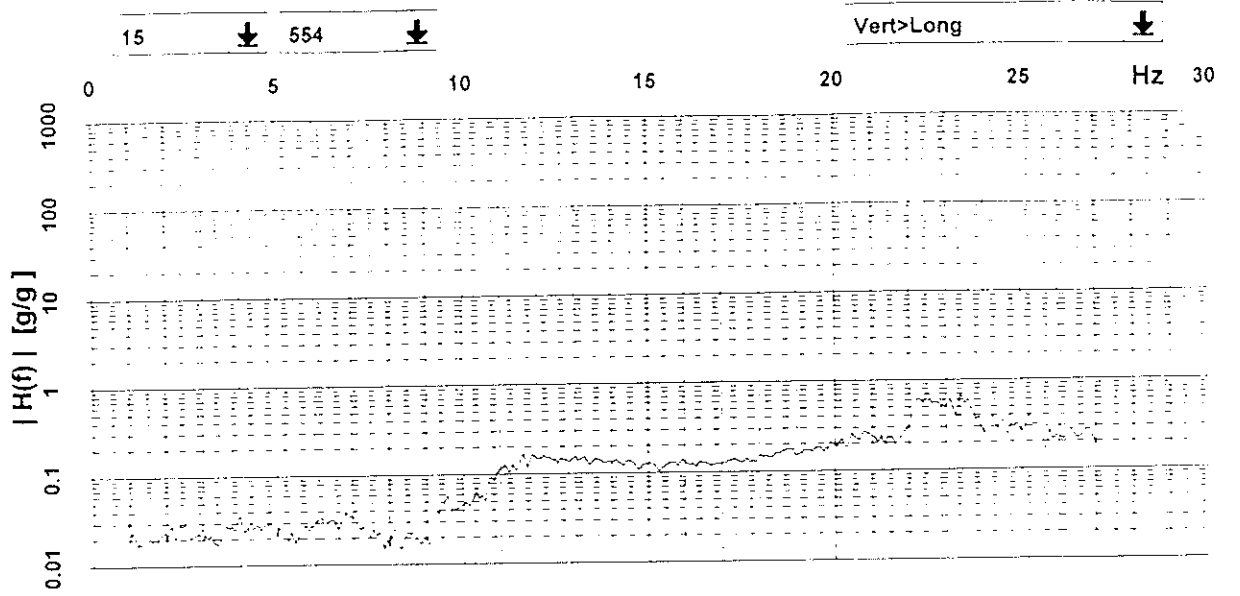




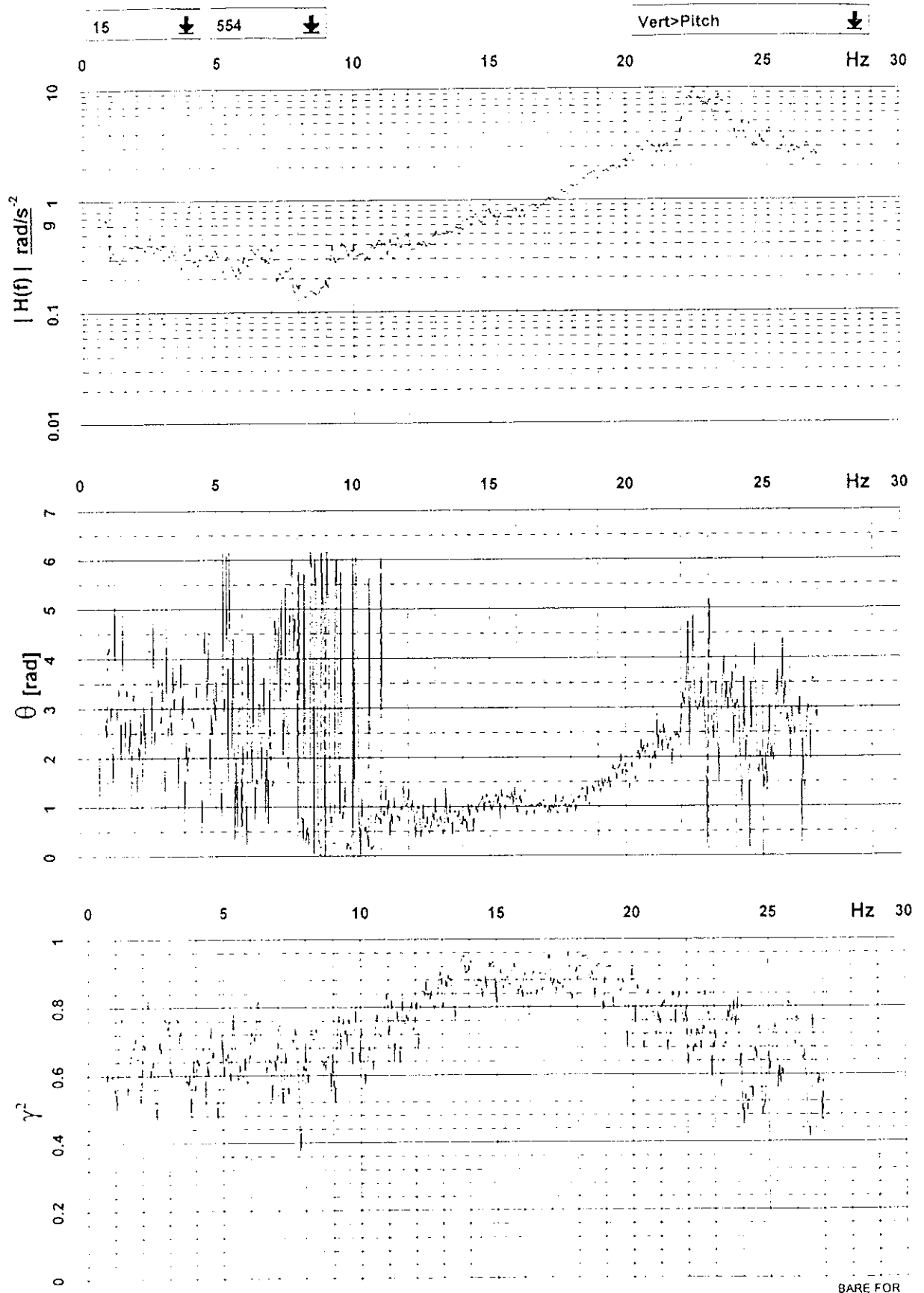
BARE FOR

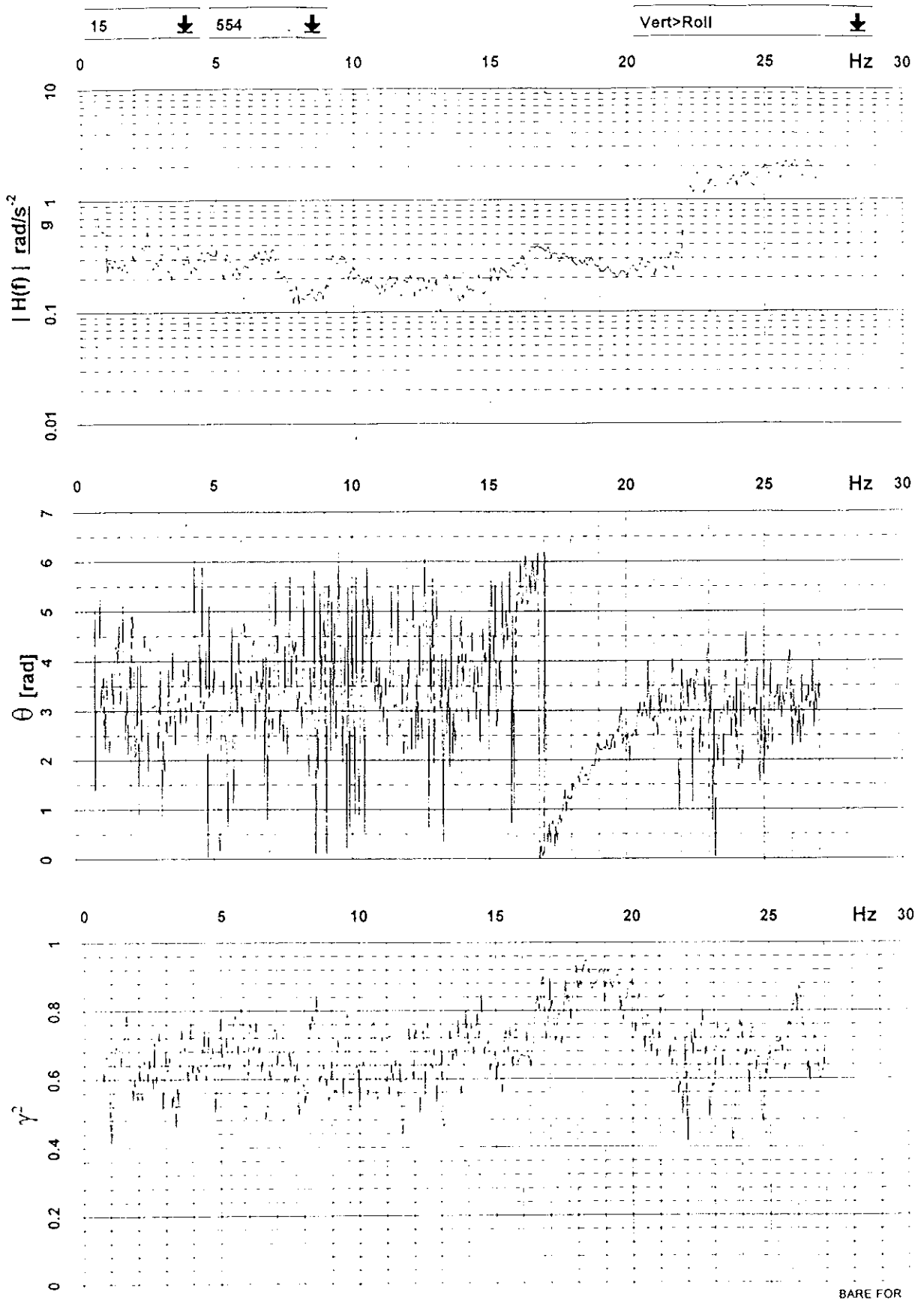


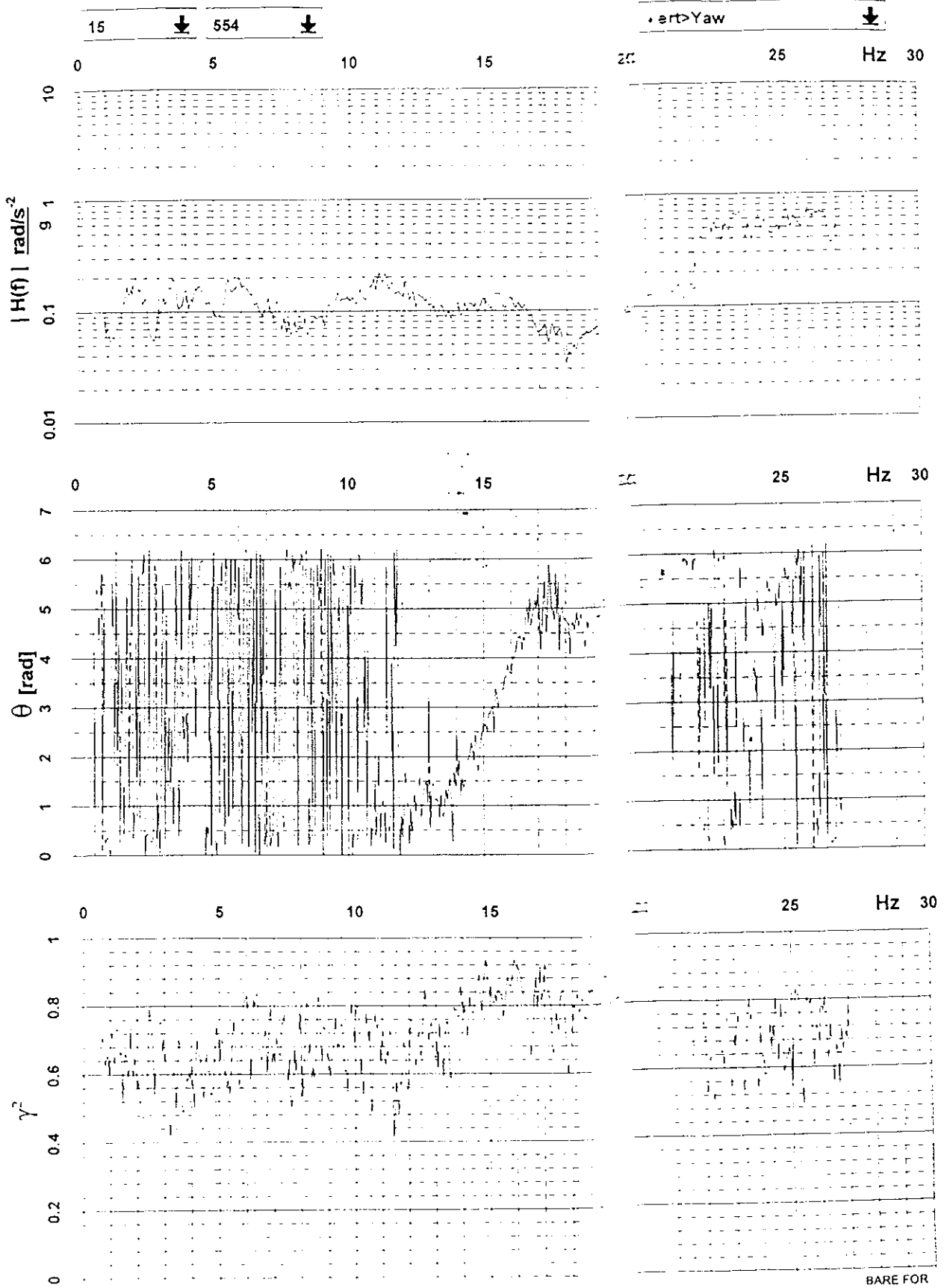




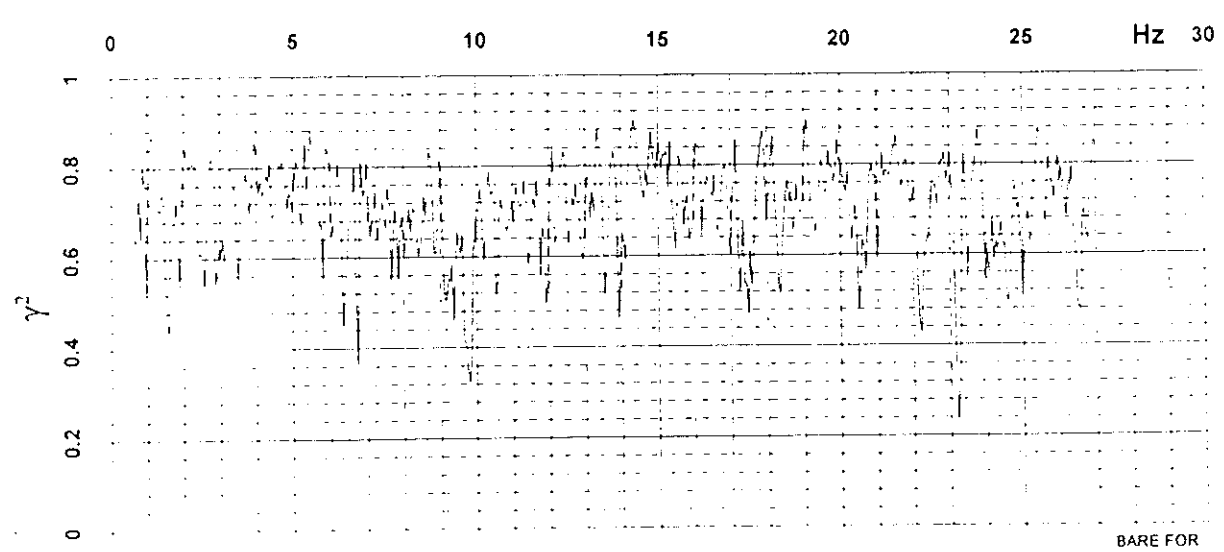
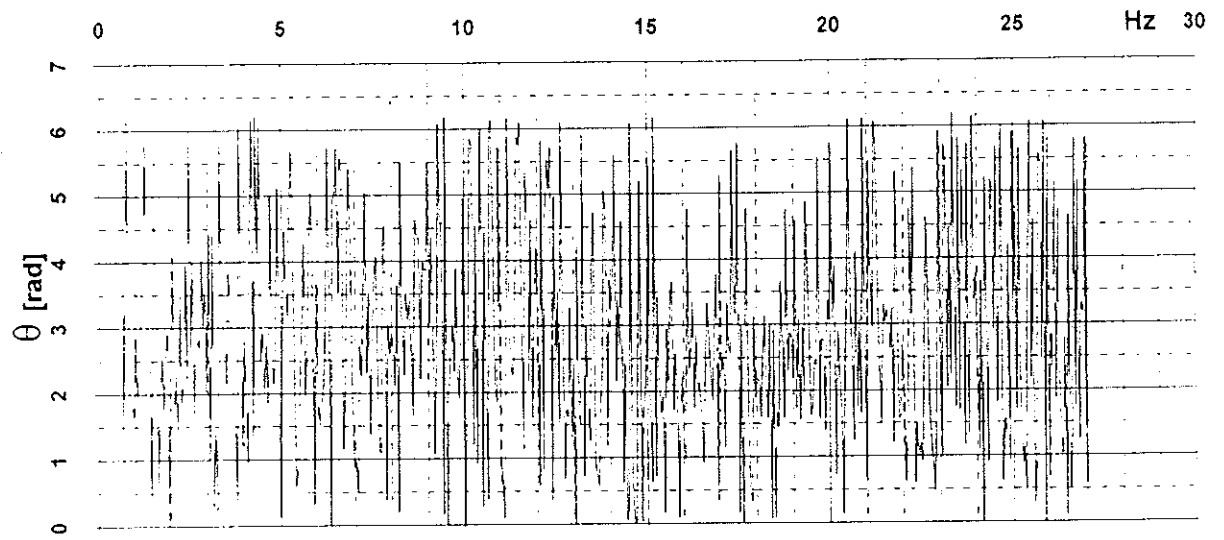
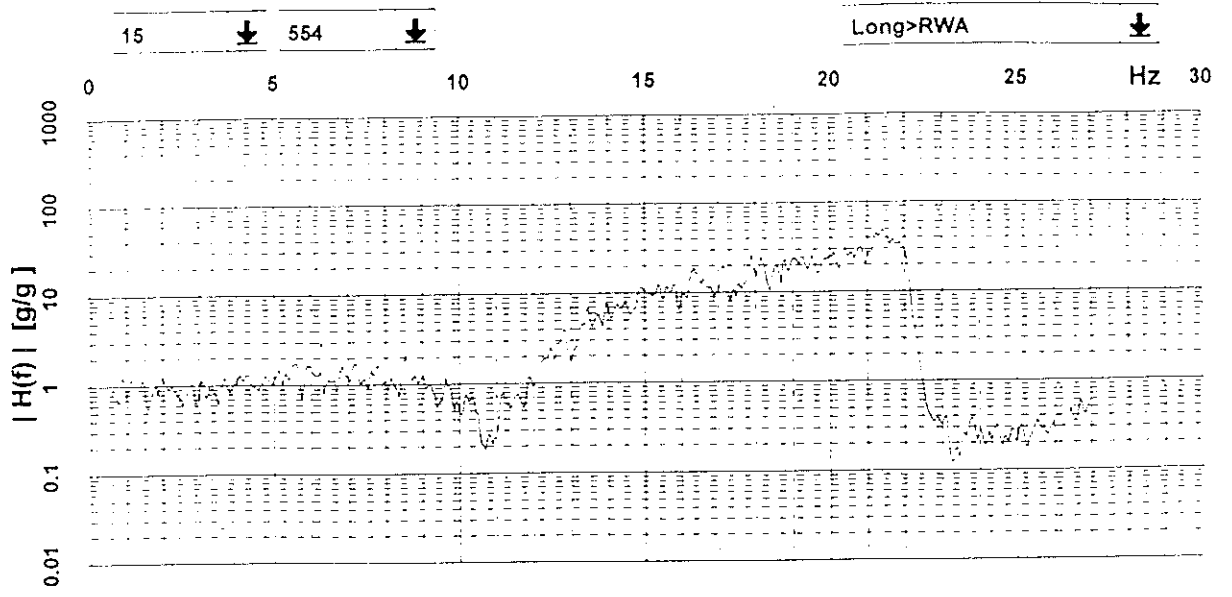
BARE FOR



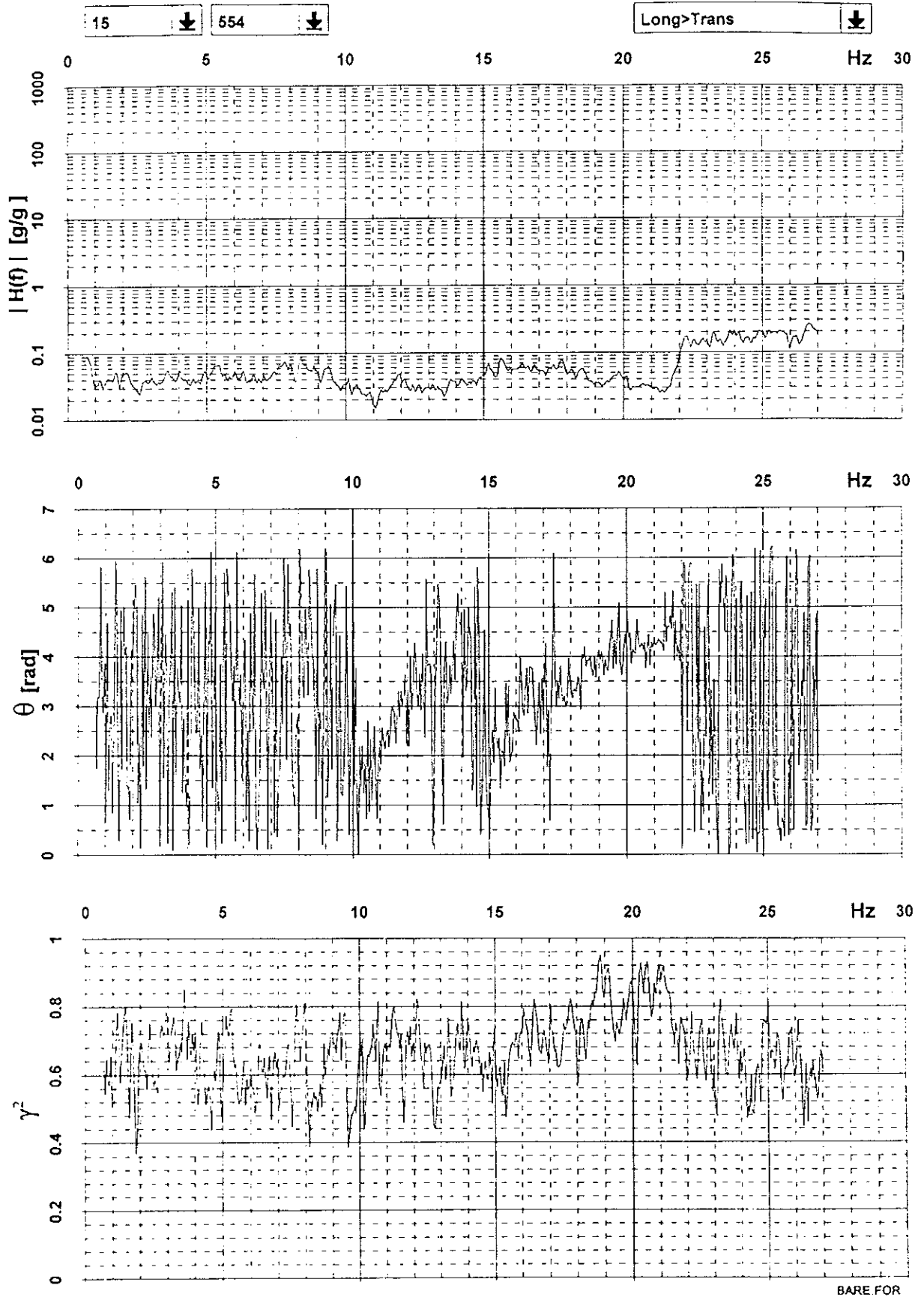




BARE FOR

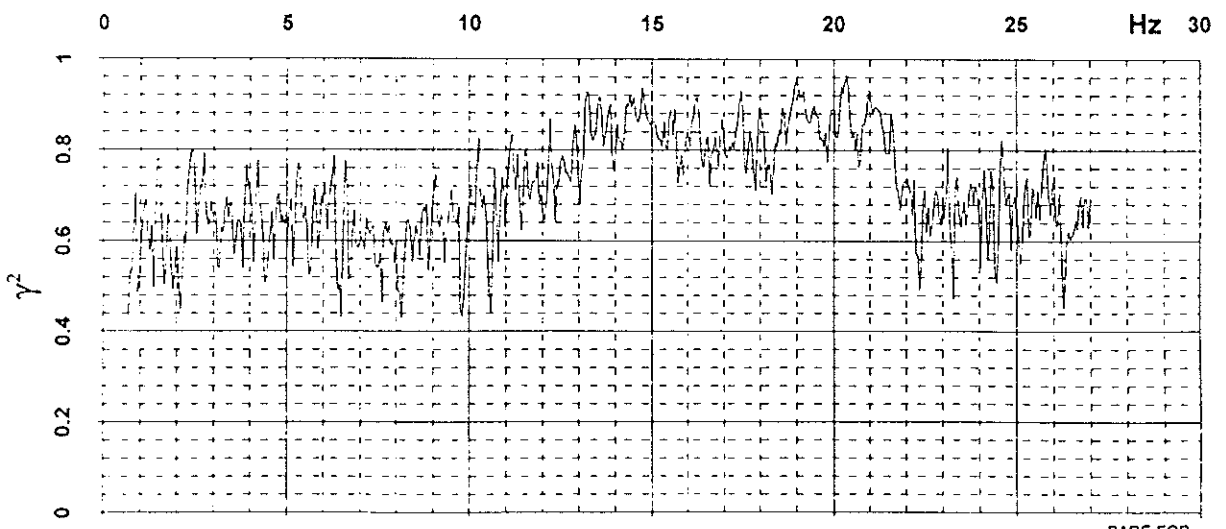
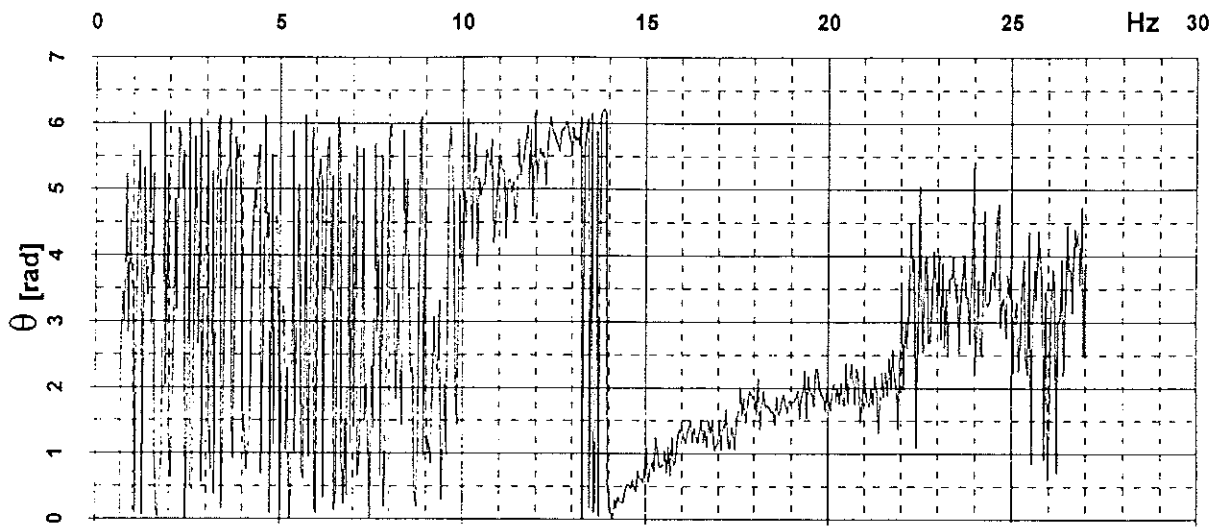
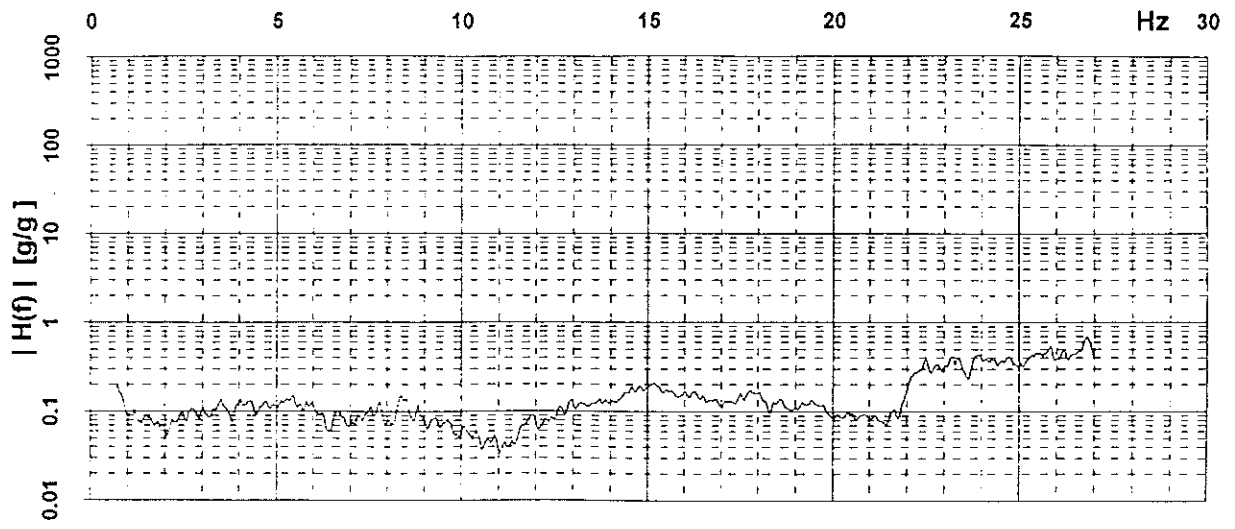


BARE FOR

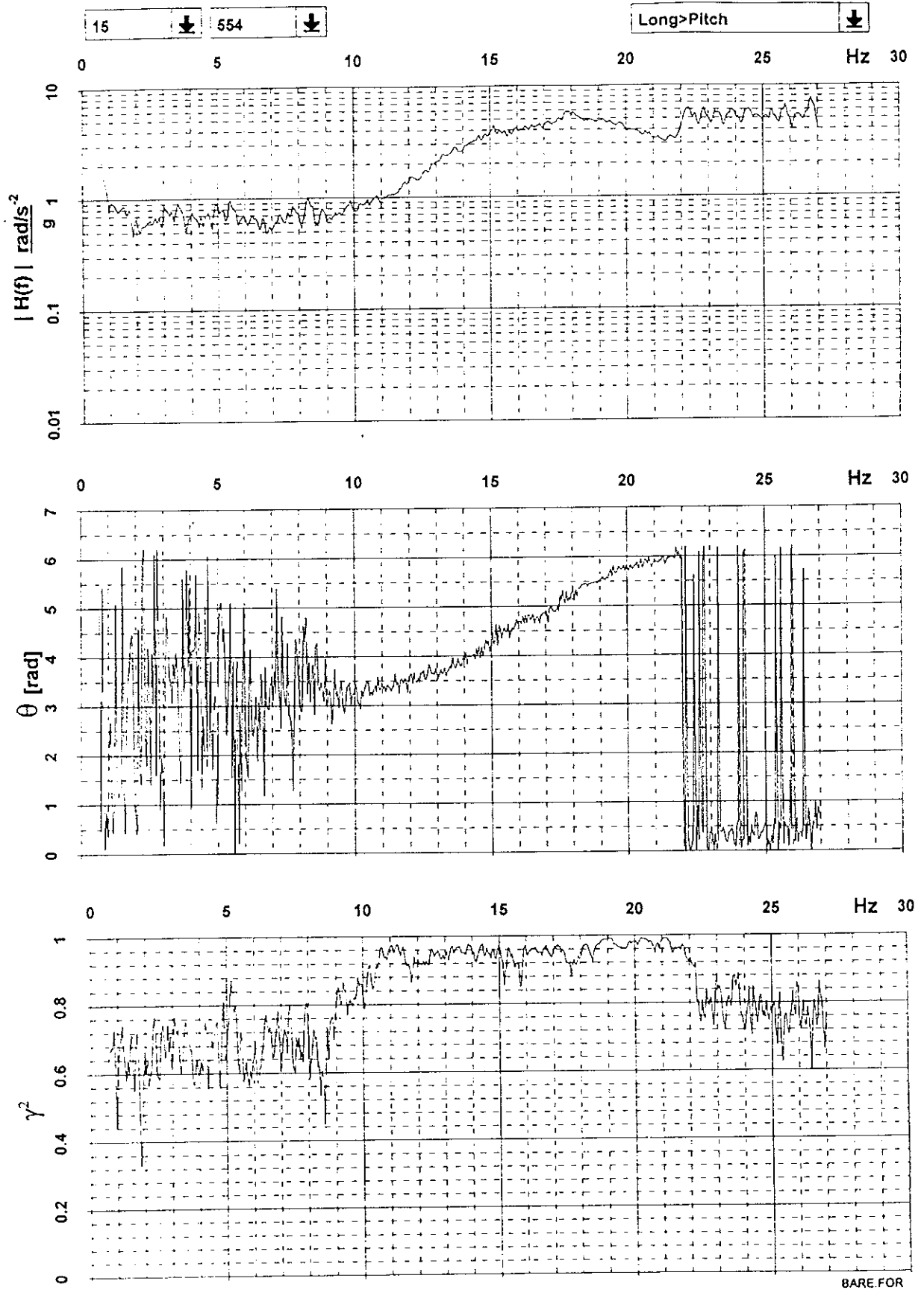


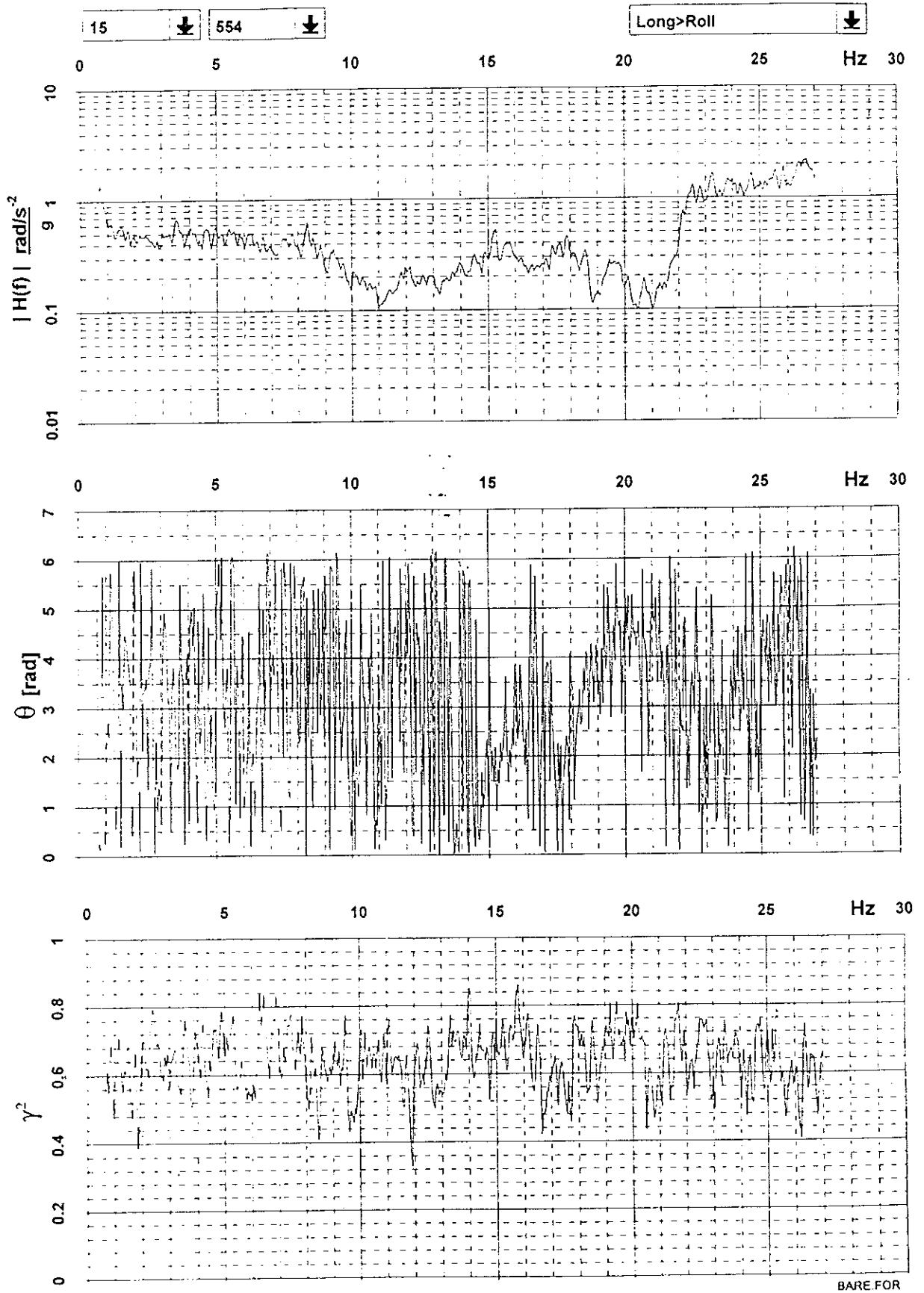
15 ↓ 554 ↓

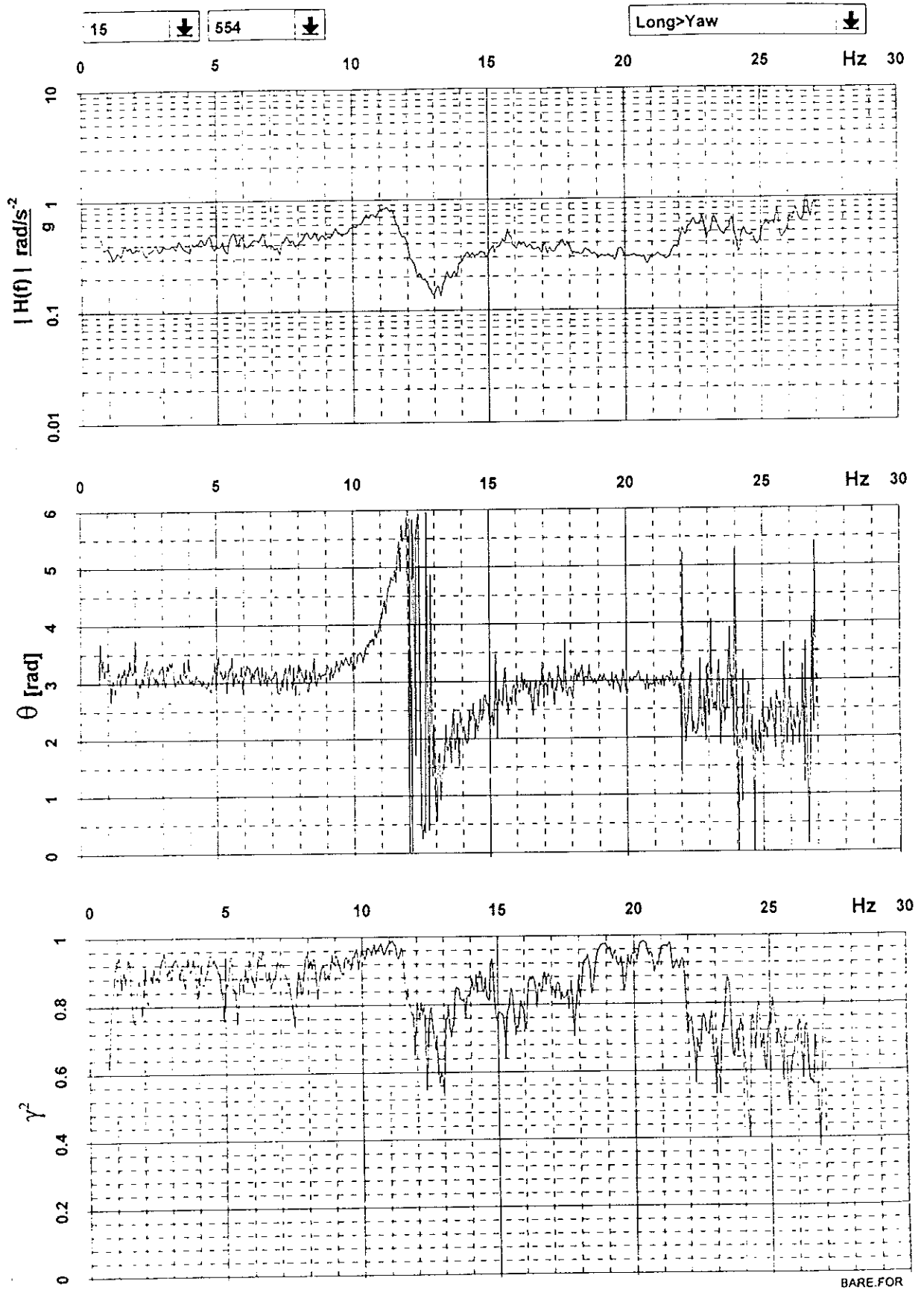
Long>Vert ↓



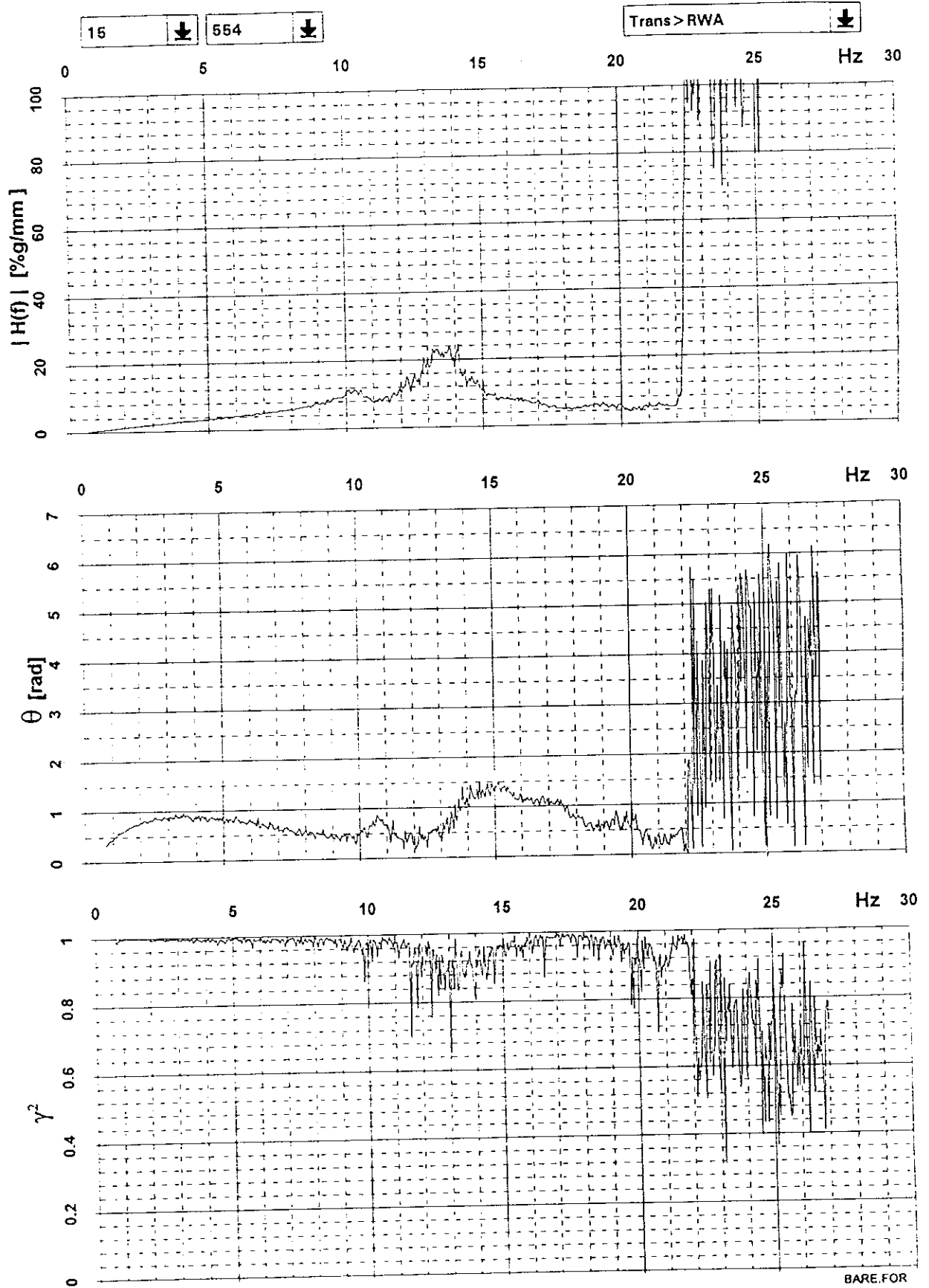
BARE.FOR

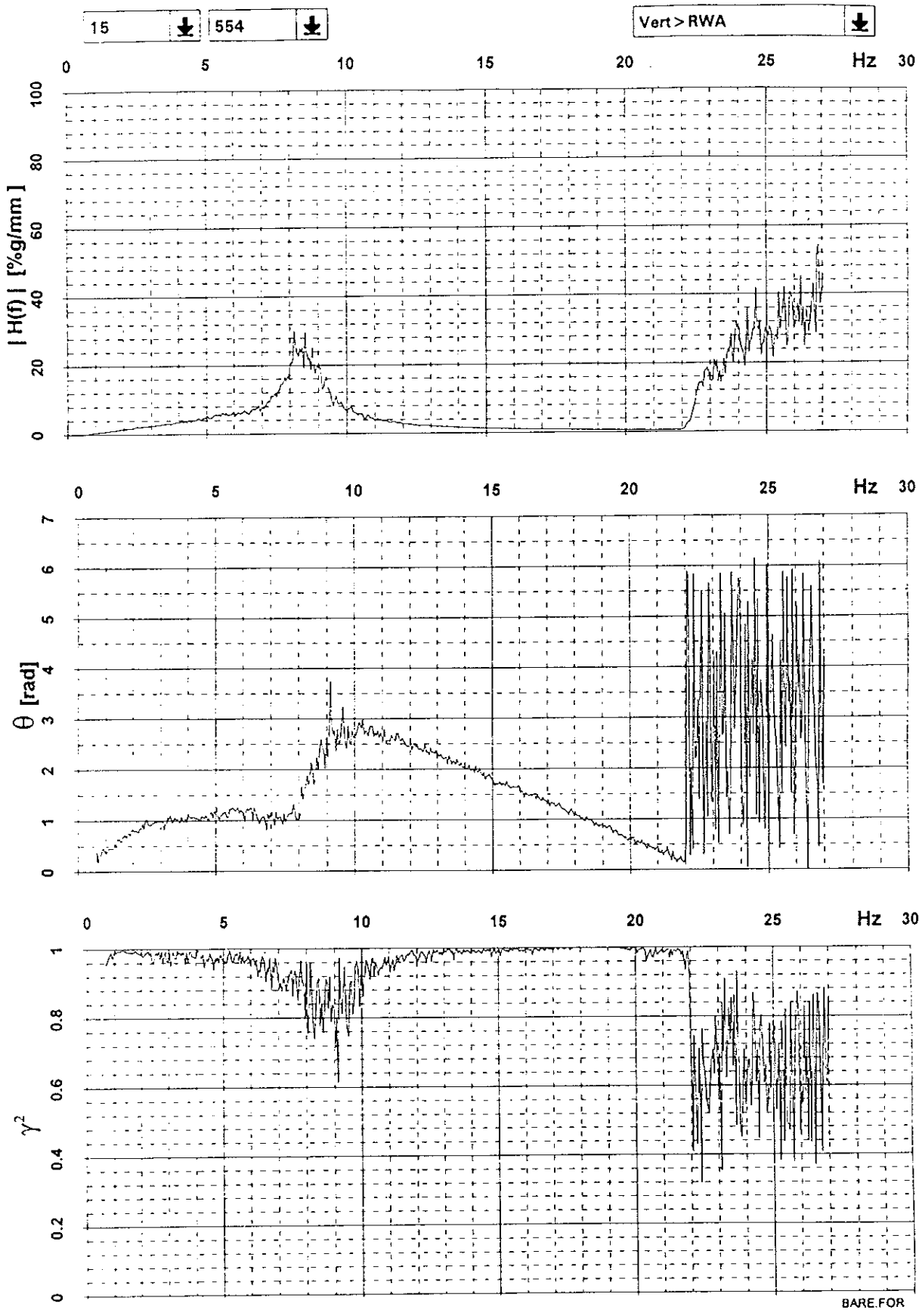






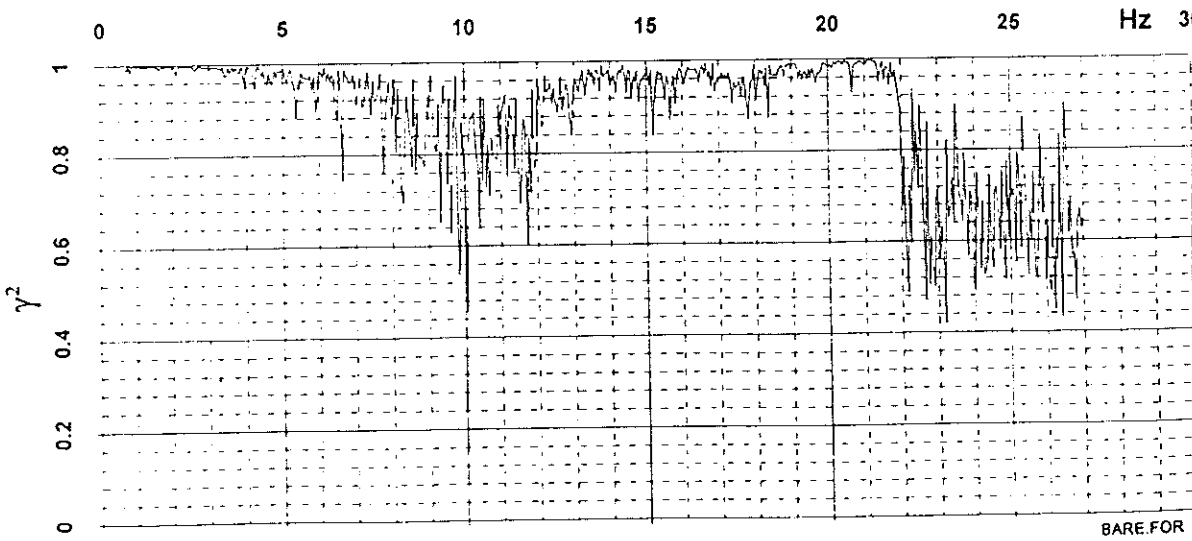
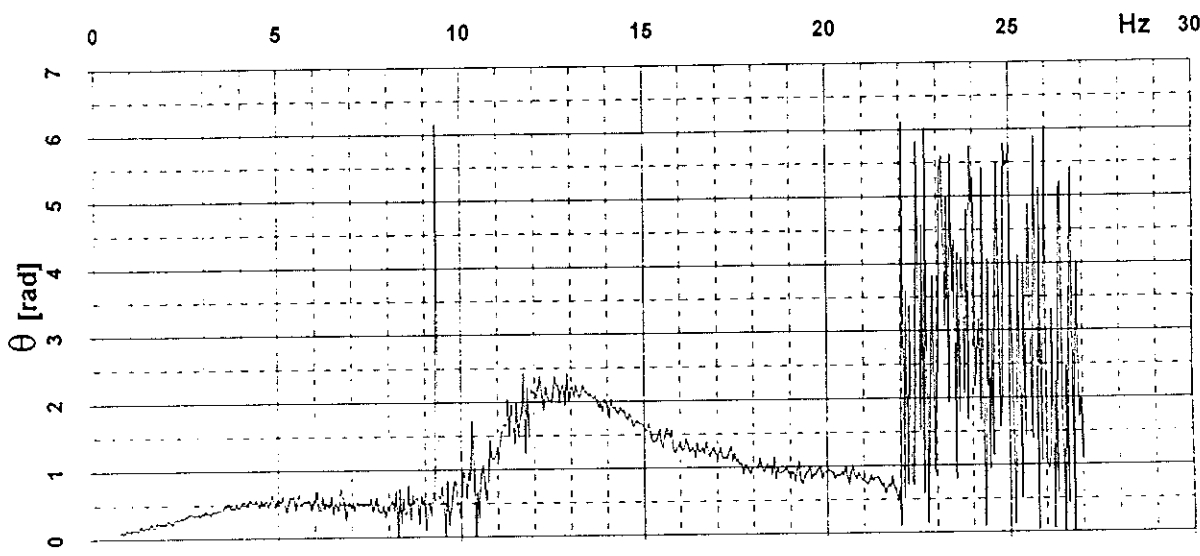
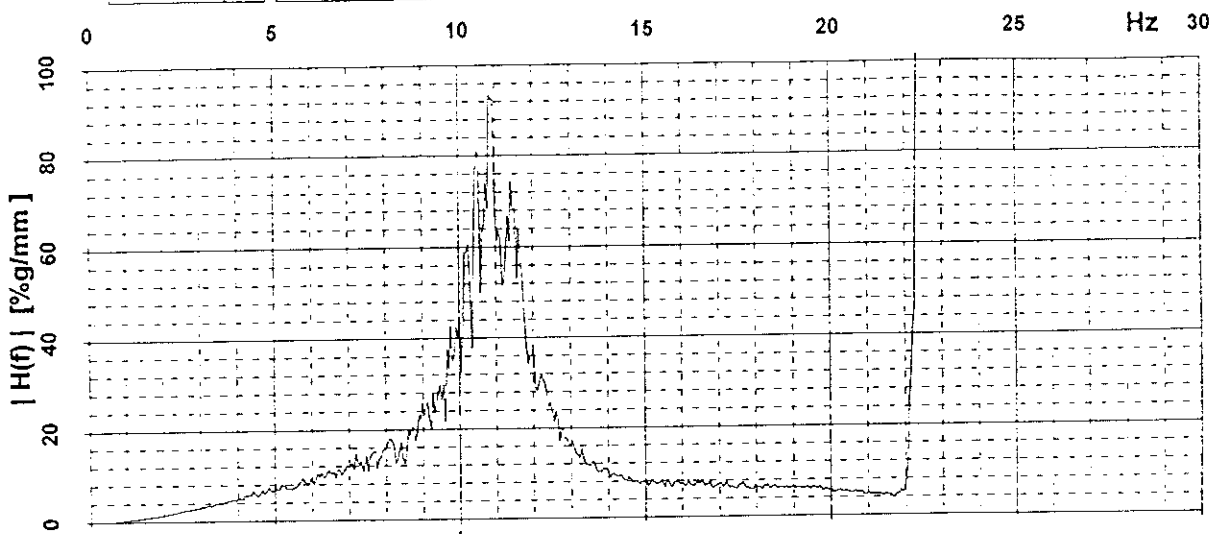
BARE.FOR





15 ↓ 554 ↓

Long > RWA ↓



BARE.FOR

APPENDIX IV

FREQUENCY RESPONSE FUNCTIONS

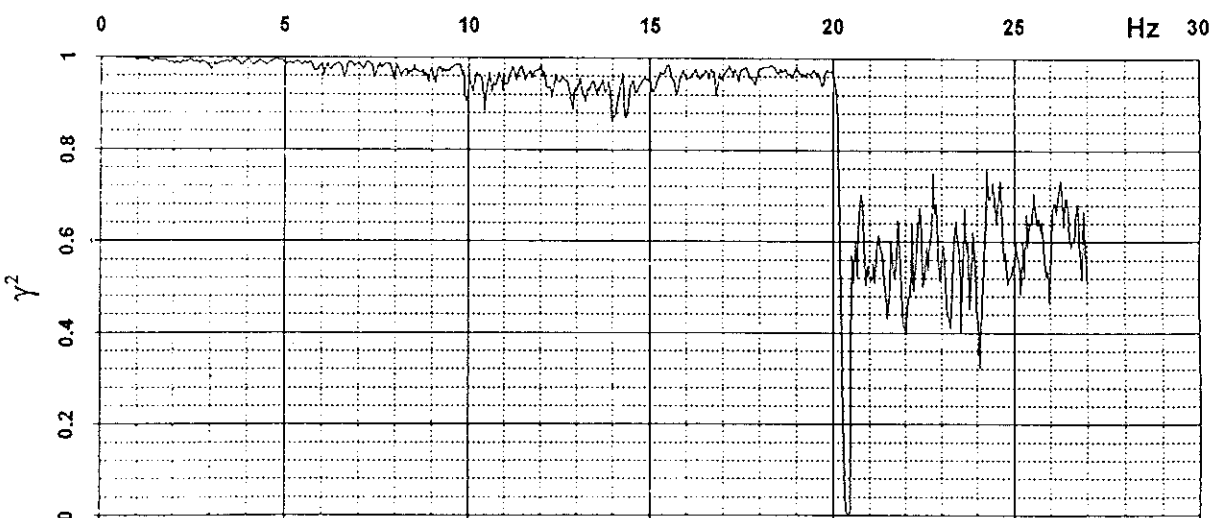
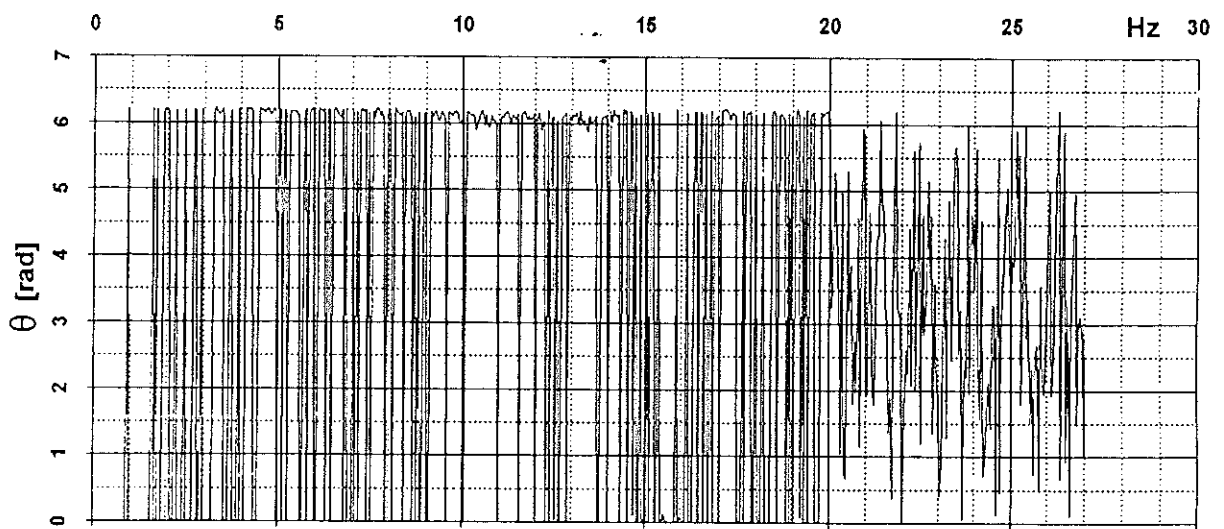
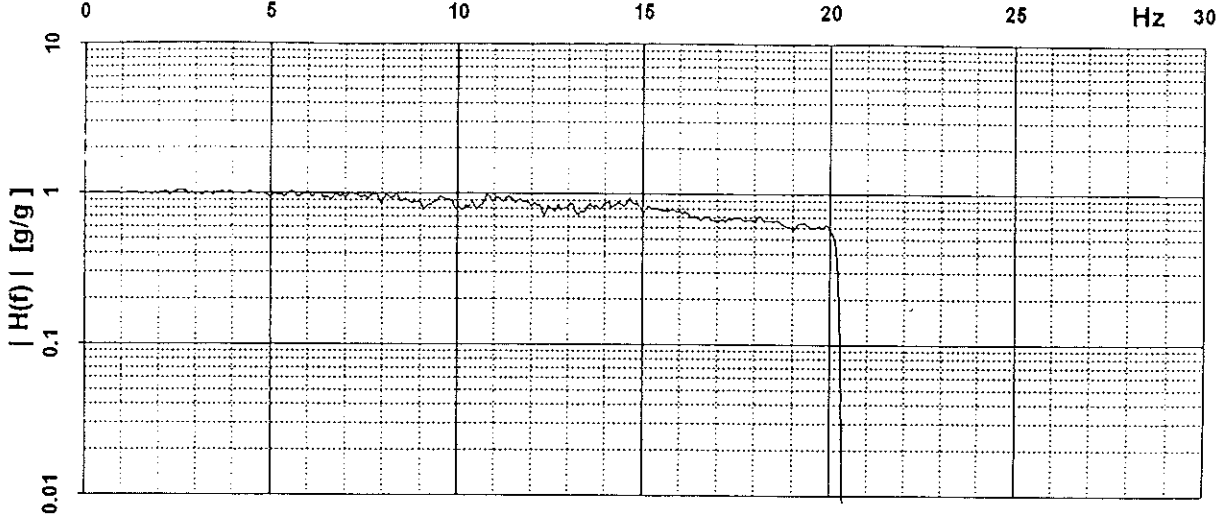
ADAPTED TEST WITHOUT MODEL

List of Figures

- AIV.1 - Modulus, Phase and Coherence of FRF; input Transverse output Target Signal
- AIV.2 - Modulus, Phase and Coherence of FRF; input Transverse output Vertical
- AIV.3 - Modulus, Phase and Coherence of FRF; input Transverse output Longitudinal
- AIV.4 - Modulus, Phase and Coherence of FRF; input Transverse output Pitch
- AIV.5 - Modulus, Phase and Coherence of FRF; input Transverse output Roll
- AIV.6 - Modulus, Phase and Coherence of FRF; input Transverse output Yaw
- AIV.7 - Modulus, Phase and Coherence of FRF; input Vertical output Target Signal
- AIV.8 - Modulus, Phase and Coherence of FRF; input Vertical output Transverse
- AIV.9 - Modulus, Phase and Coherence of FRF; input Vertical output Longitudinal
- AIV.10 - Modulus, Phase and Coherence of FRF; input Vertical output Pitch
- AIV.11 - Modulus, Phase and Coherence of FRF; input Vertical output Roll
- AIV.12 - Modulus, Phase and Coherence of FRF; input Vertical output Yaw
- AIV.13 - Modulus, Phase and Coherence of FRF; input Longitudinal output Target Signal
- AIV.14 - Modulus, Phase and Coherence of FRF; input Longitudinal output Transverse
- AIV.15 - Modulus, Phase and Coherence of FRF; input Longitudinal output Vertical
- AIV.16 - Modulus, Phase and Coherence of FRF; input Longitudinal output Pitch
- AIV.17 - Modulus, Phase and Coherence of FRF; input Longitudinal output Roll
- AIV.18 - Modulus, Phase and Coherence of FRF; input Longitudinal output Yaw

15 ↓ 554 ↓

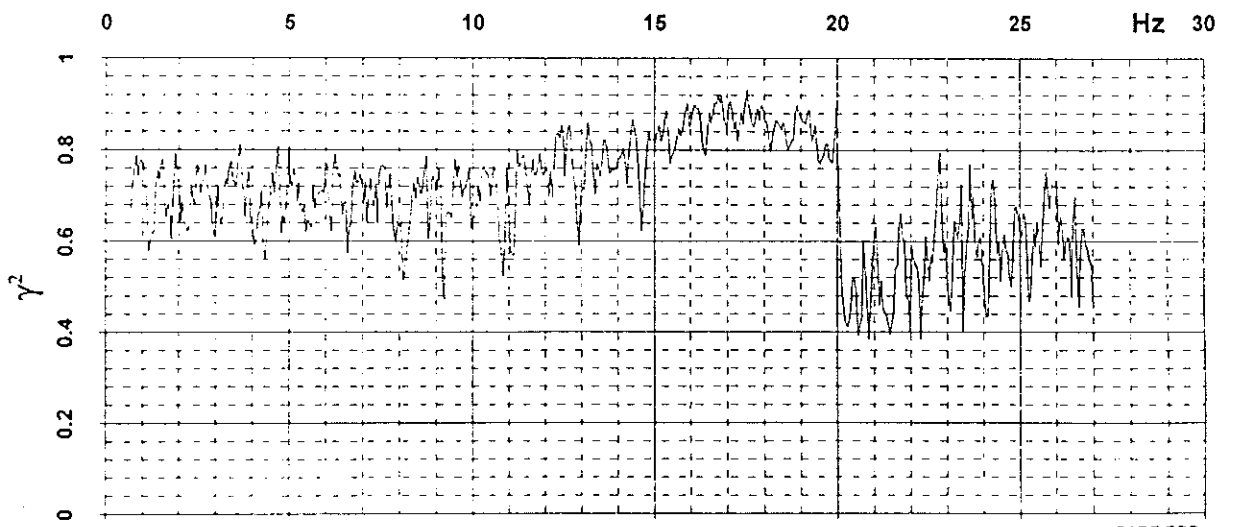
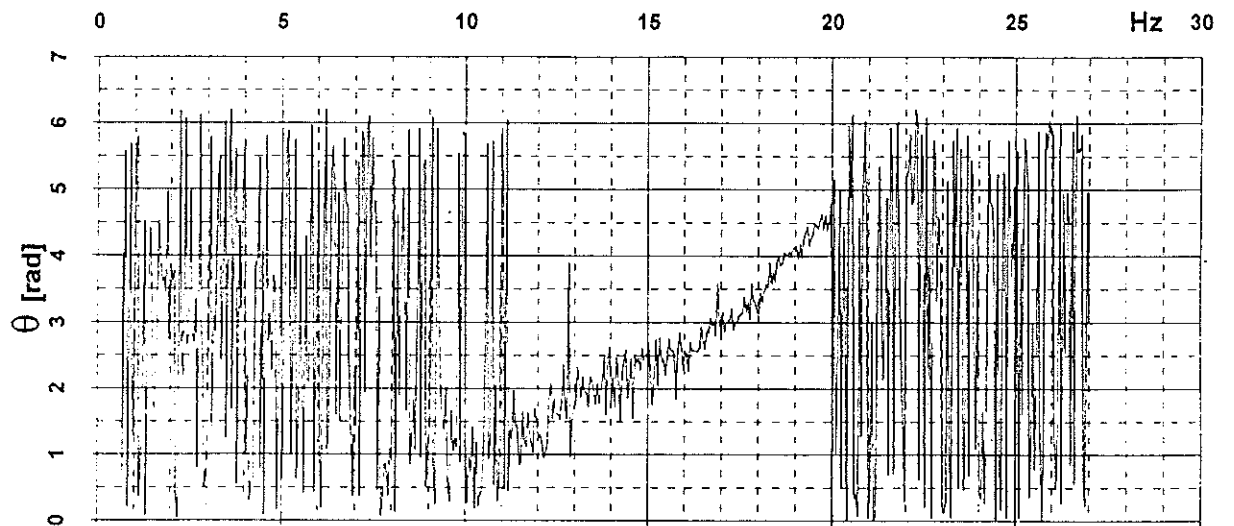
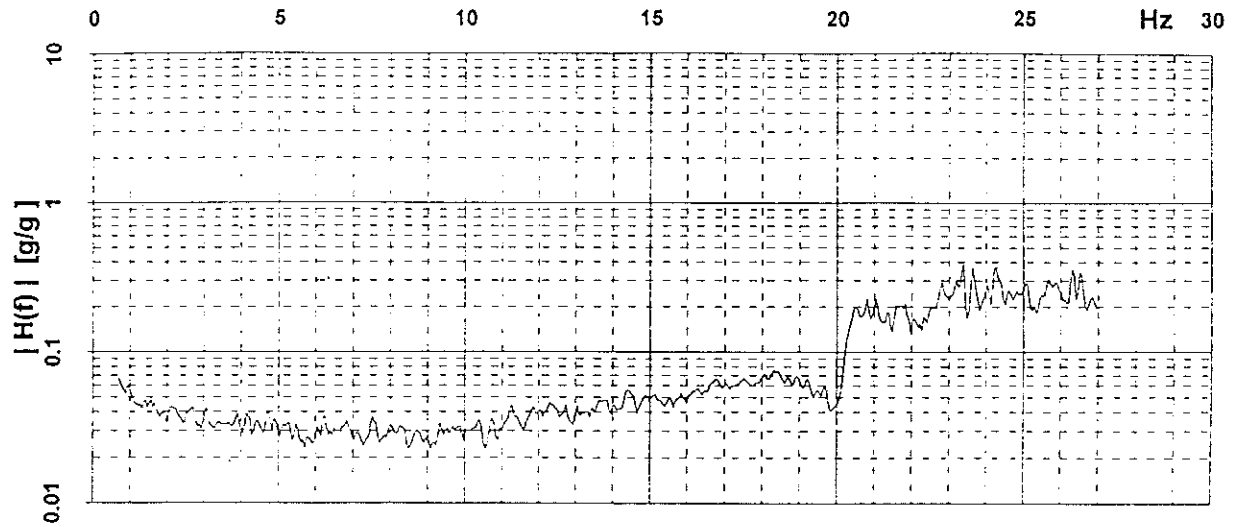
Trans > RWA ↓



BARE.FOR

15 ↓ 554 ↓

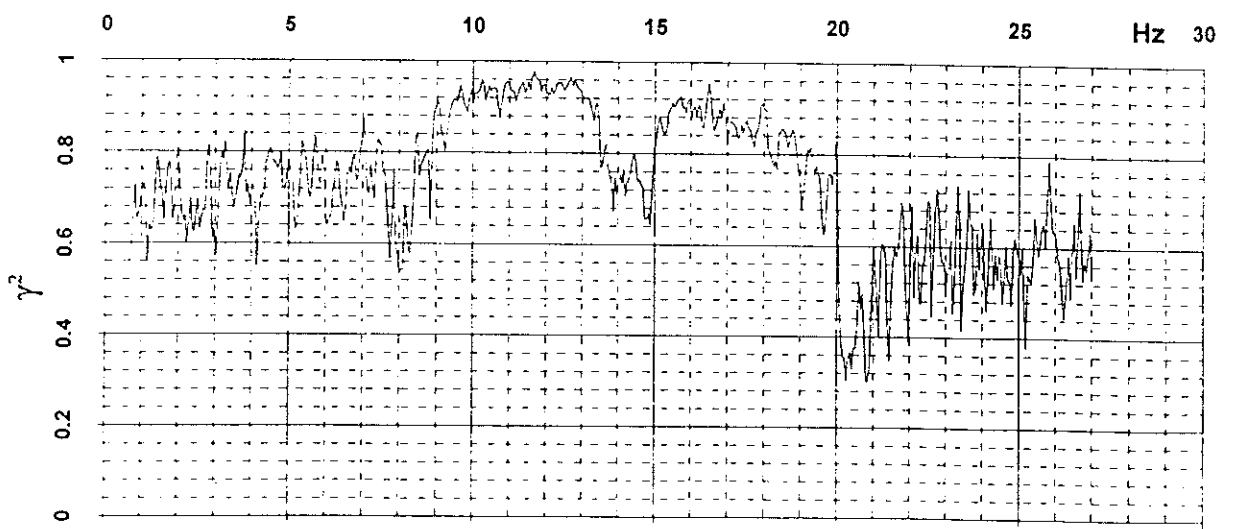
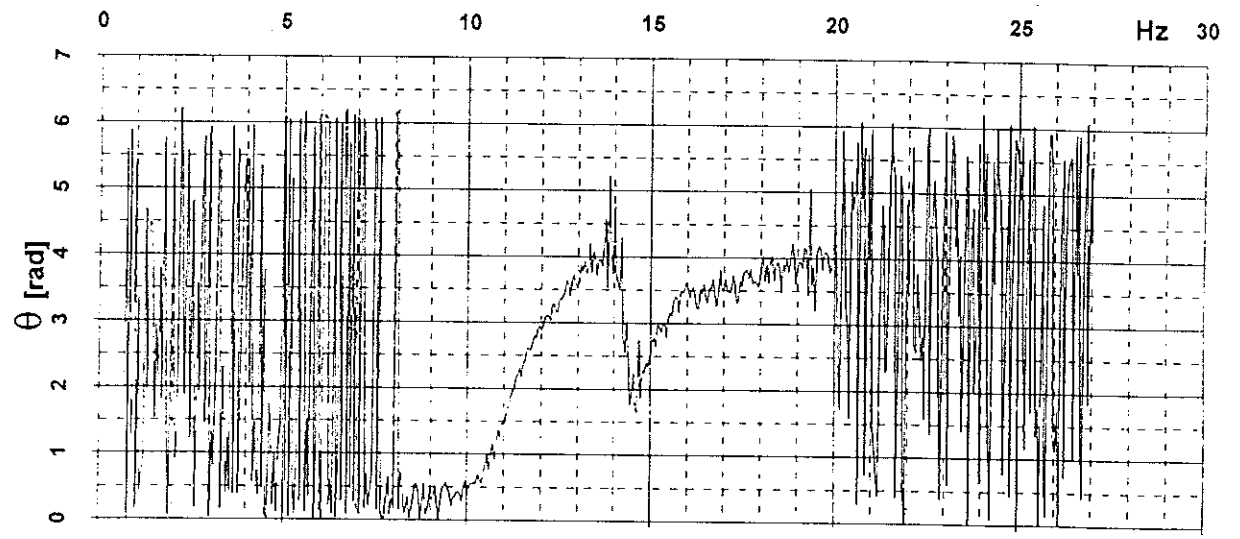
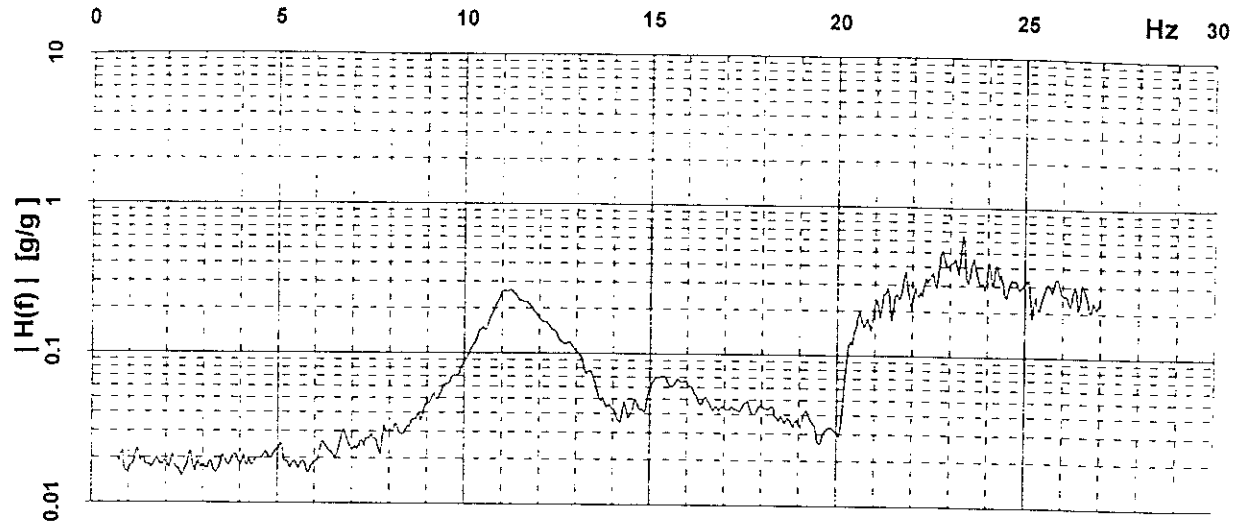
Trans>Vert ↓



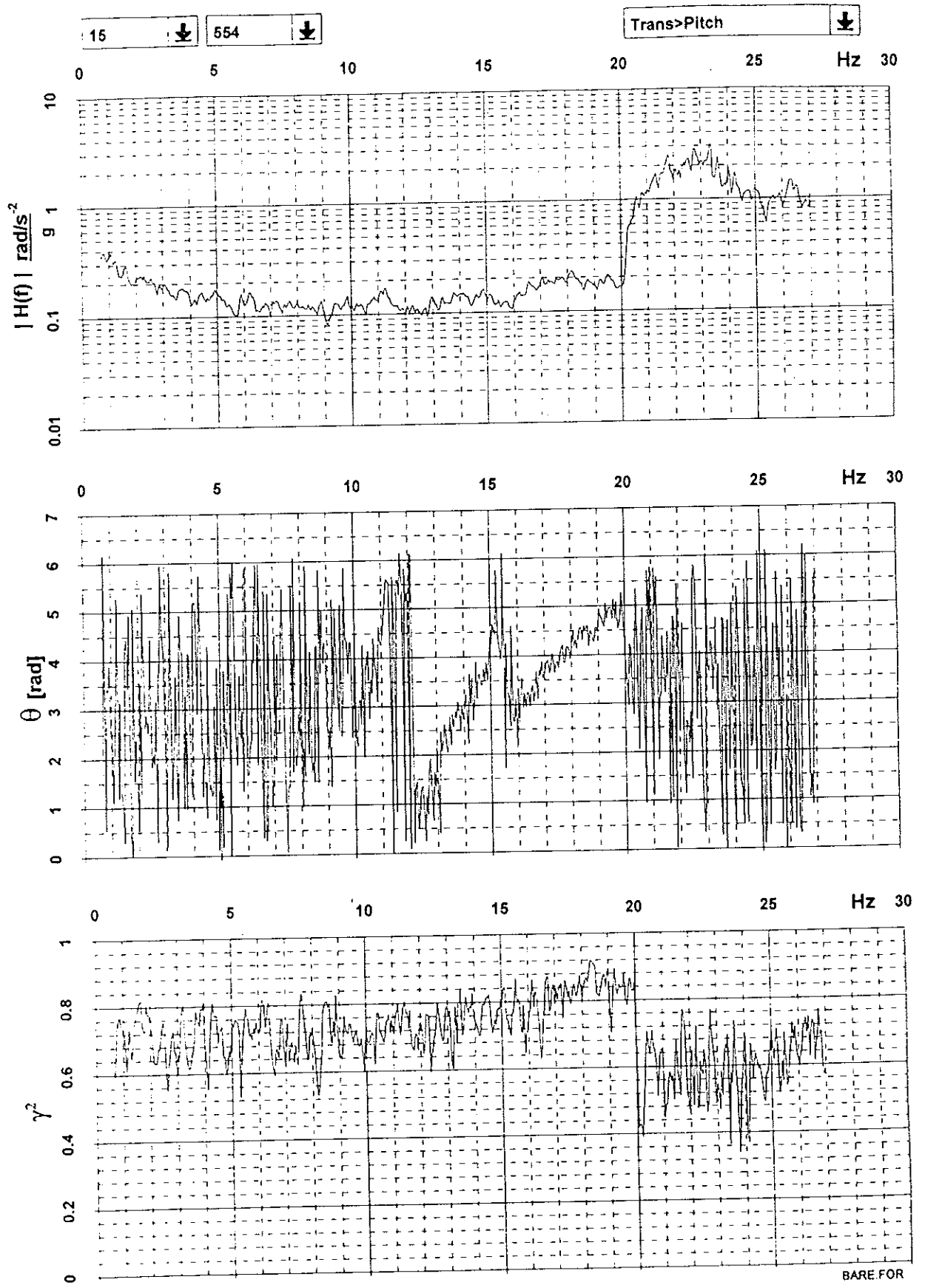
BARE.FOR

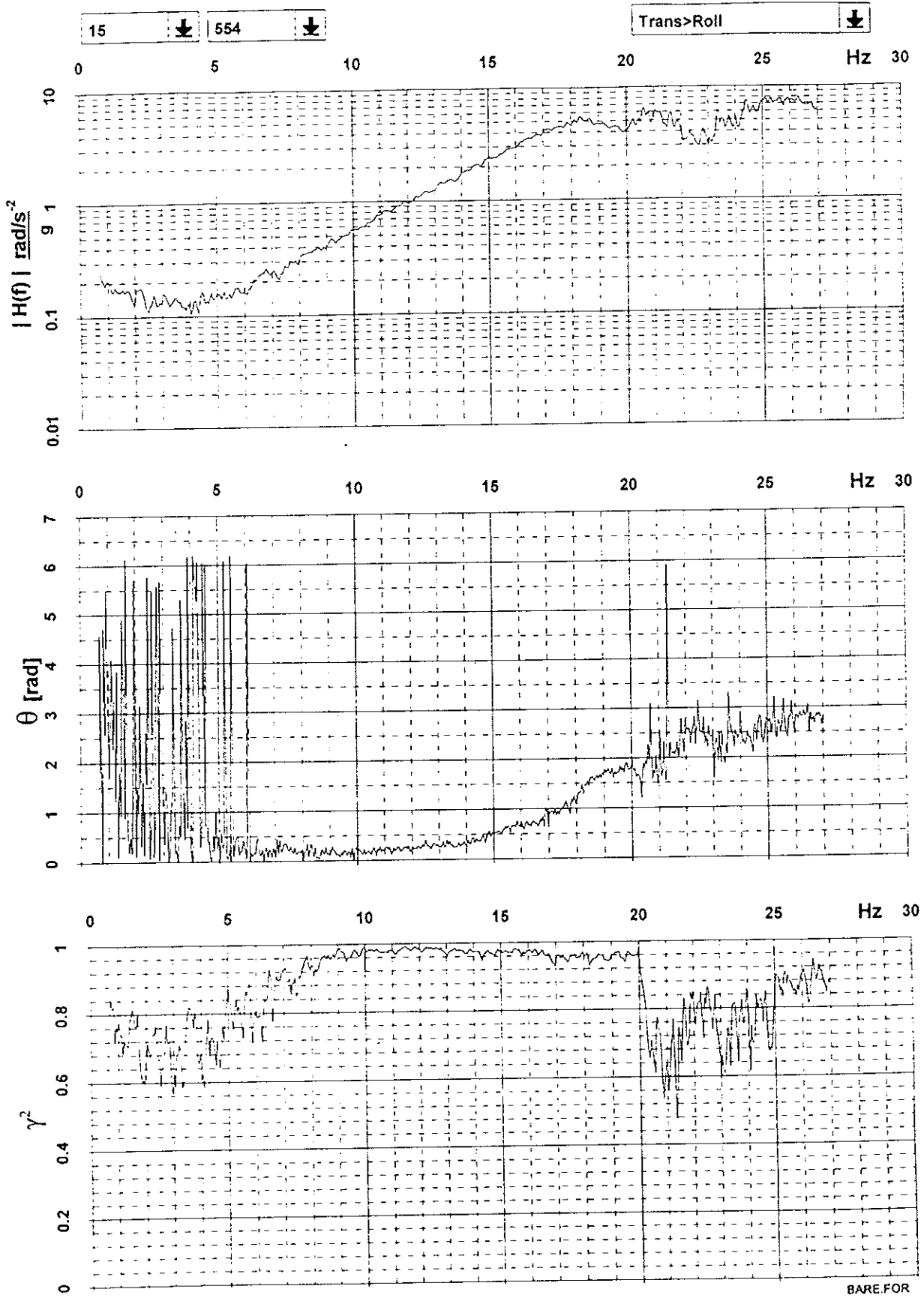
15 ↓ 554 ↓

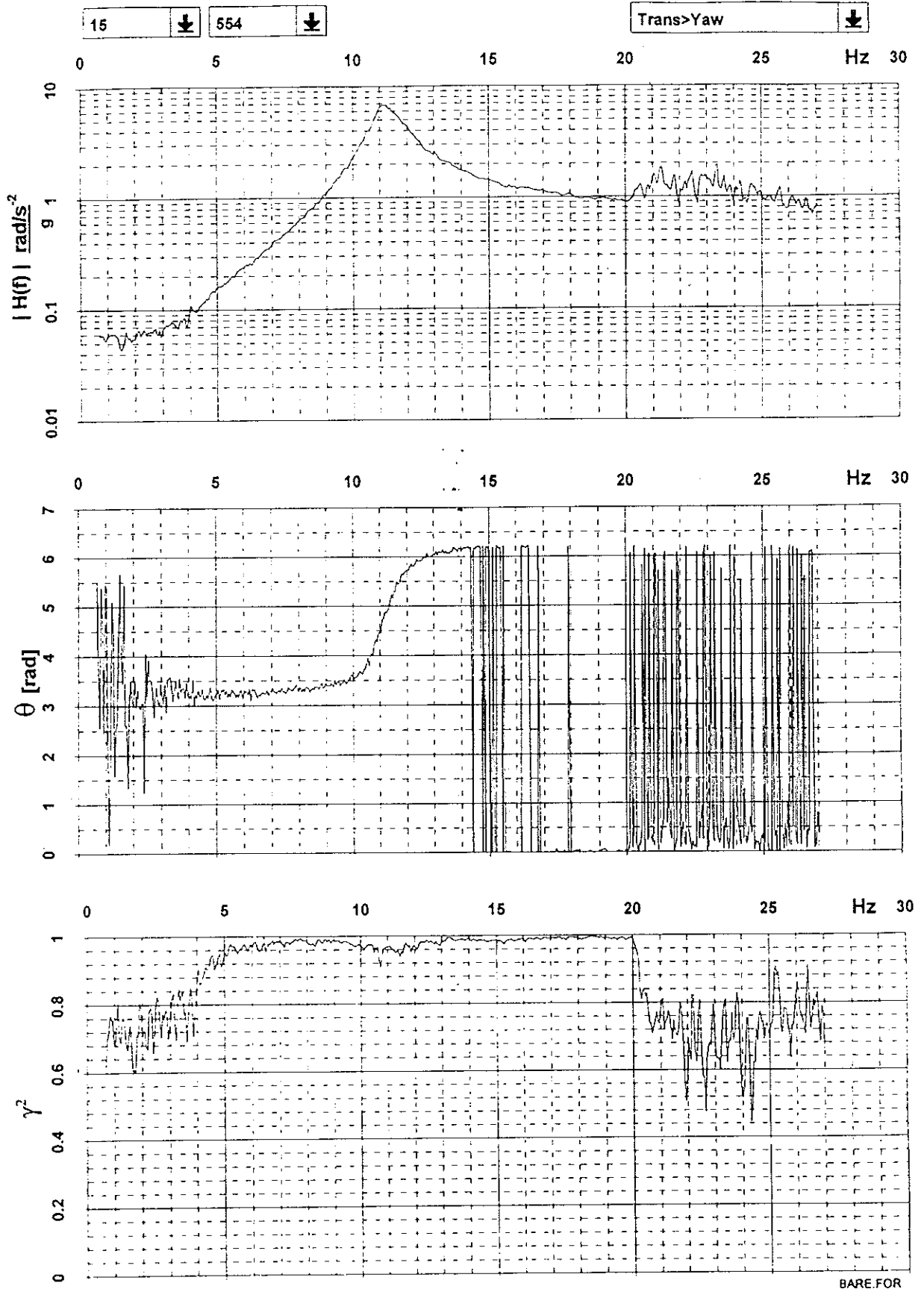
Trans>Long ↓



BARE.FOR

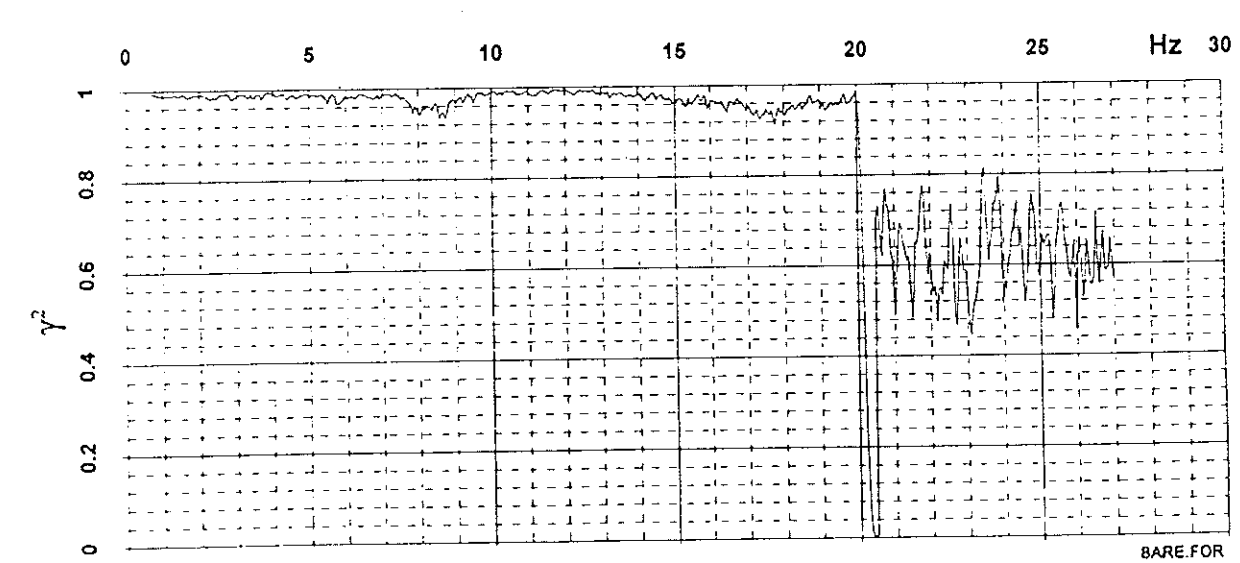
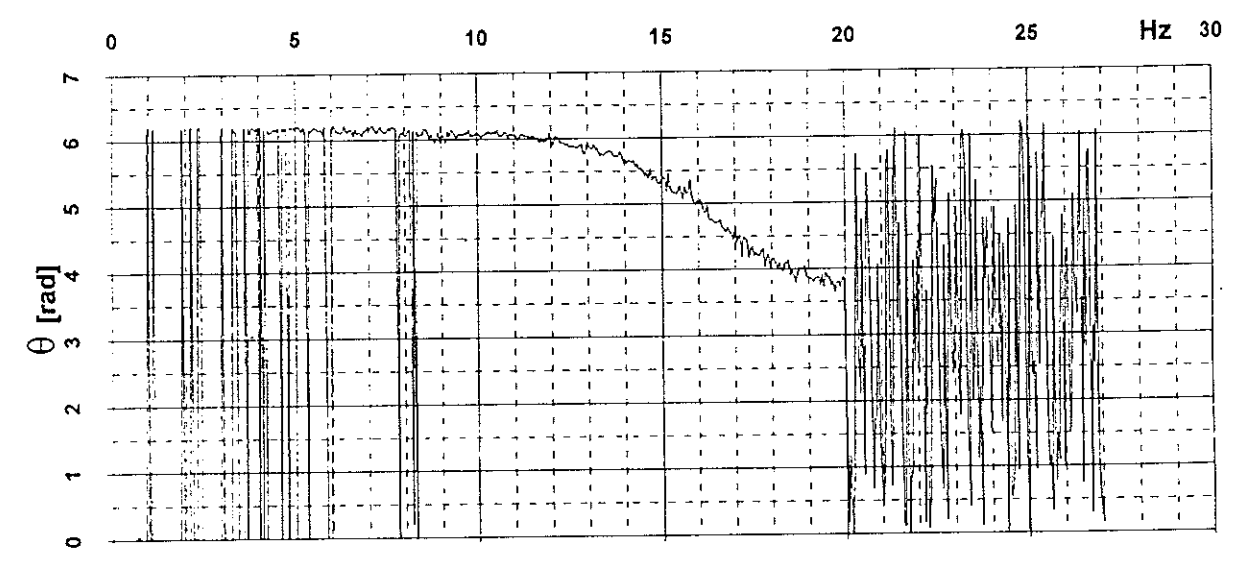
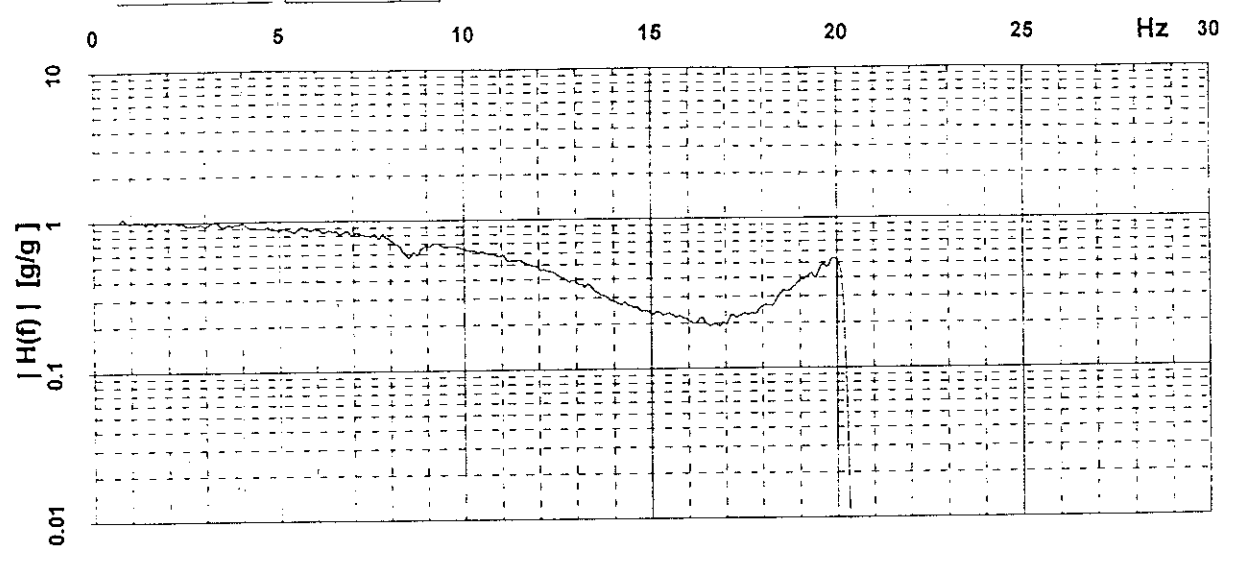






15 ↓ 554 ↓

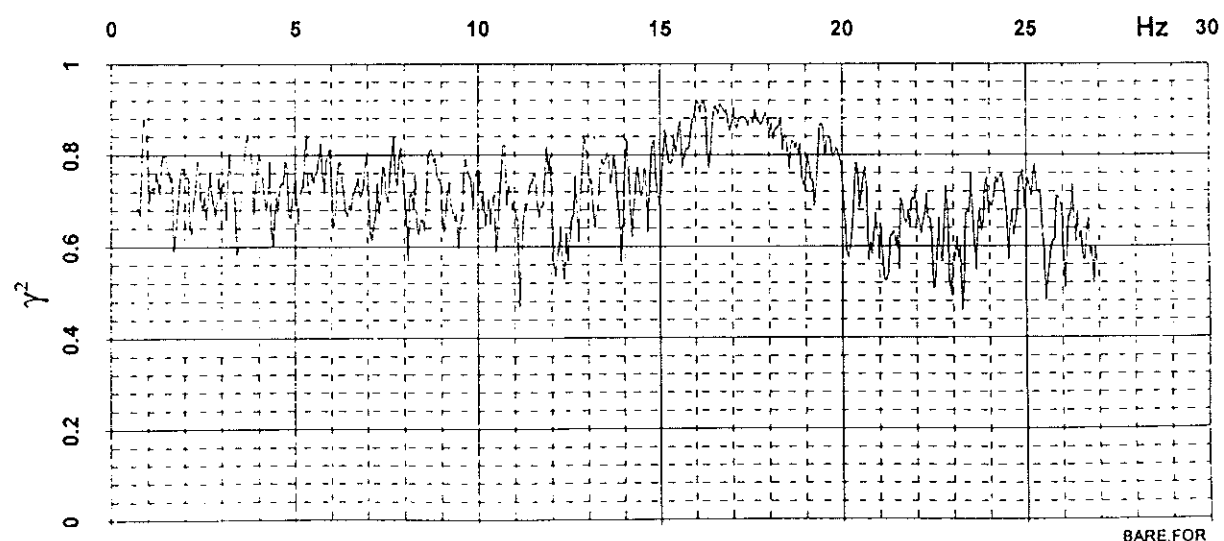
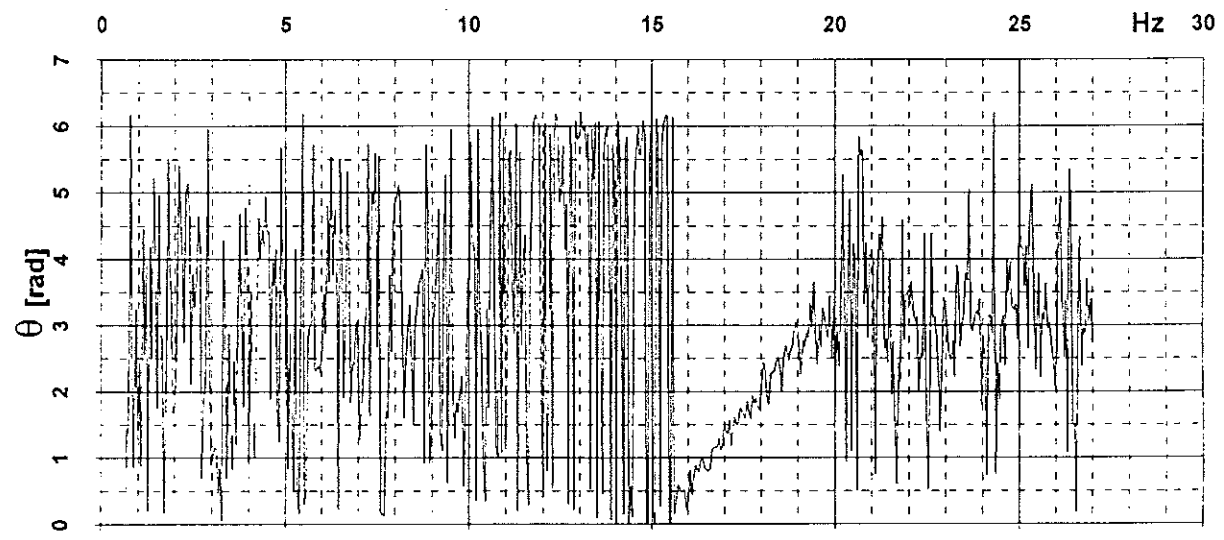
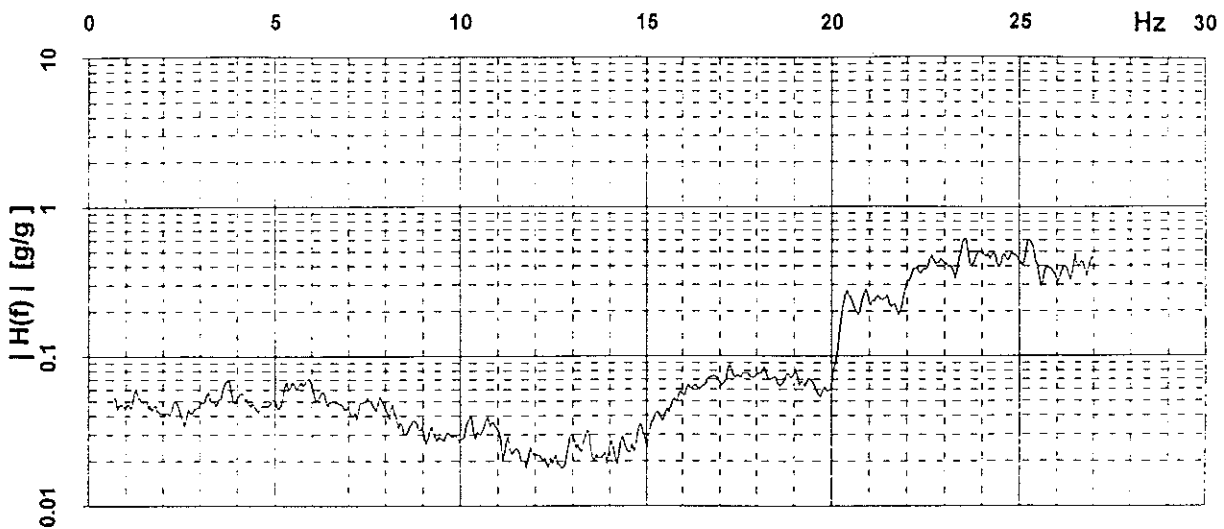
Vert>RWA ↓



BARE.FOR

15 ↓ 554 ↓

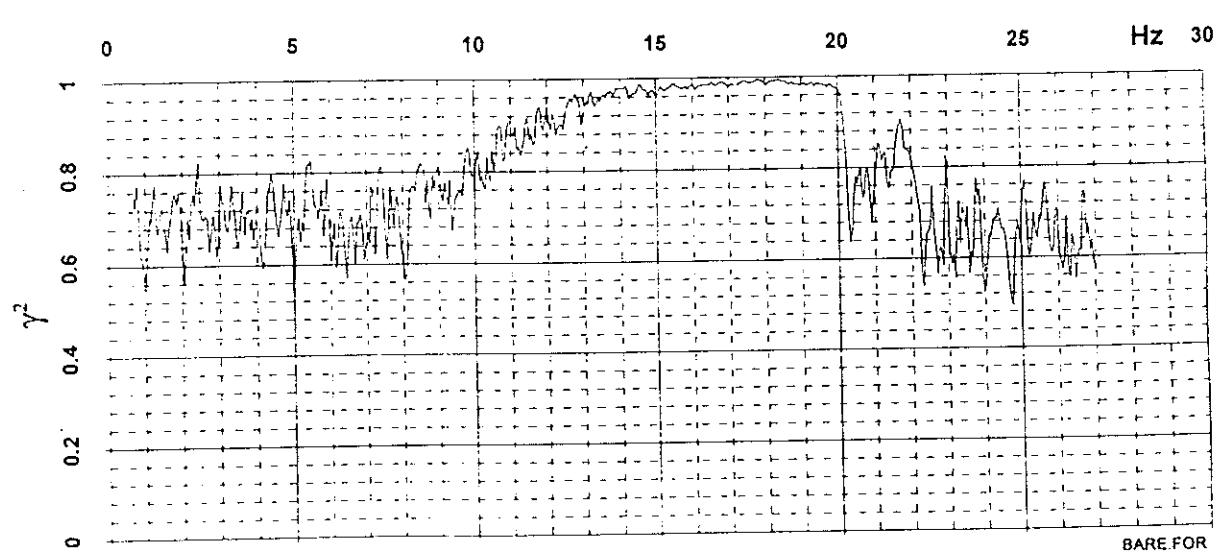
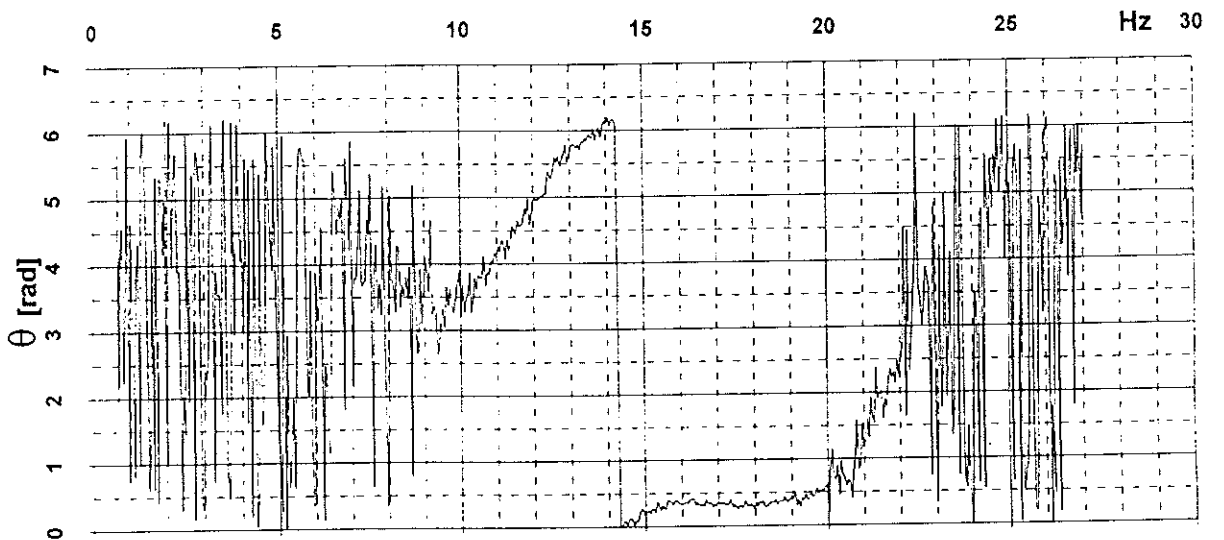
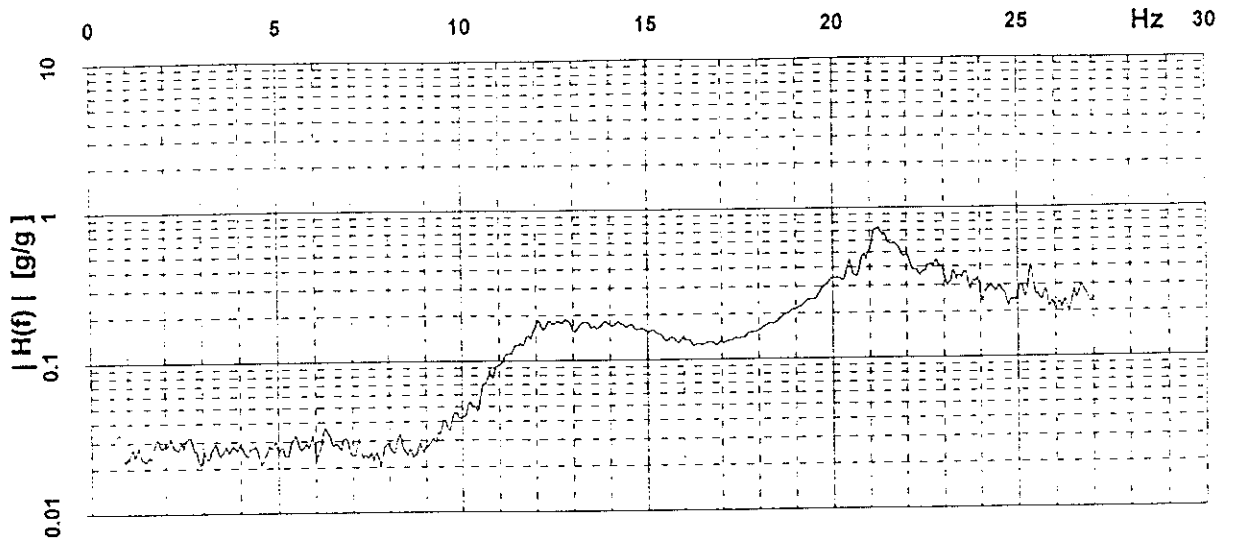
Vert>Trans ↓



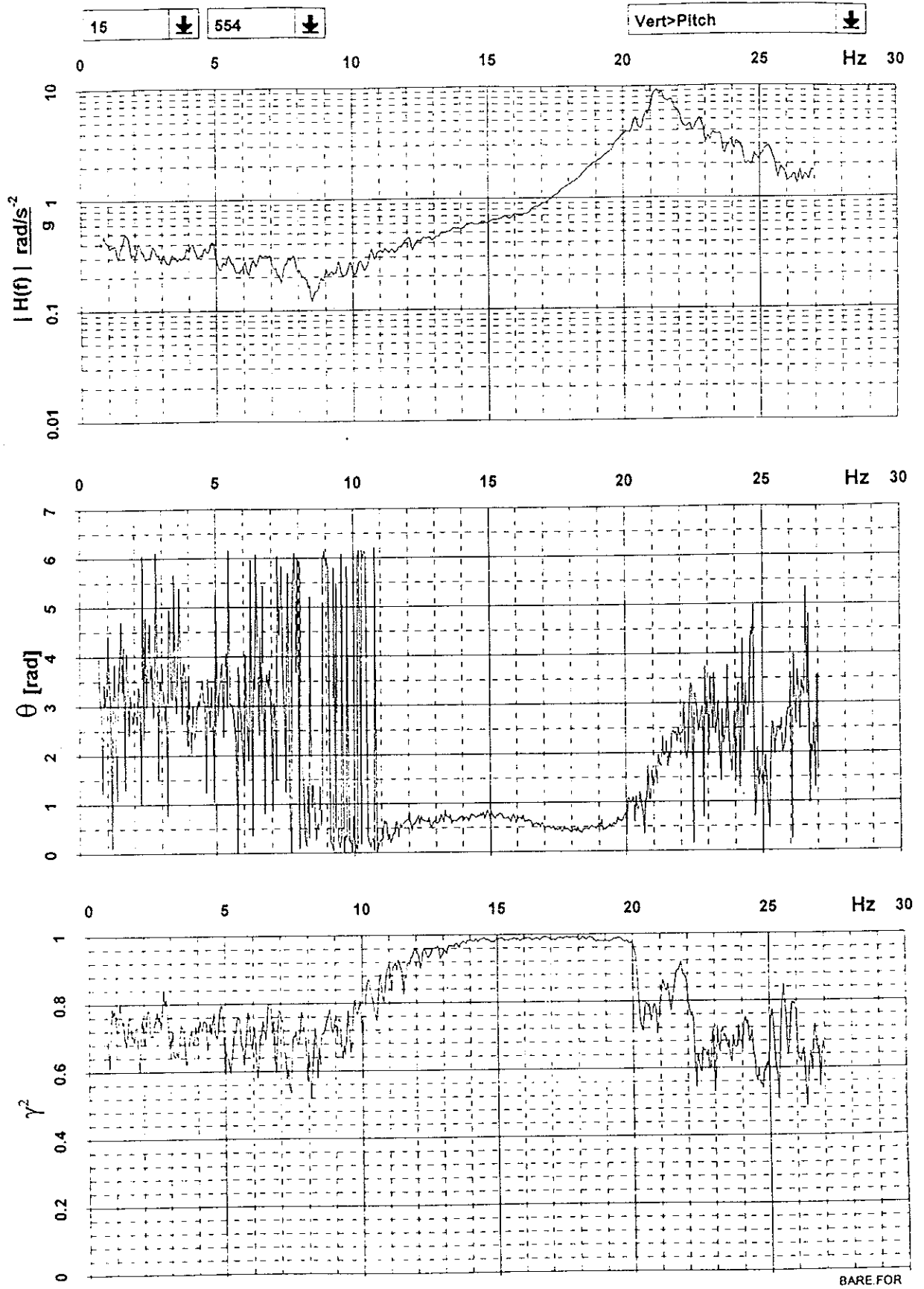
BARE.FOR

15 ↓ 554 ↓

Vert>Long ↓

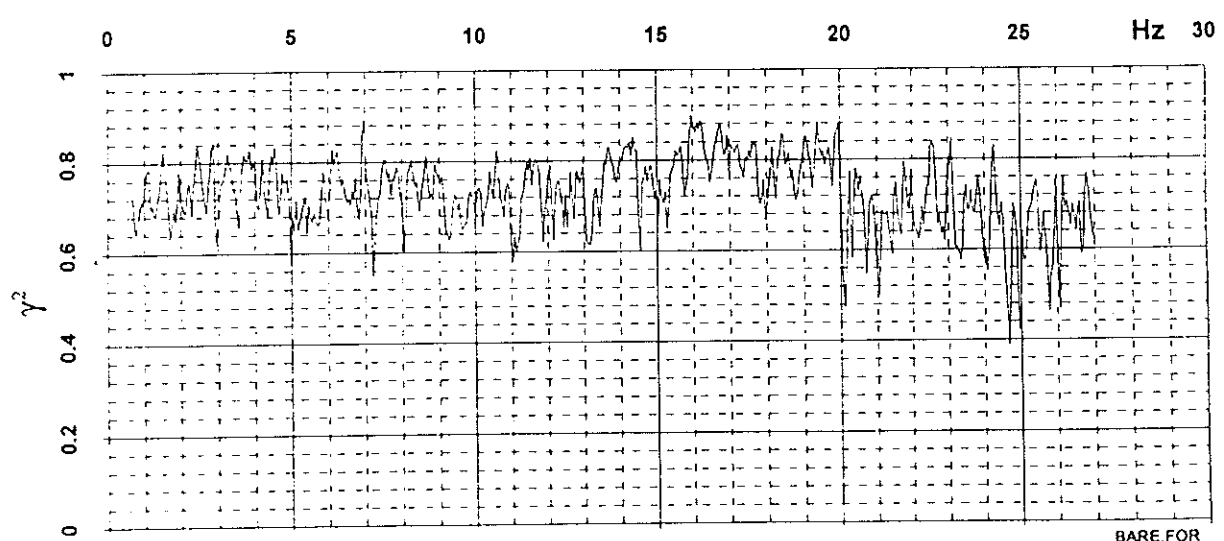
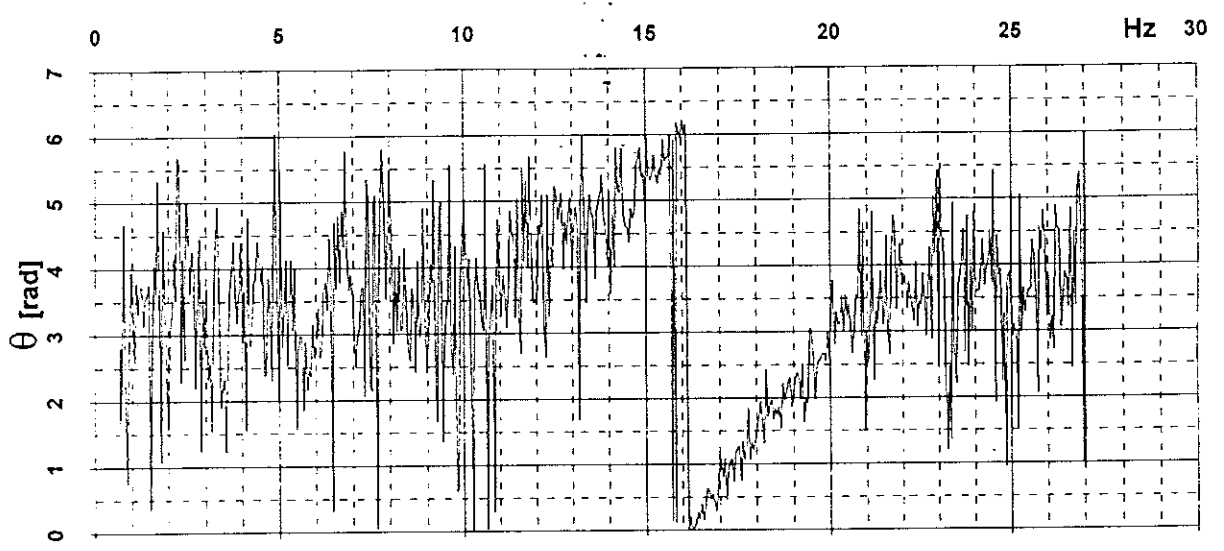
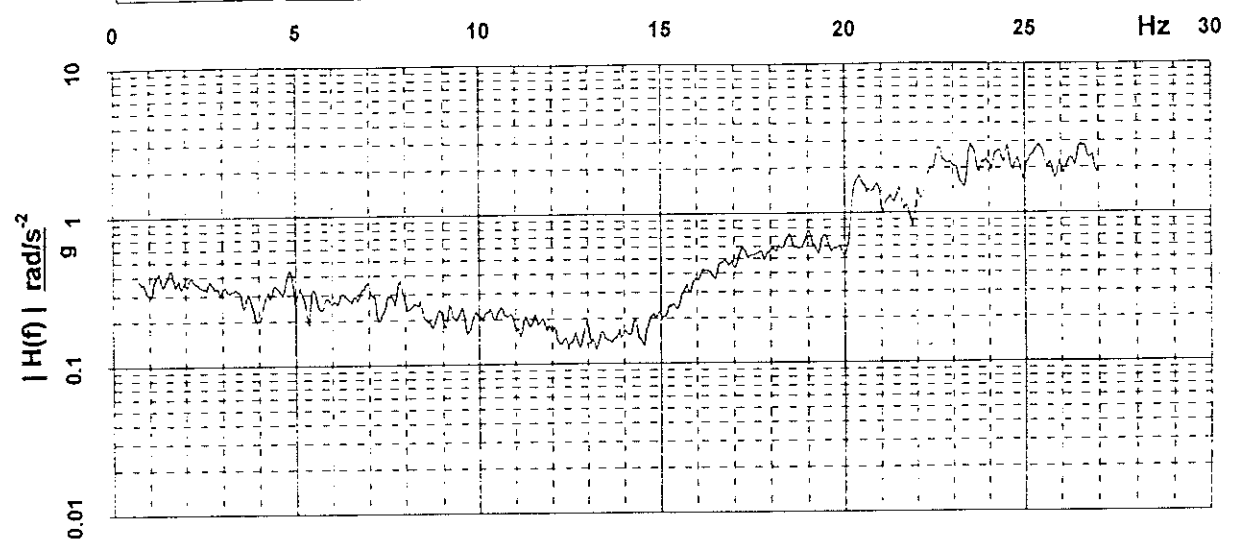


BARE FOR

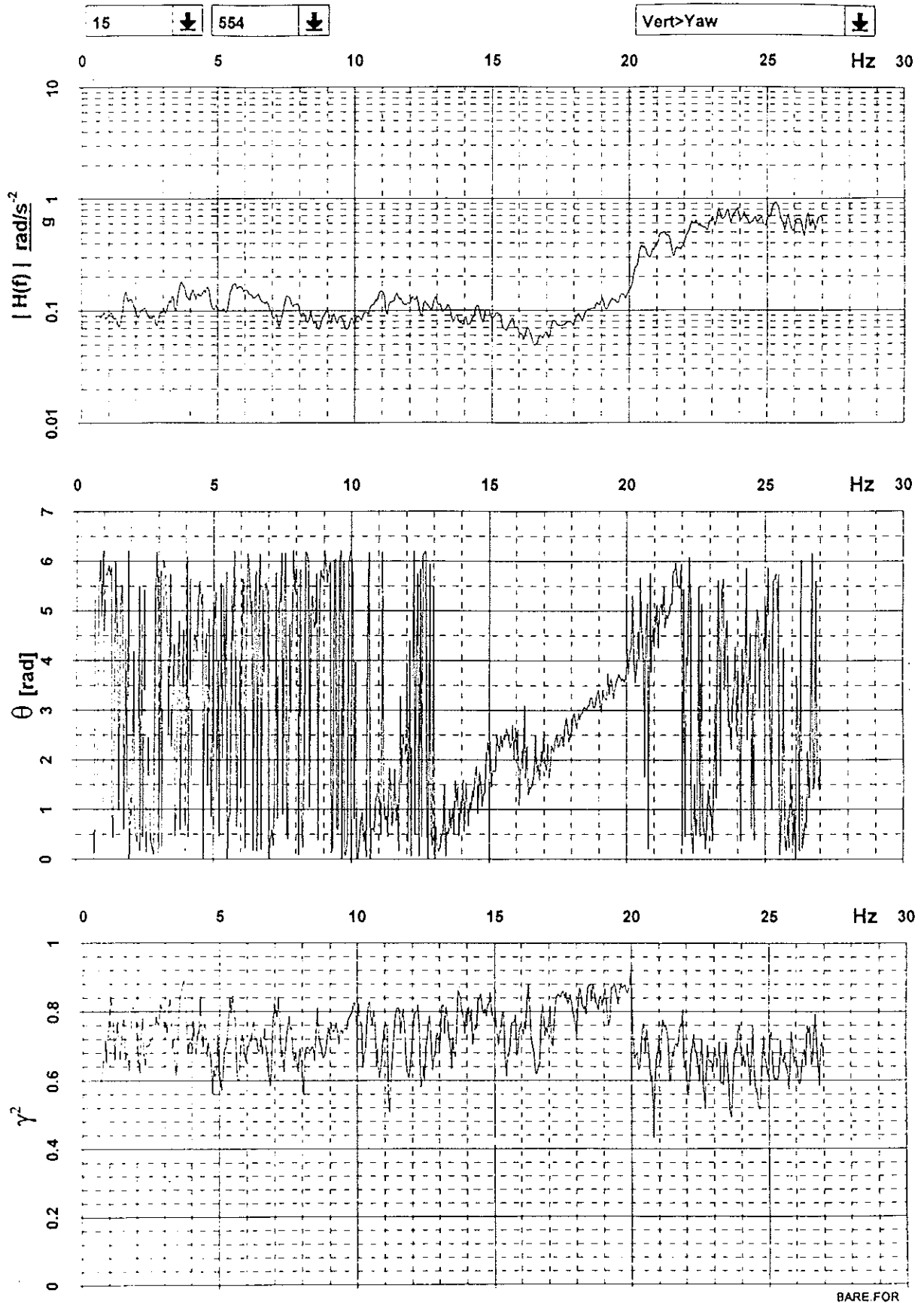


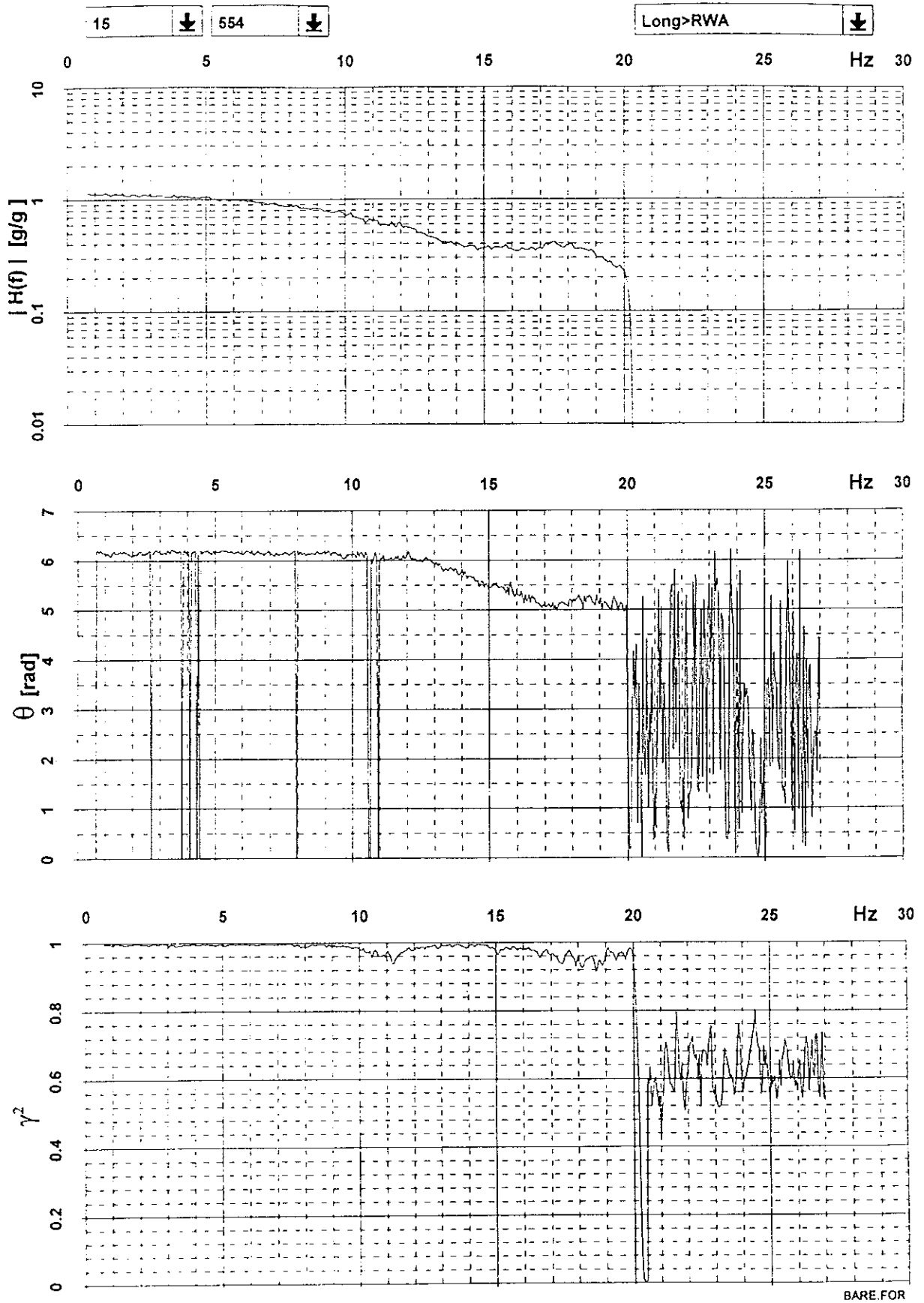
15 ↓ 554 ↓

Vert>Roll ↓



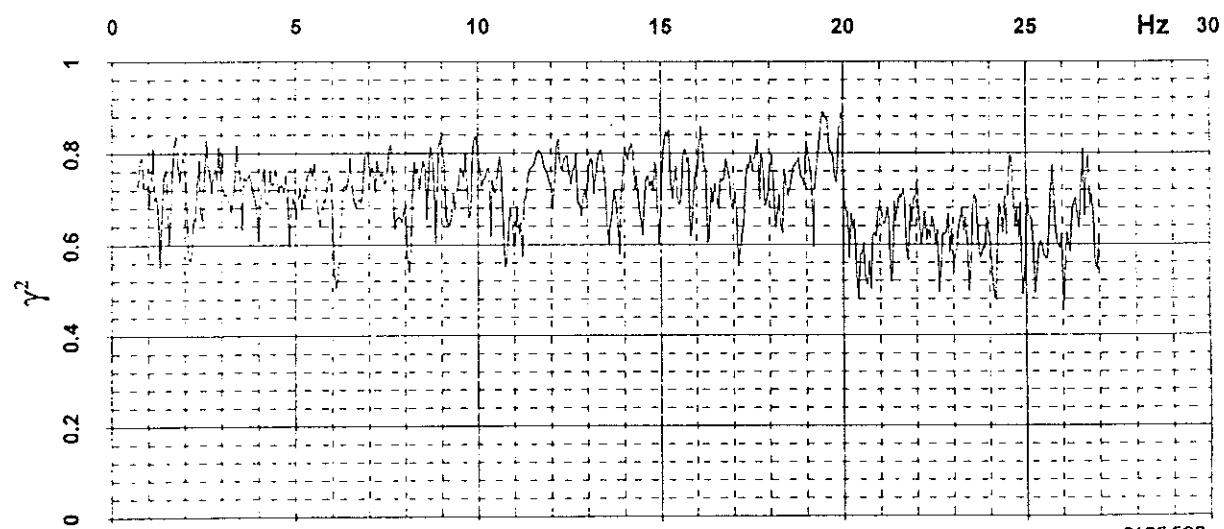
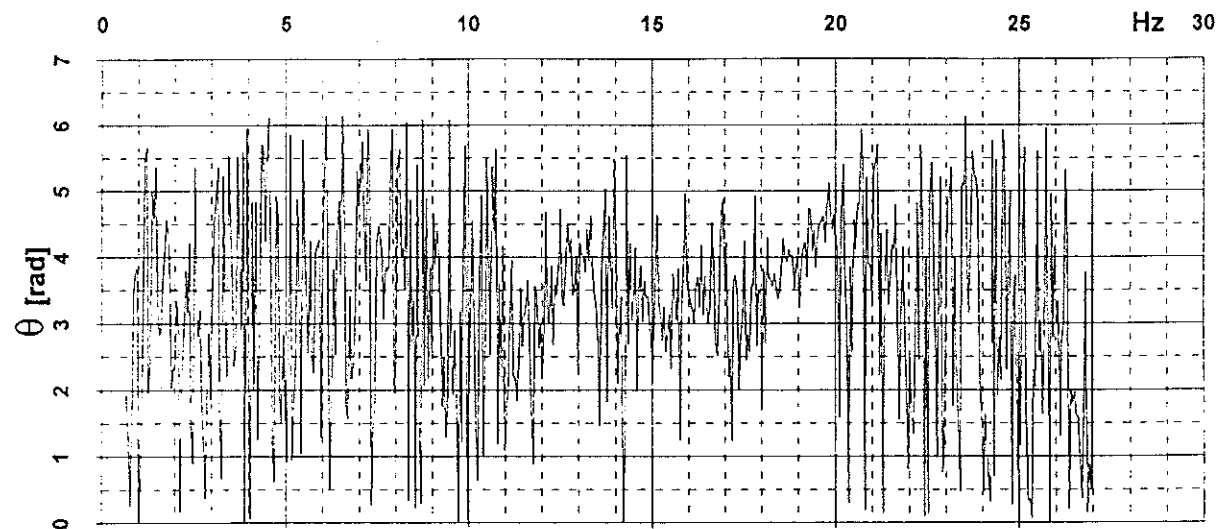
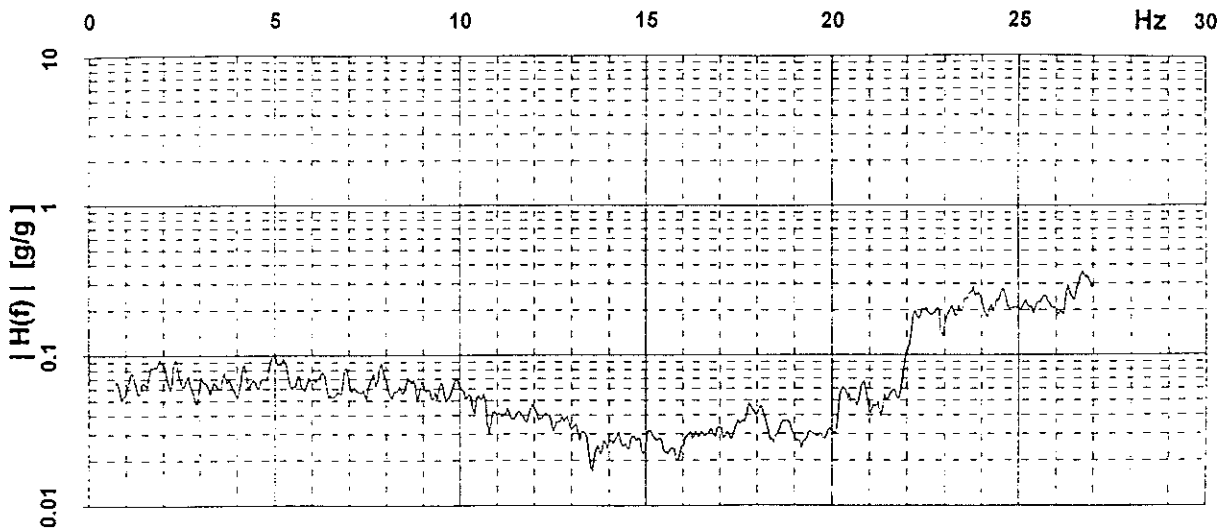
BARE FOR





15 ↓ 554 ↓

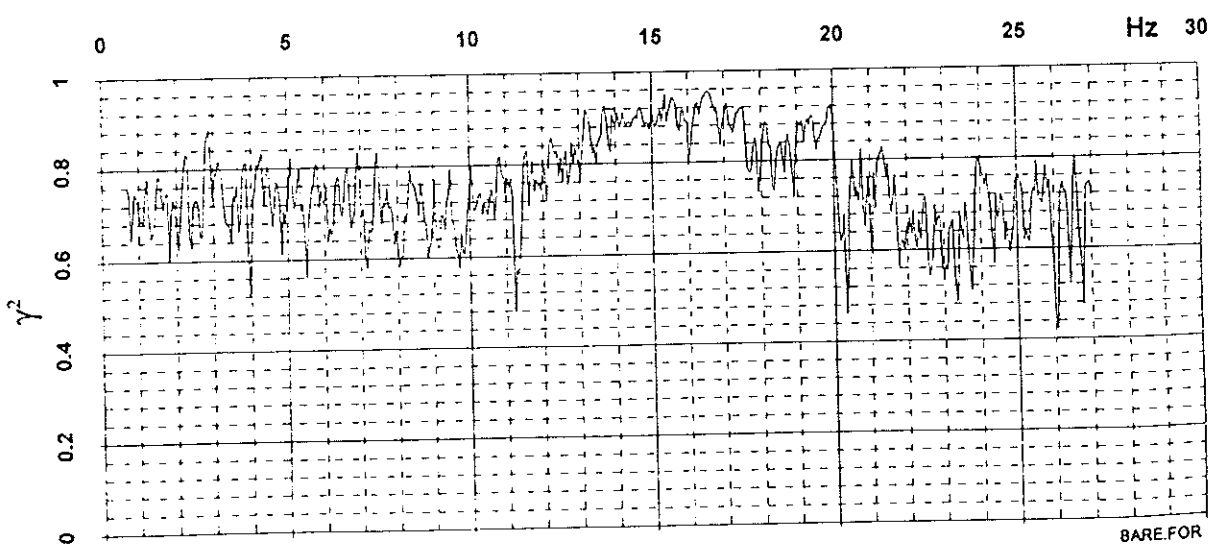
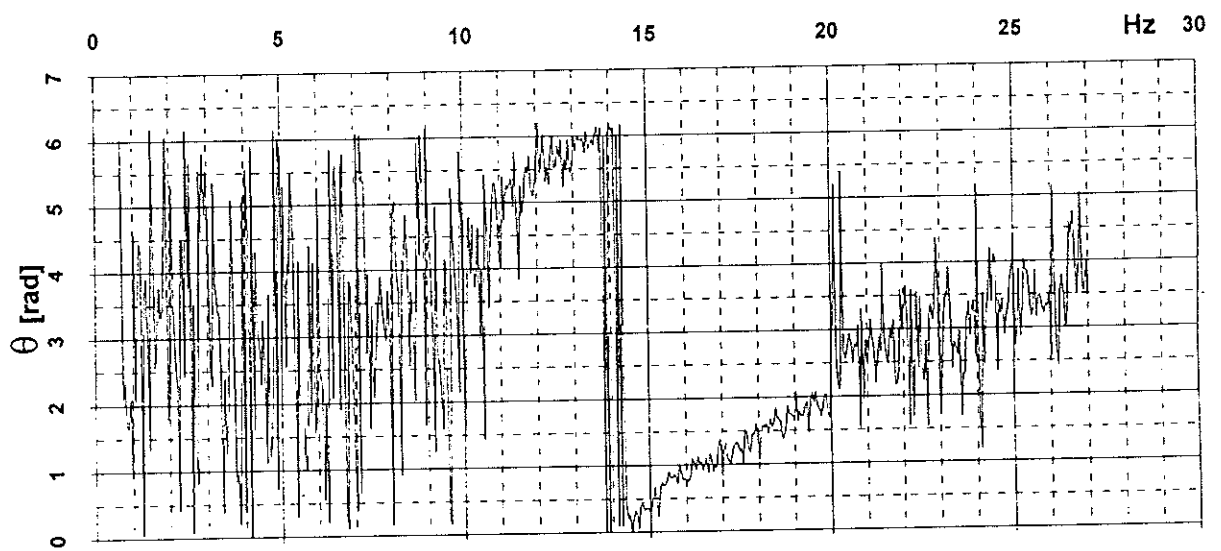
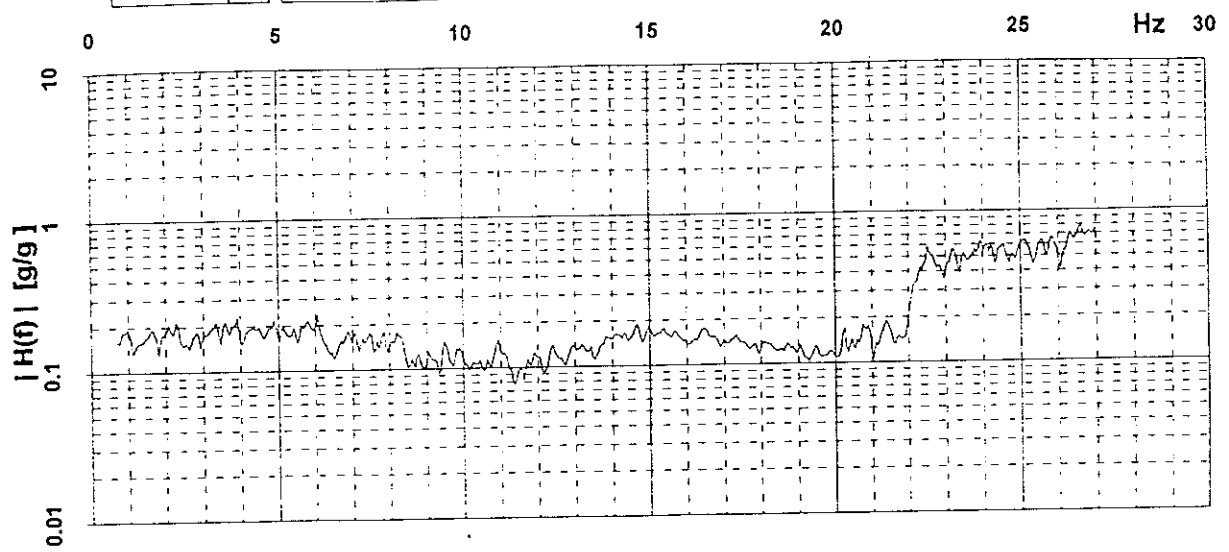
Long>Trans ↓



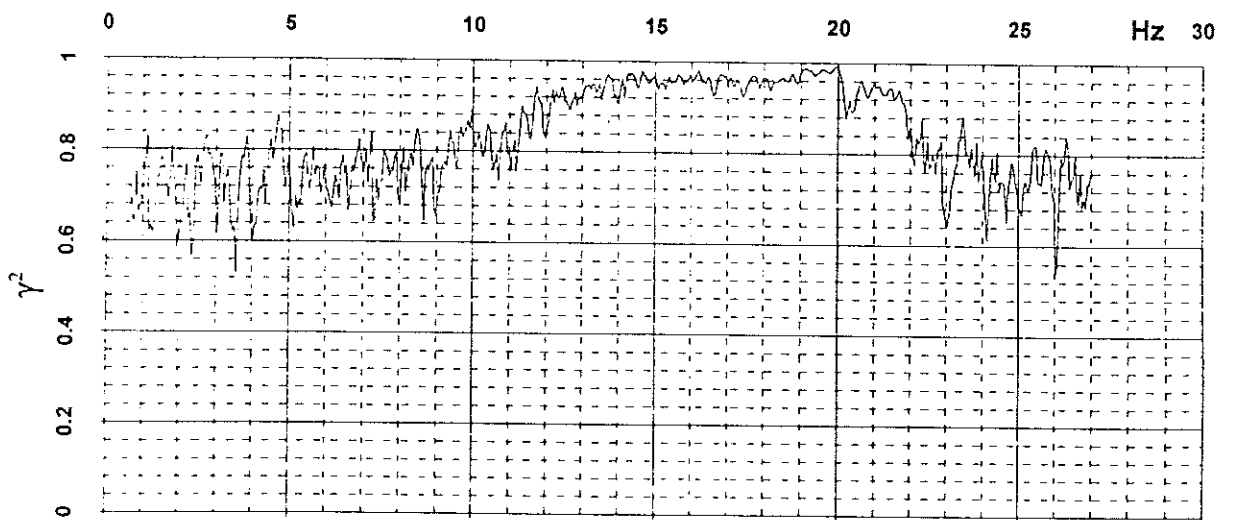
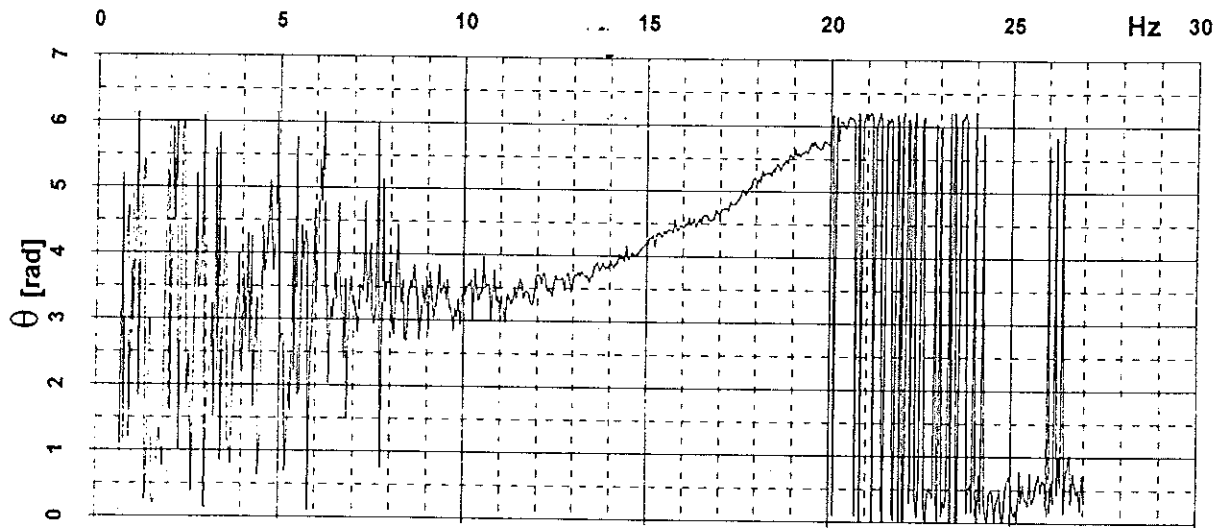
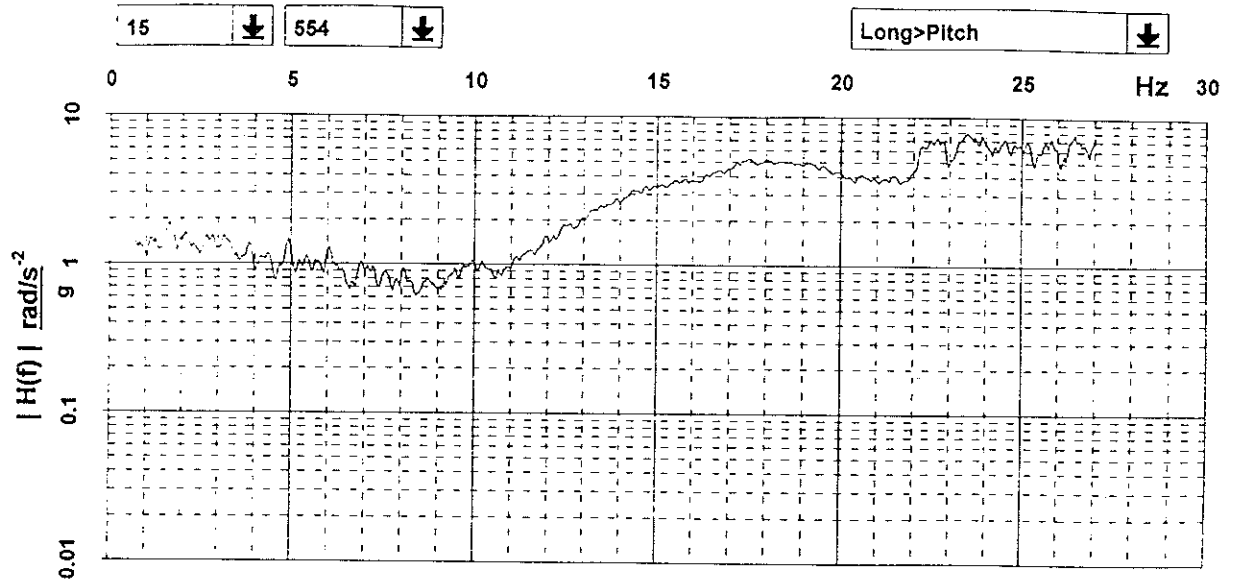
BARE.FOR

15 ↓ 554 ↓

Long>Vert ↓



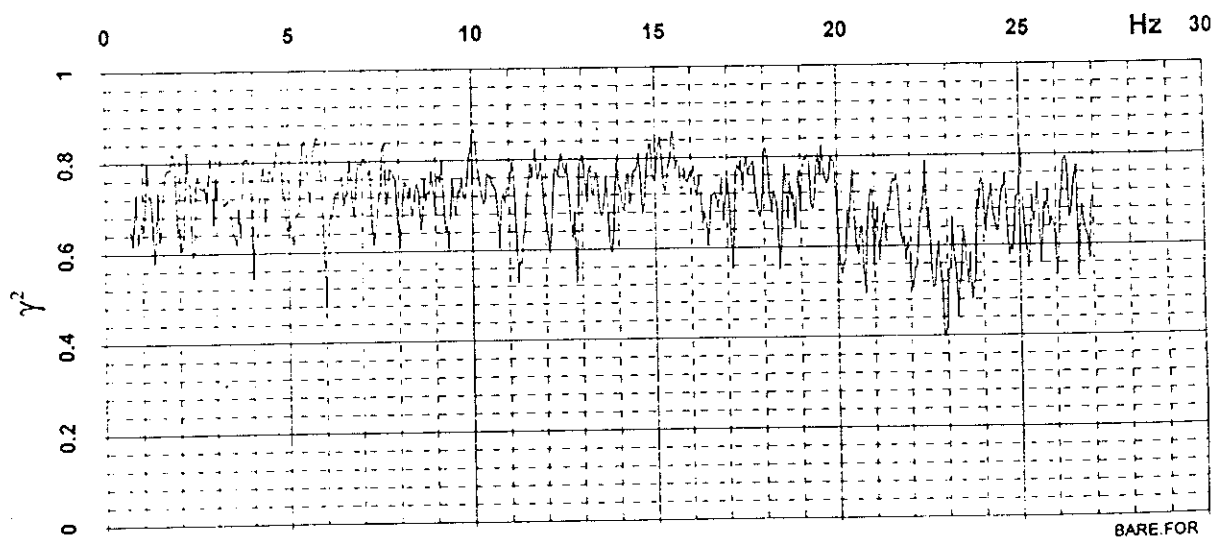
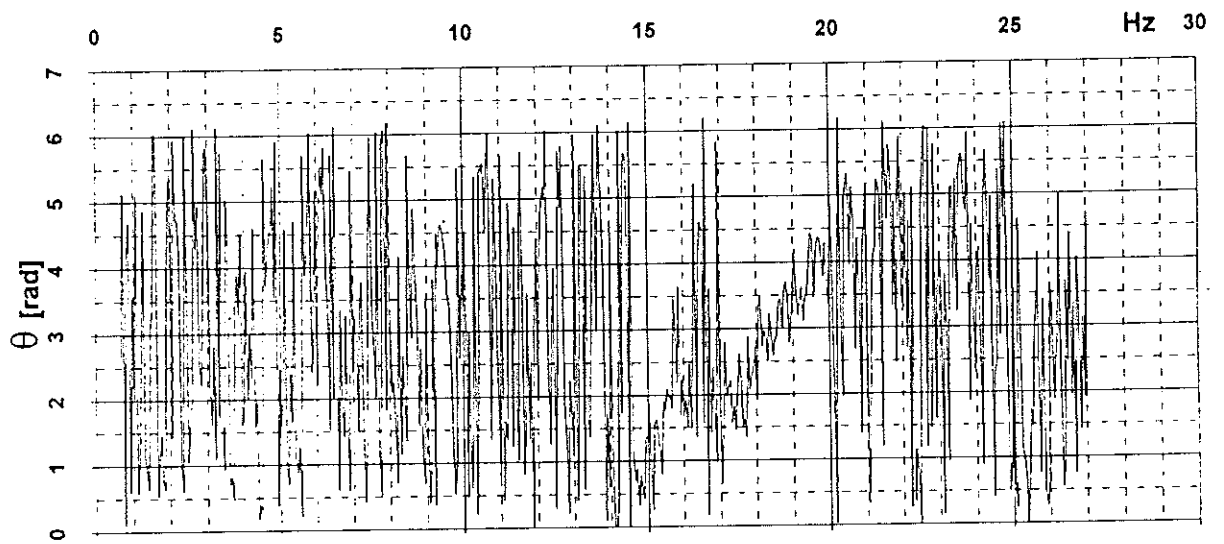
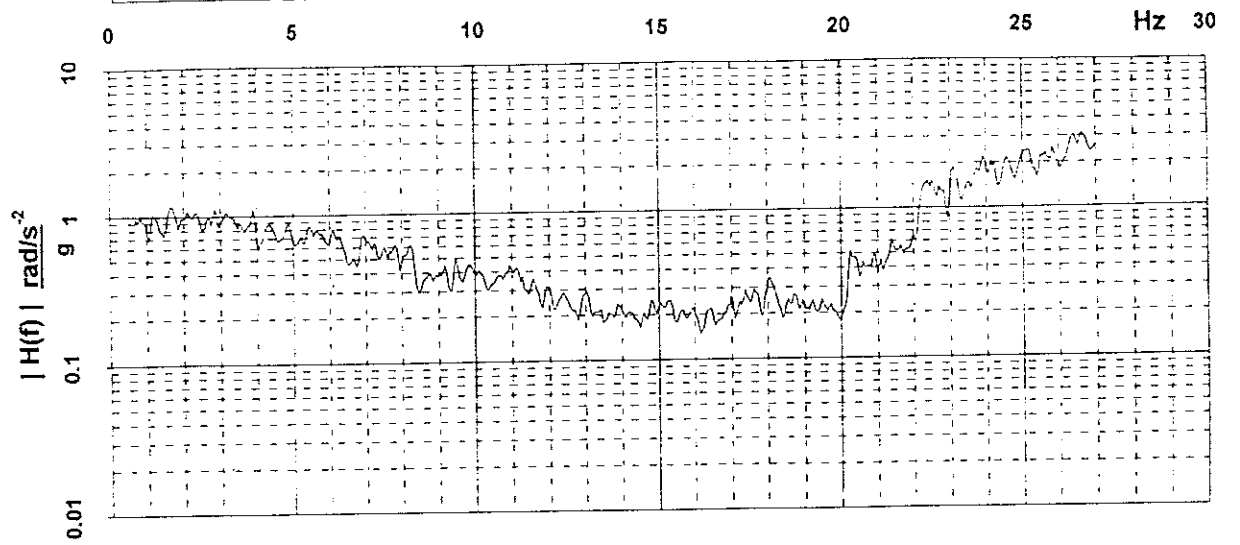
BARE FOR



BARE.FOR

15 ↓ 554 ↓

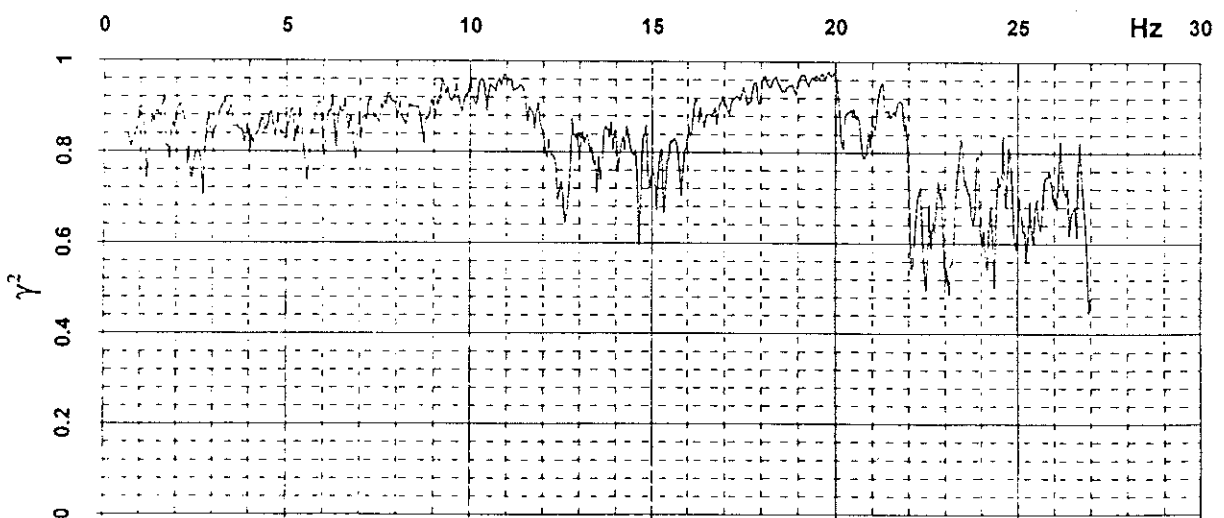
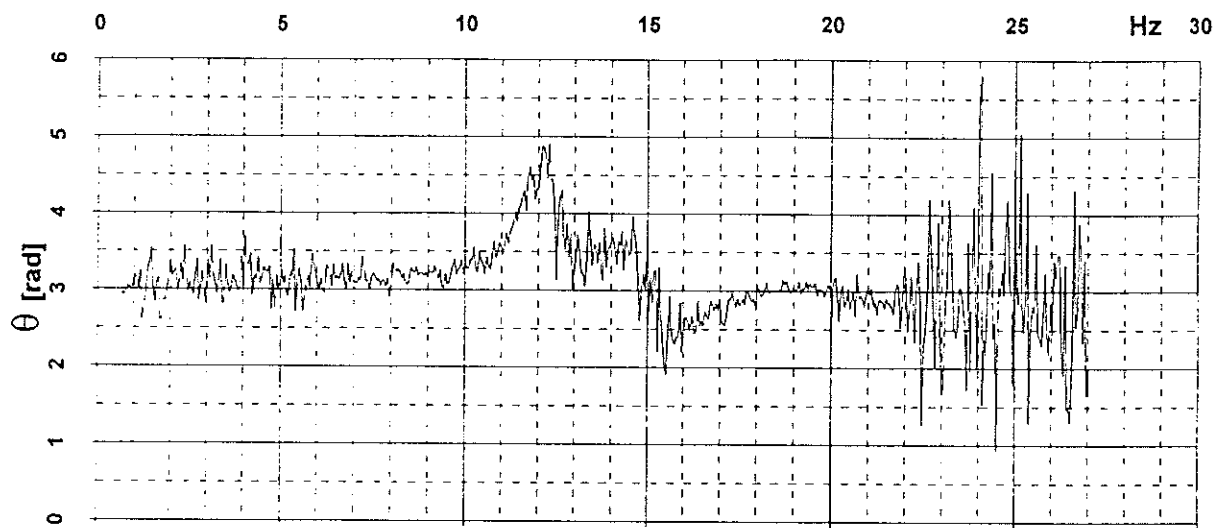
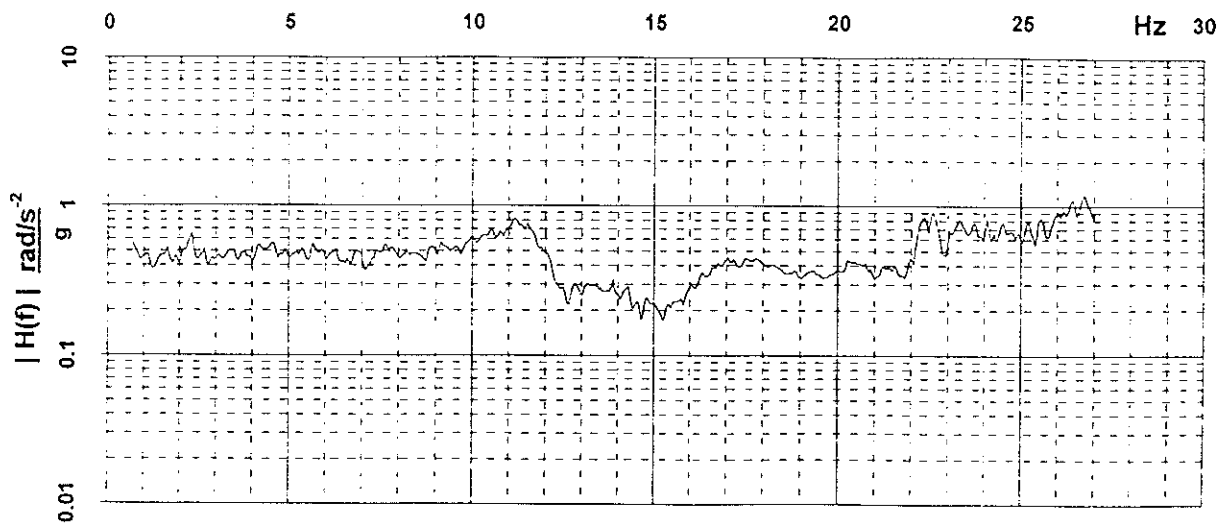
Long>Roll ↓



BARE FOR

15 ↓ 554 ↓

Long>Yaw ↓



BARE.FOR

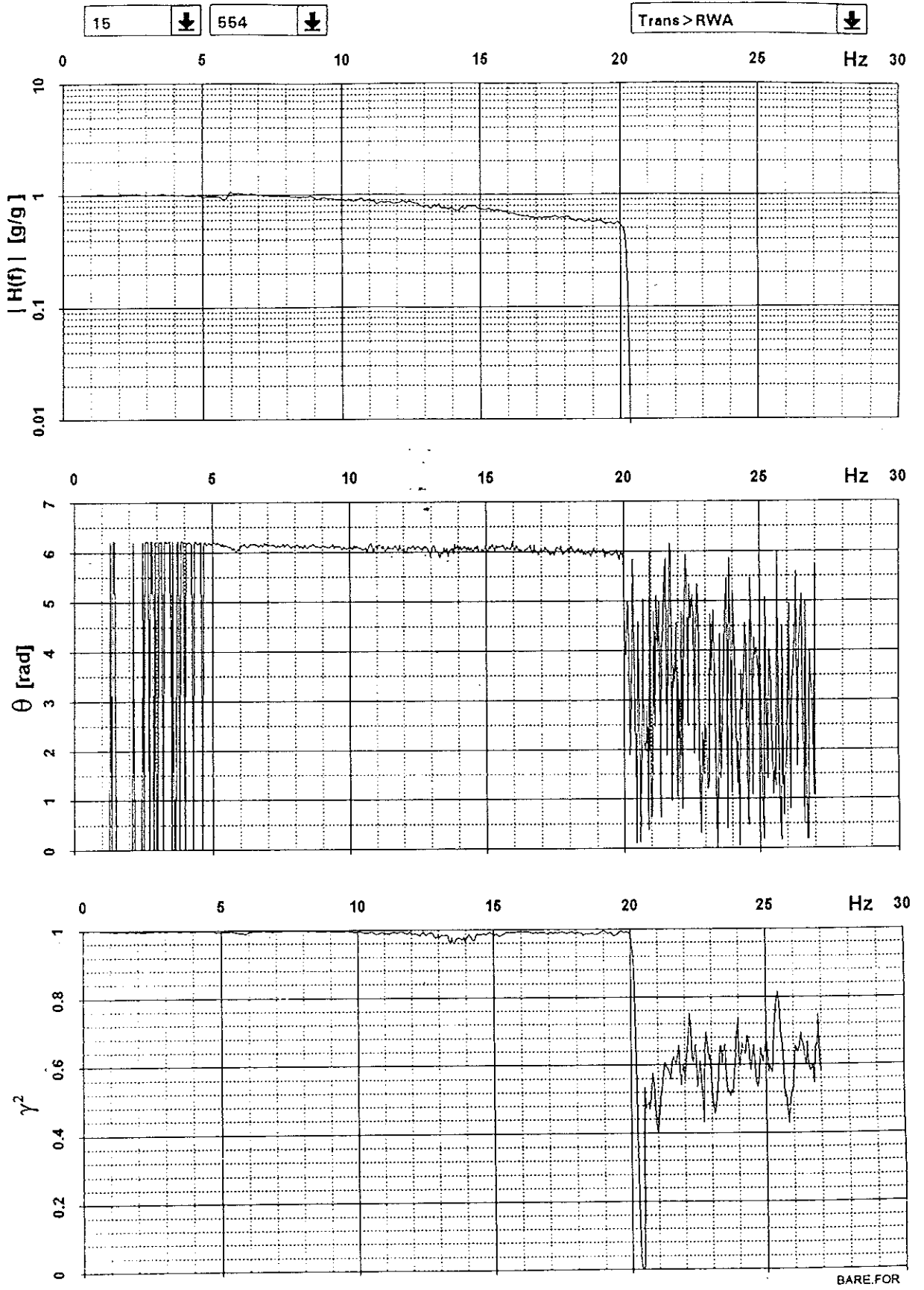
APPENDIX V

FREQUENCY RESPONSE FUNCTIONS

ADAPTED TEST WITH MODEL

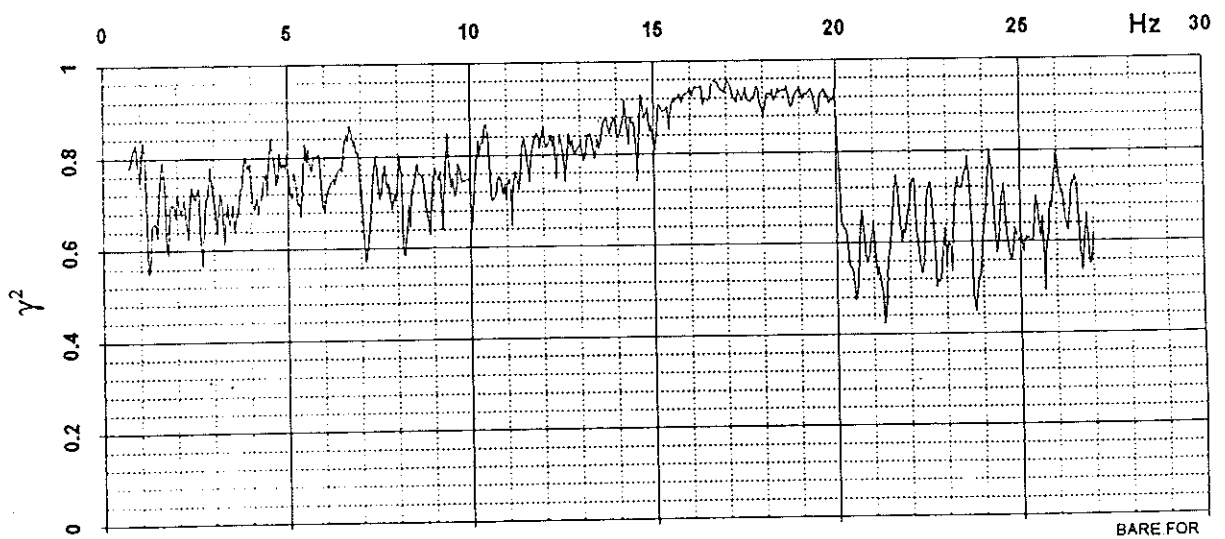
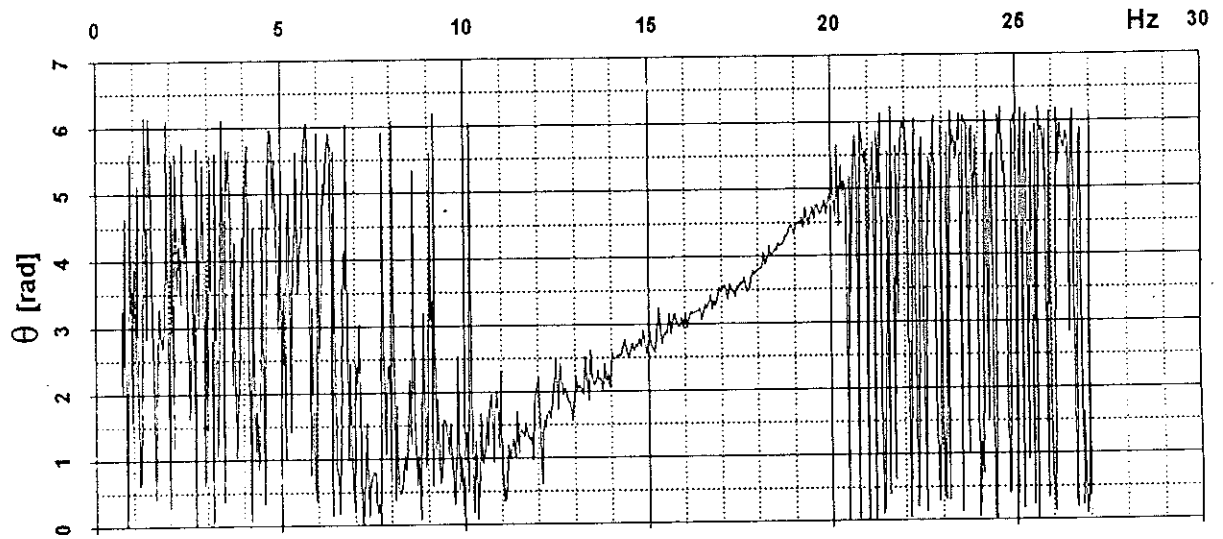
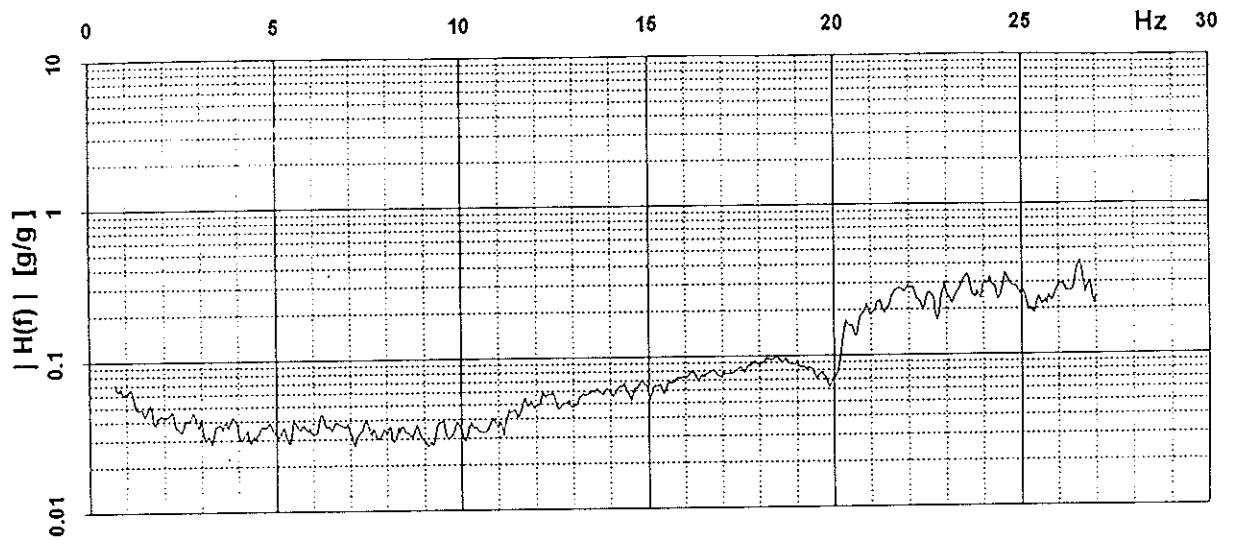
List of Figures

- AV.1 - Modulus, Phase and Coherence of FRF; input Transverse output Target Signal
- AV.2 - Modulus, Phase and Coherence of FRF; input Transverse output Vertical
- AV.3 - Modulus, Phase and Coherence of FRF; input Transverse output Longitudinal
- AV.4 - Modulus, Phase and Coherence of FRF; input Transverse output Pitch
- AV.5 - Modulus, Phase and Coherence of FRF; input Transverse output Roll
- AV.6 - Modulus, Phase and Coherence of FRF; input Transverse output Yaw
- AV.7 - Modulus, Phase and Coherence of FRF; input Vertical output Target Signal
- AV.8 - Modulus, Phase and Coherence of FRF; input Vertical output Transverse
- AV.9 - Modulus, Phase and Coherence of FRF; input Vertical output Longitudinal
- AV.10 - Modulus, Phase and Coherence of FRF; input Vertical output Pitch
- AV.11 - Modulus, Phase and Coherence of FRF; input Vertical output Roll
- AV.12 - Modulus, Phase and Coherence of FRF; input Vertical output Yaw
- AV.13 - Modulus, Phase and Coherence of FRF; input Longitudinal output Target Signal
- AV.14 - Modulus, Phase and Coherence of FRF; input Longitudinal output Transverse
- AV.15 - Modulus, Phase and Coherence of FRF; input Longitudinal output Vertical
- AV.16 - Modulus, Phase and Coherence of FRF; input Longitudinal output Pitch
- AV.17 - Modulus, Phase and Coherence of FRF; input Longitudinal output Roll
- AV.18 - Modulus, Phase and Coherence of FRF; input Longitudinal output Yaw
- AV.19 - Modulus, Phase and Coherence of FRF; input Transverse output Transverse Model
- AV.20 - Modulus, Phase and Coherence of FRF; input Transverse output Longitudinal Model
- AV.21 - Modulus, Phase and Coherence of FRF; input Longitudinal output Longitudinal Model
- AV.22 - Modulus, Phase and Coherence of FRF; input Longitudinal output Transverse Model

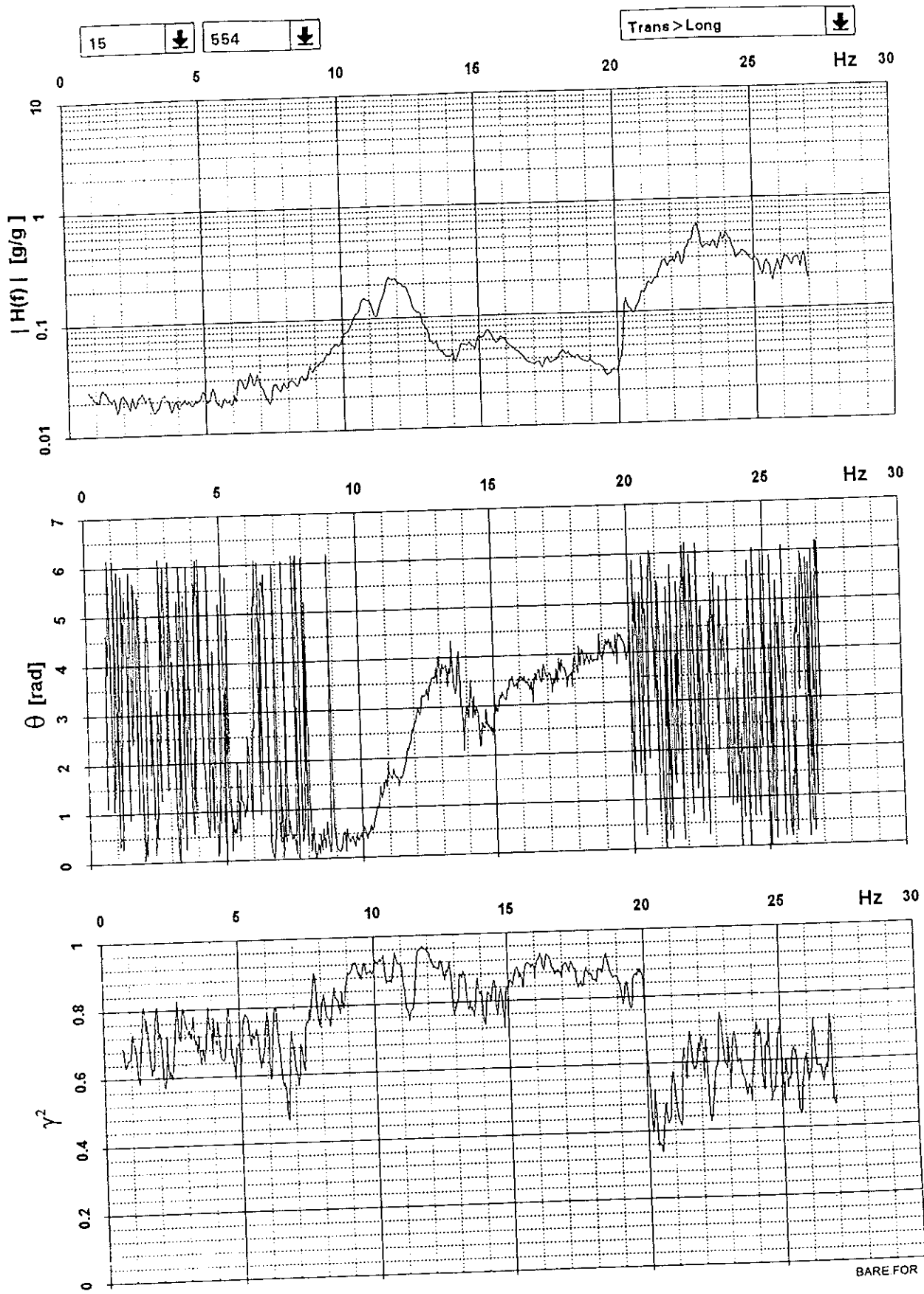


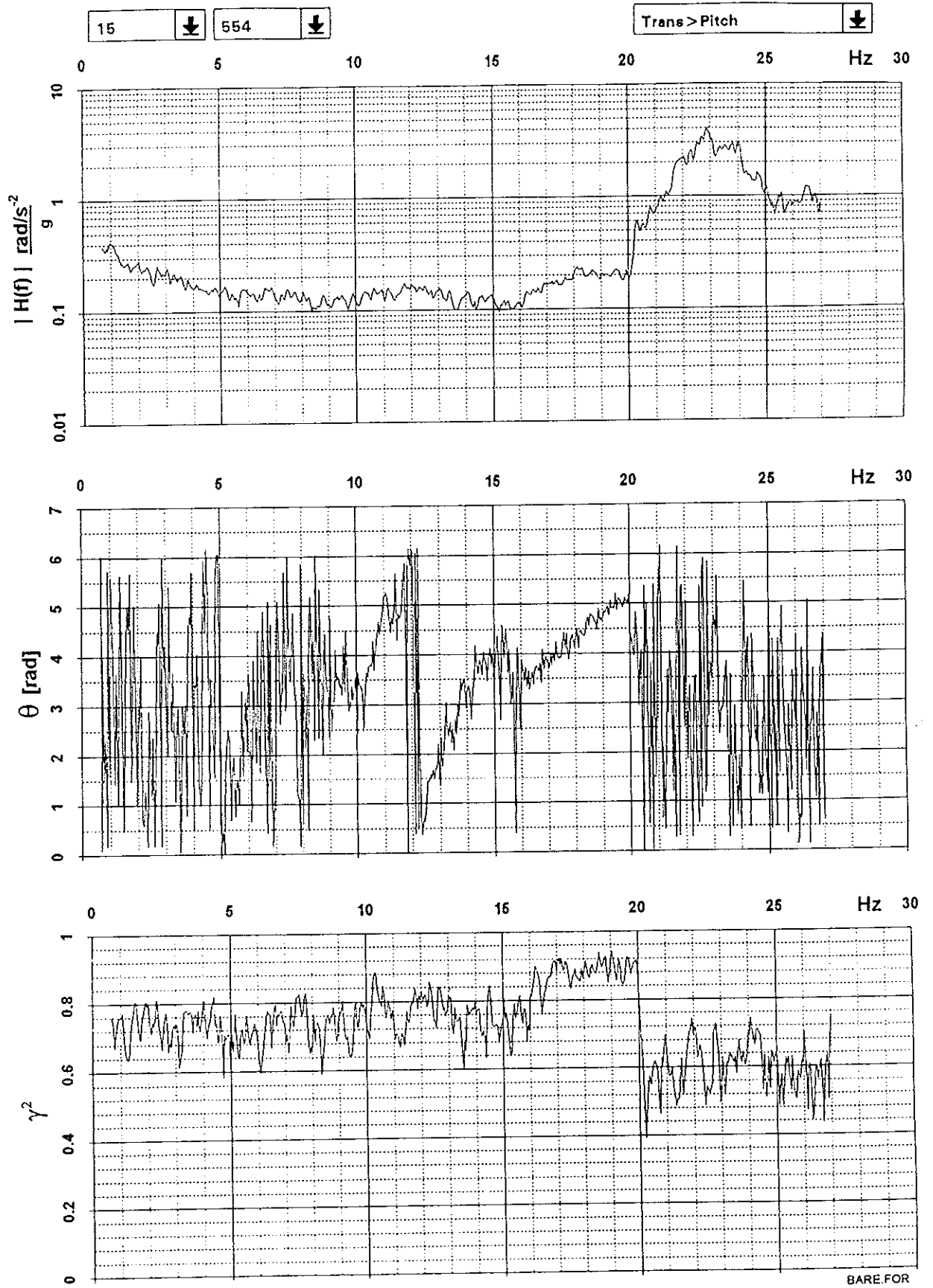
15 ↓ 554 ↓

Trans > Vert ↓



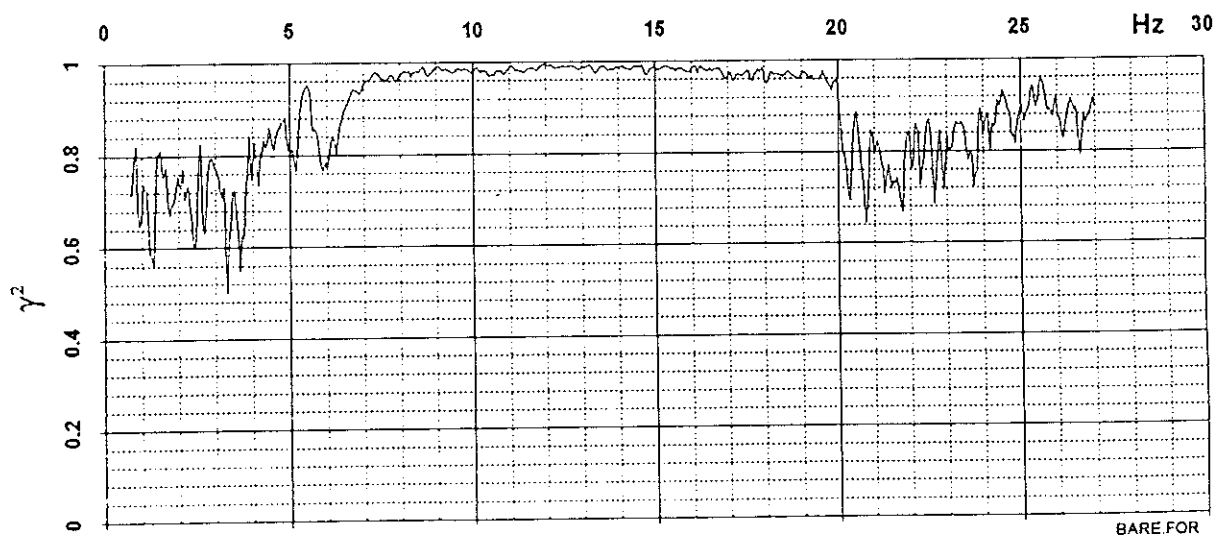
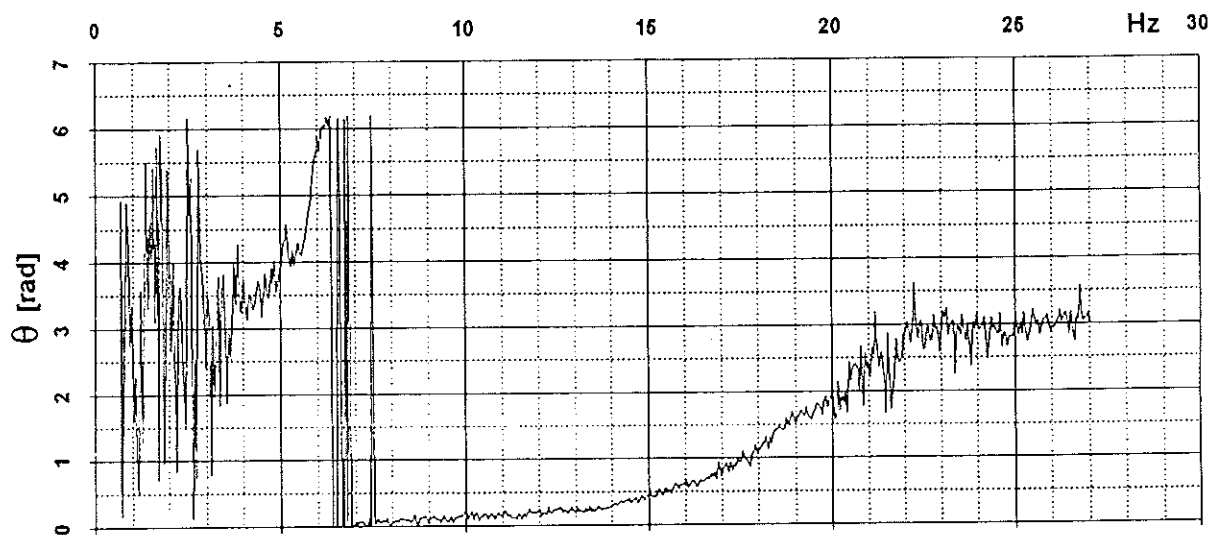
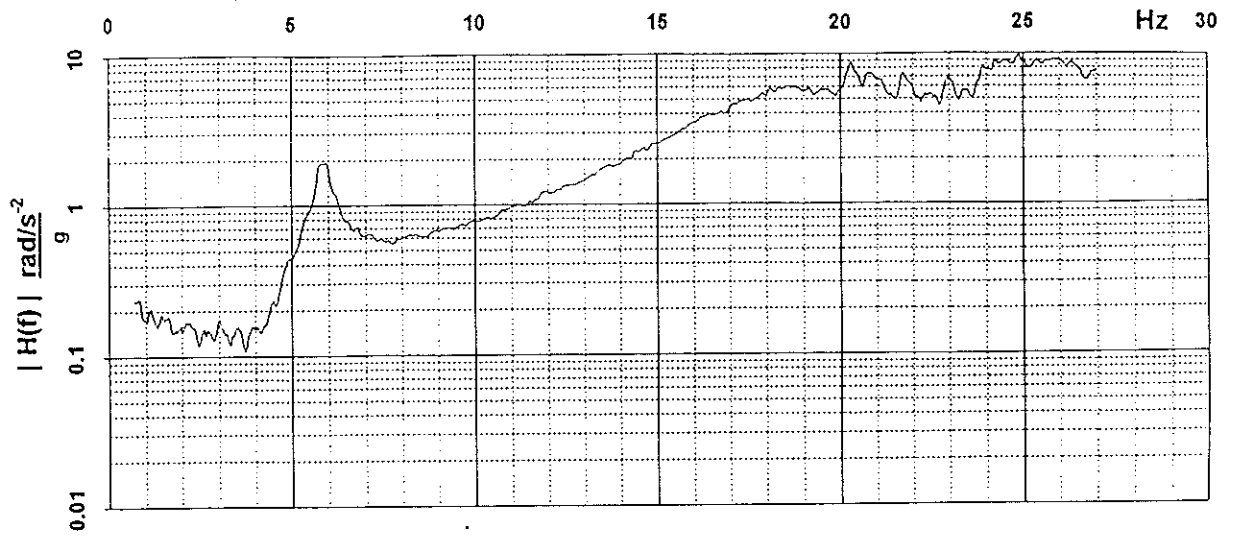
BARE FOR



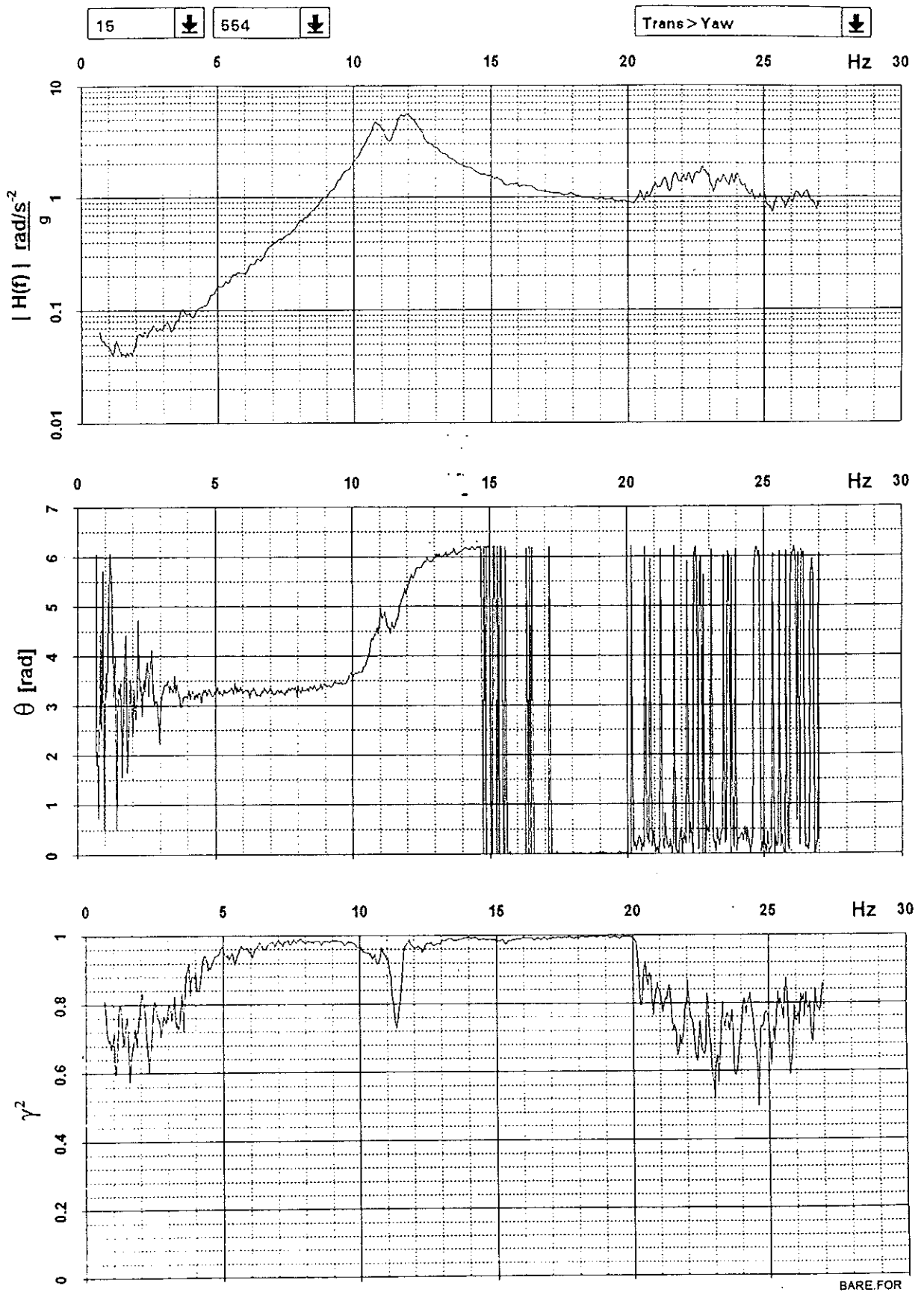


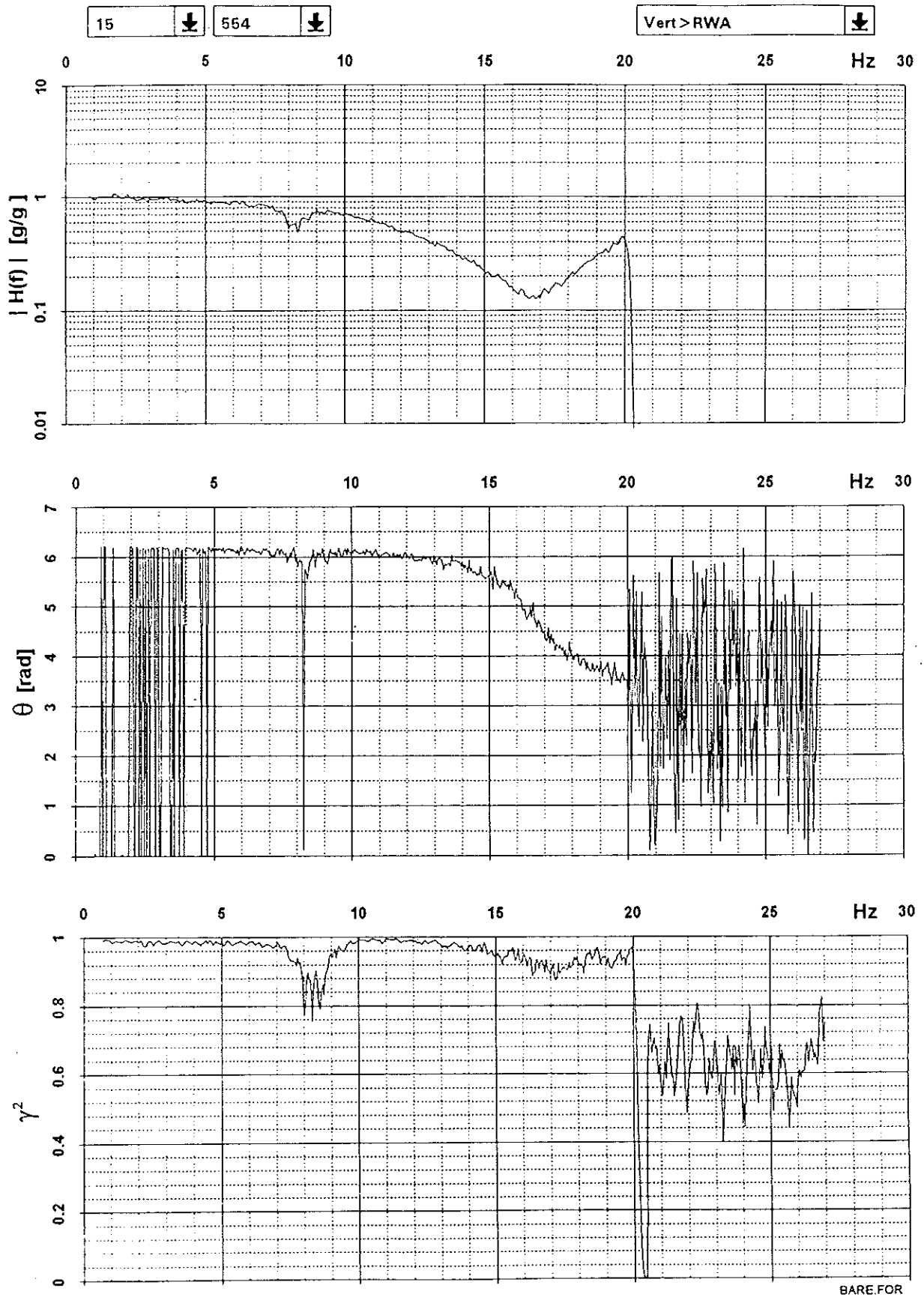
15 ↓ 554 ↓

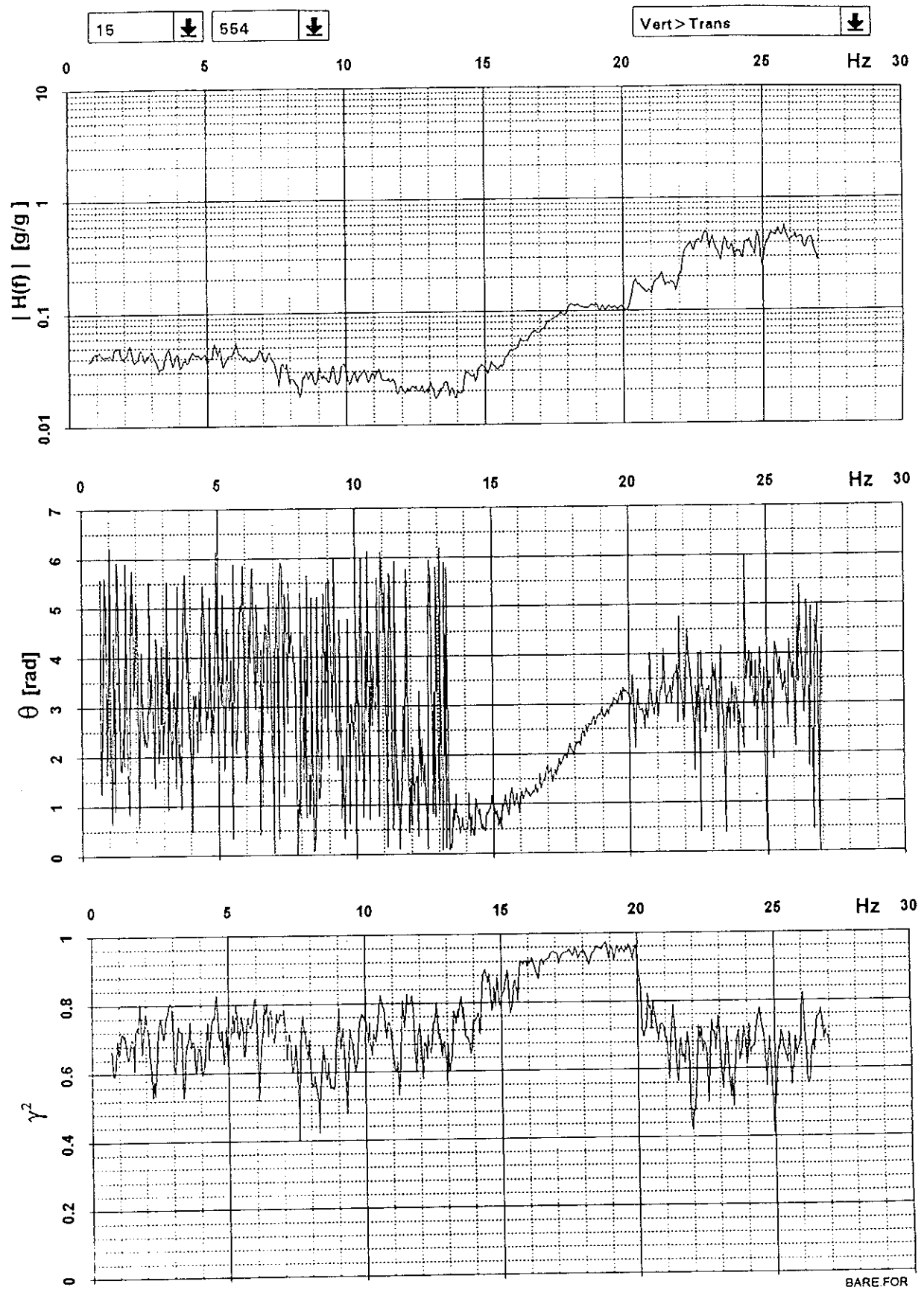
Trans > Roll ↓



BARE.FOR

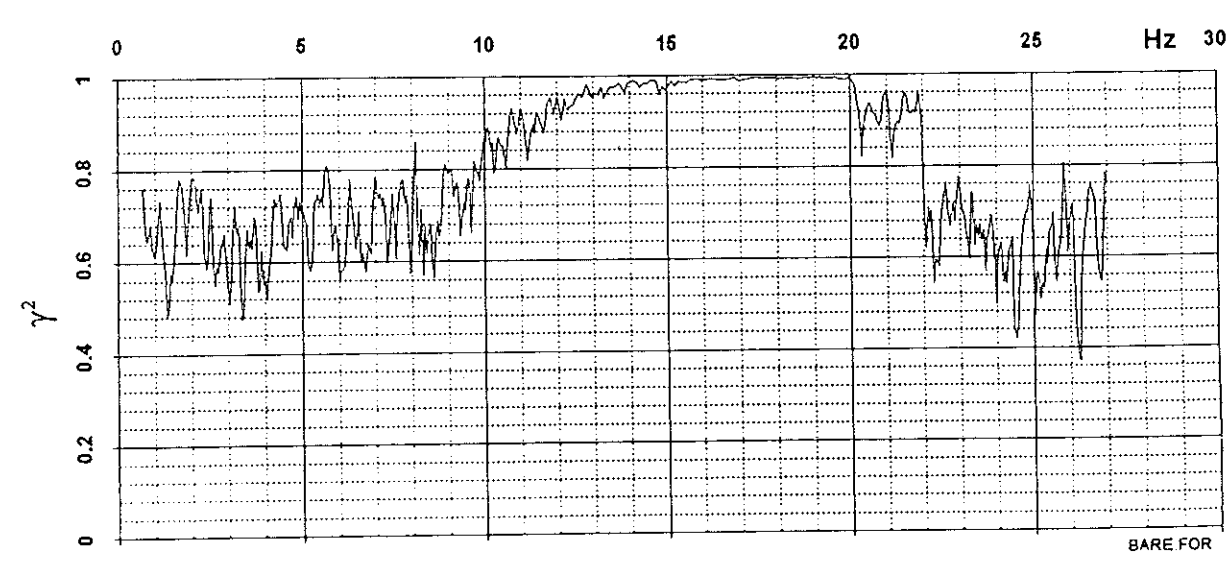
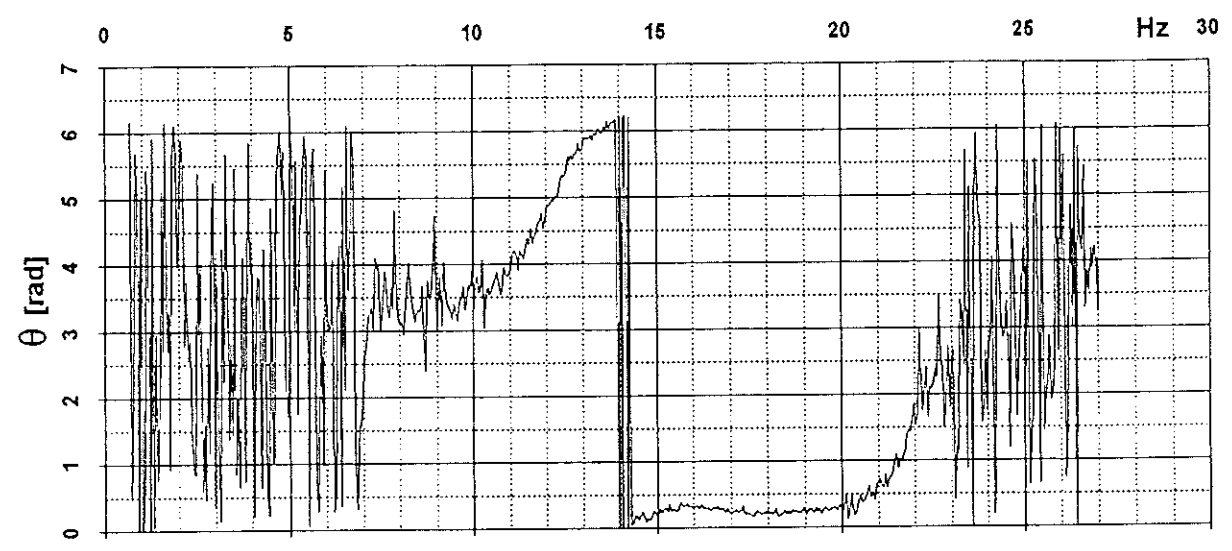
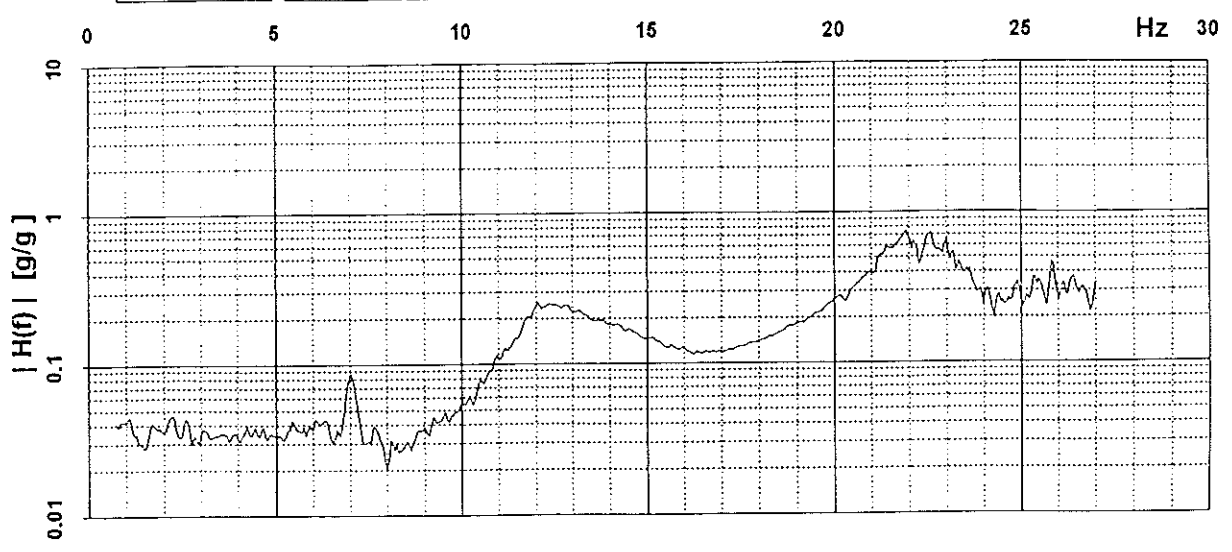




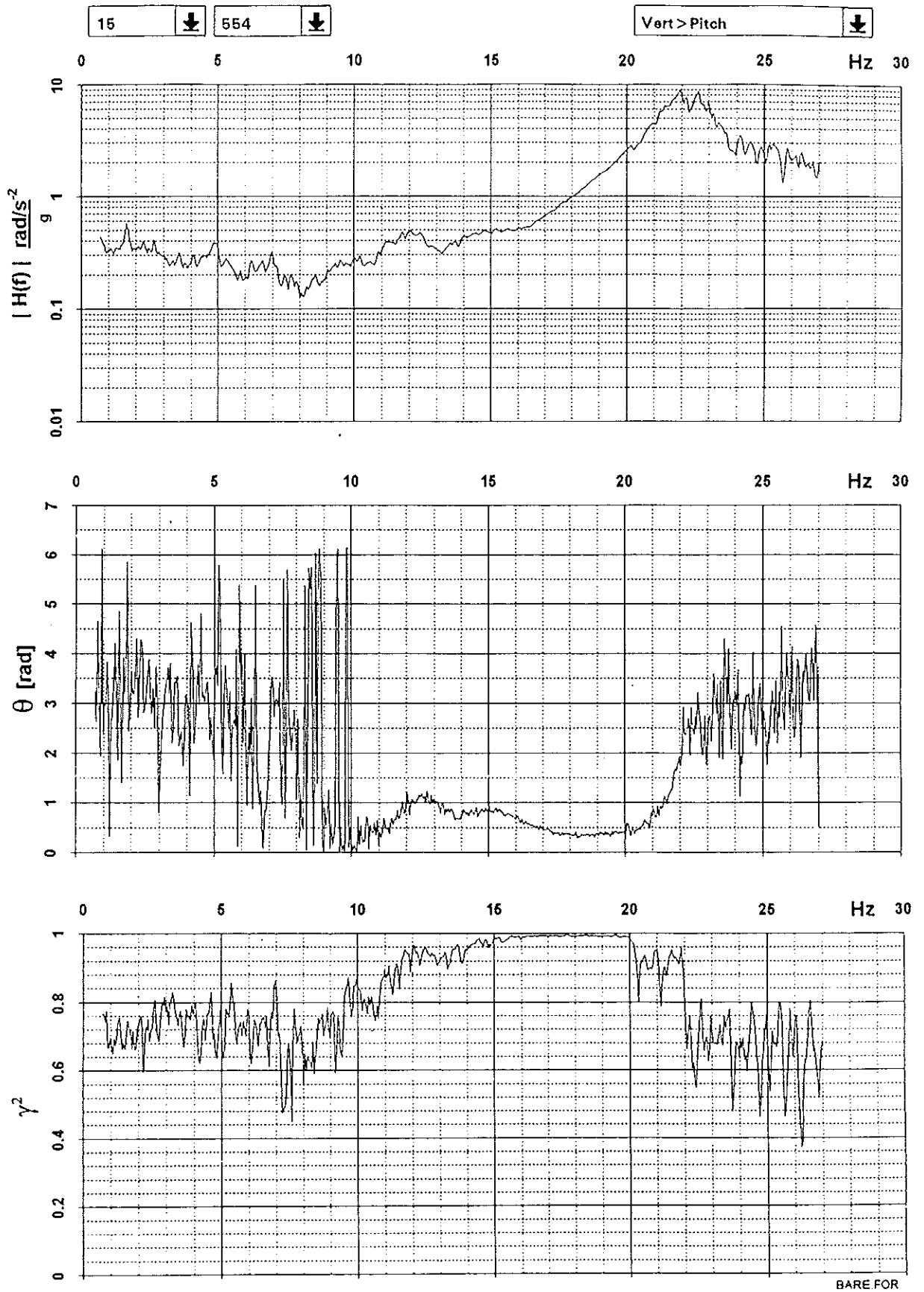


15 ↓ 554 ↓

Vert > Long ↓

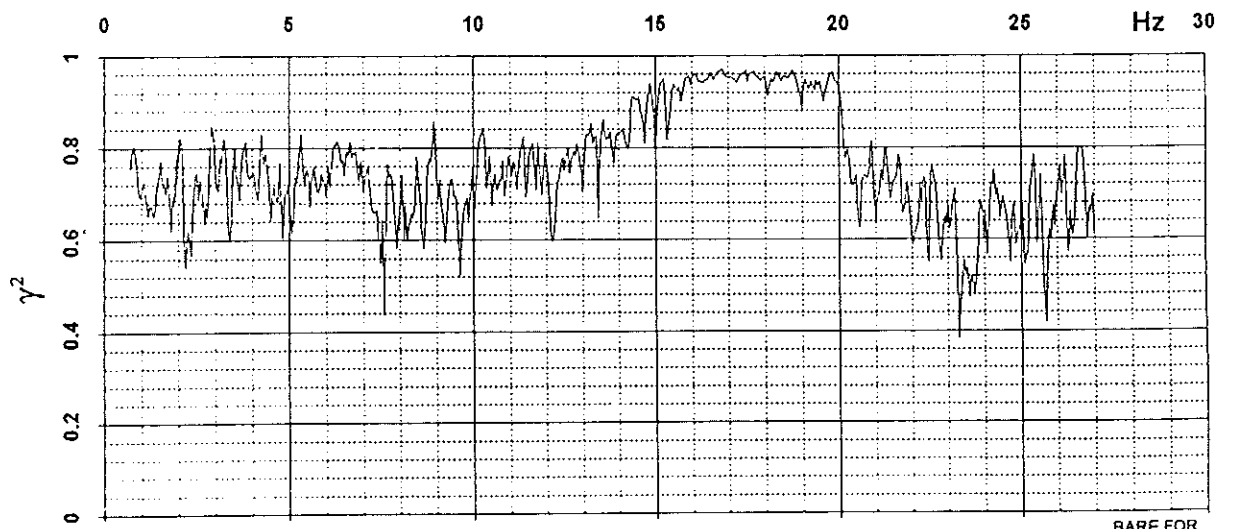
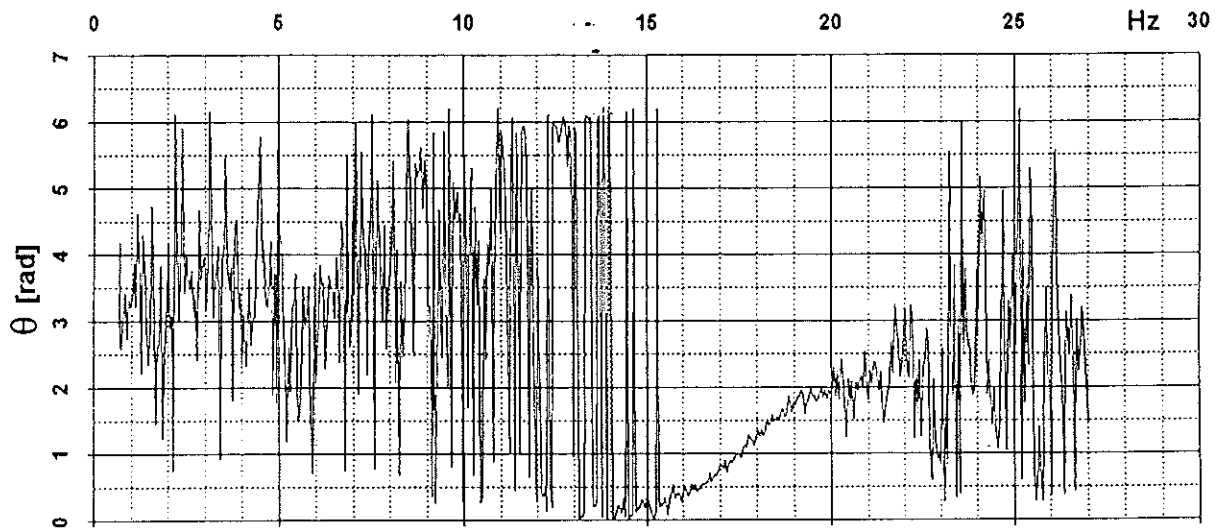
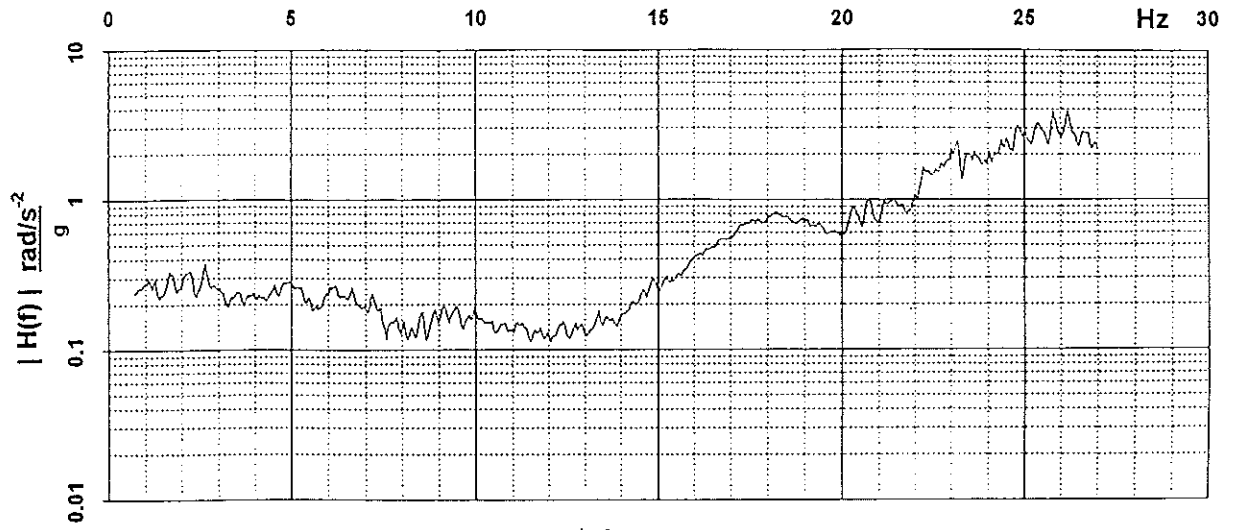


BARE FOR



15 ↓ 554 ↓

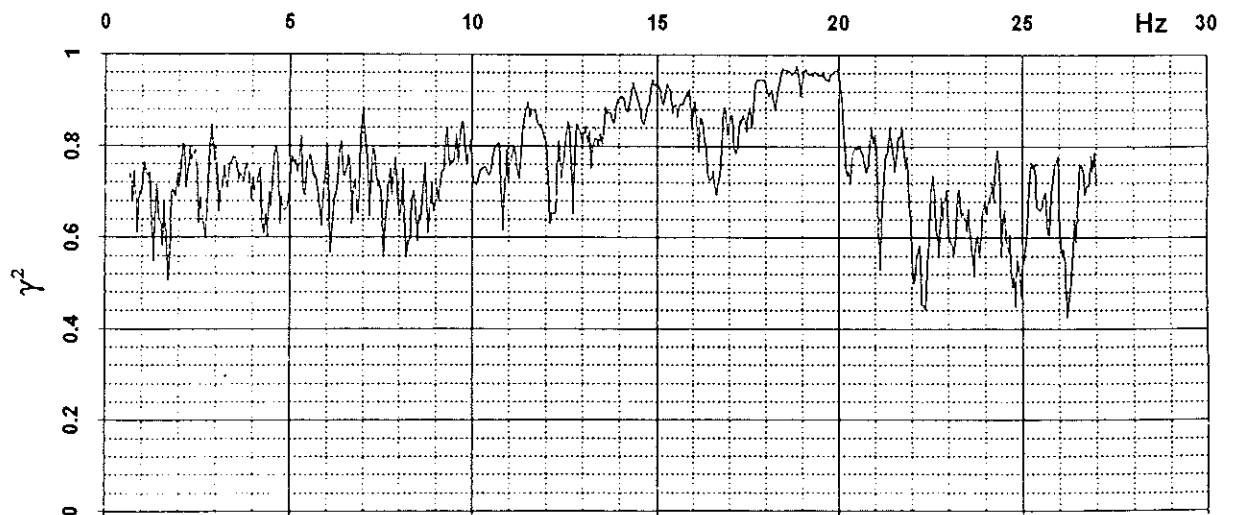
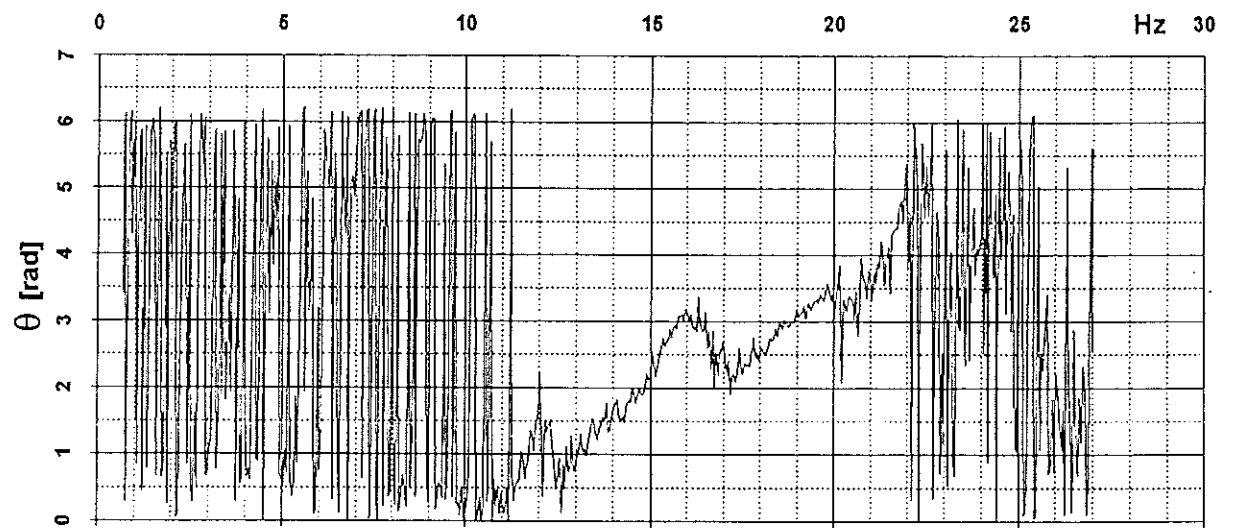
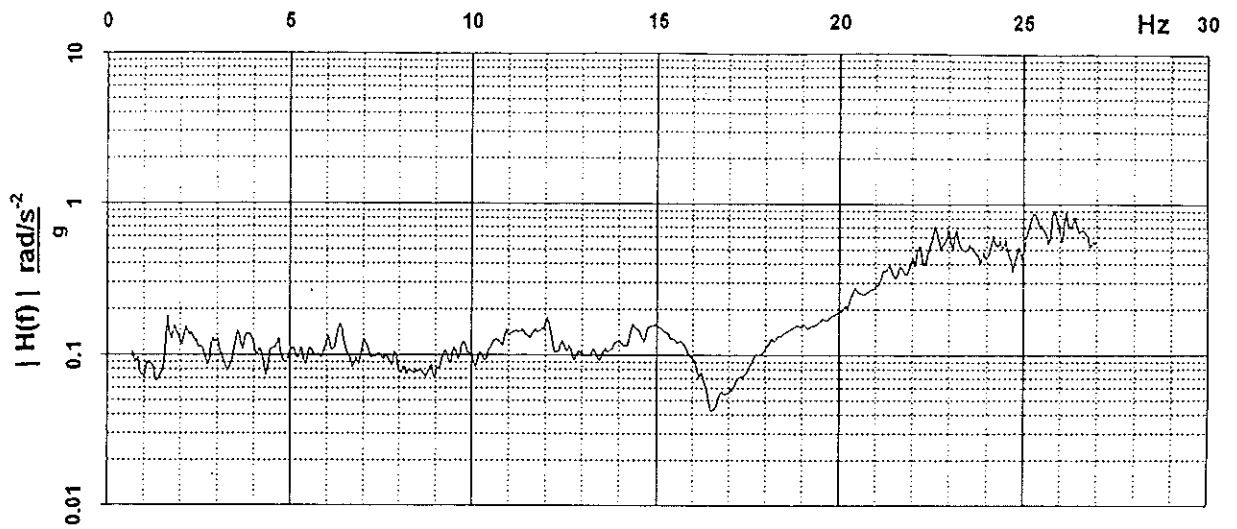
Vert > Roll ↓



BARE.FOR

15 ↓ 554 ↓

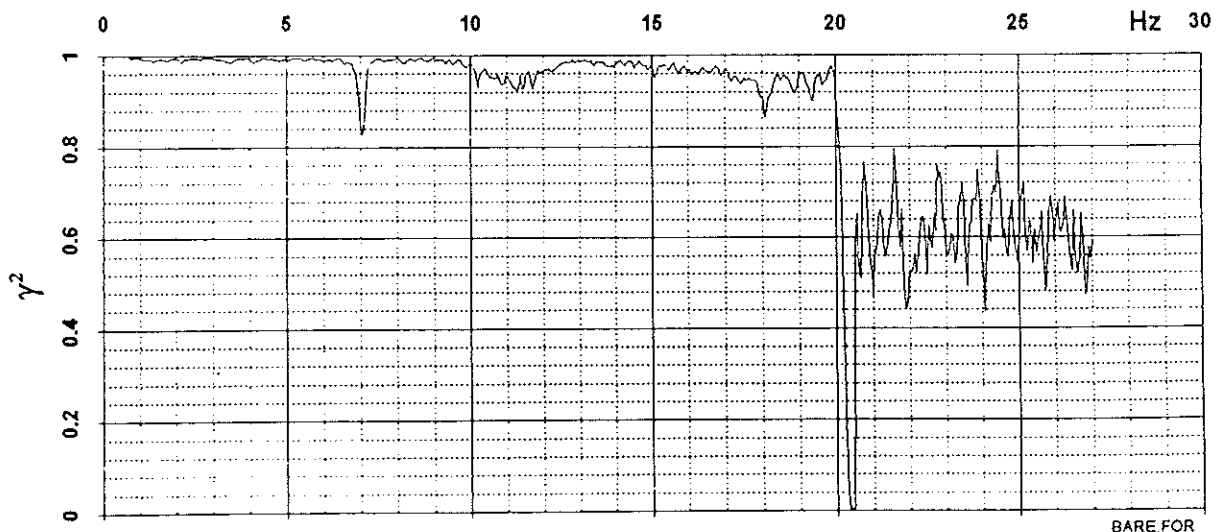
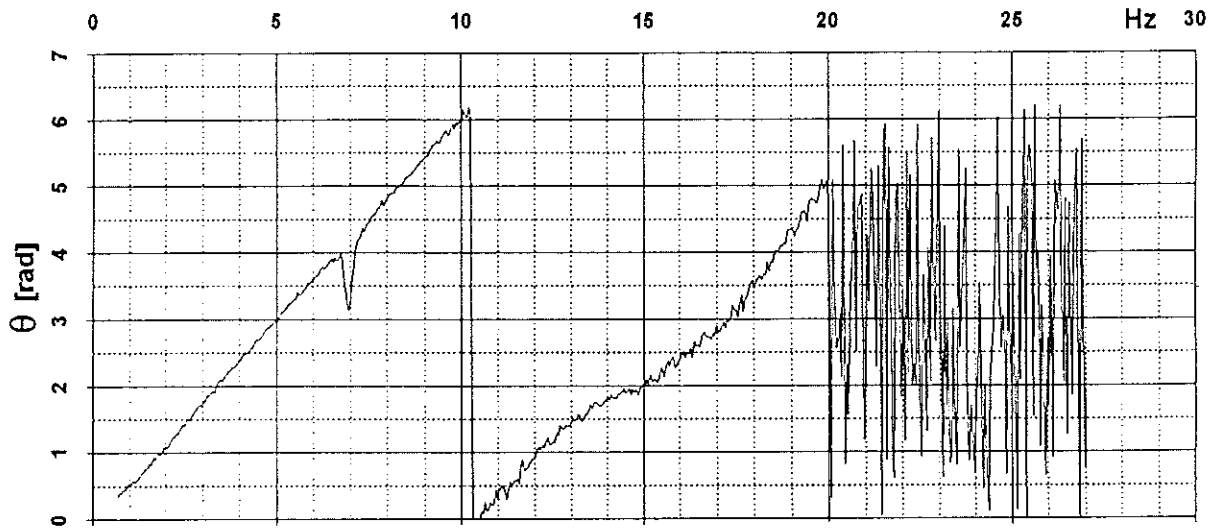
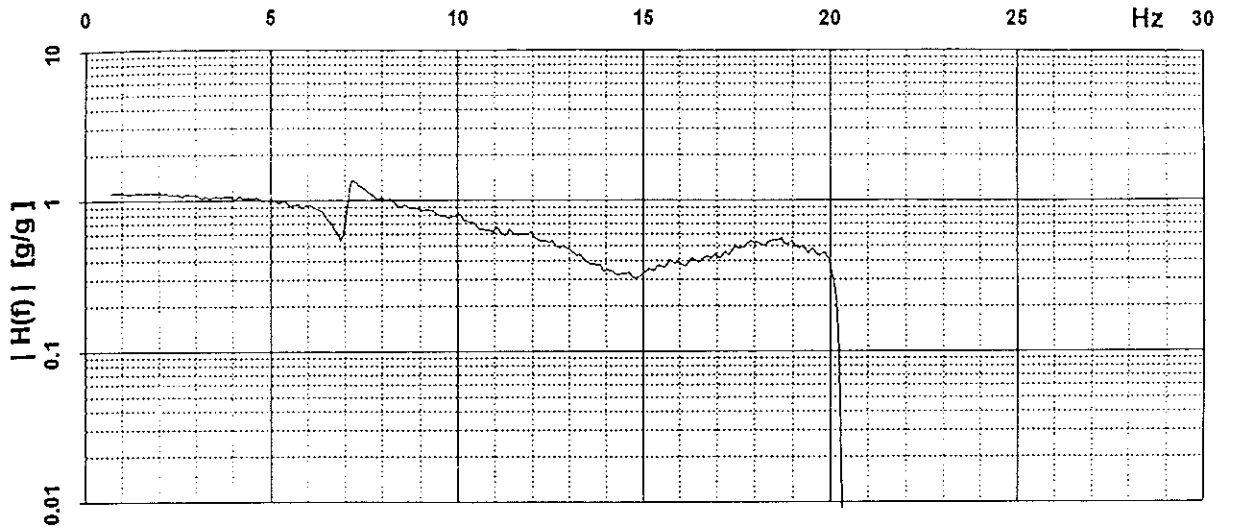
Vert > Yaw ↓



BARE.FOR

15 554

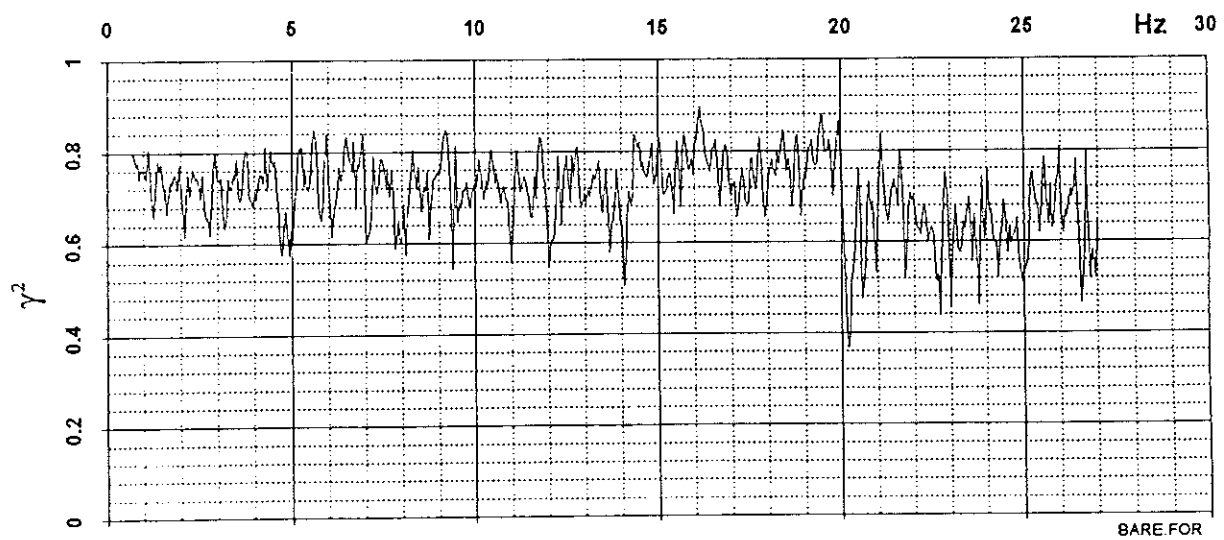
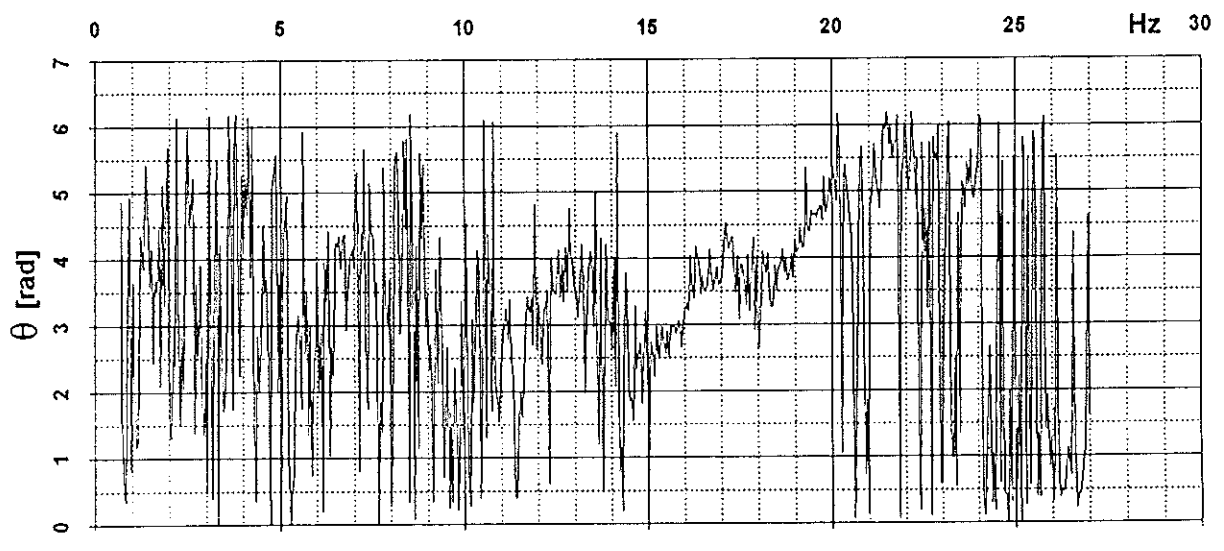
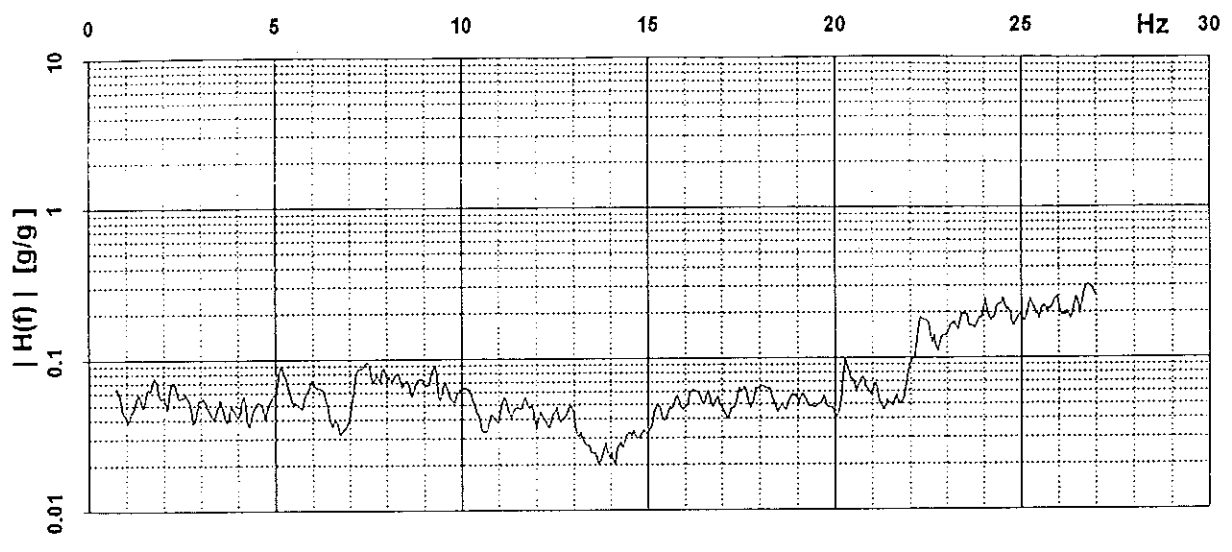
Long > RWA



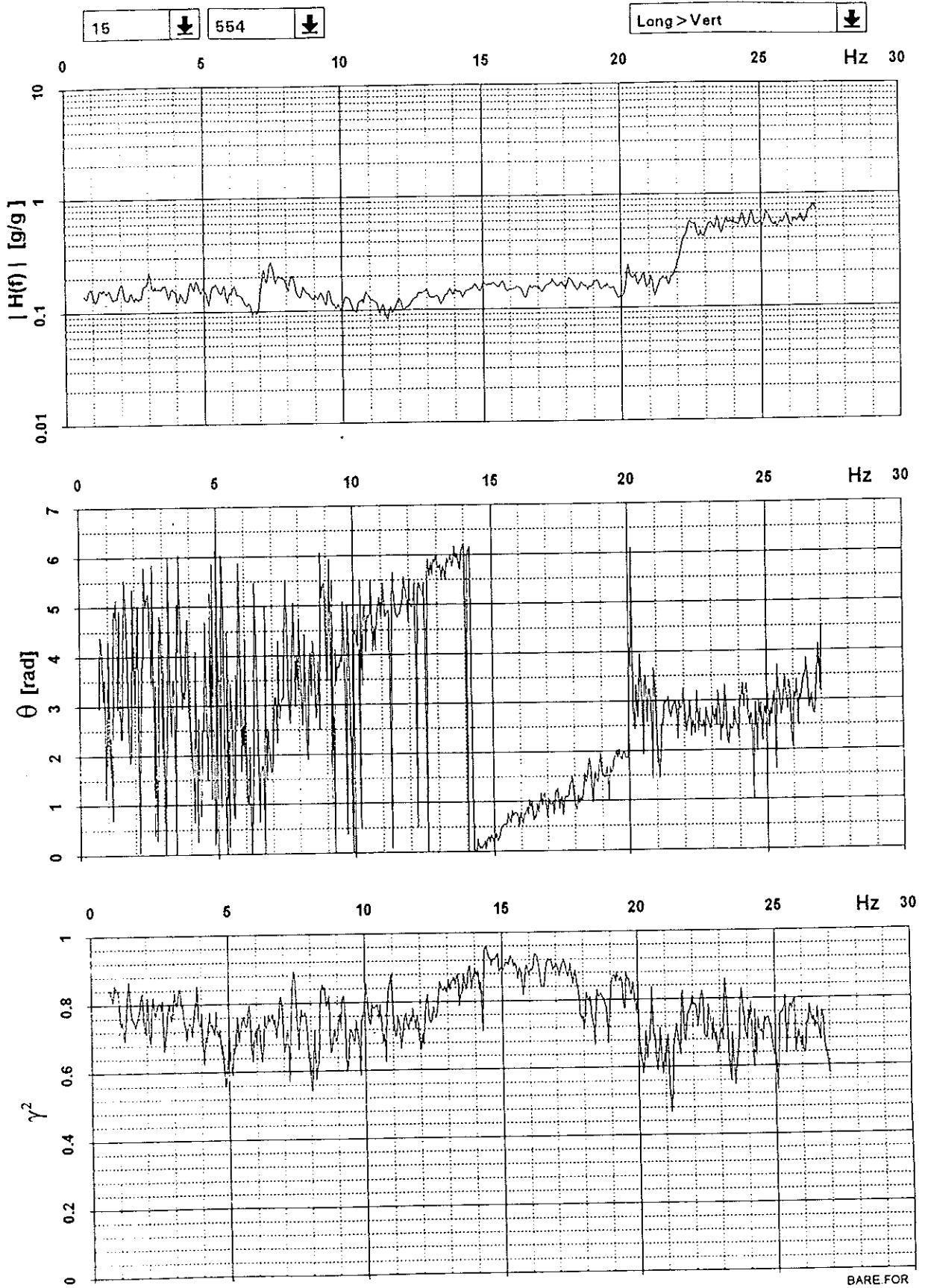
BARE FOR

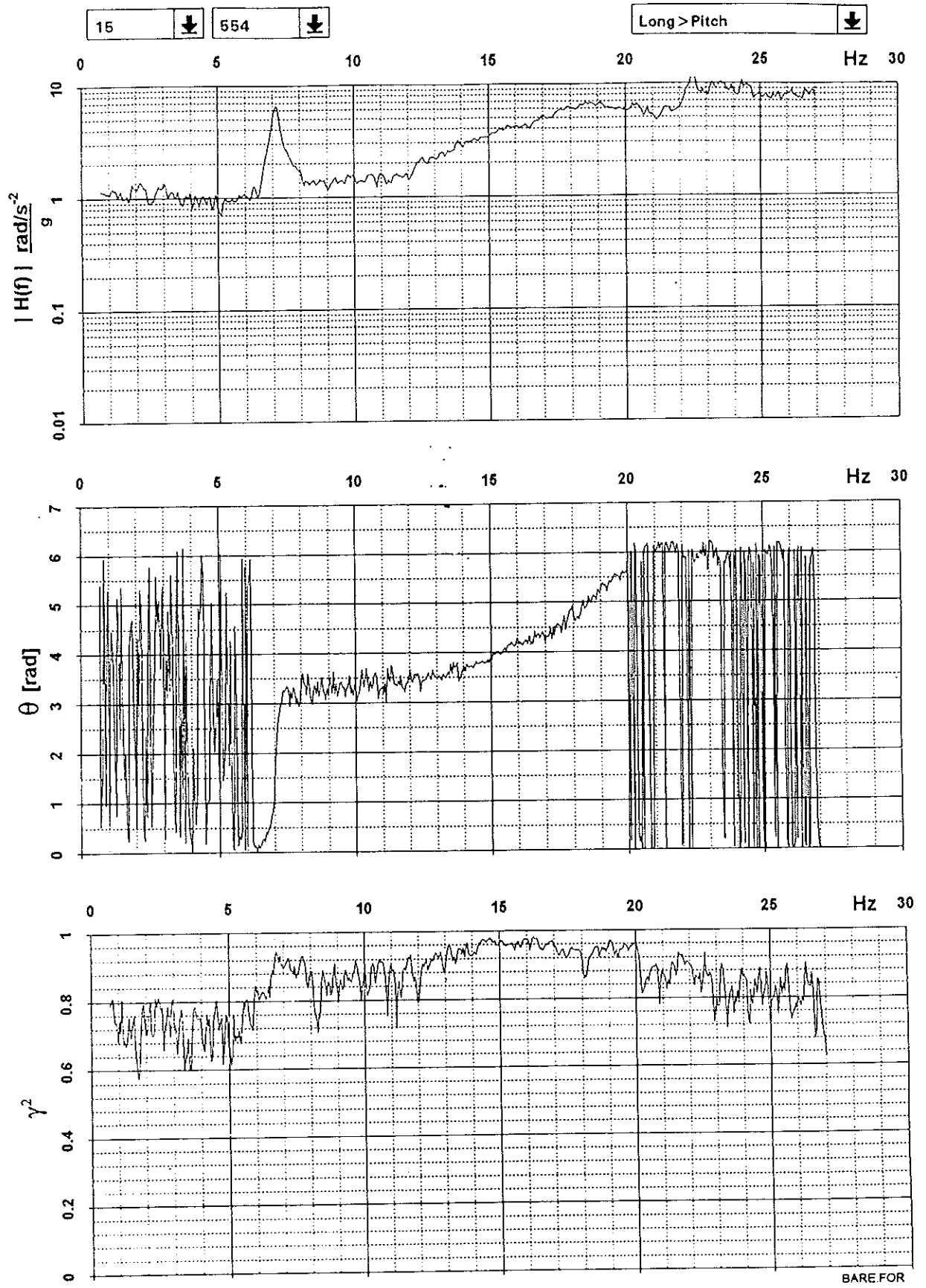
15 ↓ 554 ↓

Long > Trans ↓



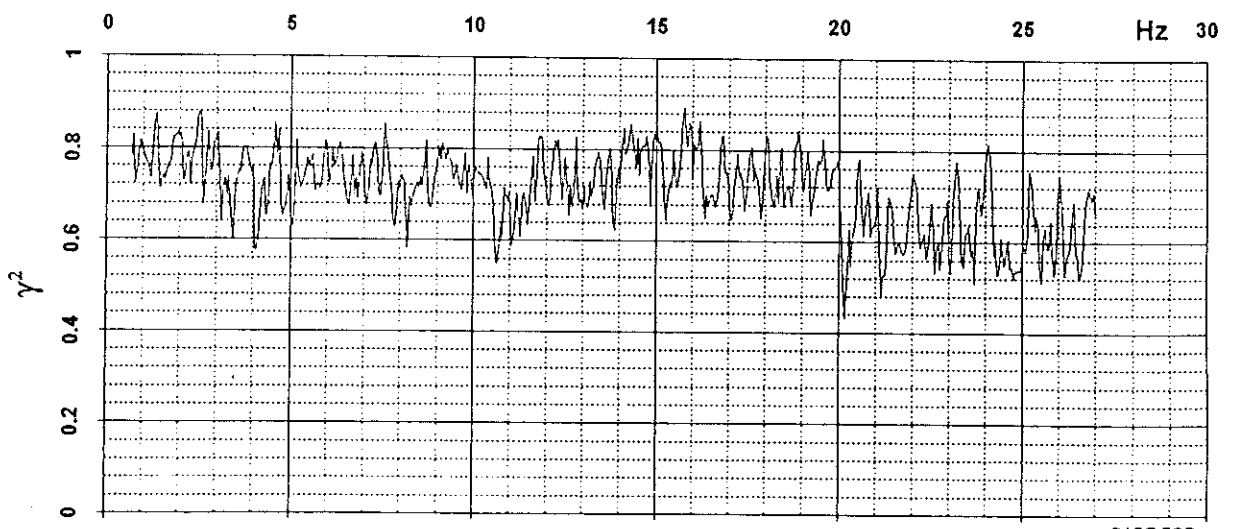
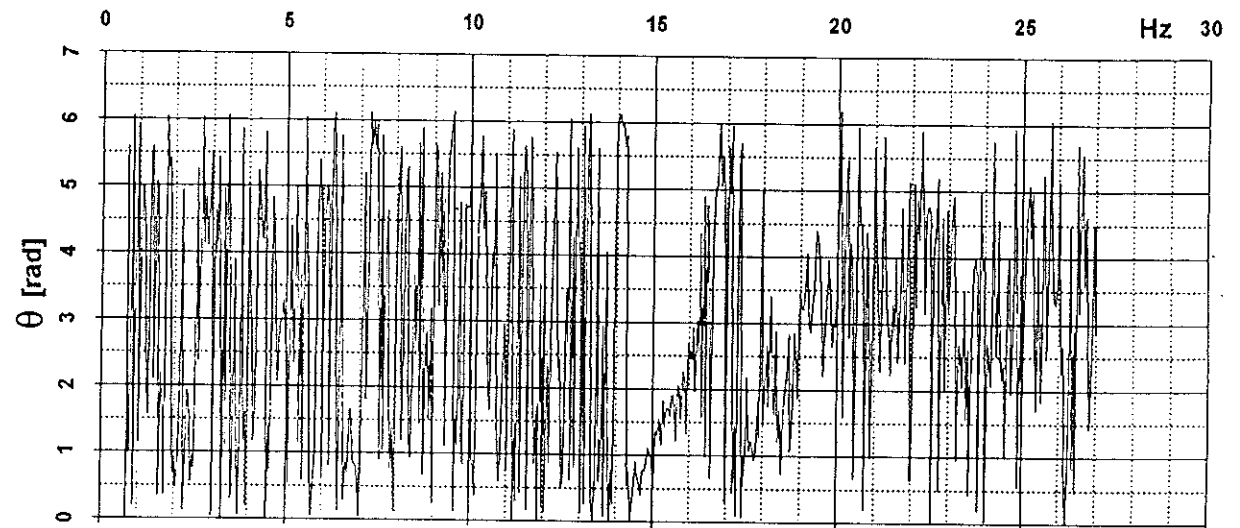
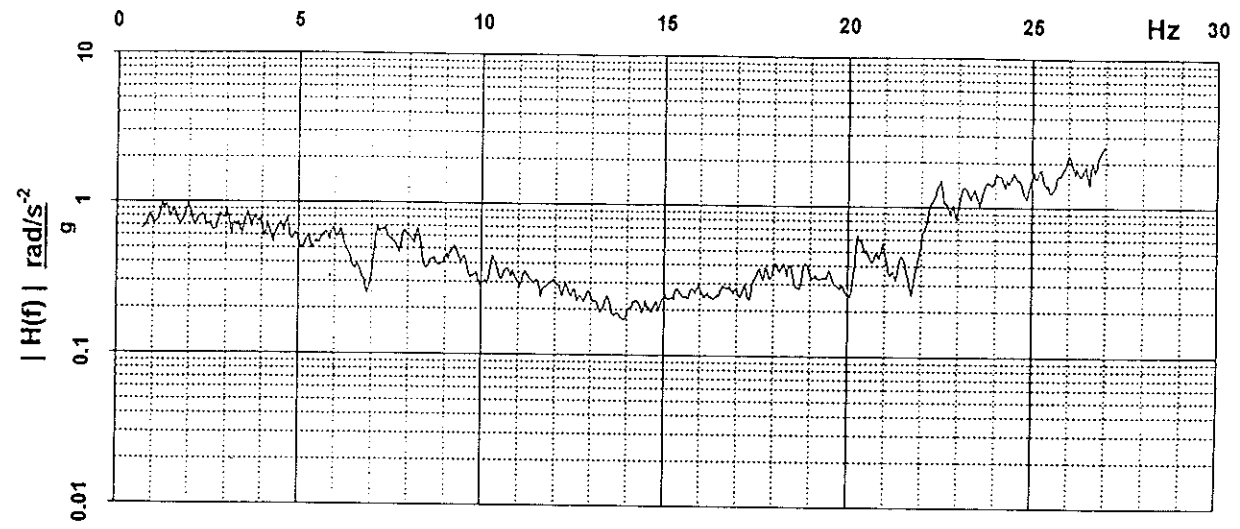
BARE FOR





15 ↓ 554 ↓

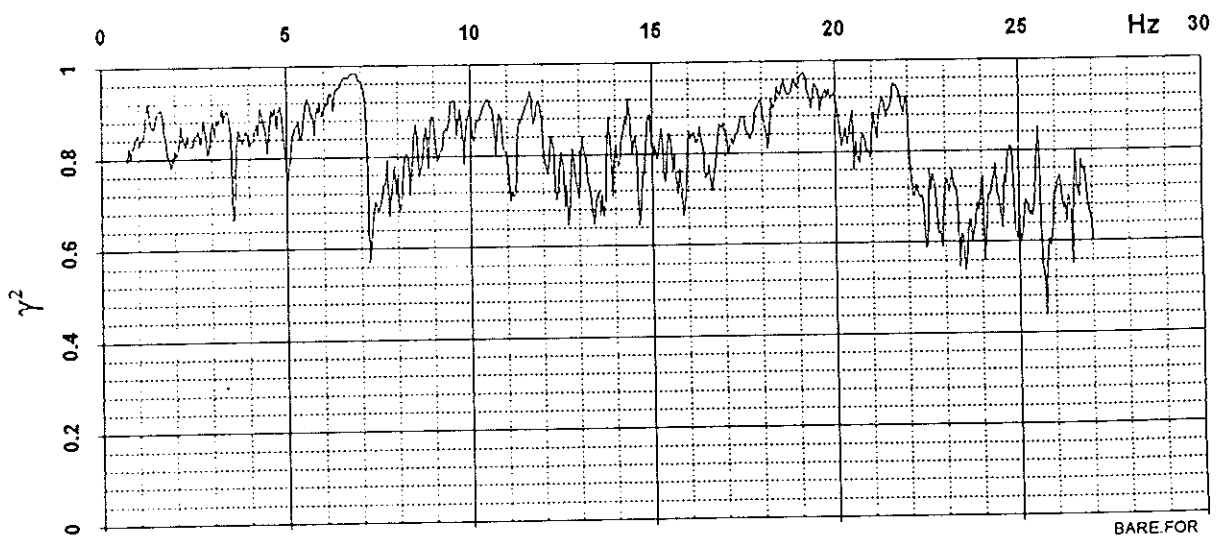
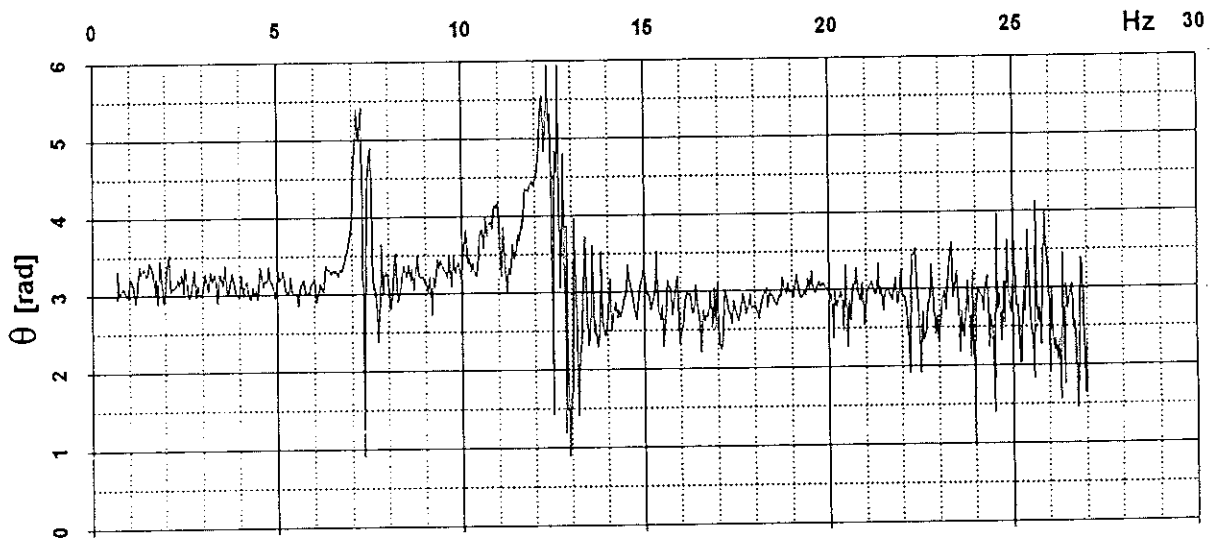
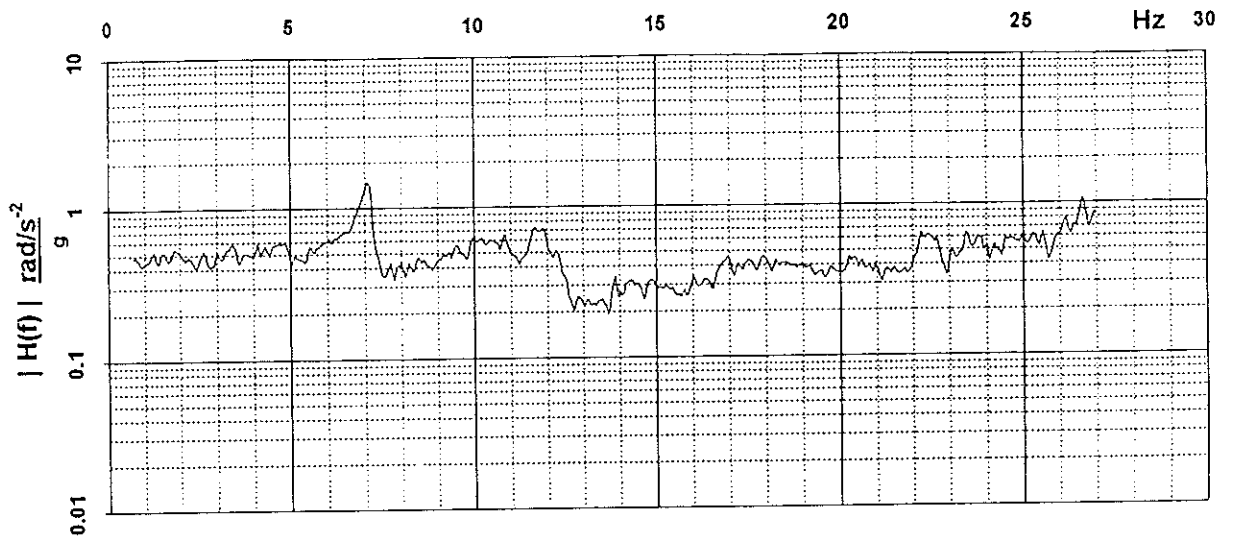
Long > Roll ↓



BARE.FOR

15 554

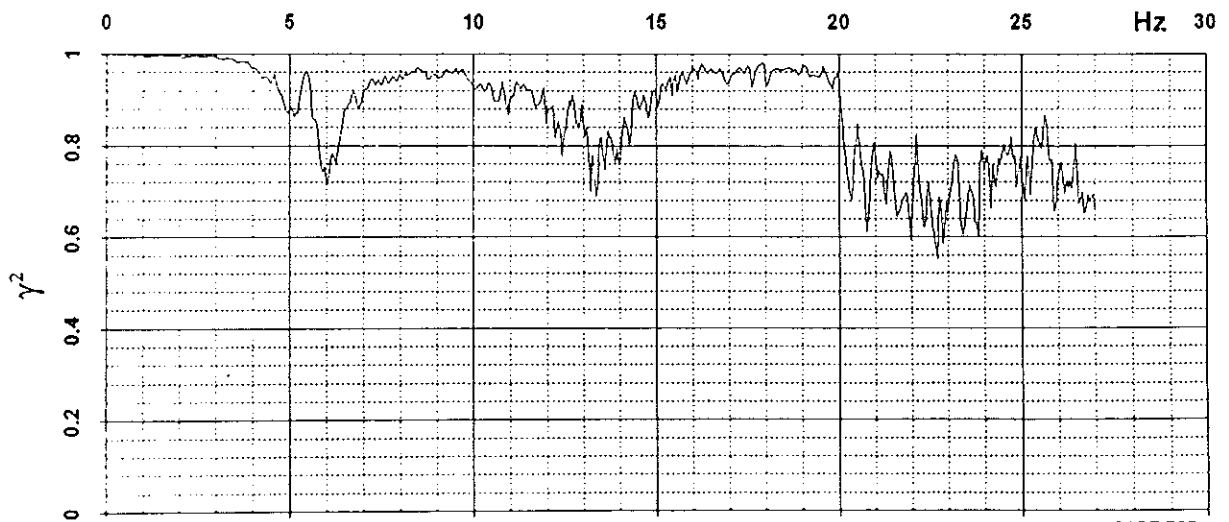
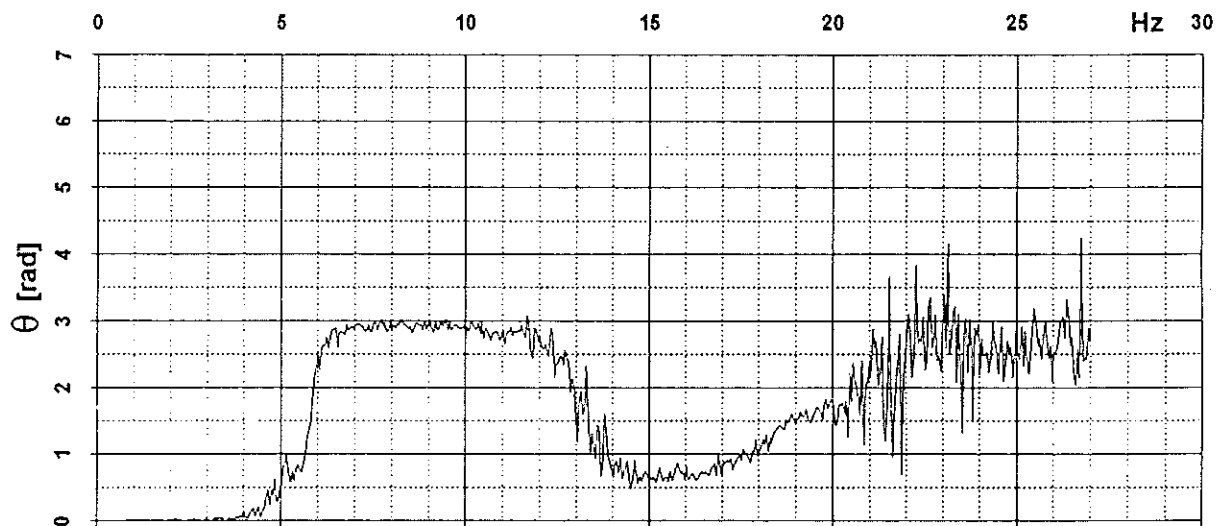
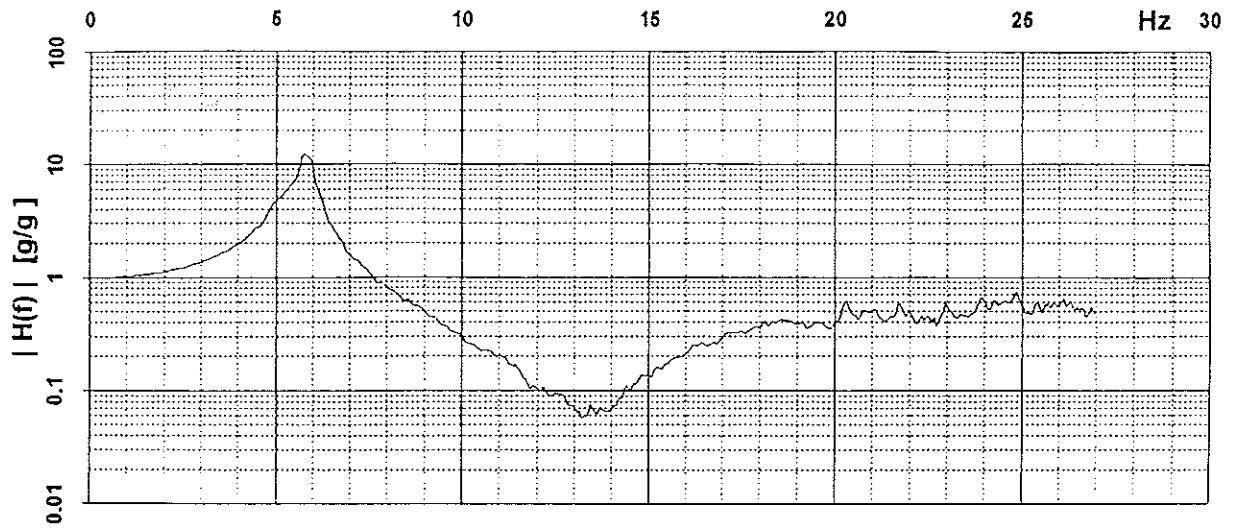
Long > Yaw



BARE FOR

15 ↓ 554 ↓

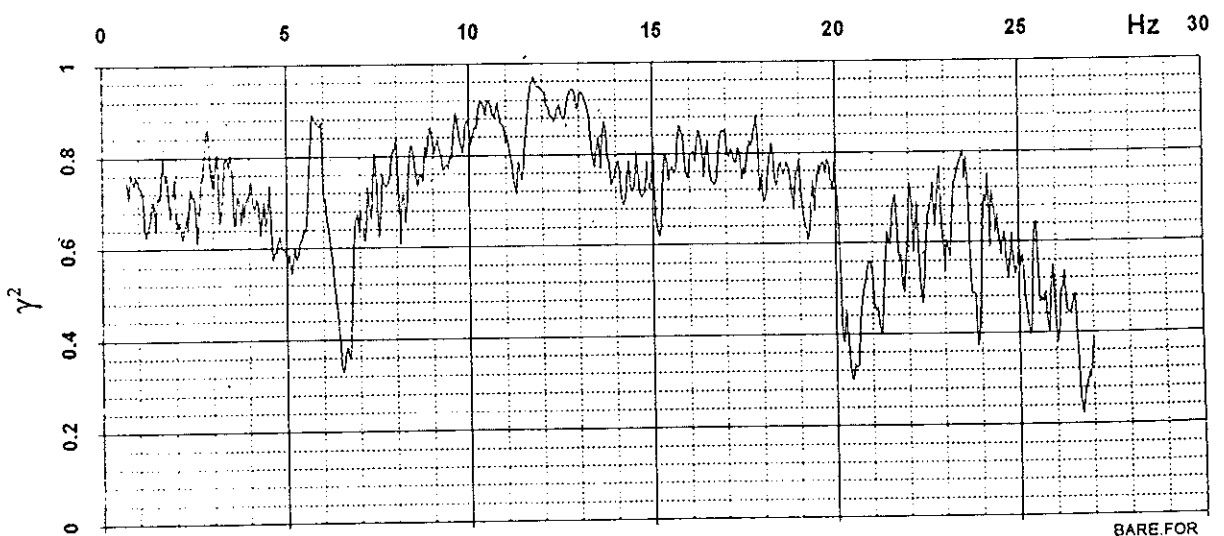
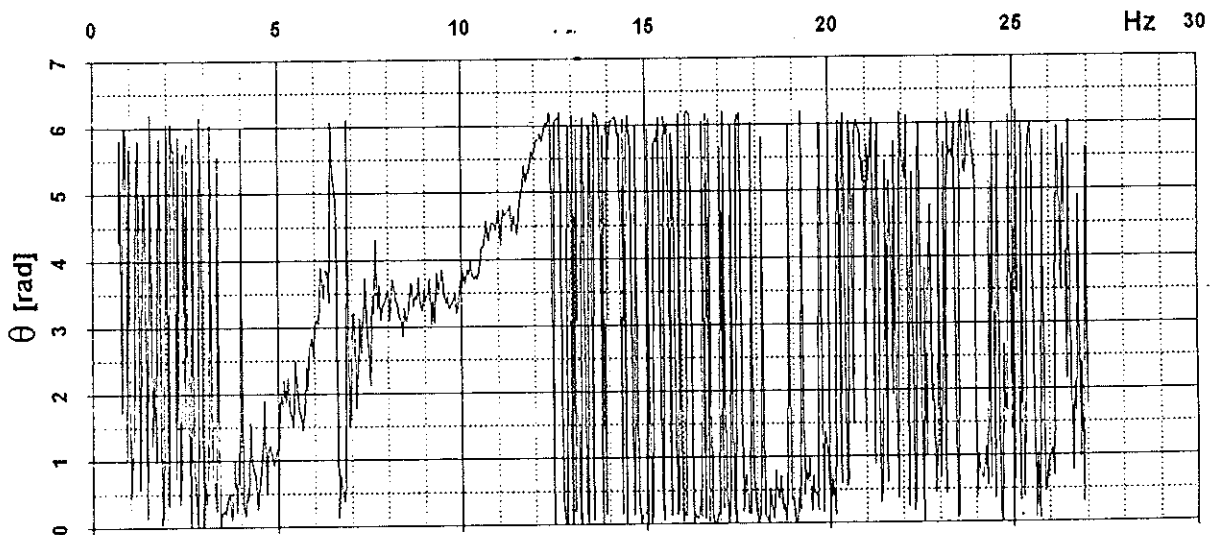
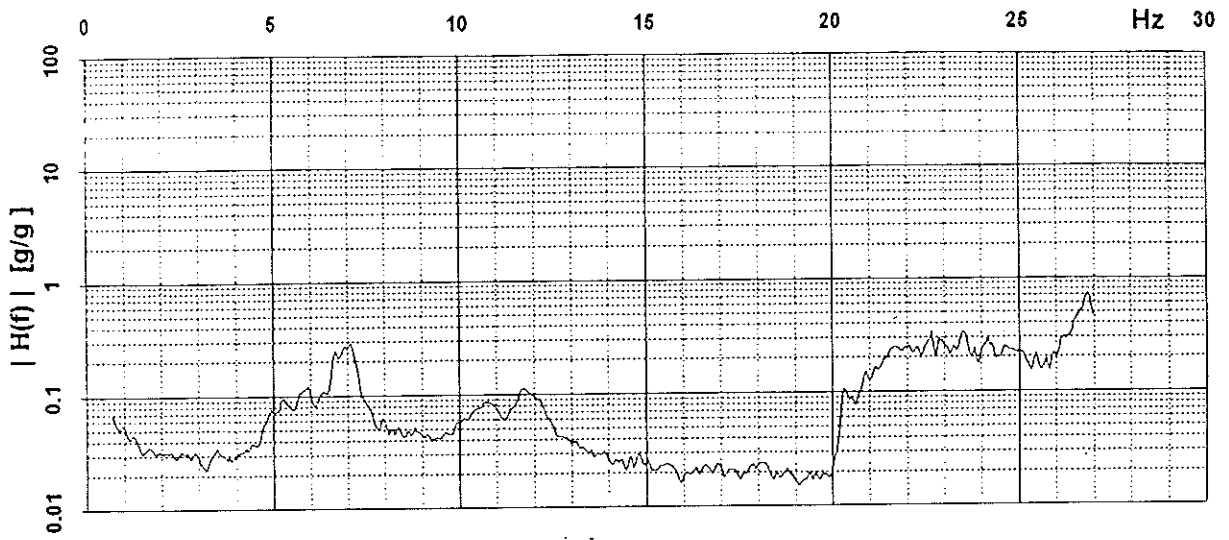
Trans > ModT ↓



BARE.FOR

15 ↓ 554 ↓

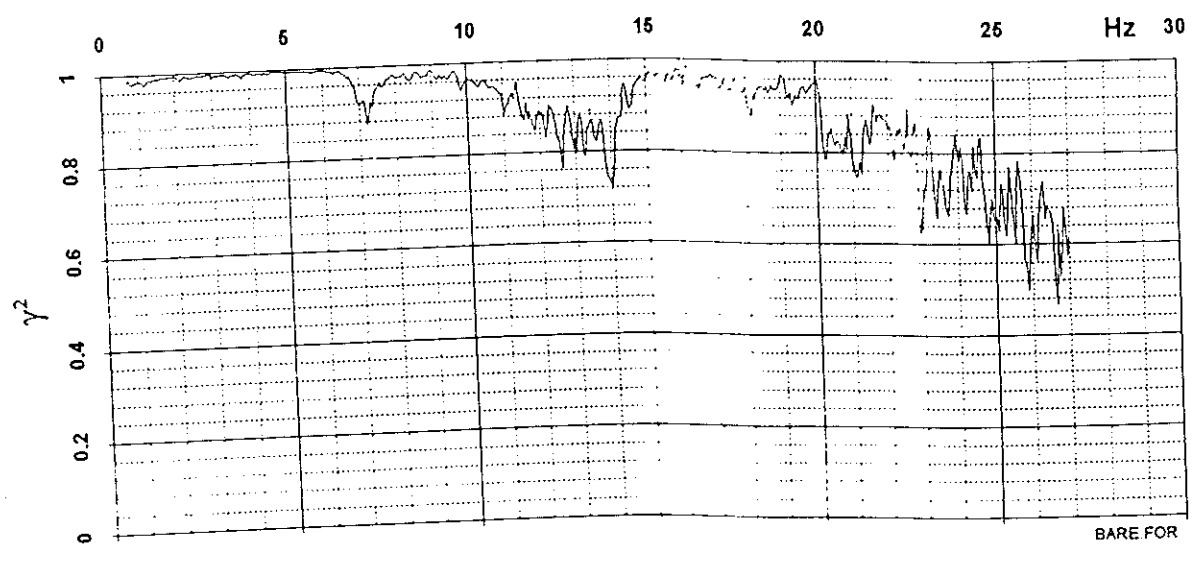
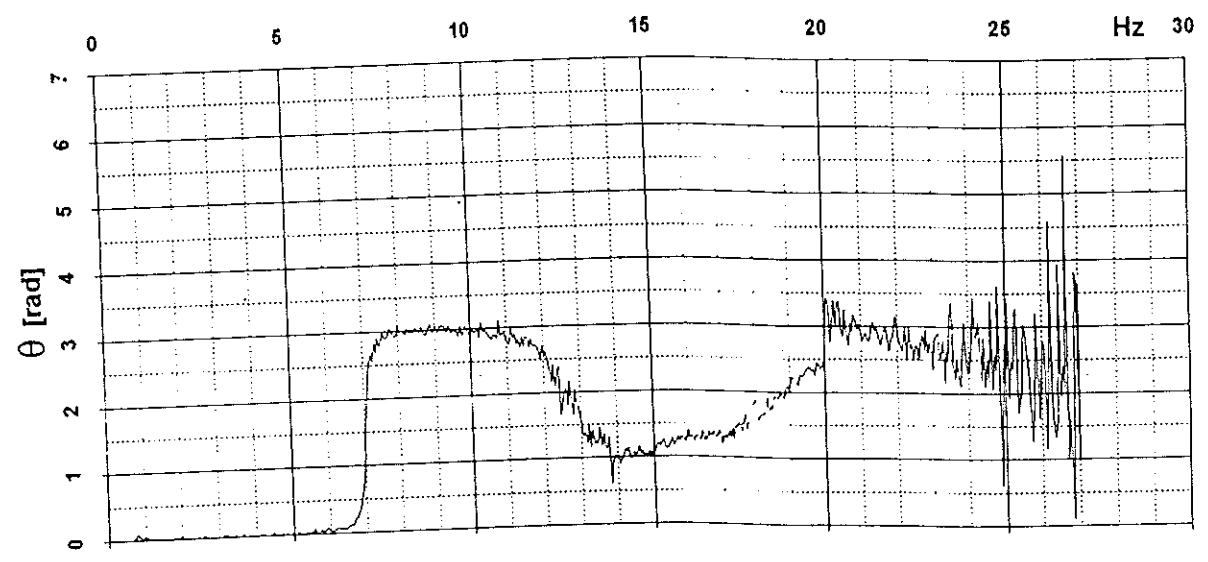
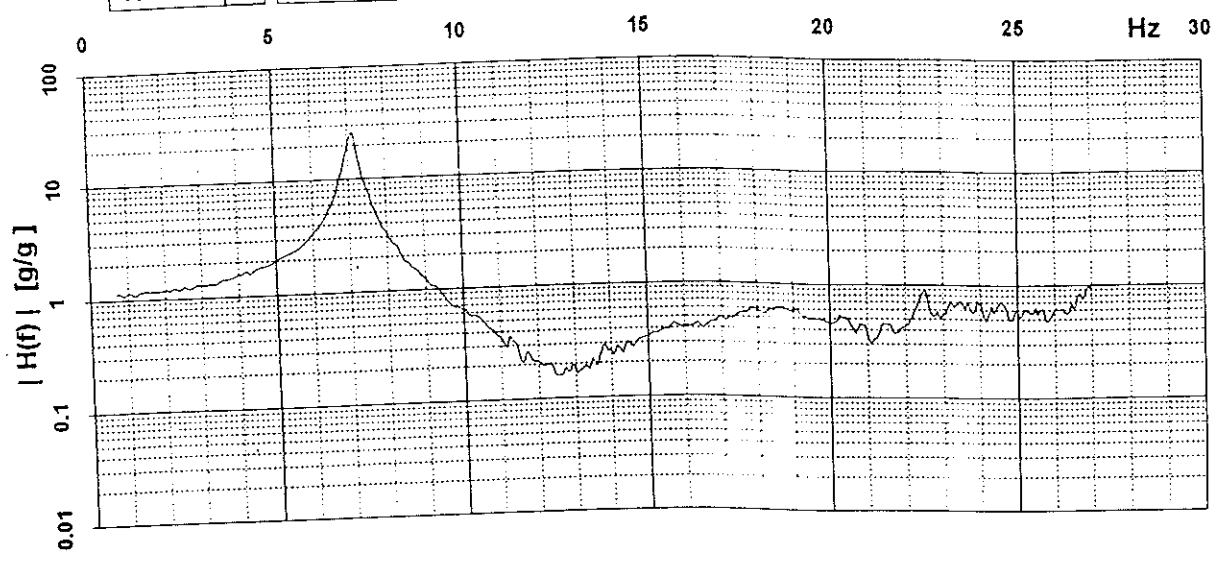
Trans > ModL ↓



BARE.FOR

15 ↓ 554 ↓

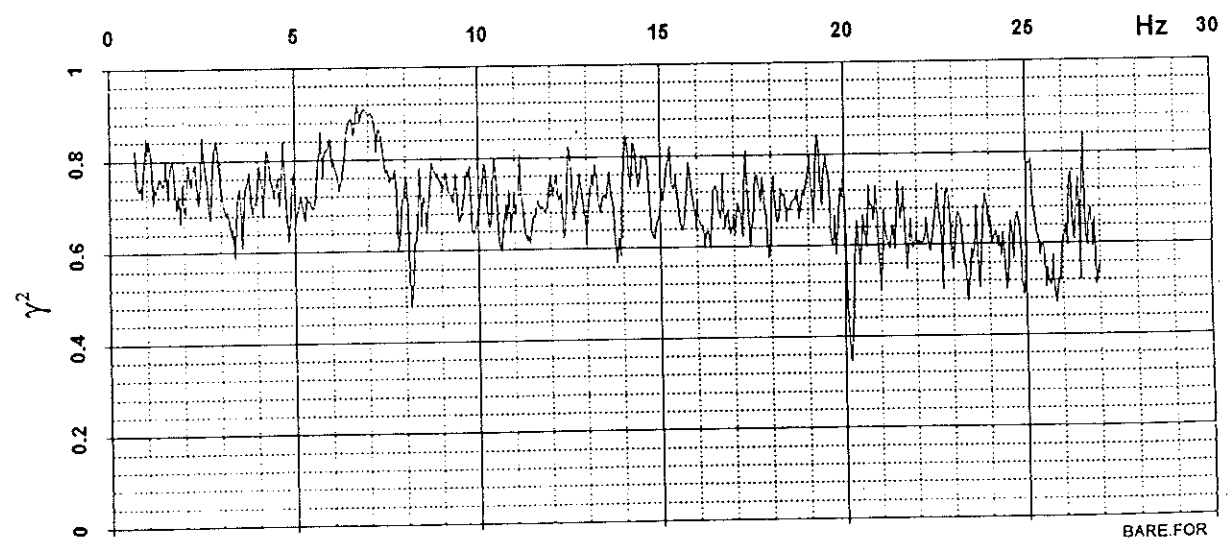
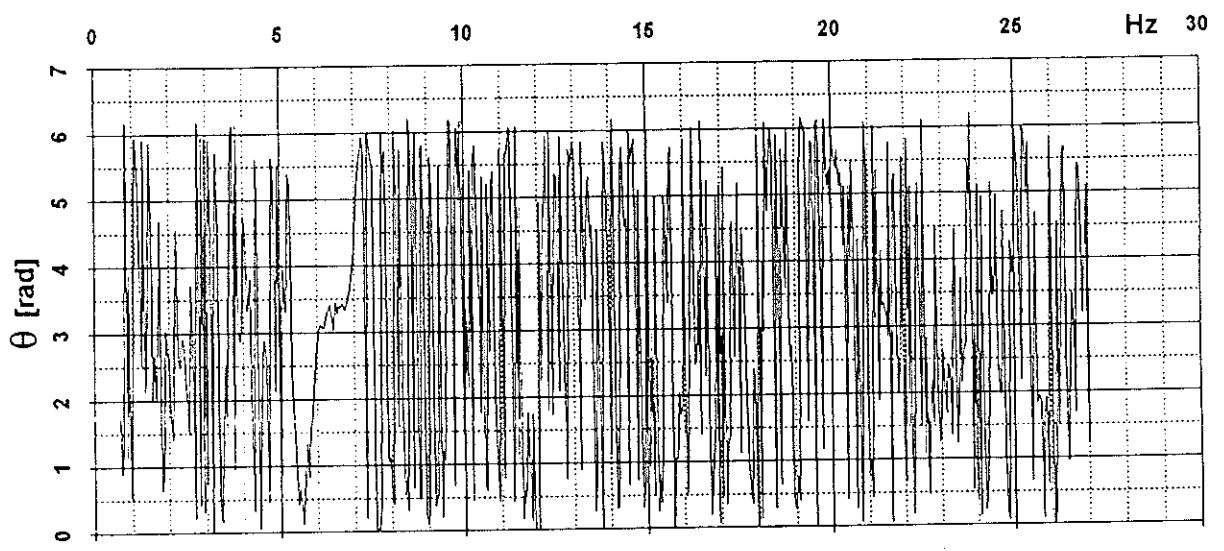
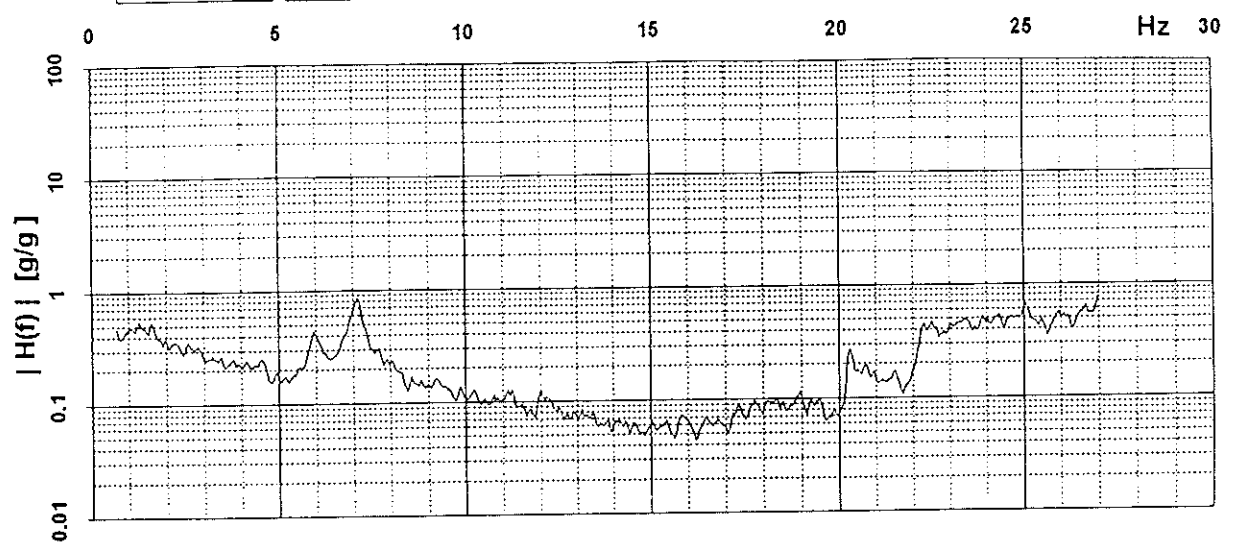
Long > ModL ↓



BARE FOR

15 ↓ 554 ↓

Long > ModT ↓



BARE FOR

APPENDIX VI

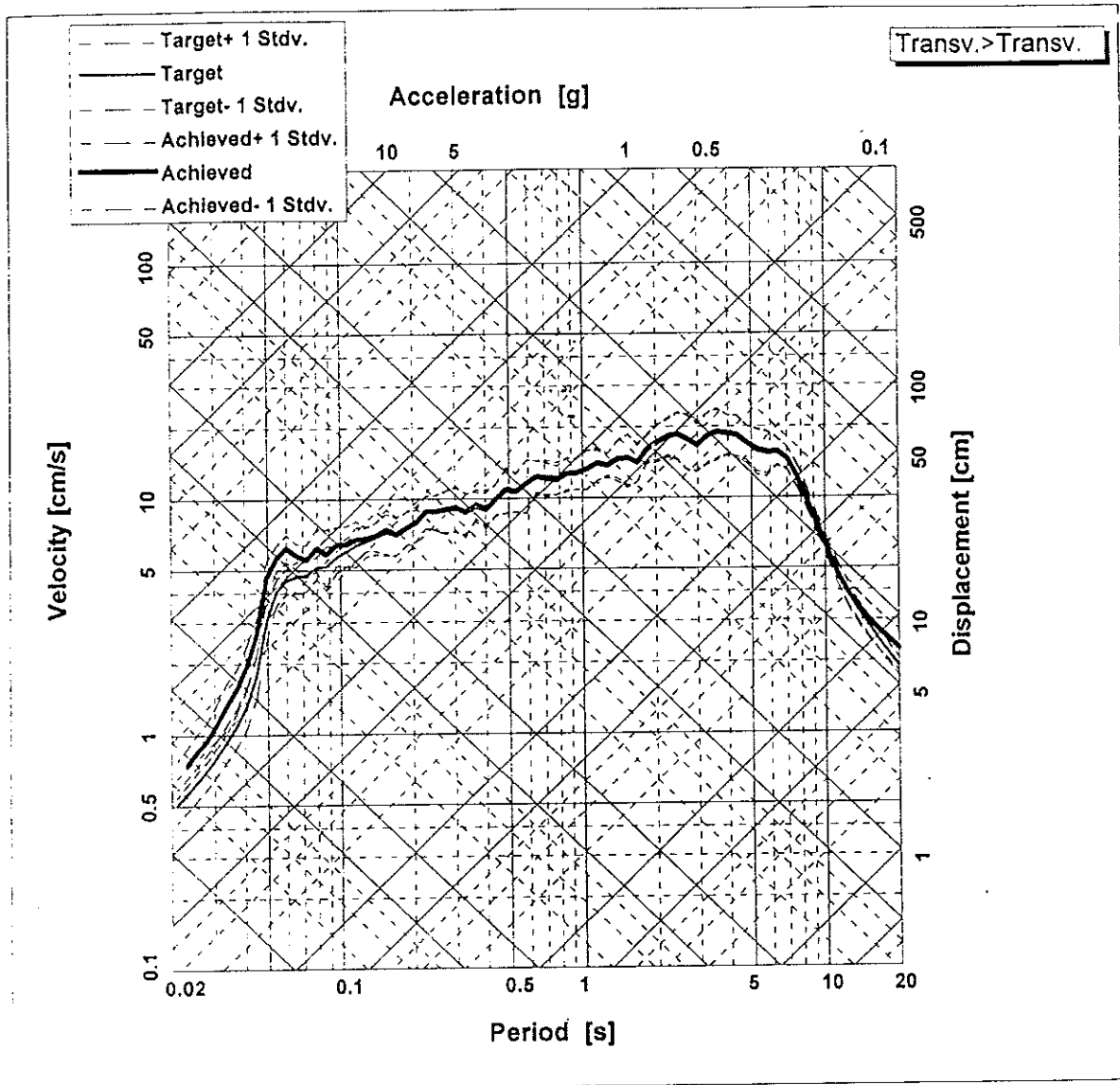
CONTROL FIDELITY

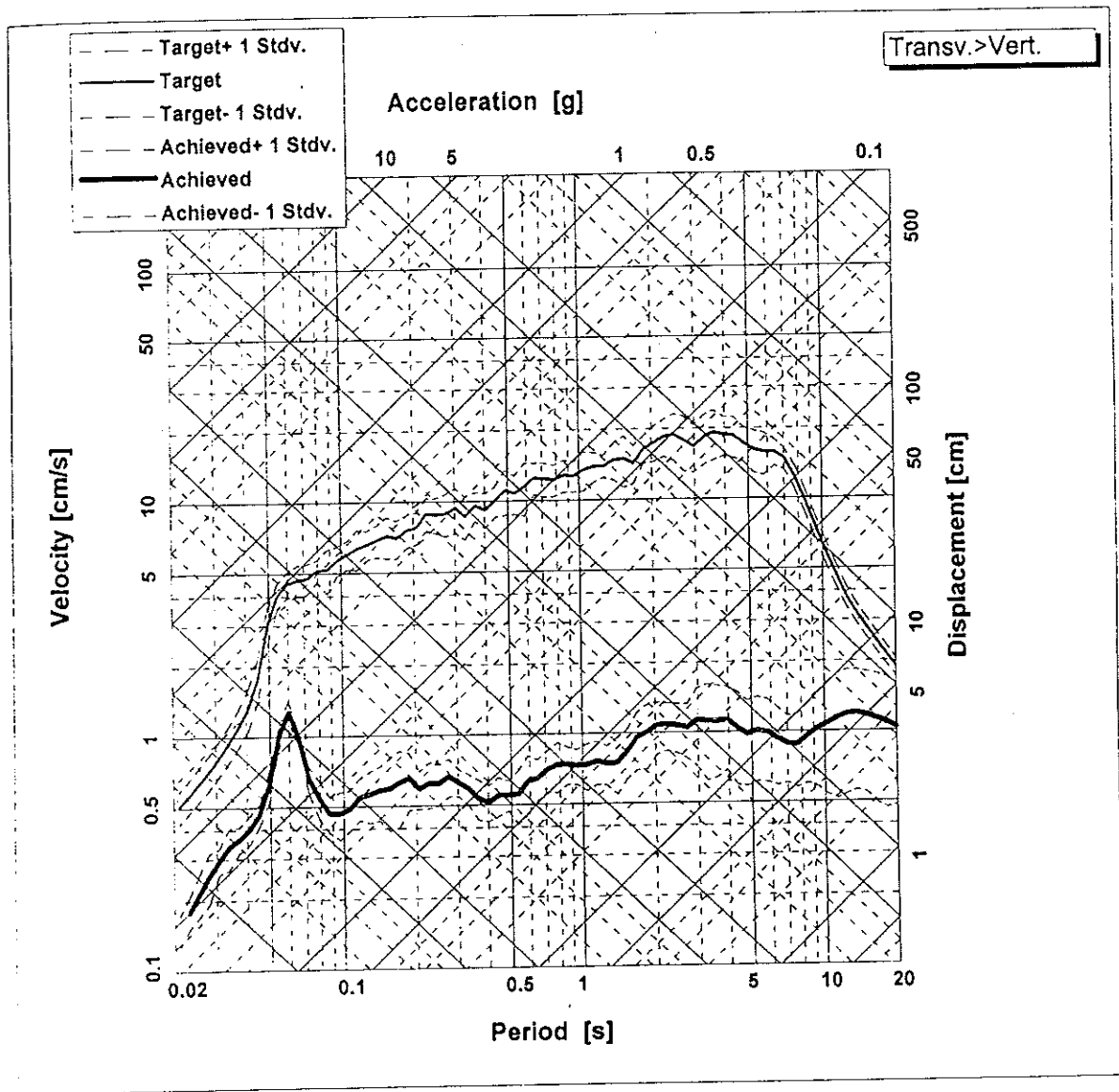
**RESPONSE SPECTRA OF TARGET AND ACHIEVED MOTION
RANDOM WHITE NOISE**

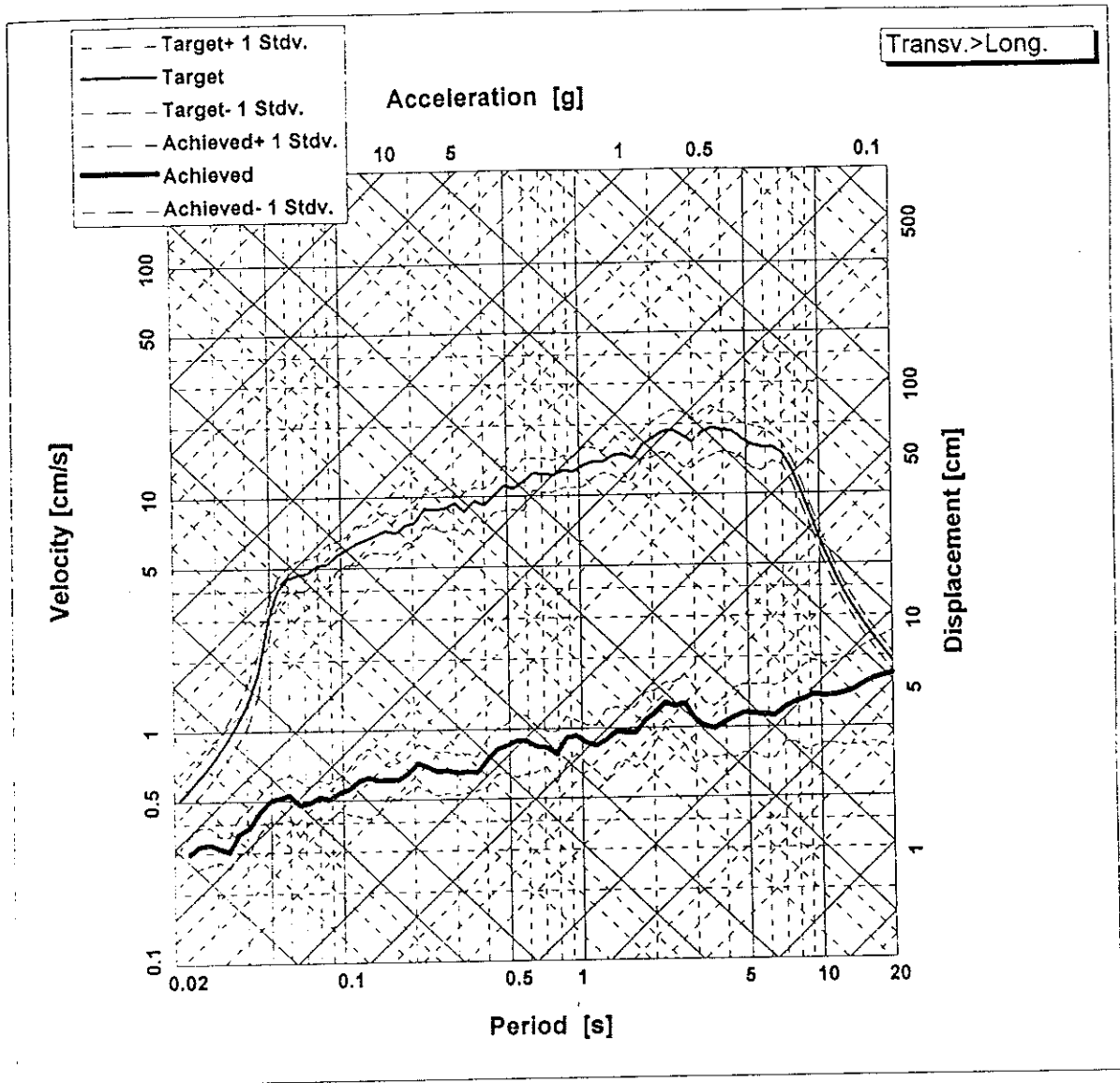
List of Figures

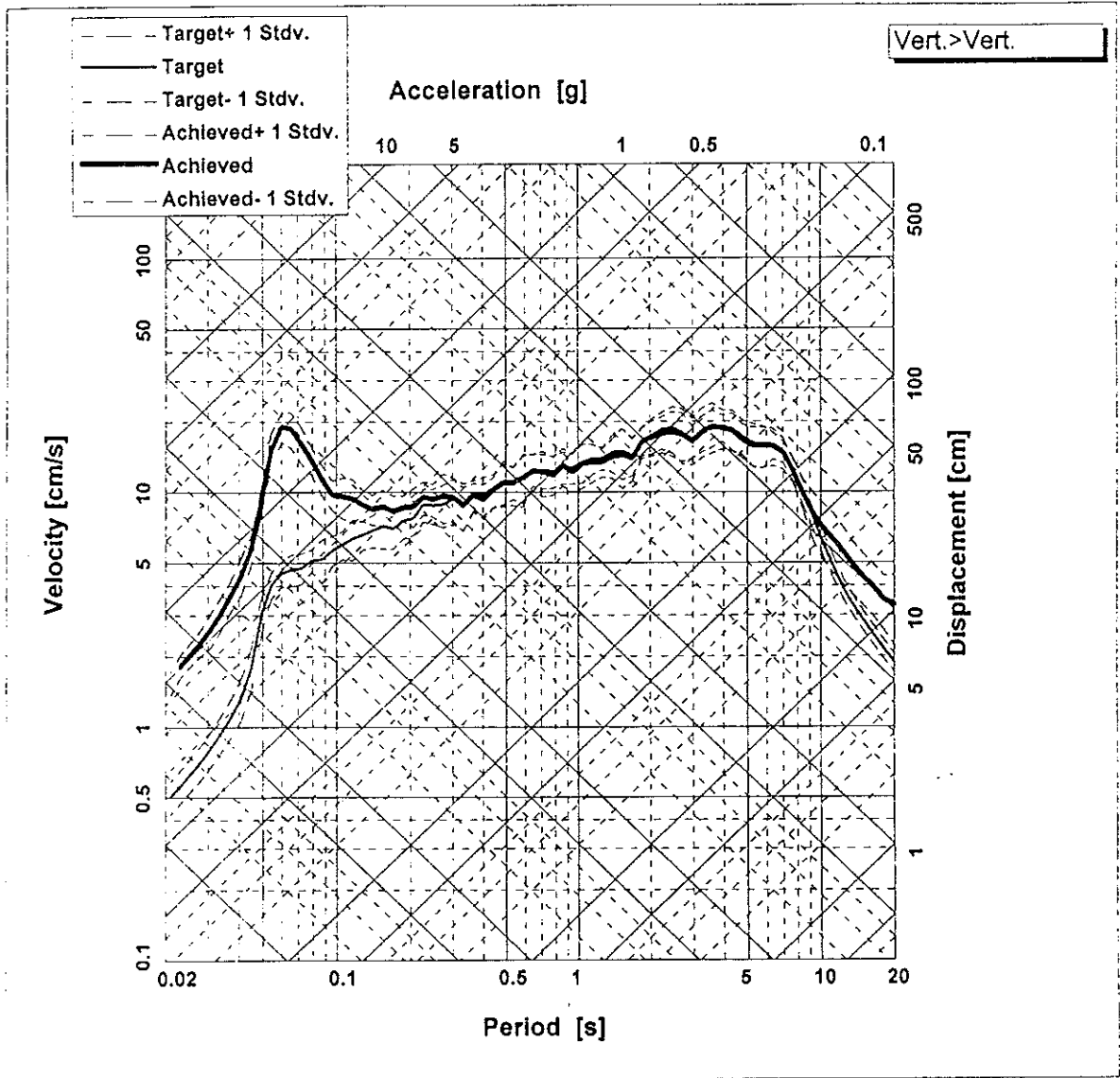
- AVI.1 - Response spectra (without model) of transverse achieved and target motion
- AVI.2 - Response spectra (without model) of vertical achieved motion
- AVI.3 - Response spectra (without model) of longitudinal achieved motion
- AVI.4 - Response spectra (without model) of vertical achieved and target motion
- AVI.5 - Response spectra (without model) of transverse achieved motion
- AVI.6 - Response spectra (without model) of longitudinal achieved motion
- AVI.7 - Response spectra (without model) of longitudinal achieved and target motion
- AVI.8 - Response spectra (without model) of transverse achieved motion
- AVI.9 - Response spectra (without model) of vertical achieved motion
- AVI.10 - Response spectra (with model) of transverse achieved and target motion
- AVI.11 - Response spectra (with model) of vertical achieved motion
- AVI.12 - Response spectra (with model) of longitudinal achieved motion
- AVI.13 - Response spectra (with model) of vertical achieved and target motion
- AVI.14 - Response spectra (with model) of transverse achieved motion
- AVI.15 - Response spectra (with model) of longitudinal achieved motion
- AVI.16 - Response spectra (with model) of longitudinal achieved and target motion
- AVI.17 - Response spectra (with model) of transverse achieved motion
- AVI.18 - Response spectra (with model) of vertical achieved motion

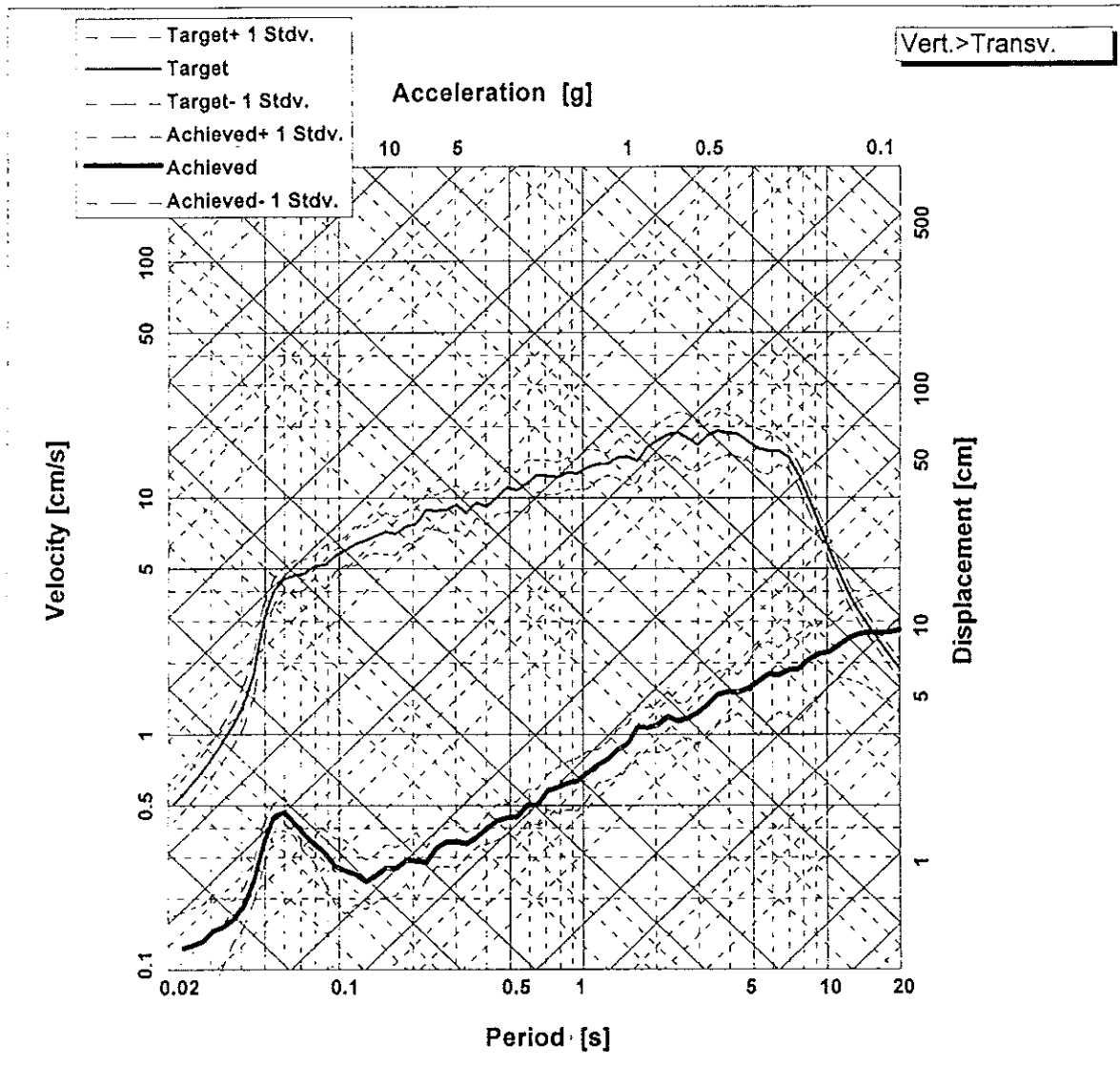
Note: In the response spectra shown in this appendix the target plot refers to the required motion for each degree of freedom. The achieved spectra refers either to same degree of freedom or to another not controlled degree of freedom.

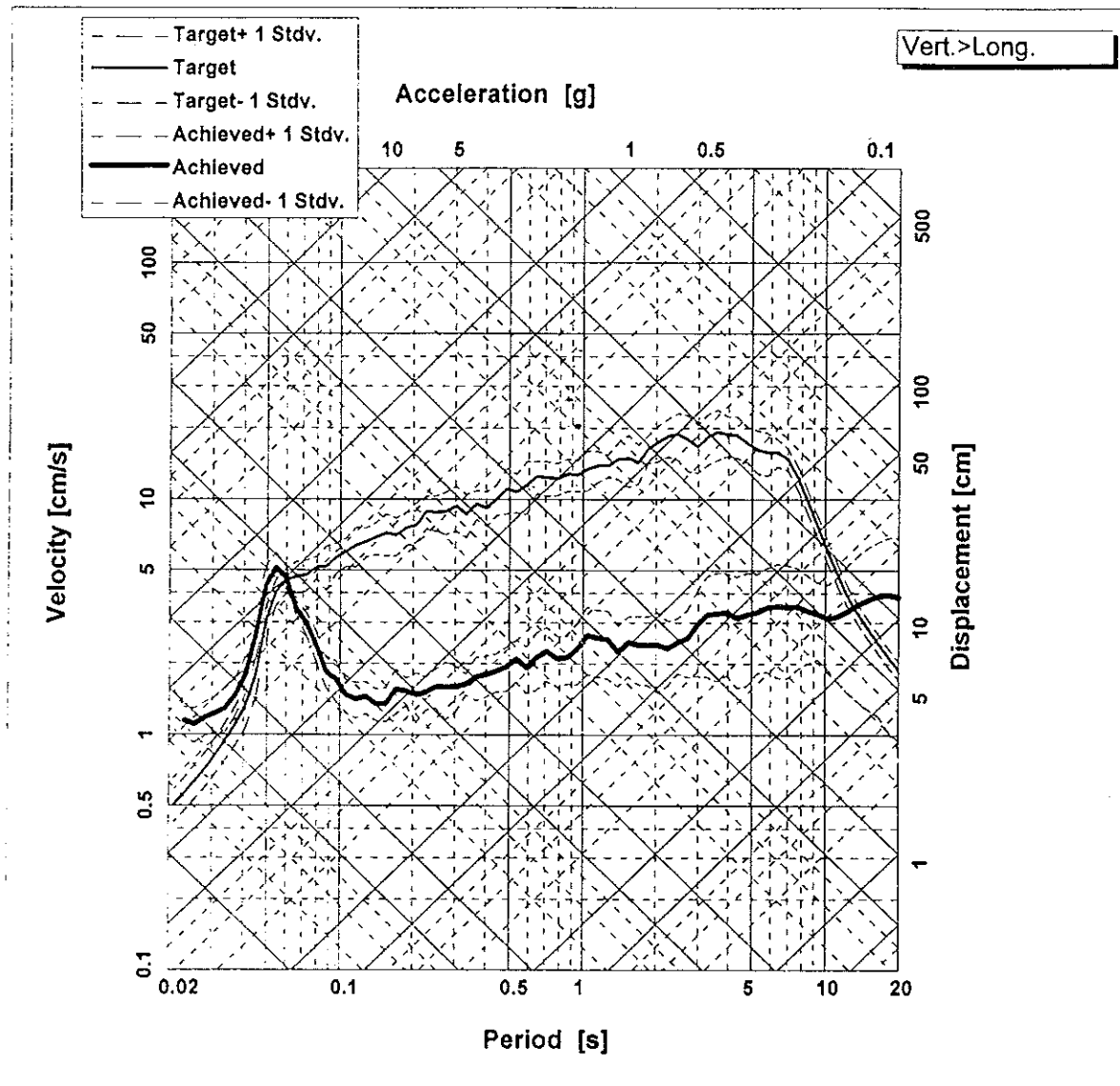


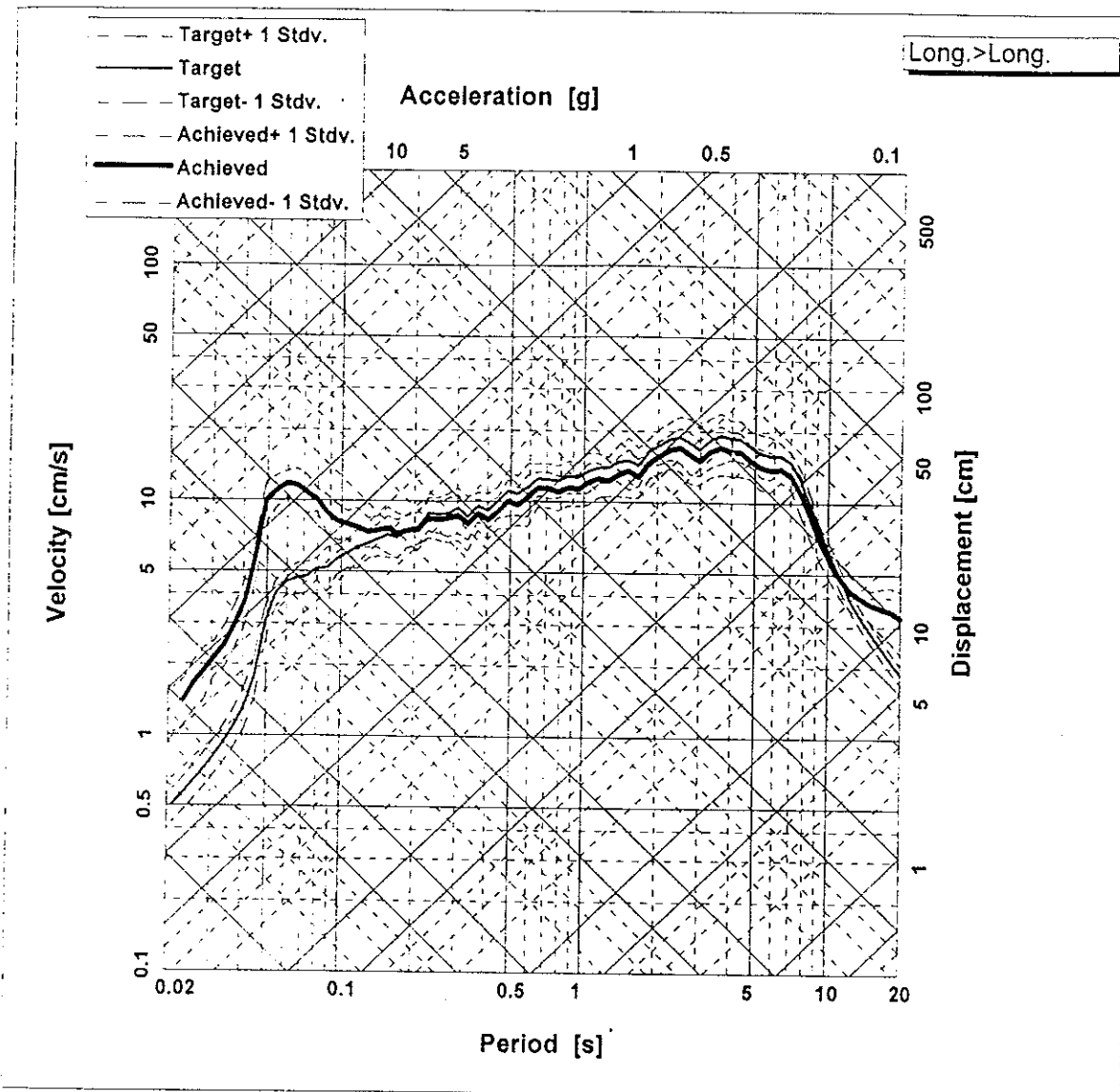


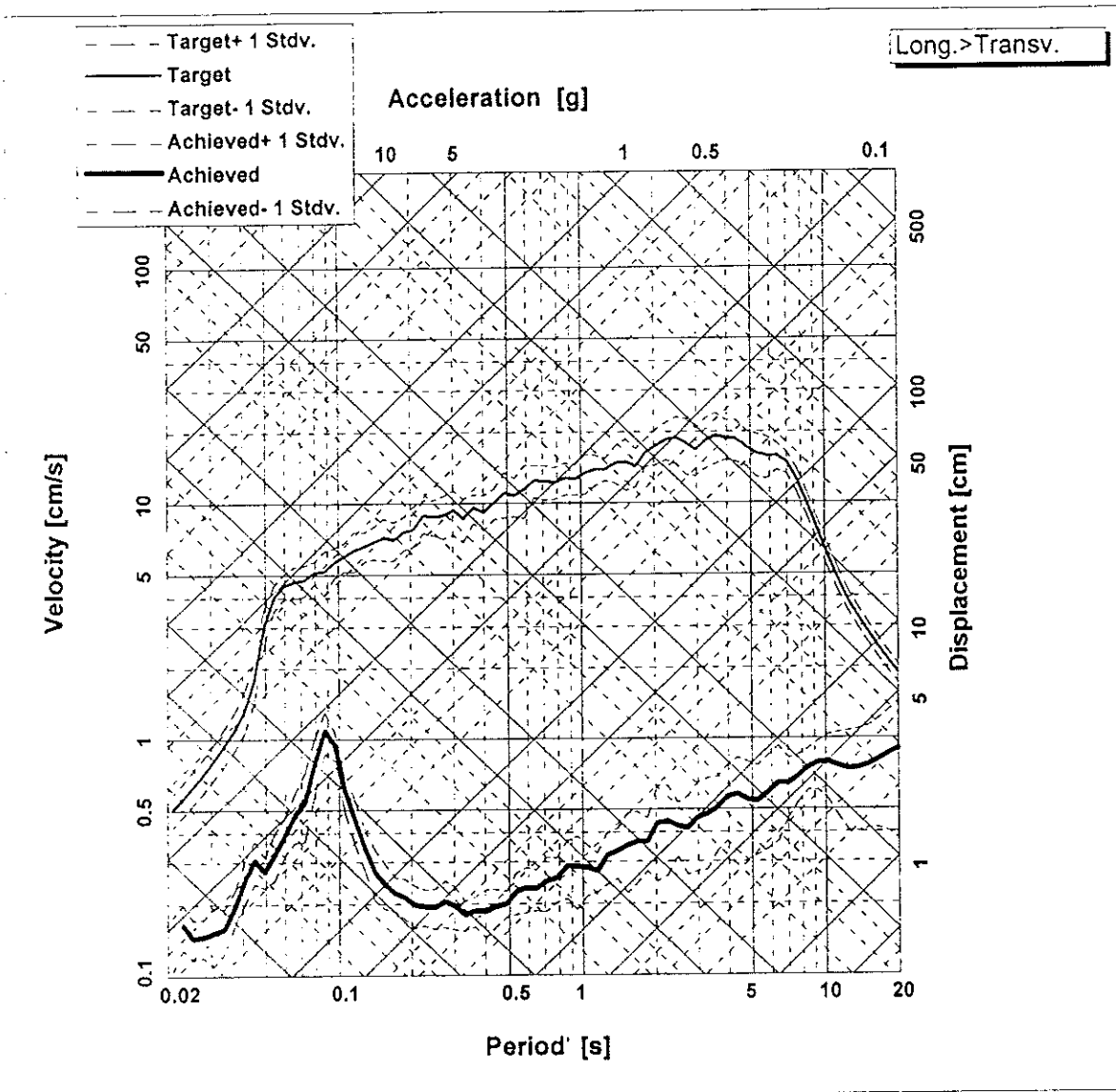


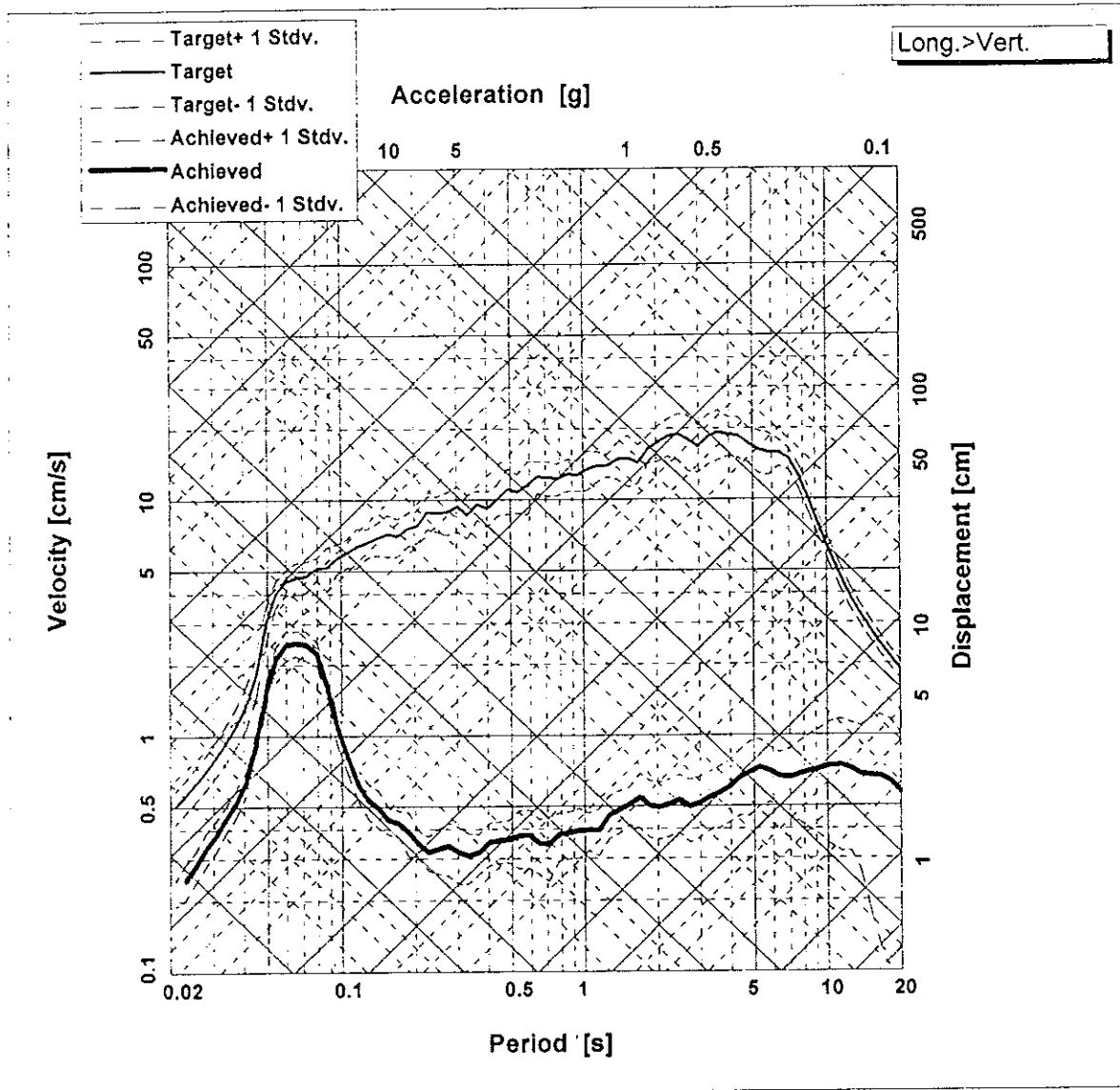


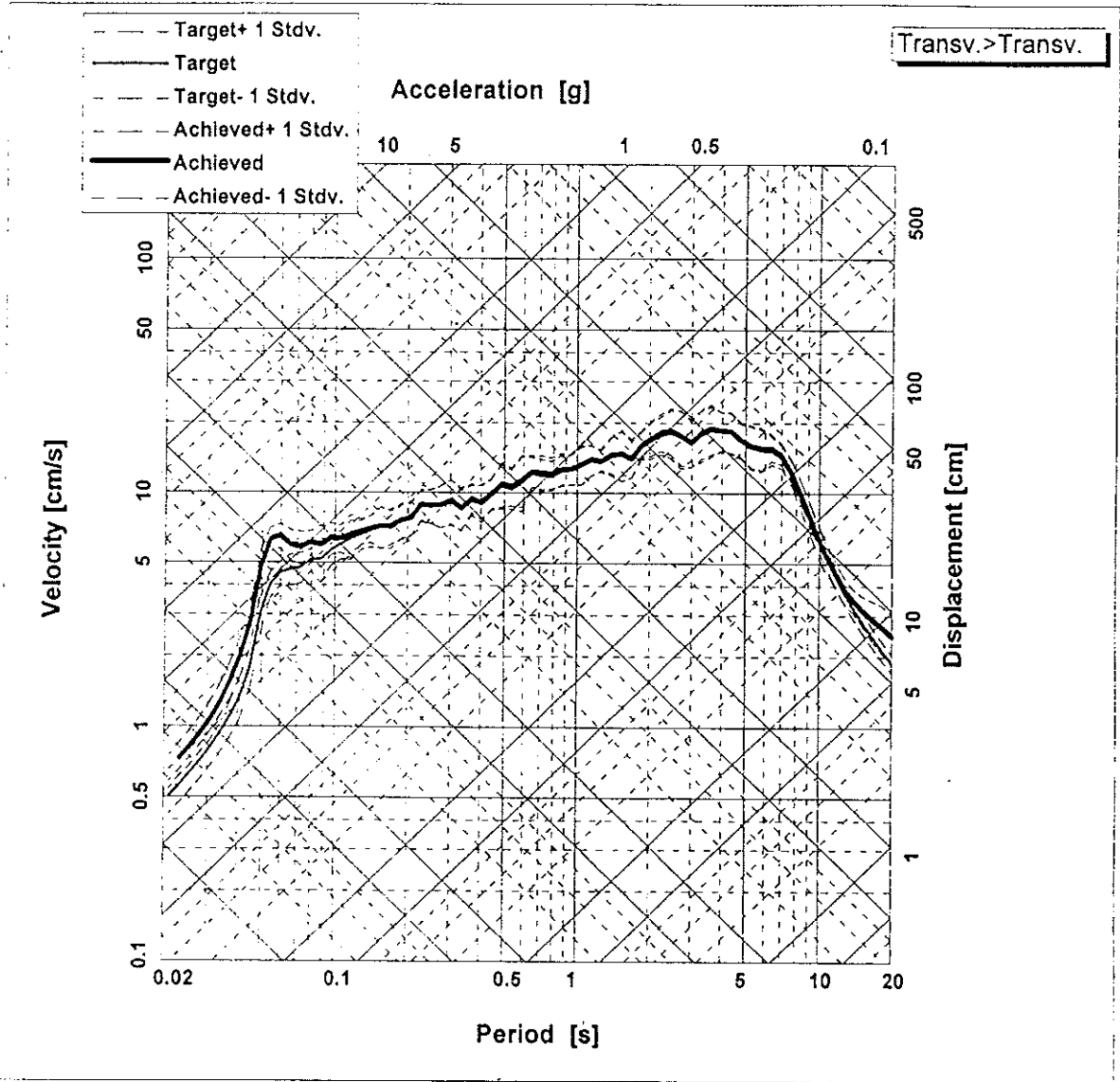


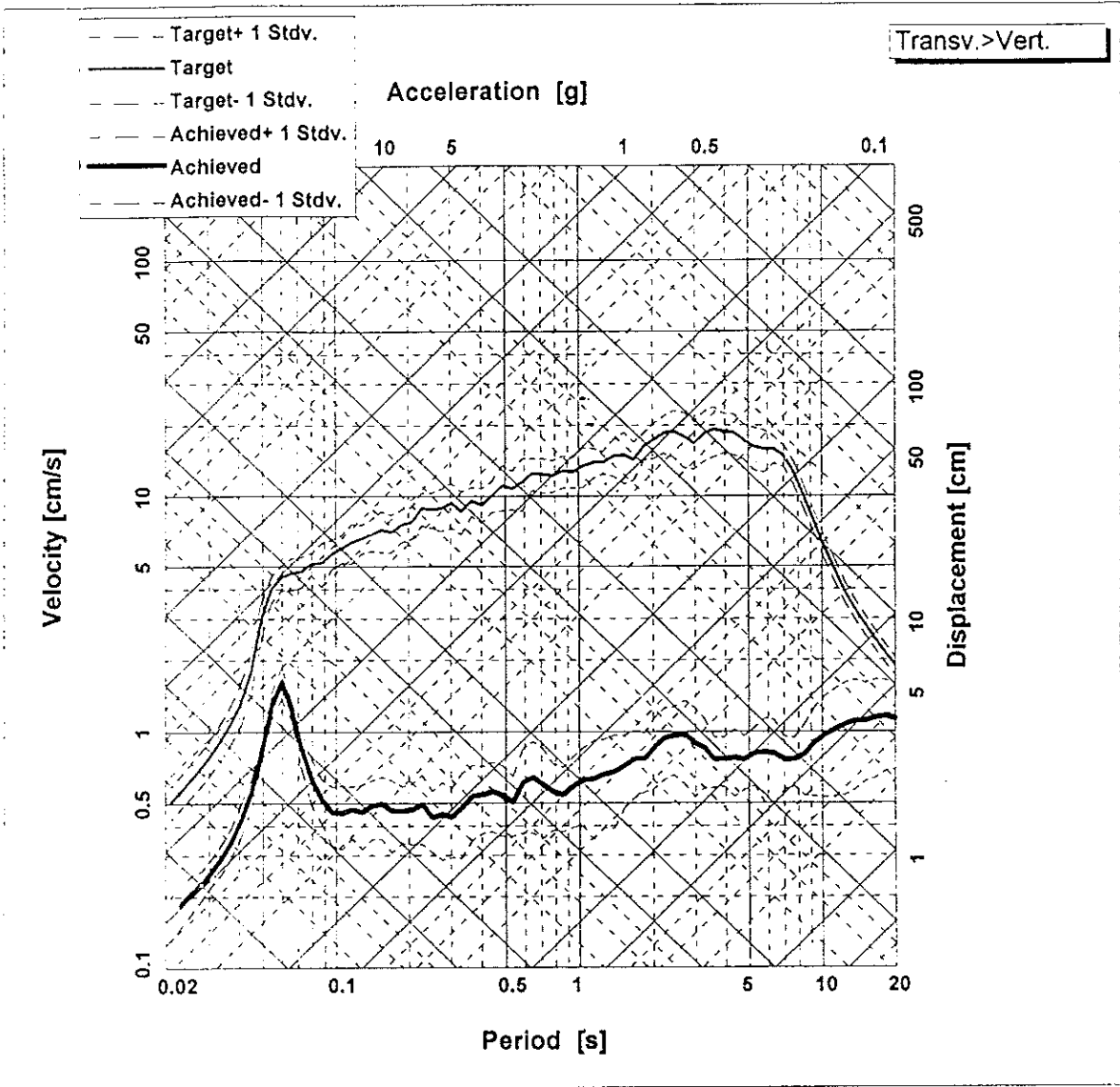


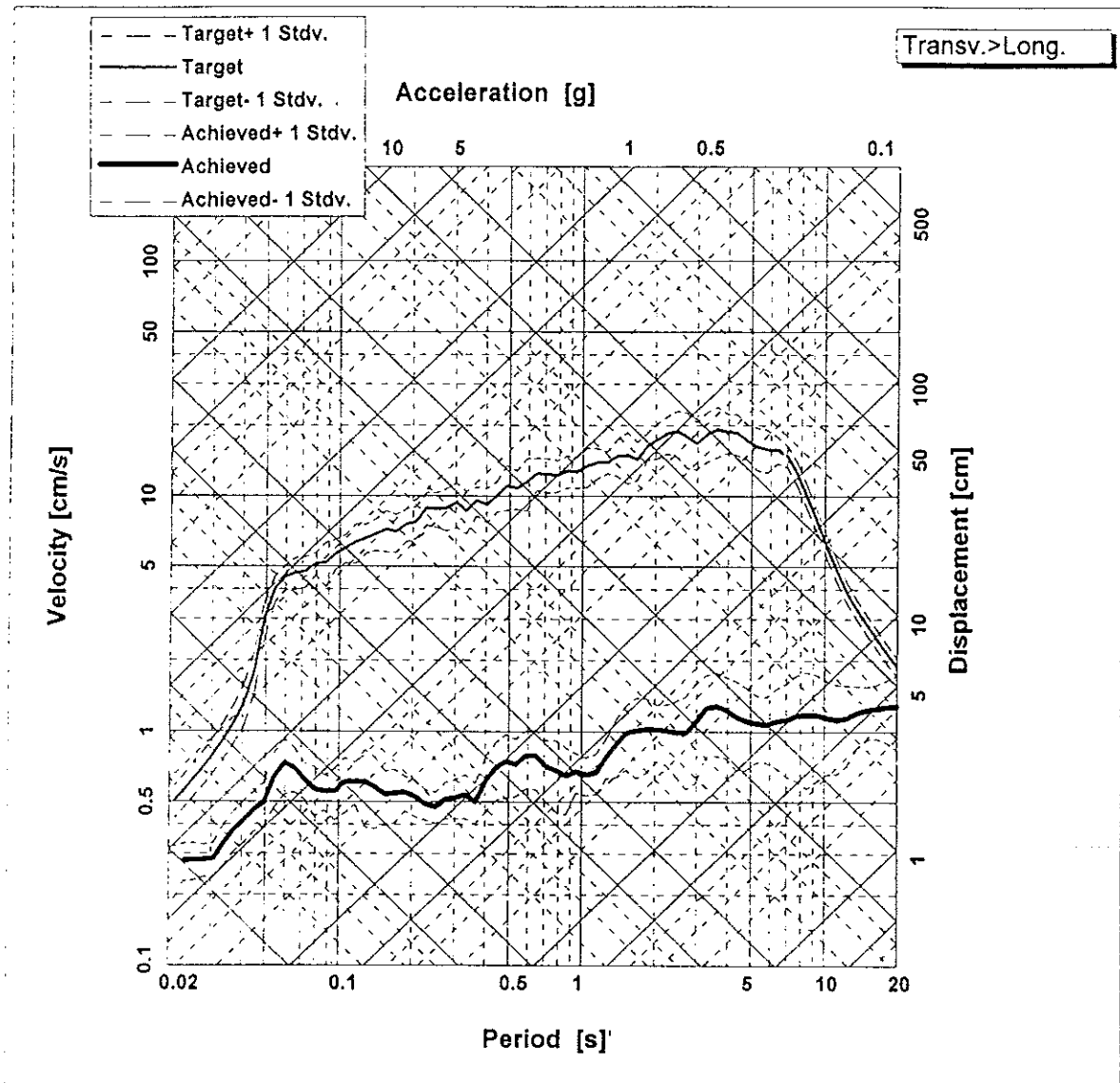


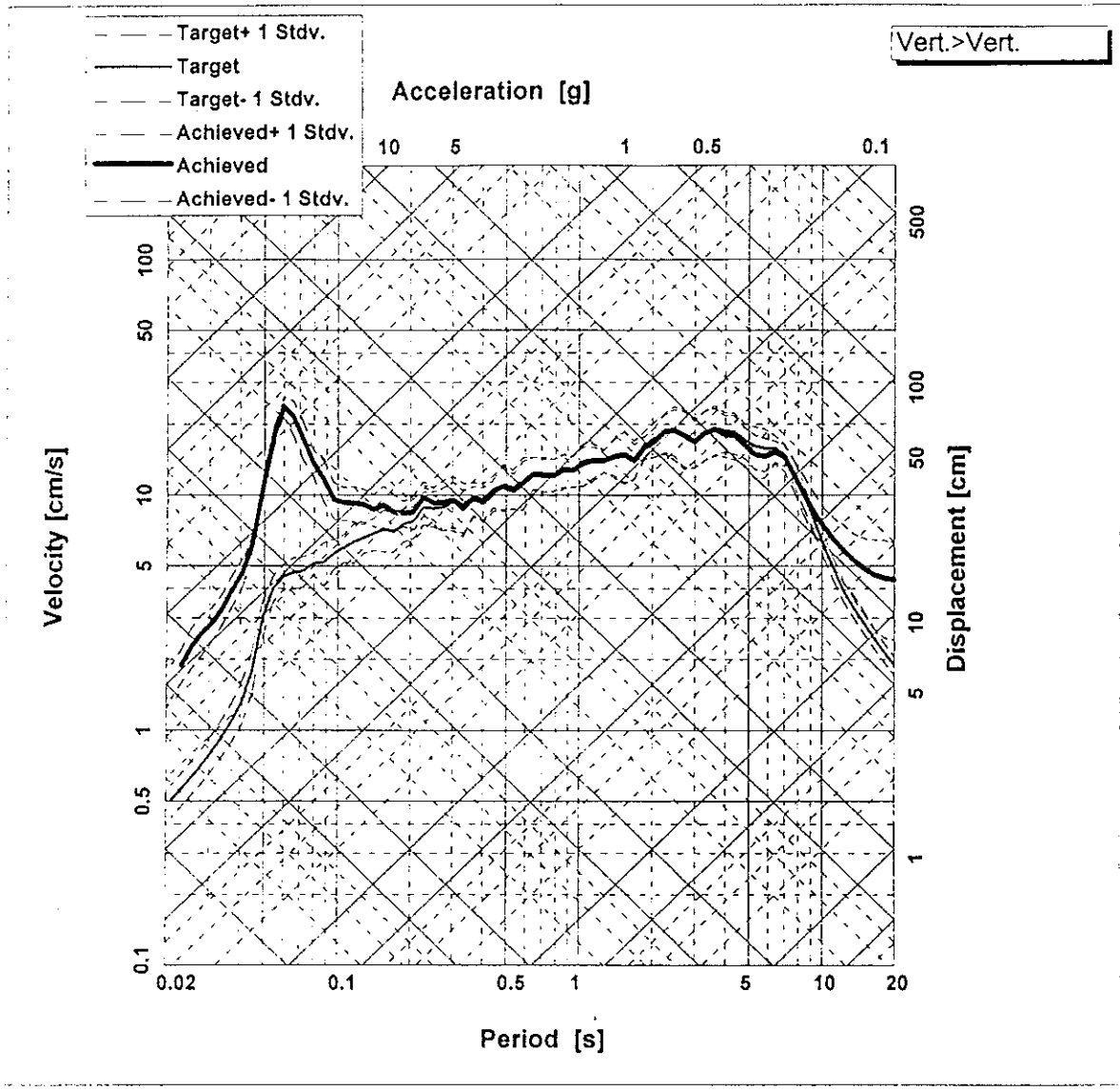


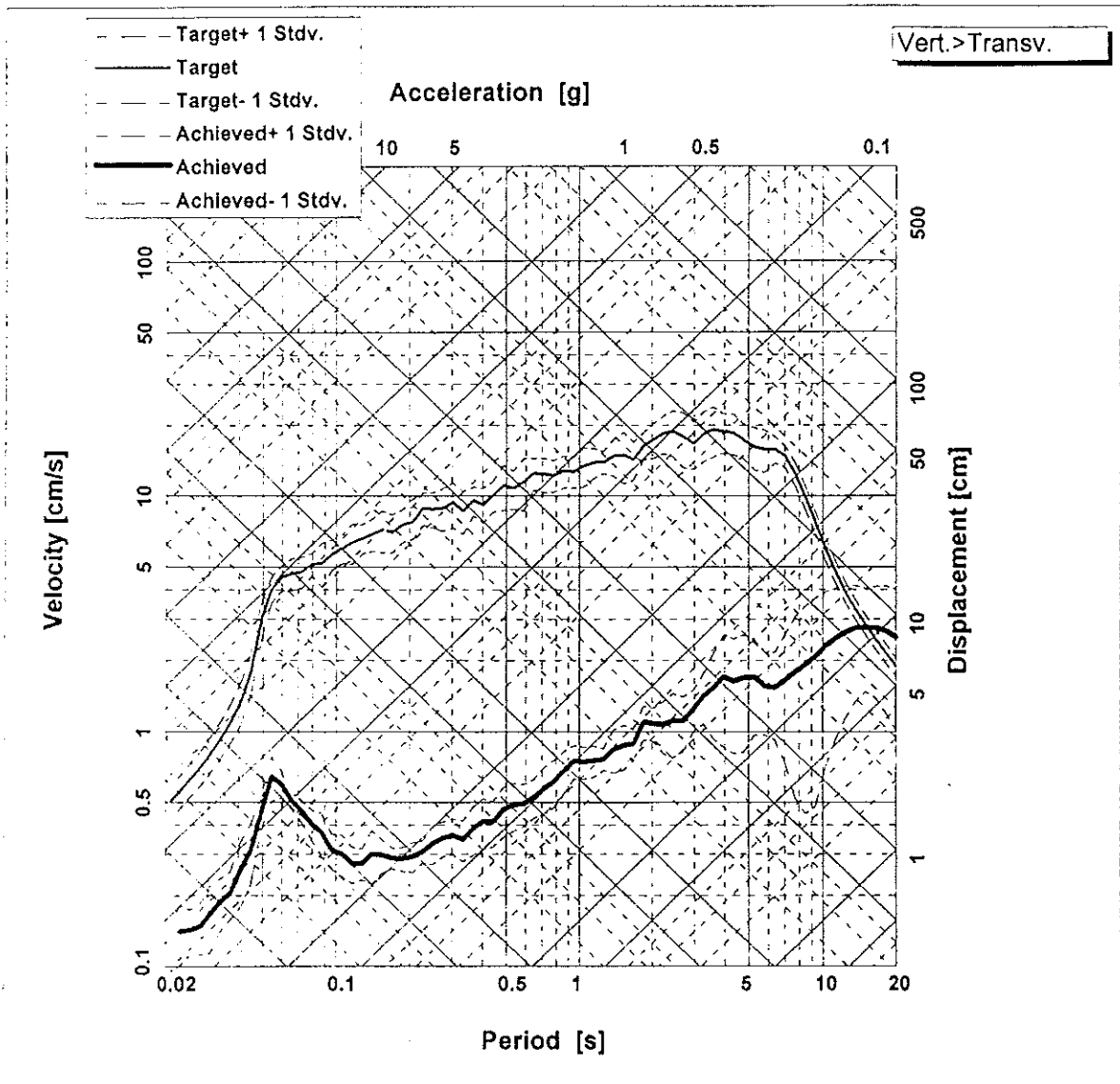


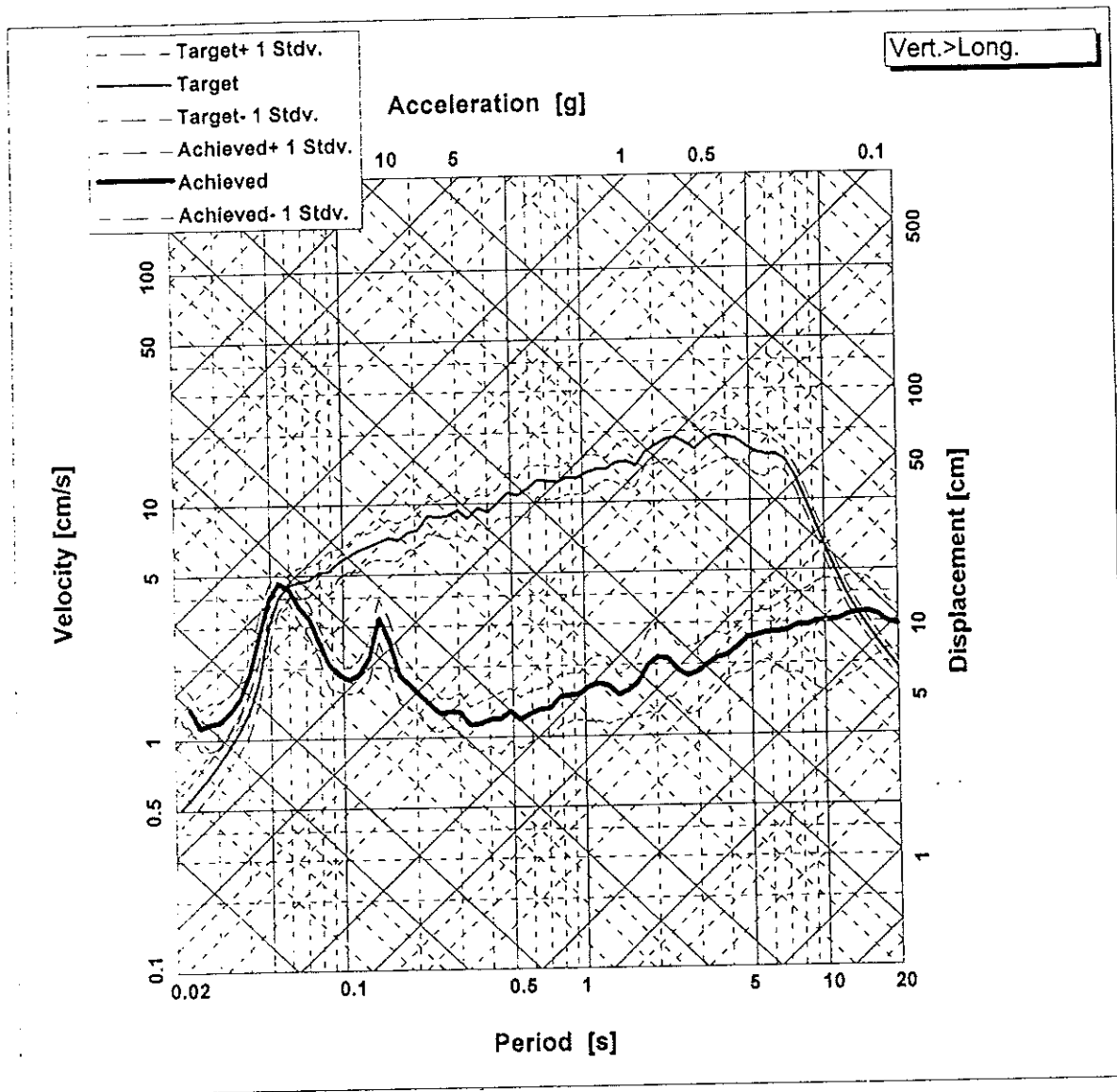


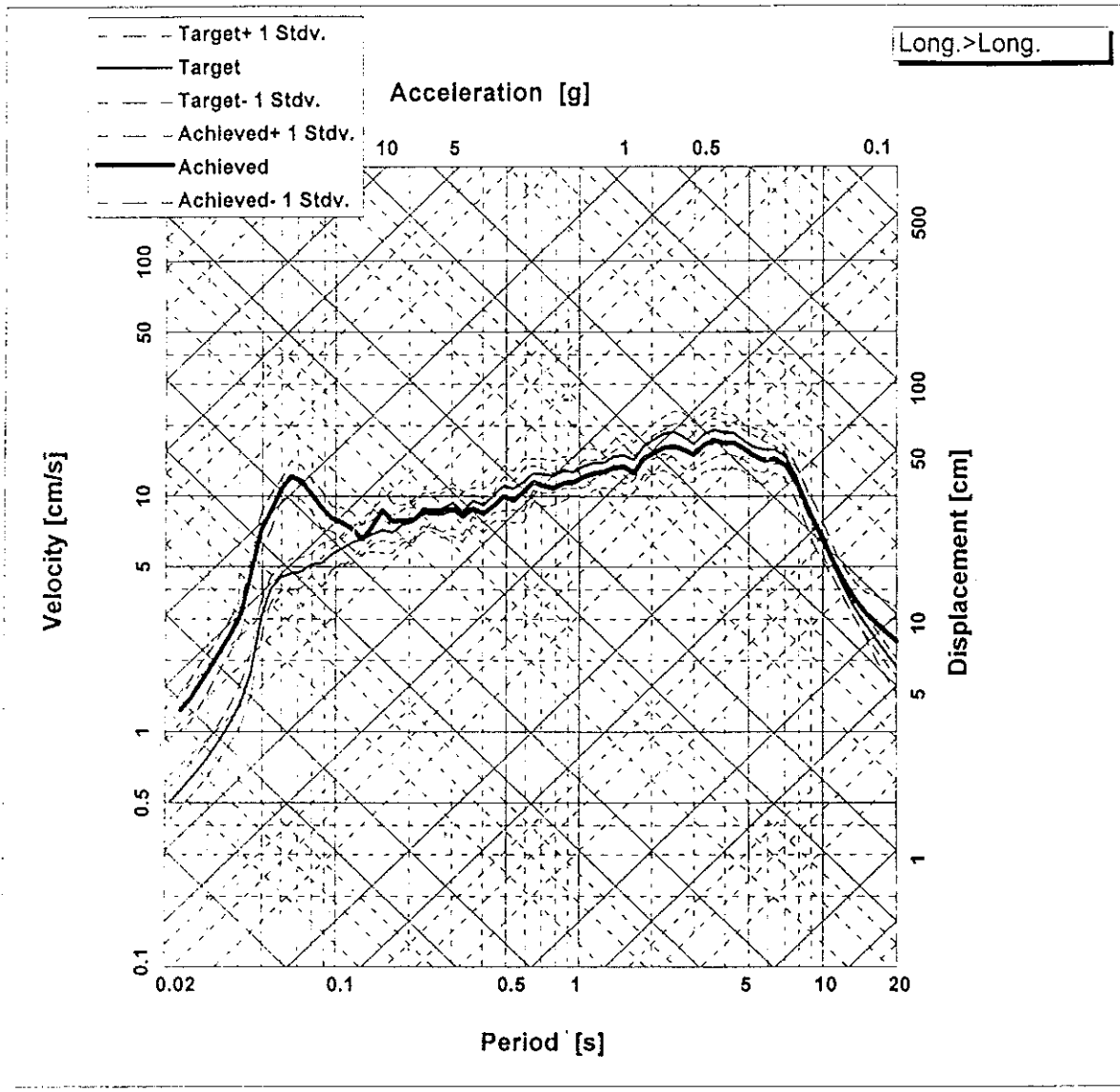


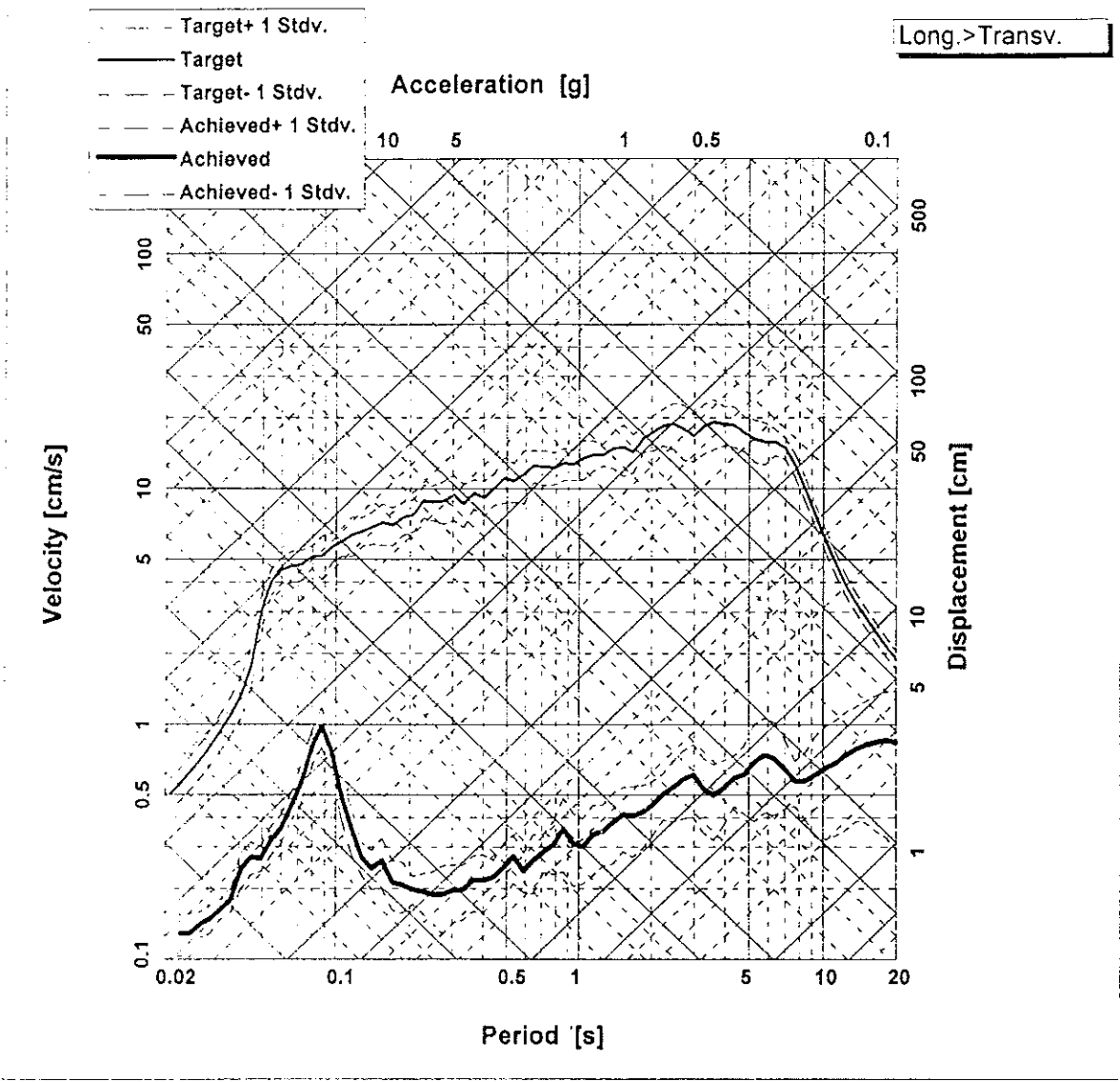


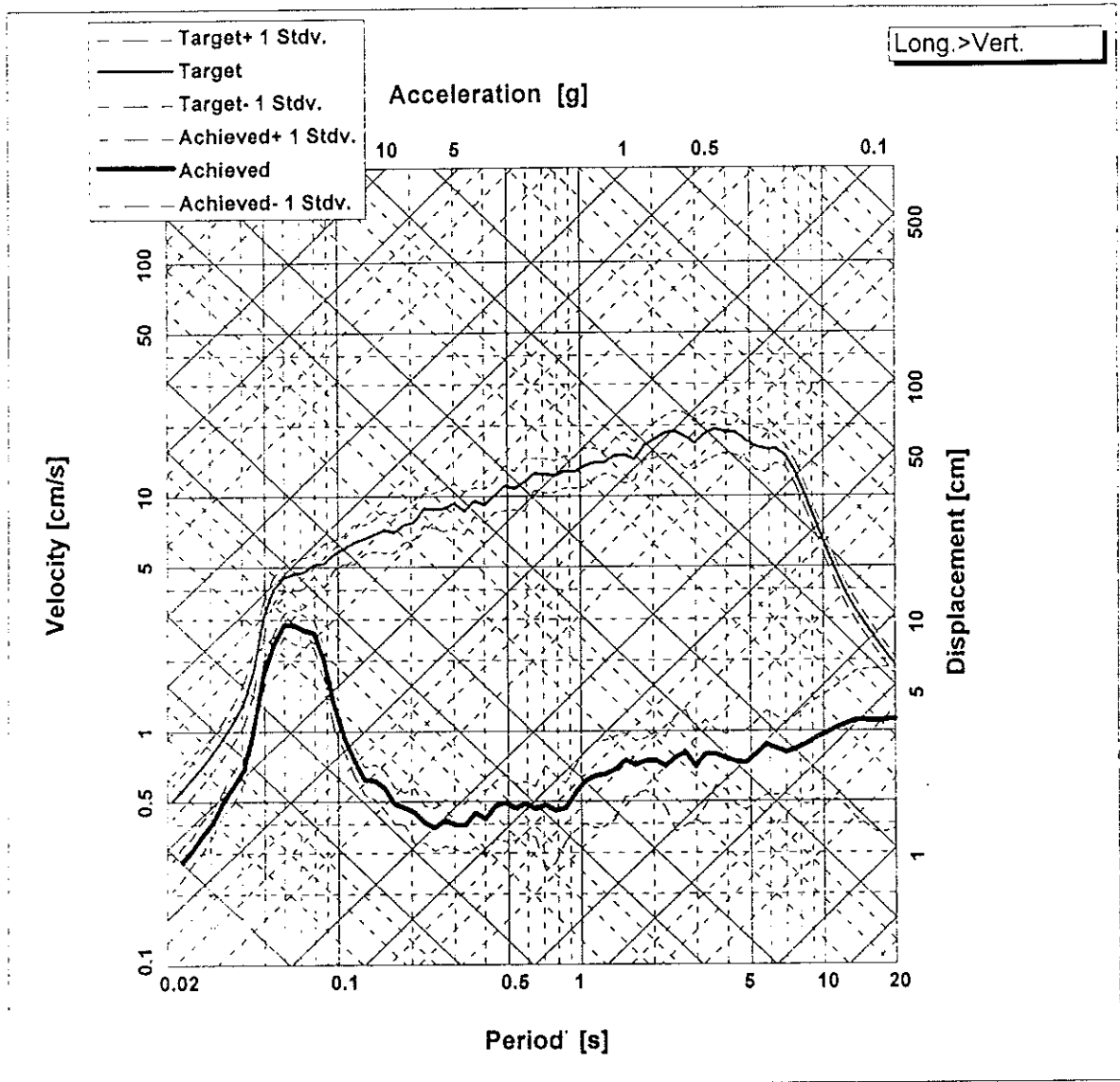












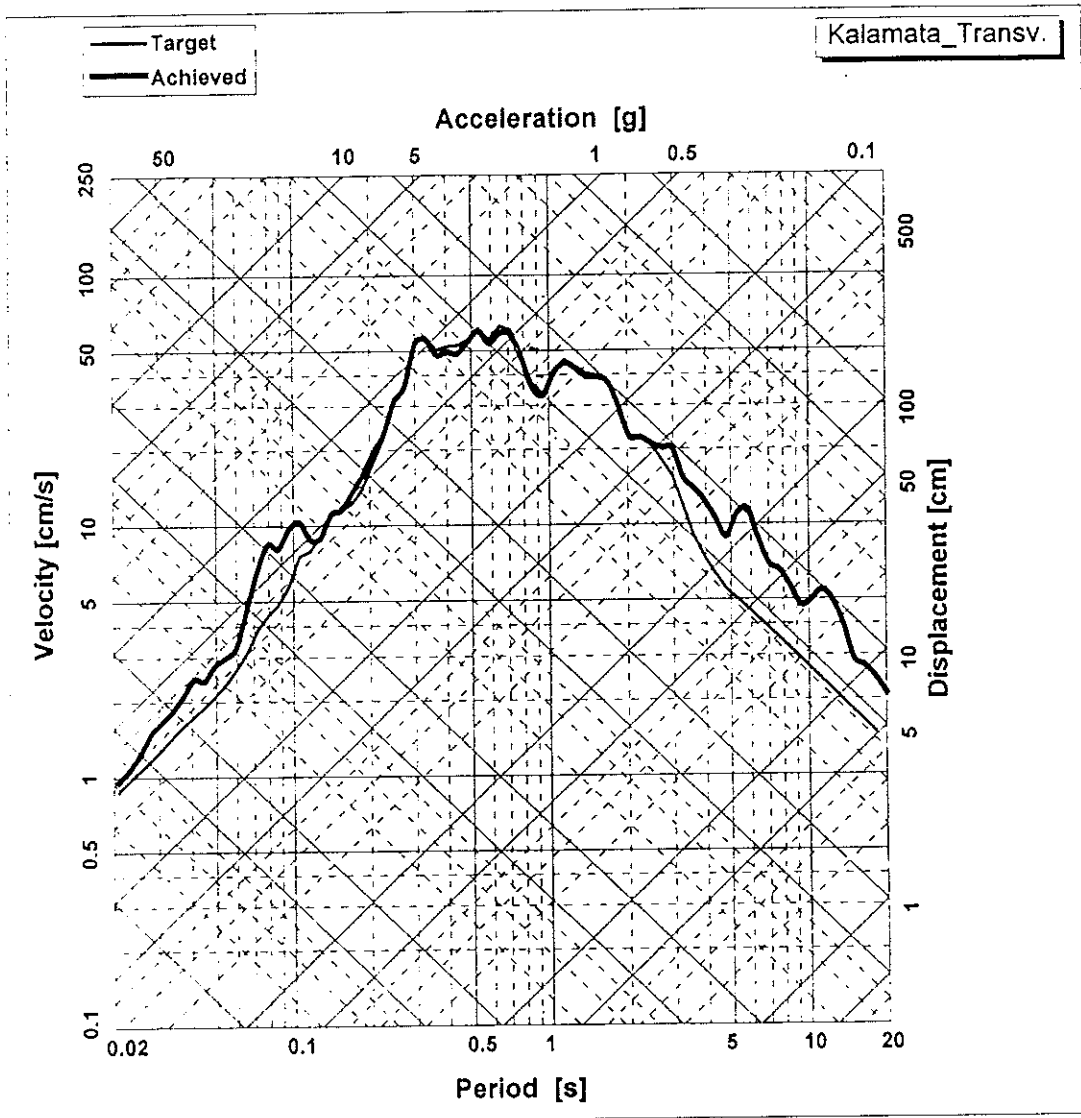
APPENDIX VII

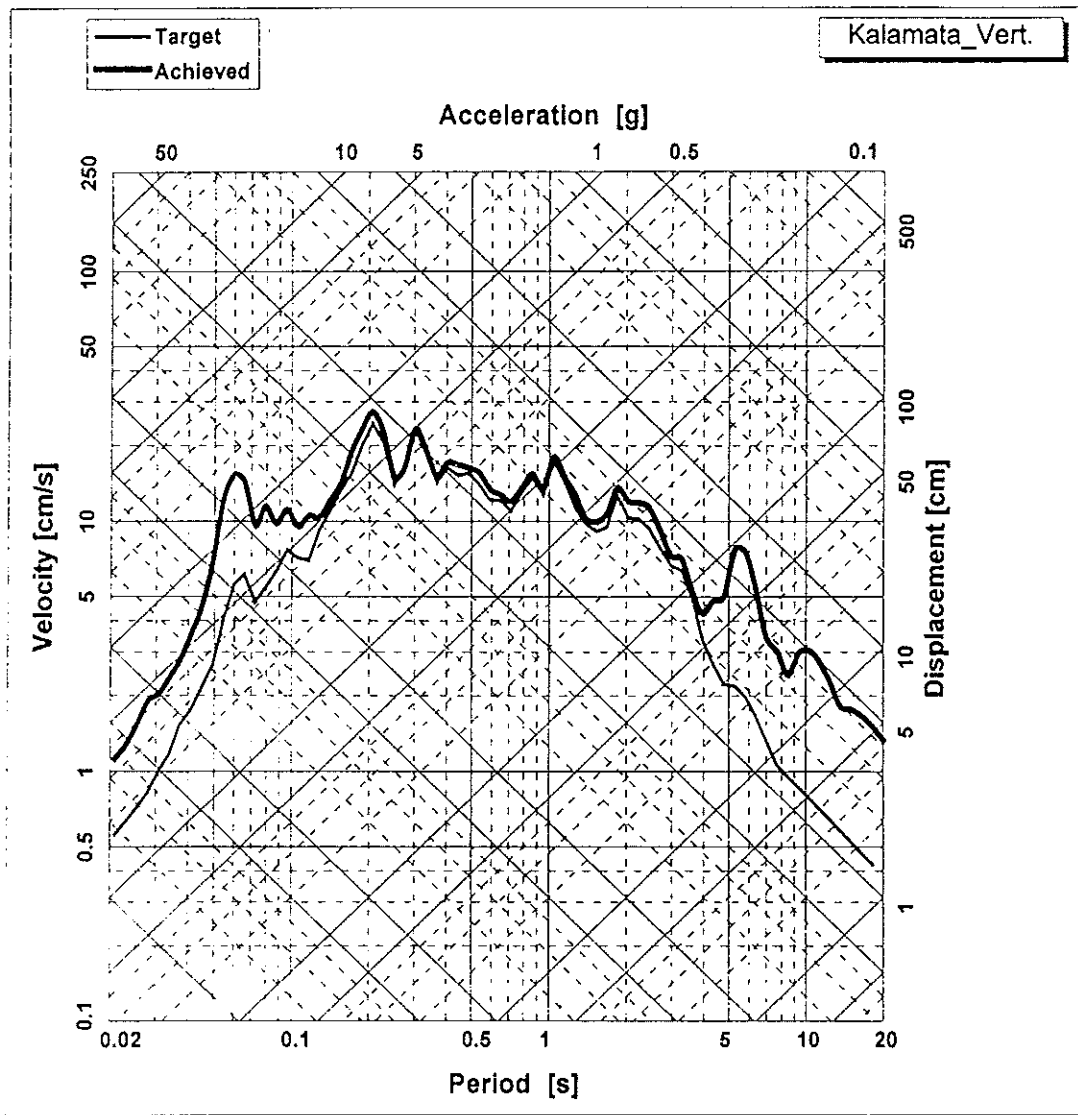
CONTROL FIDELITY

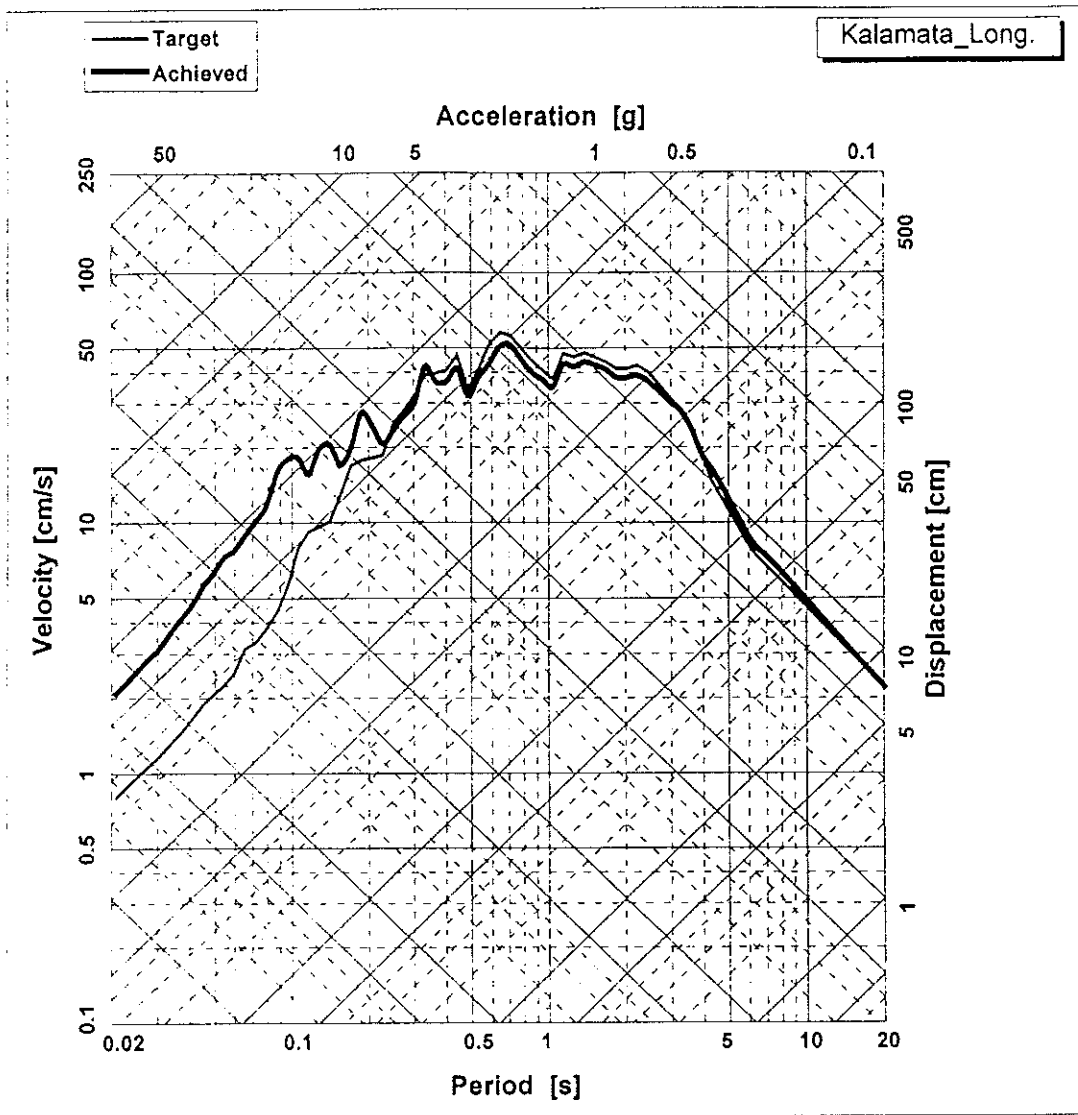
**RESPONSE SPECTRA OF TARGET AND ACHIEVED MOTION
KALAMATA EARTHQUAKE**

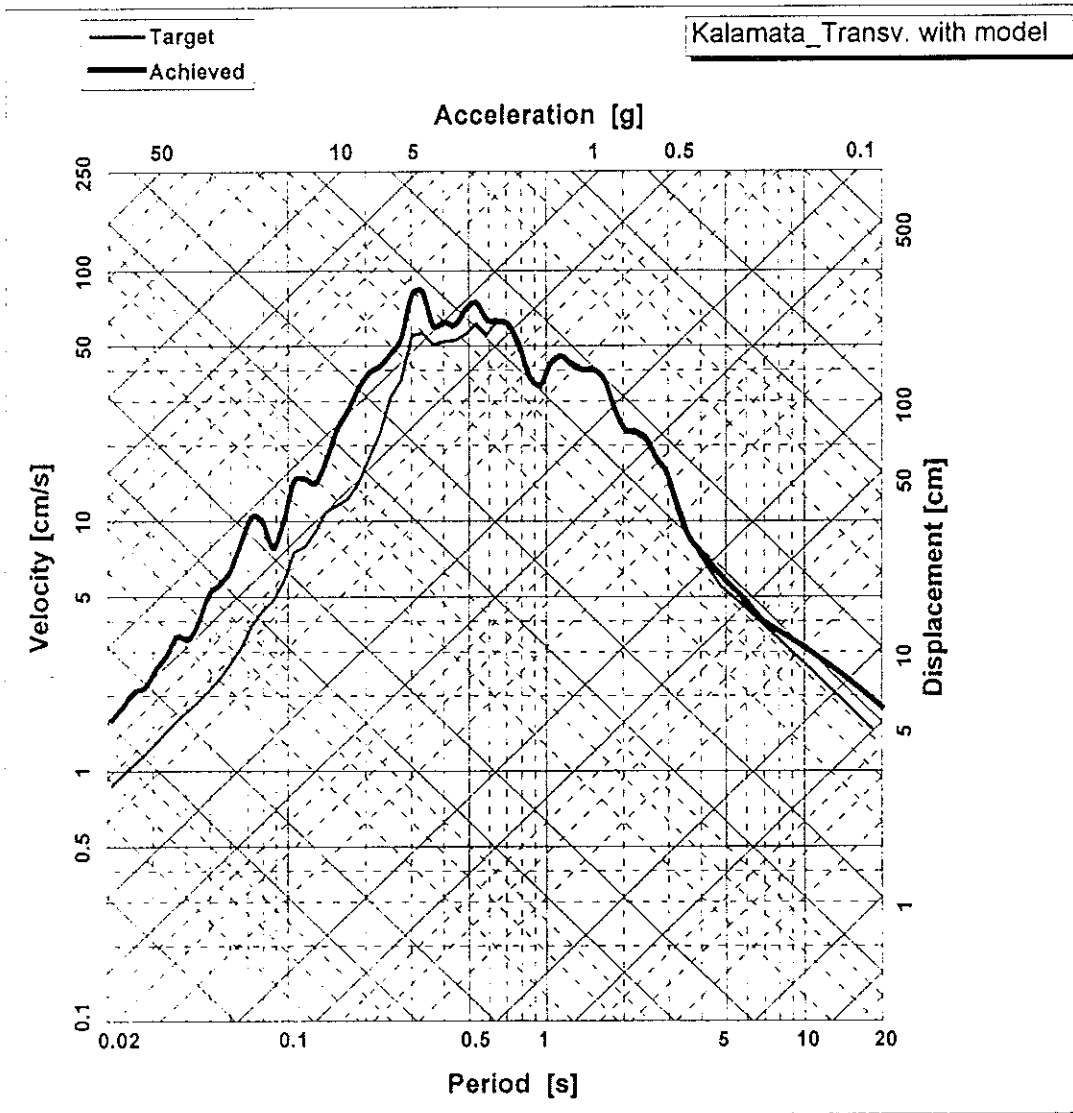
List of Figures

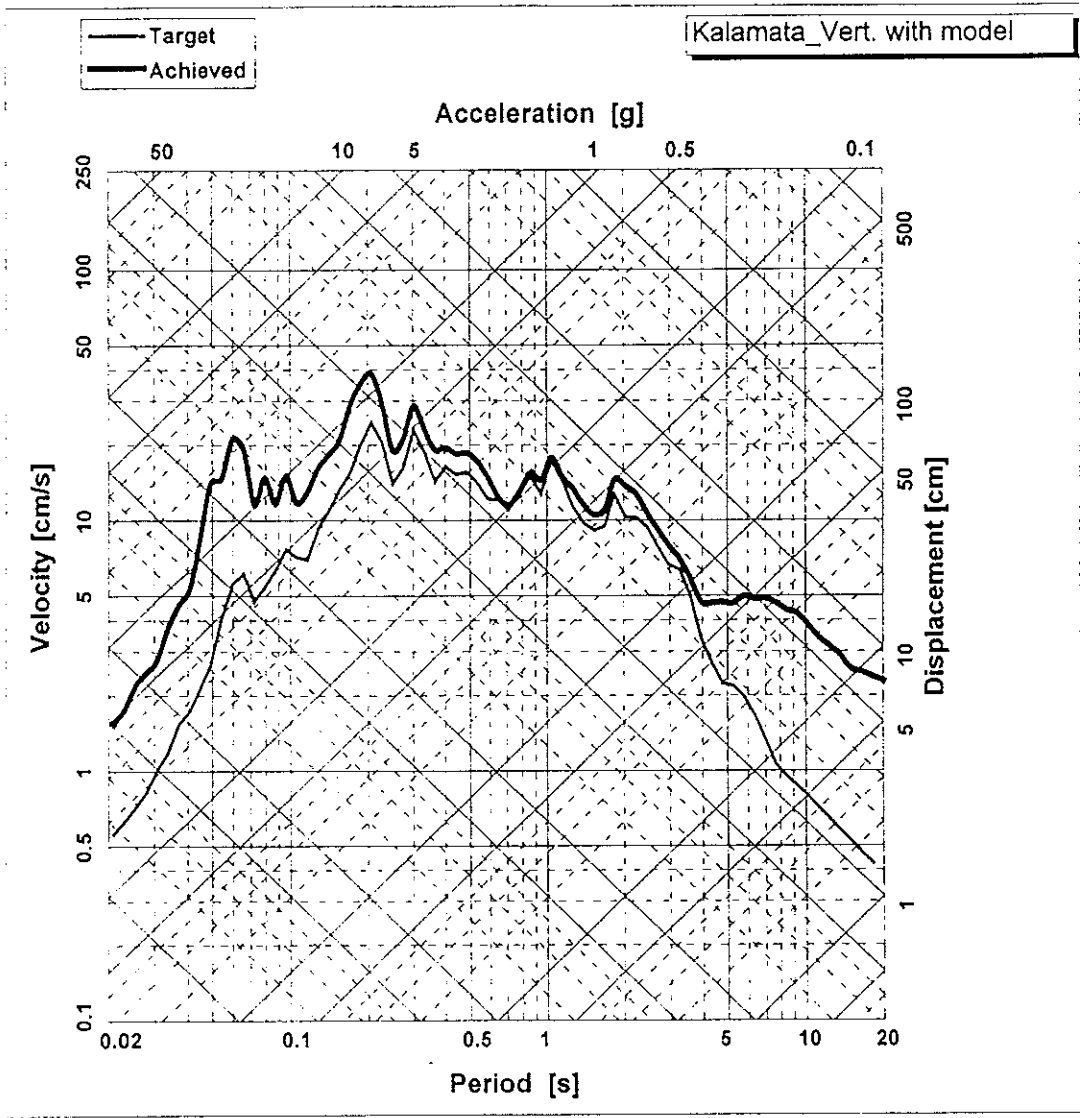
- AVII.1 - Response spectra (without model) of transverse achieved and target motion
- AVII.2 - Response spectra (without model) of vertical achieved and target motion
- AVII.3 - Response spectra (without model) of longitudinal achieved and target motion
- AVII.4 - Response spectra (with model) of transverse achieved and target motion
- AVII.5 - Response spectra (with model) of vertical achieved and target motion
- AVII.6 - Response spectra (with model) of longitudinal achieved and target motion

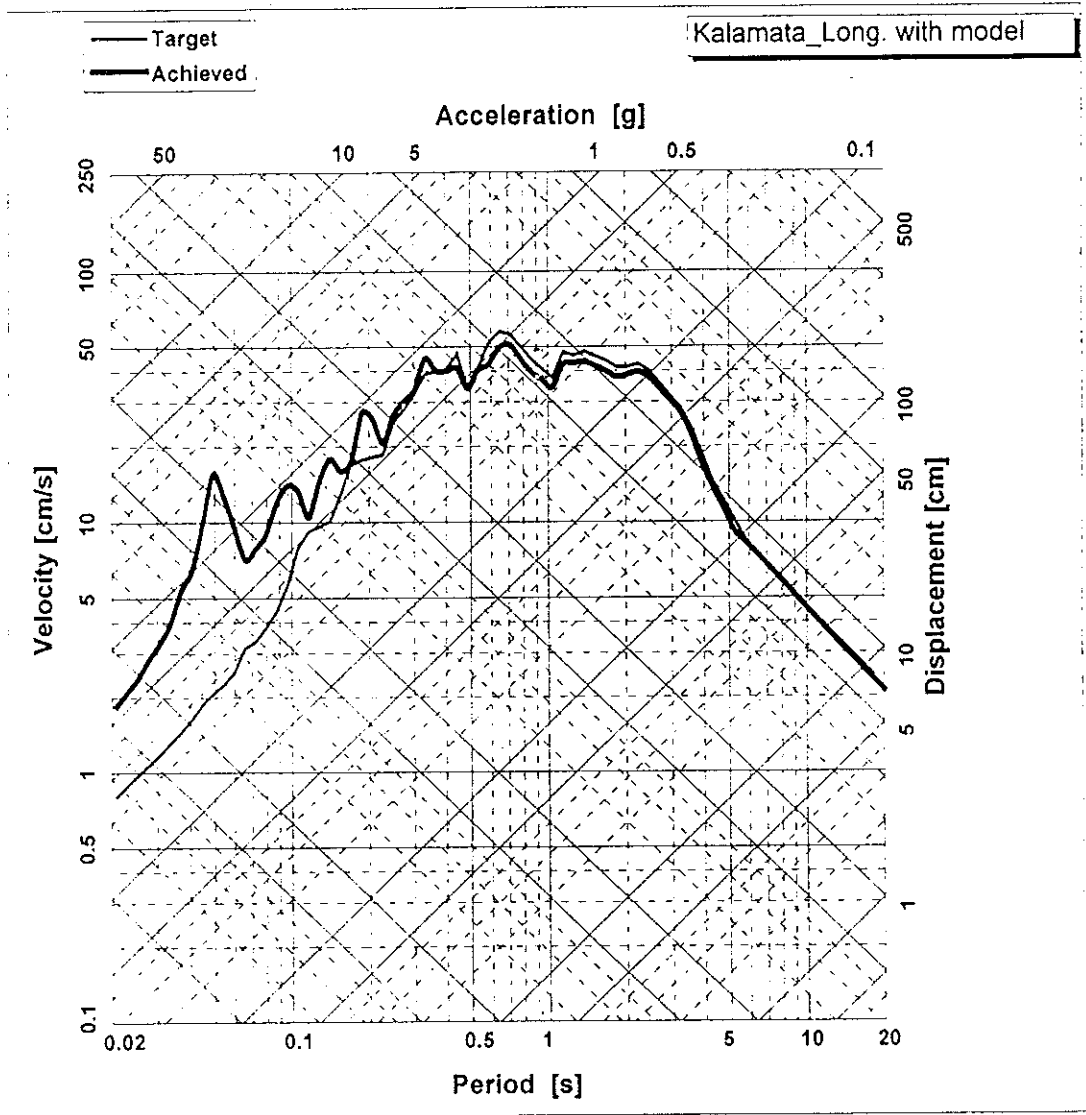










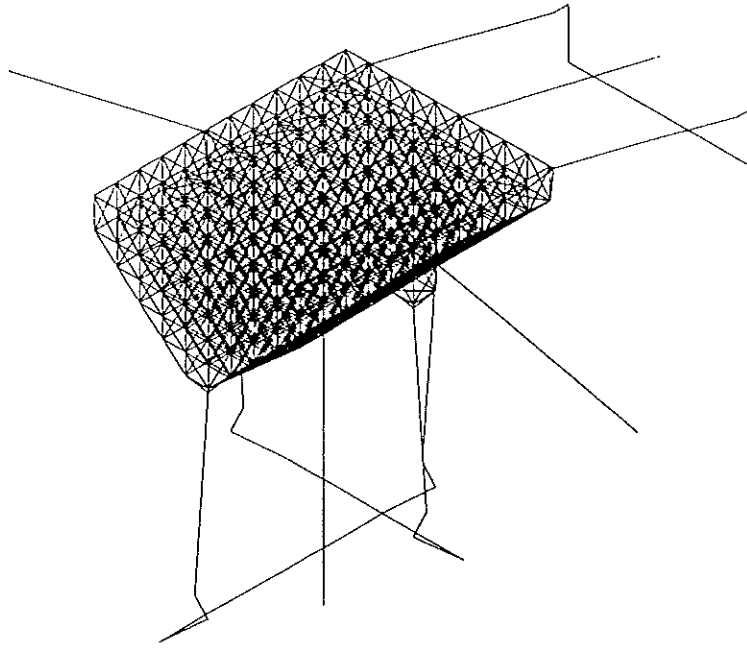
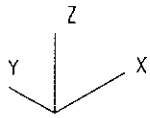


APPENDIX VIII

ANALYTICAL MODEL OF LNEC SHAKING TABLE

MODE SHAPES

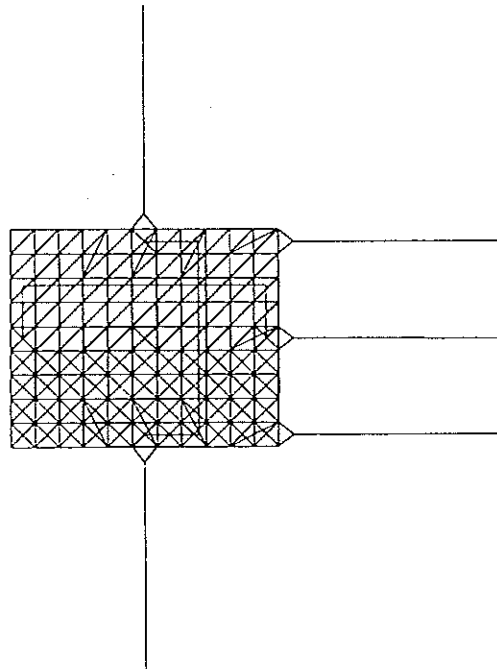
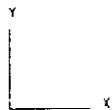
MODE NO. 1
FREQ. = 6.9707
PER. = 0.1435



Mesa Sismica 3GL

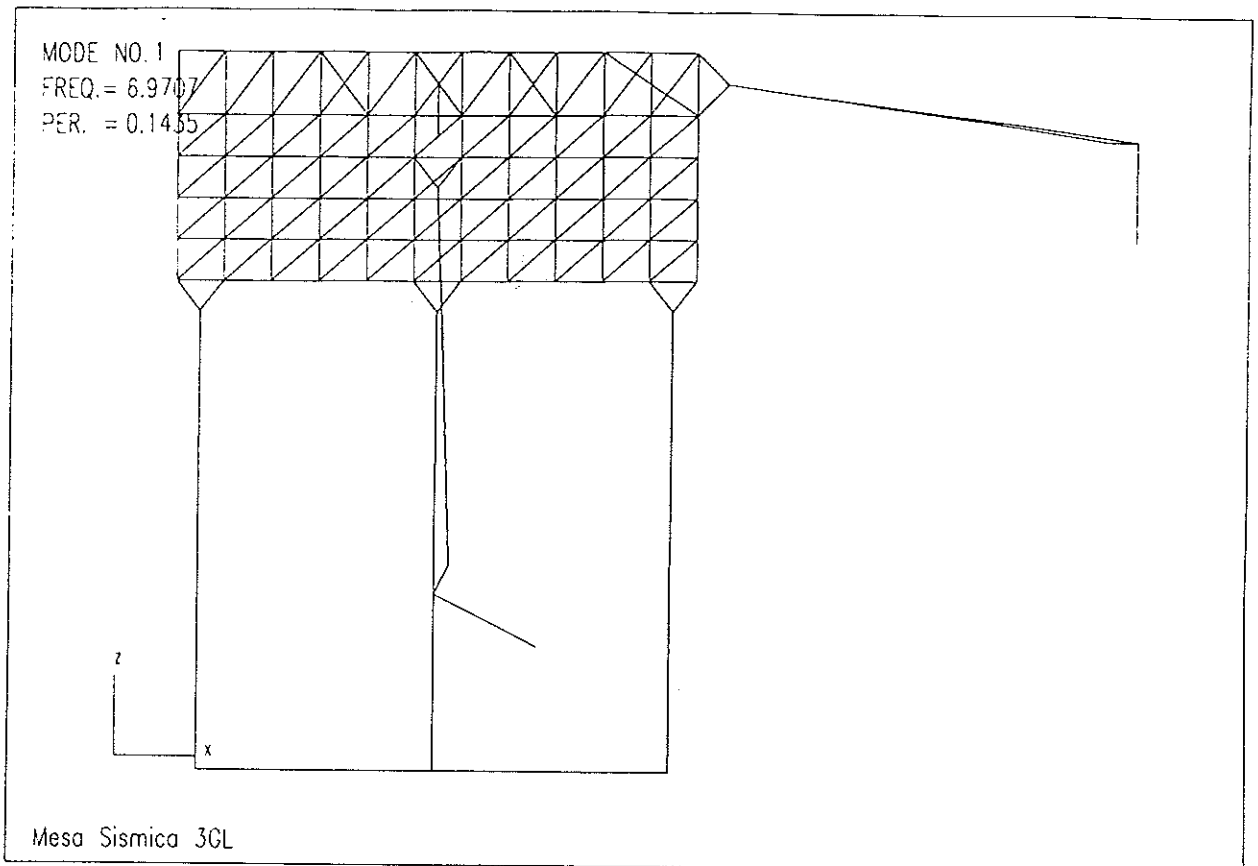
a) Isometric view

MODE NO. 1
FREQ. = 6.9707
PER. = 0.1435

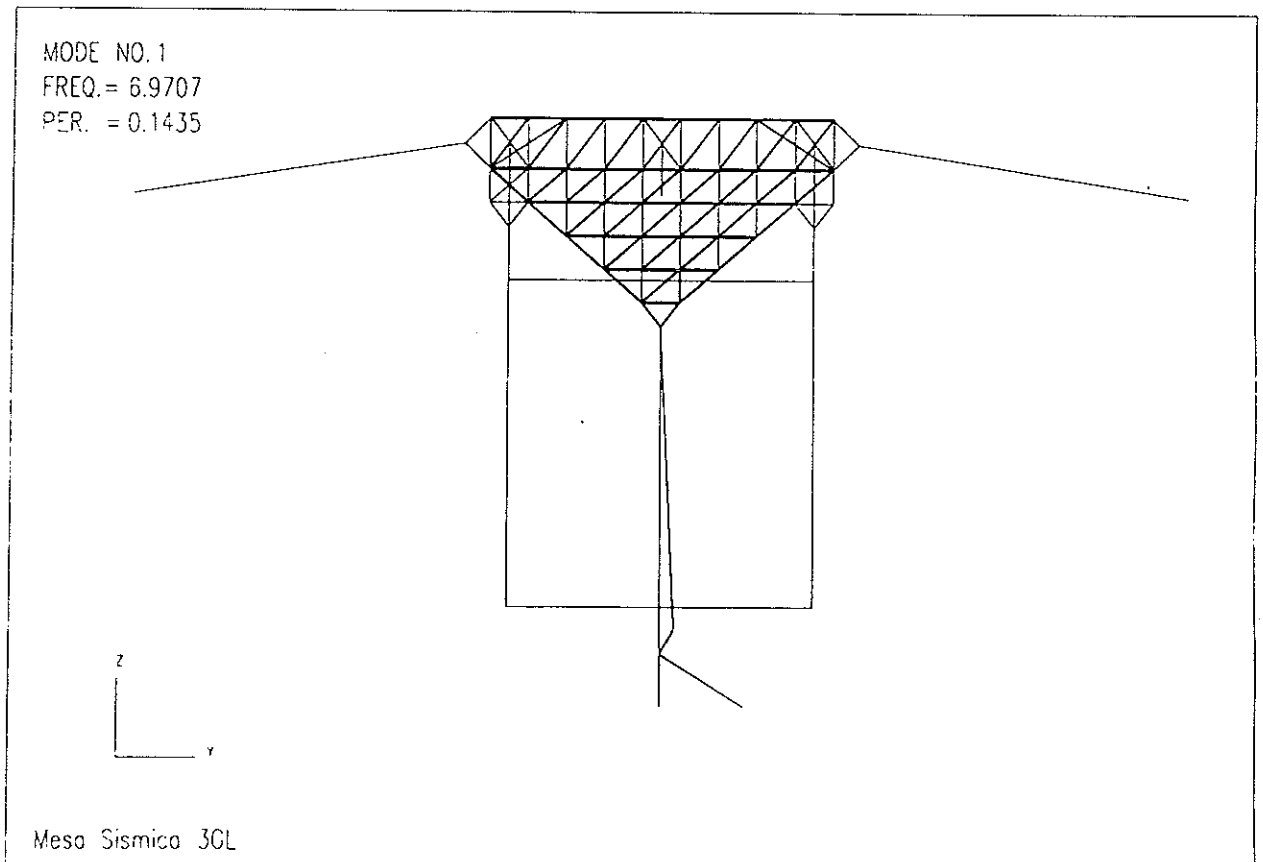


Mesa Sismica 3GL

b) Plan view

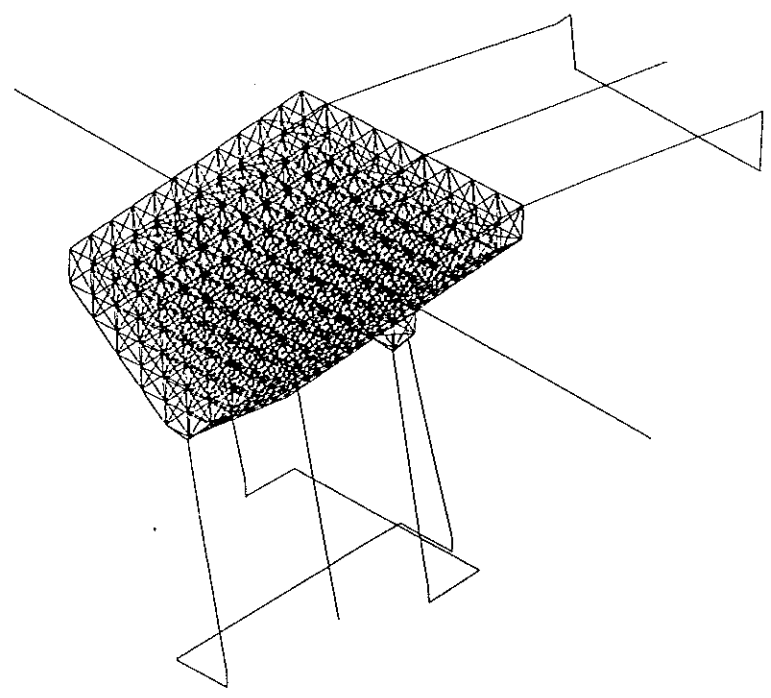
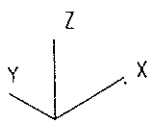


c) Transverse elevation



d) Longitudinal elevation

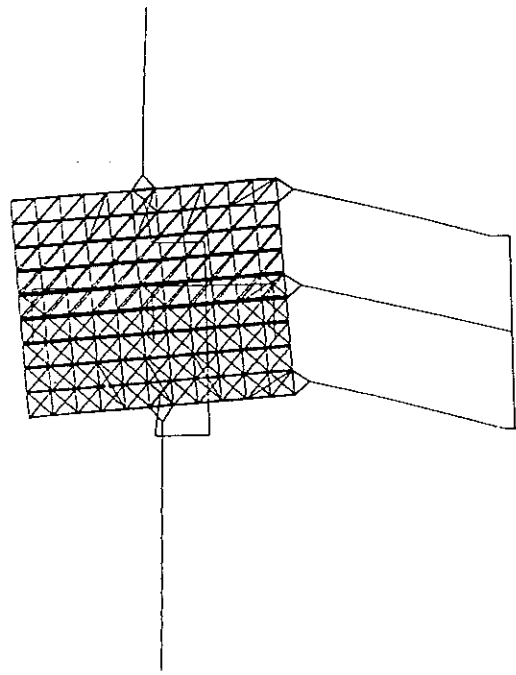
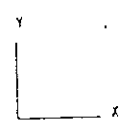
MODE NO.2
FREQ = 10.3079
PER. = 0.0970



Mesa Sismica 3GL

a) Isometric view

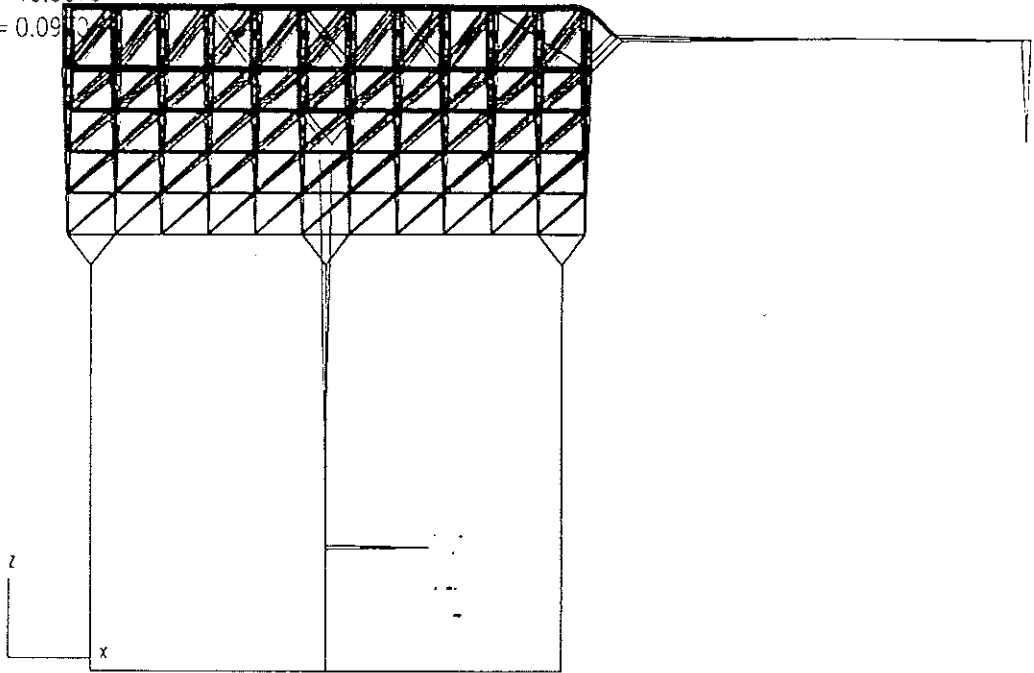
MODE NO.2
FREQ. = 10.3079
PER. = 0.0970



Mesa Sismica 3GL

b) Plan view

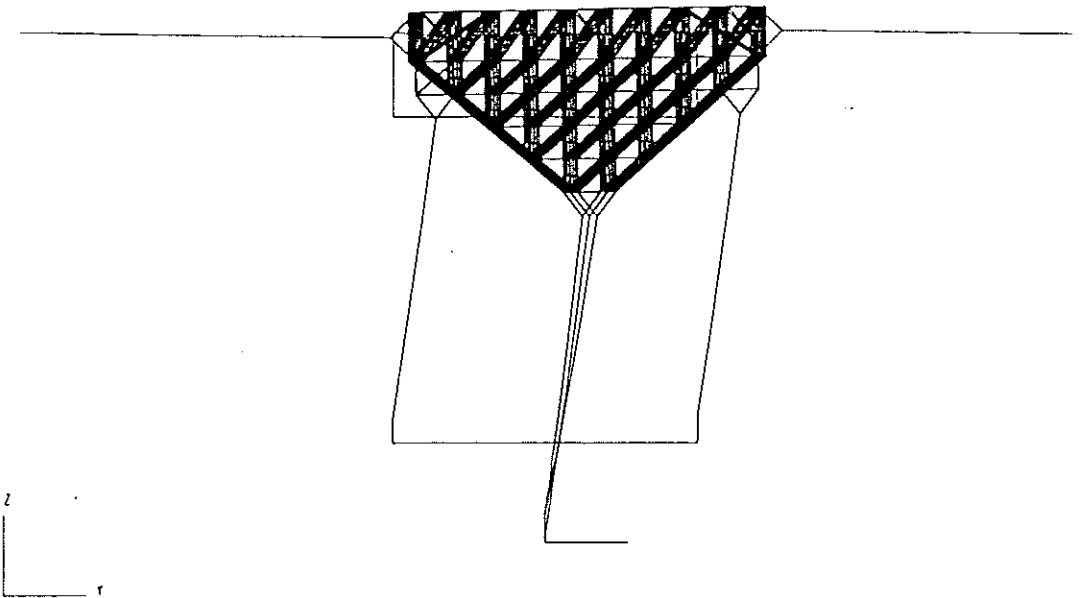
MODE NO.2
FREQ. = 10.3079
PER. = 0.0970



Meso Sismica 3GL

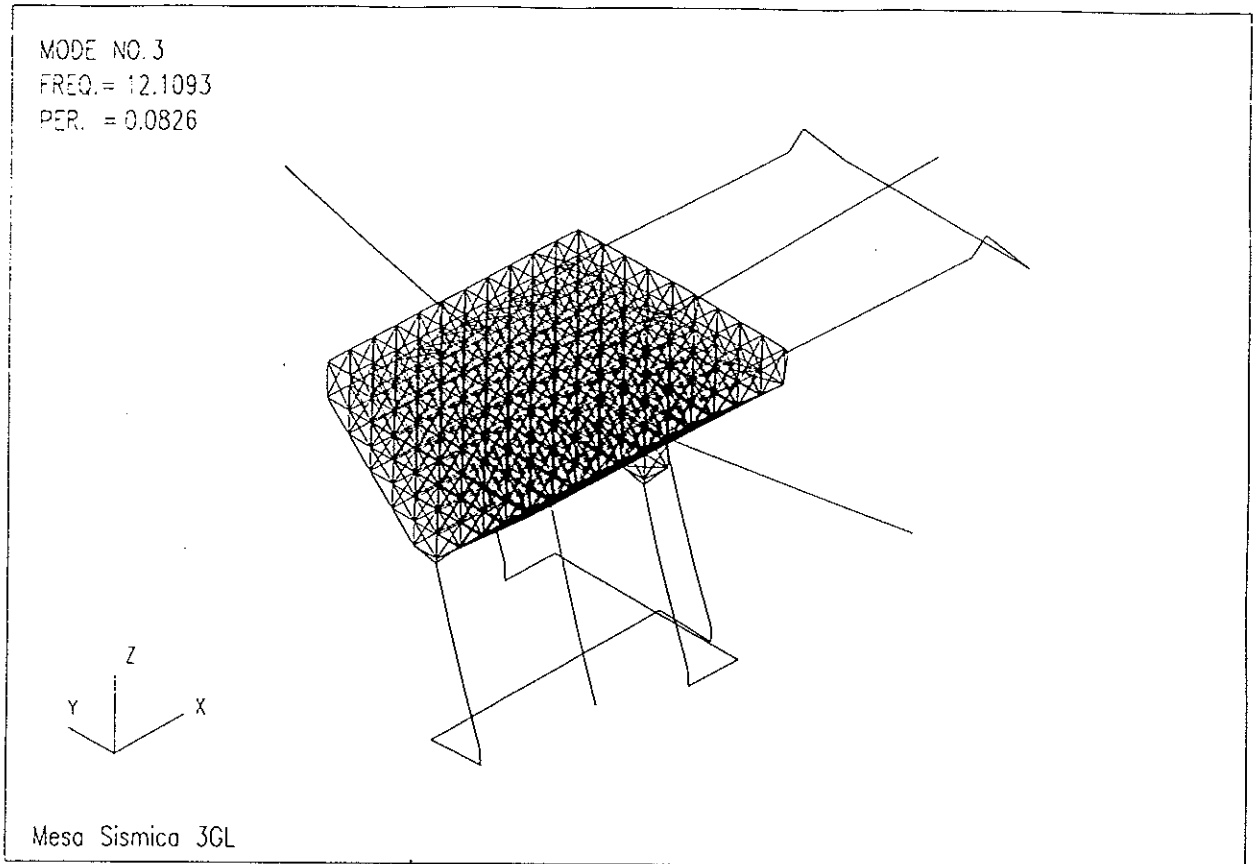
c) Transverse elevation

MODE NO.2
FREQ. = 10.3079
PER. = 0.0970

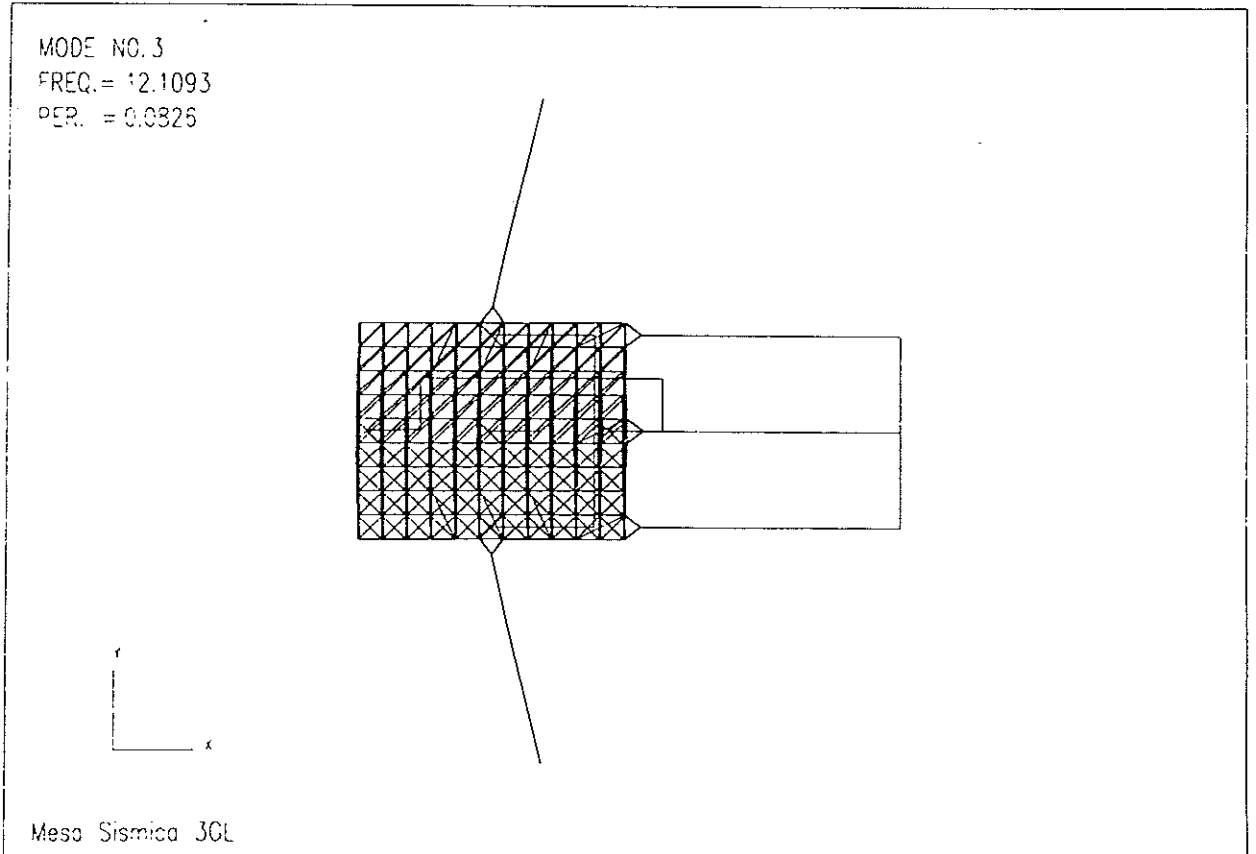


Meso Sismica 3GL

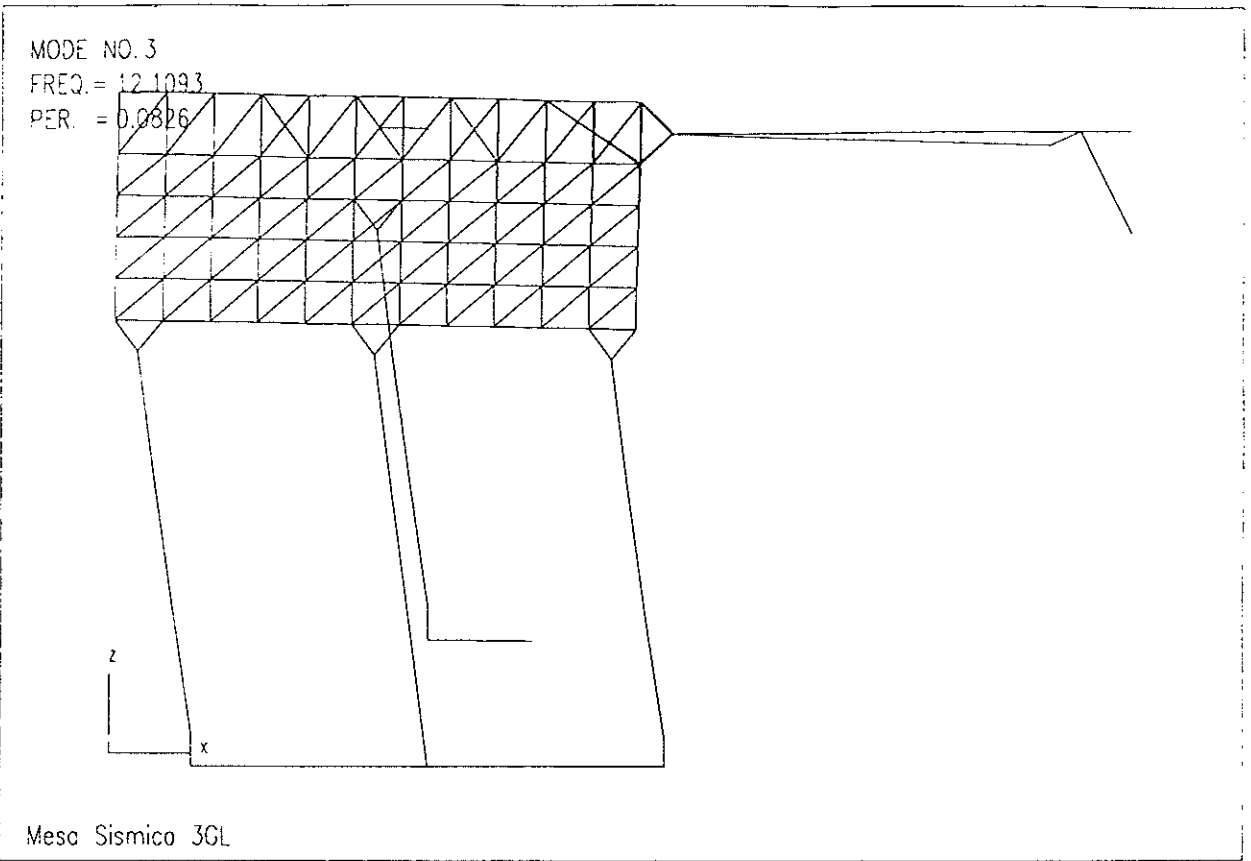
d) Longitudinal elevation



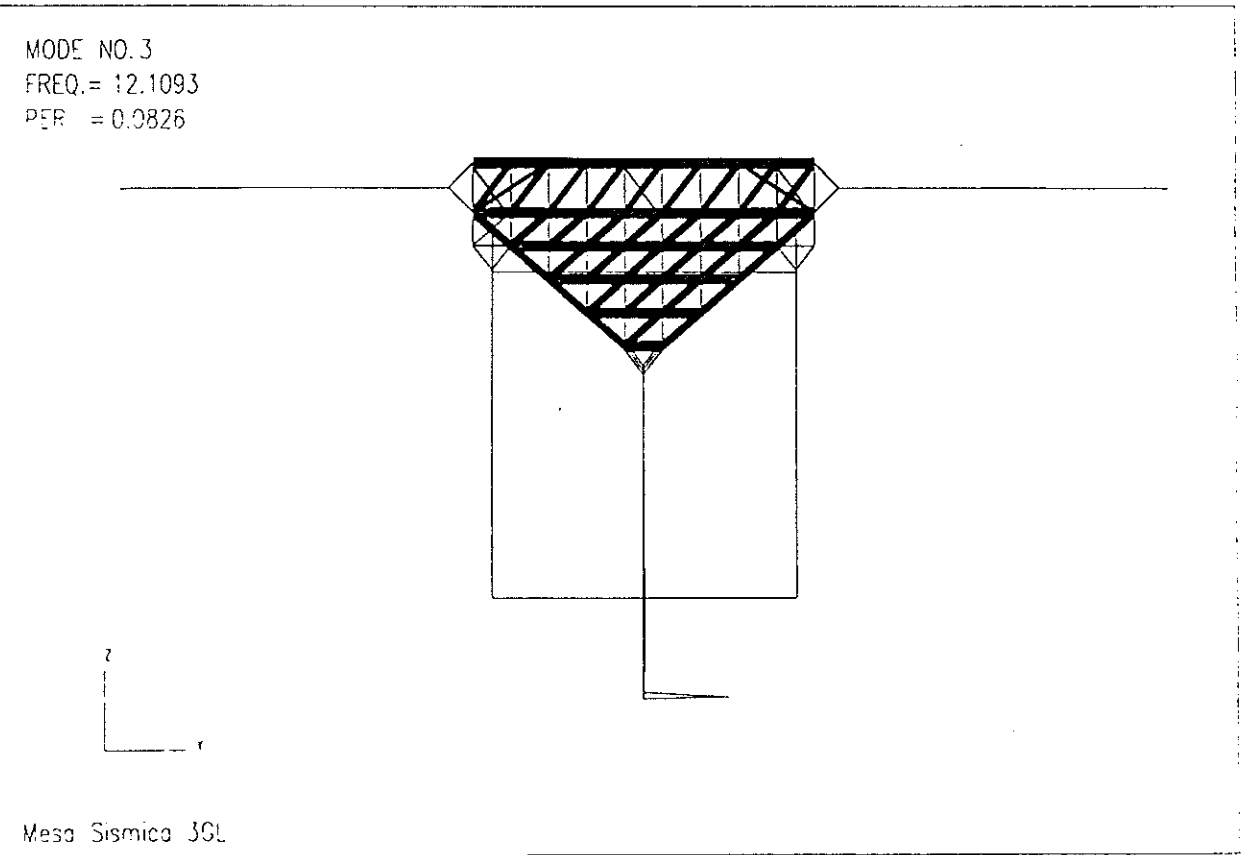
a) Isometric view



b) Plan view

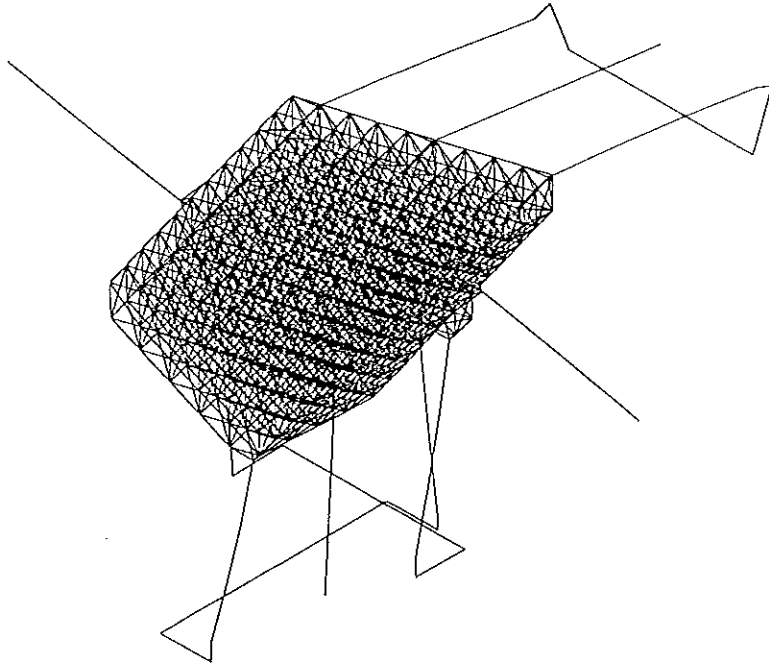
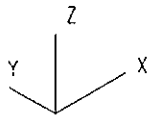


c) Transverse elevation



d) Longitudinal elevation

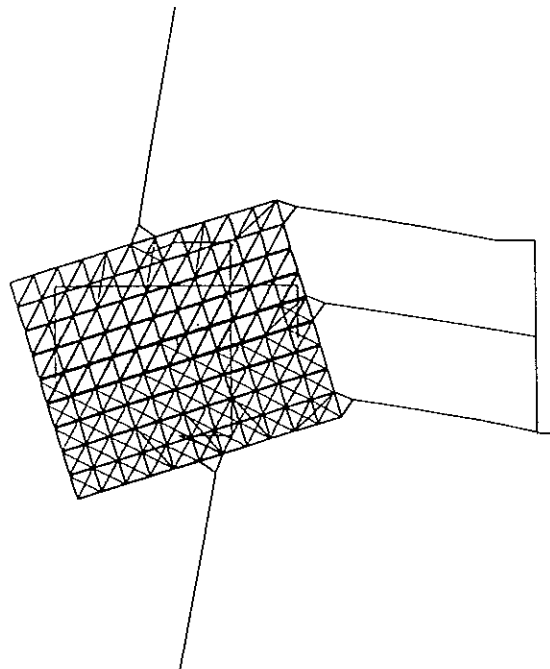
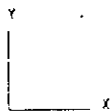
MODE NO. 4
FREQ. = 15.1092
PER. = 0.0662



Meso Sismico 3GL

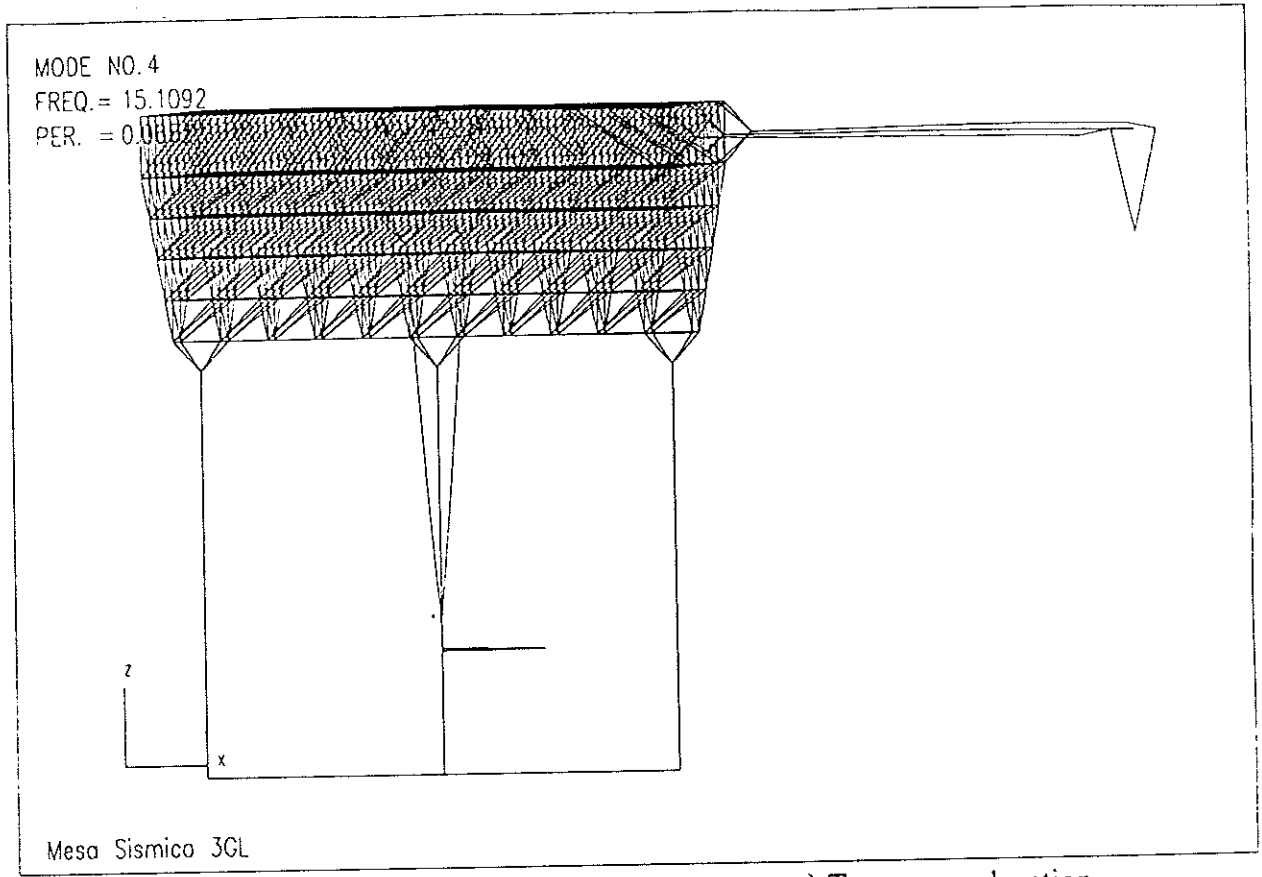
a) Isometric view

MODE NO. 4
FREQ. = 15.1092
PER. = 0.0662

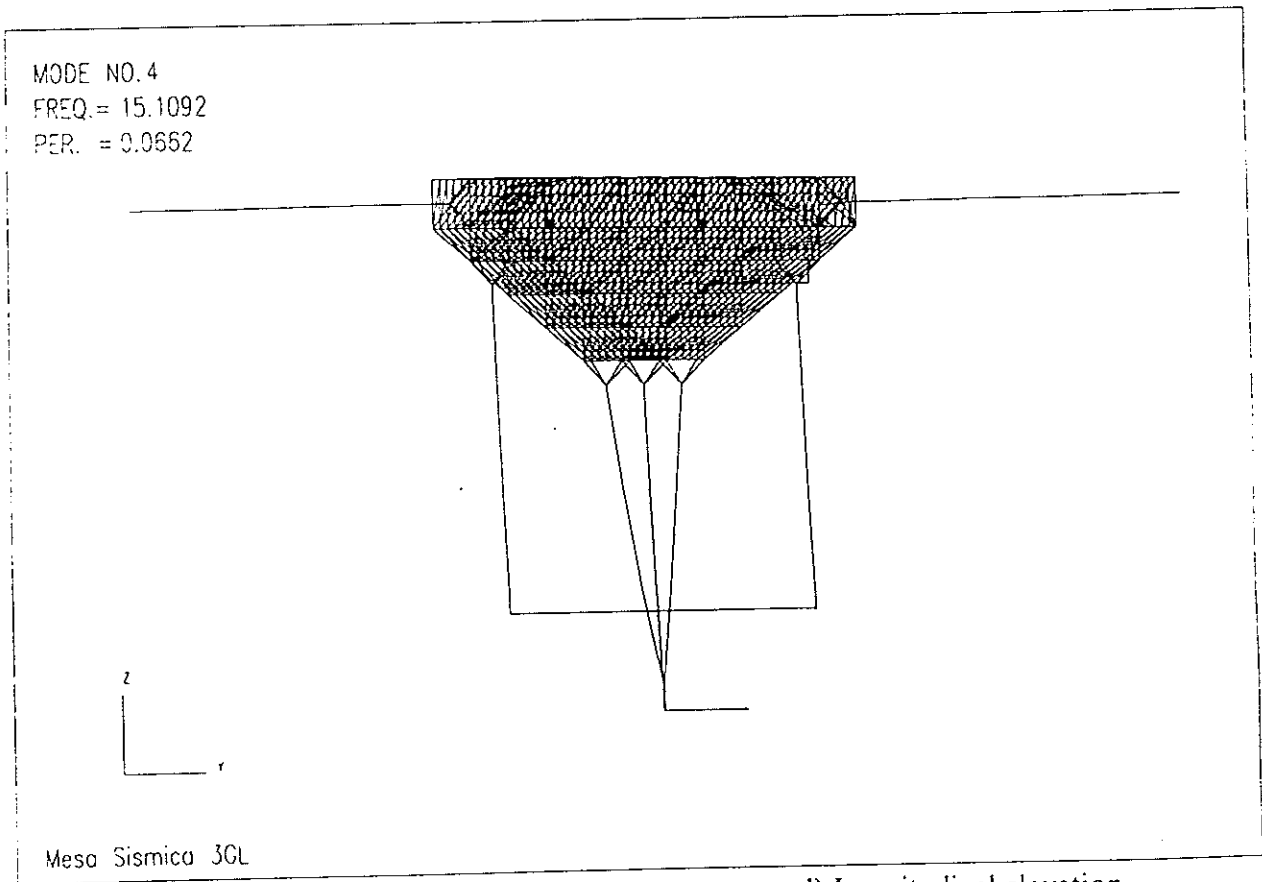


Meso Sismico 3GL

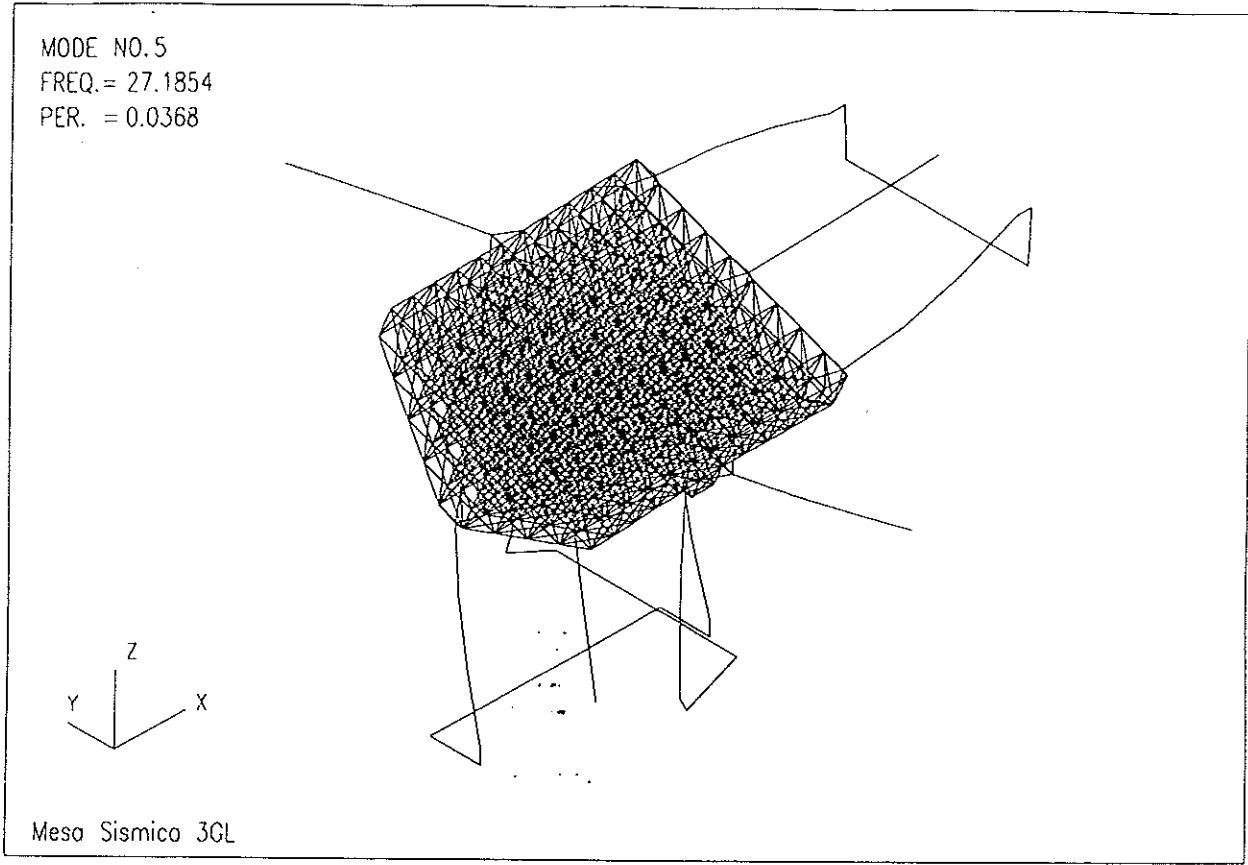
b) Plan view



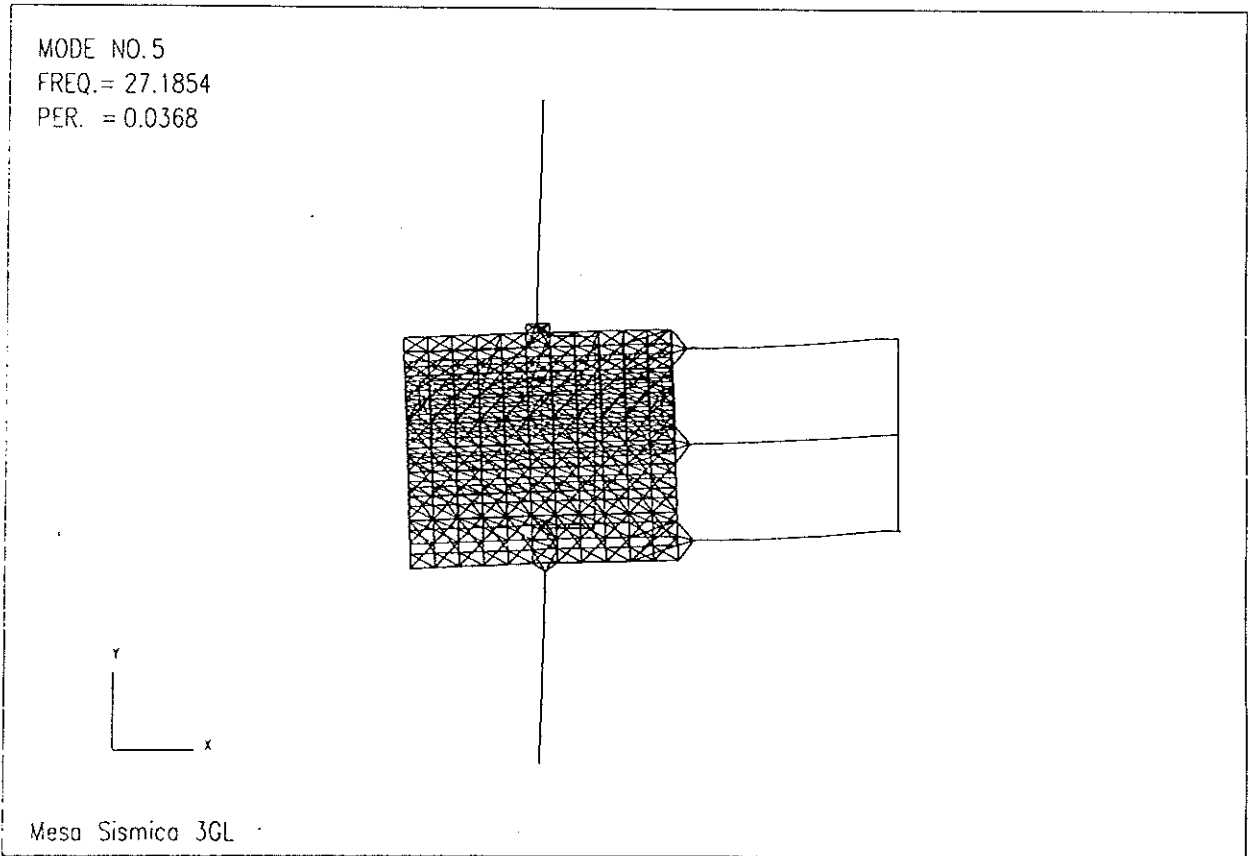
c) Transverse elevation



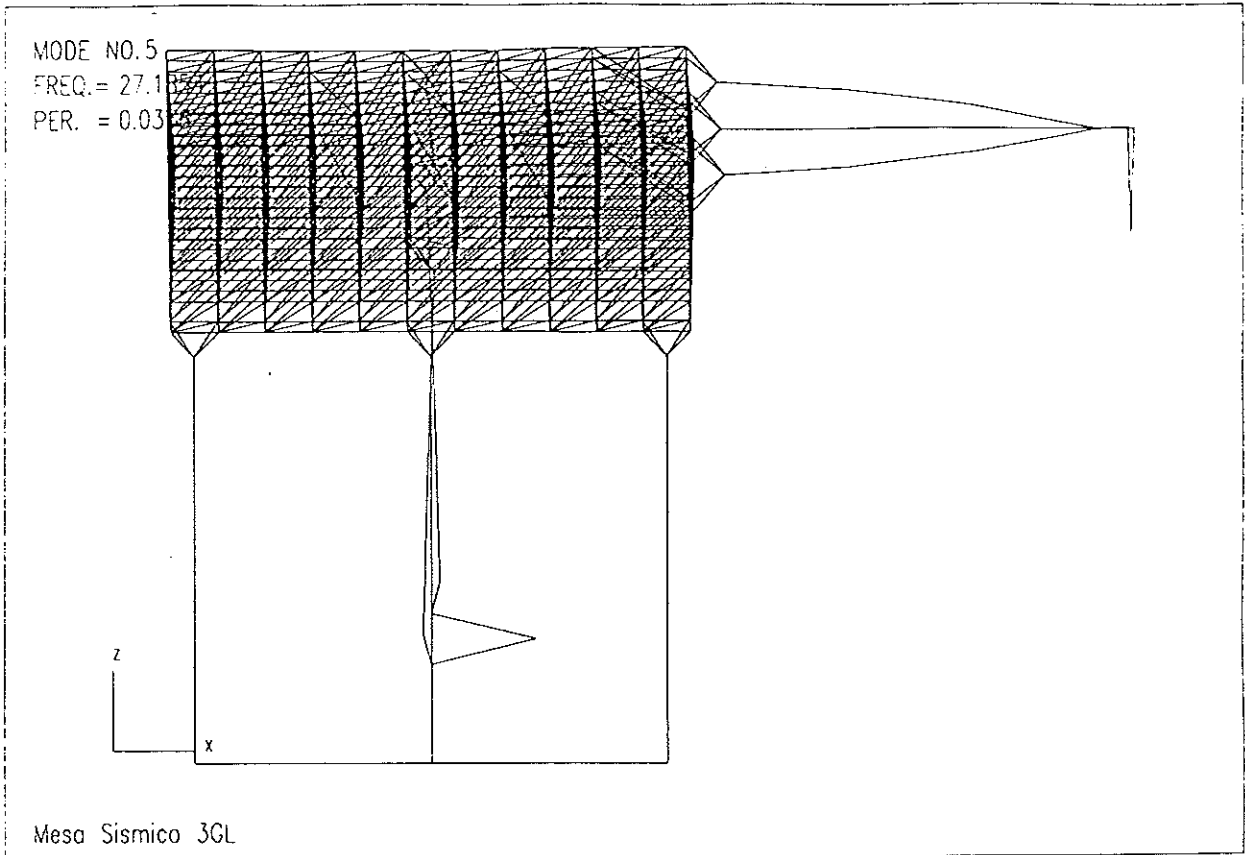
d) Longitudinal elevation



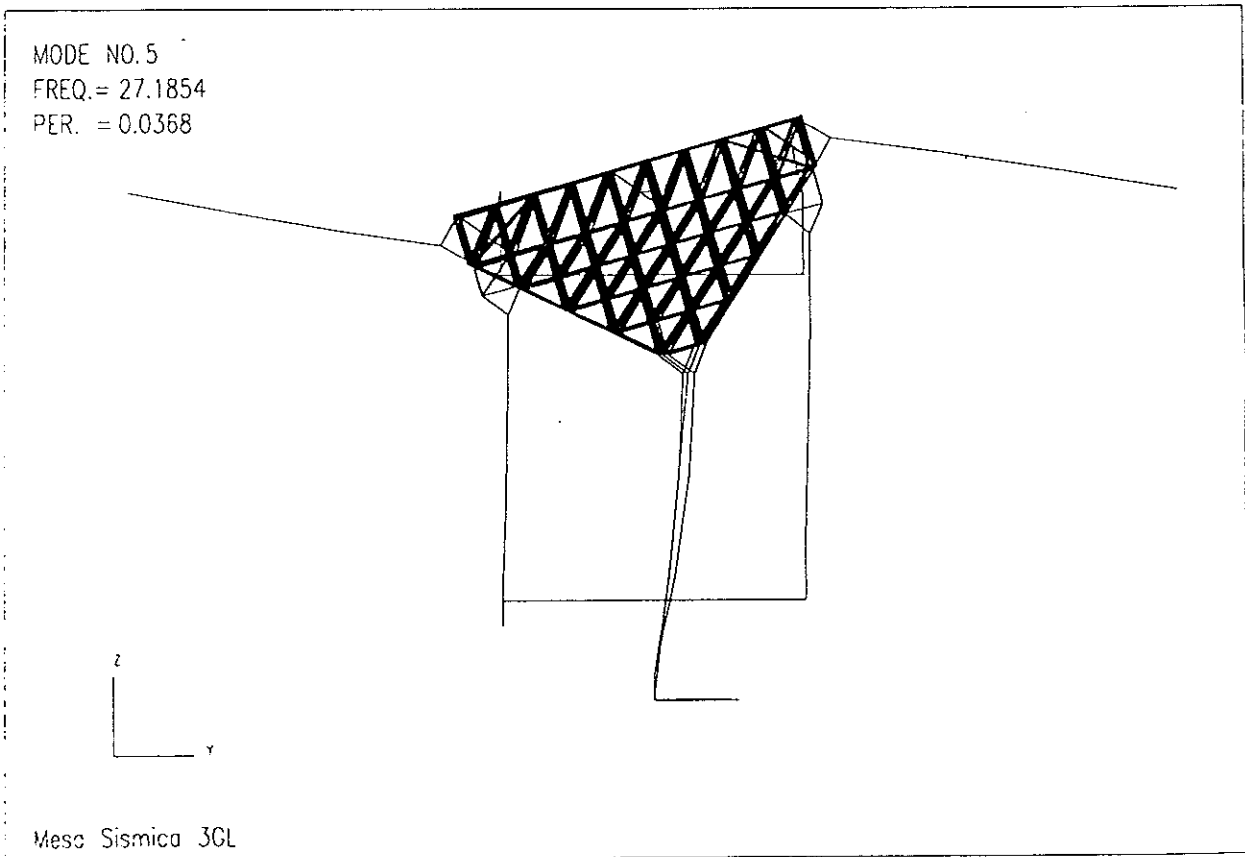
a) Isometric view



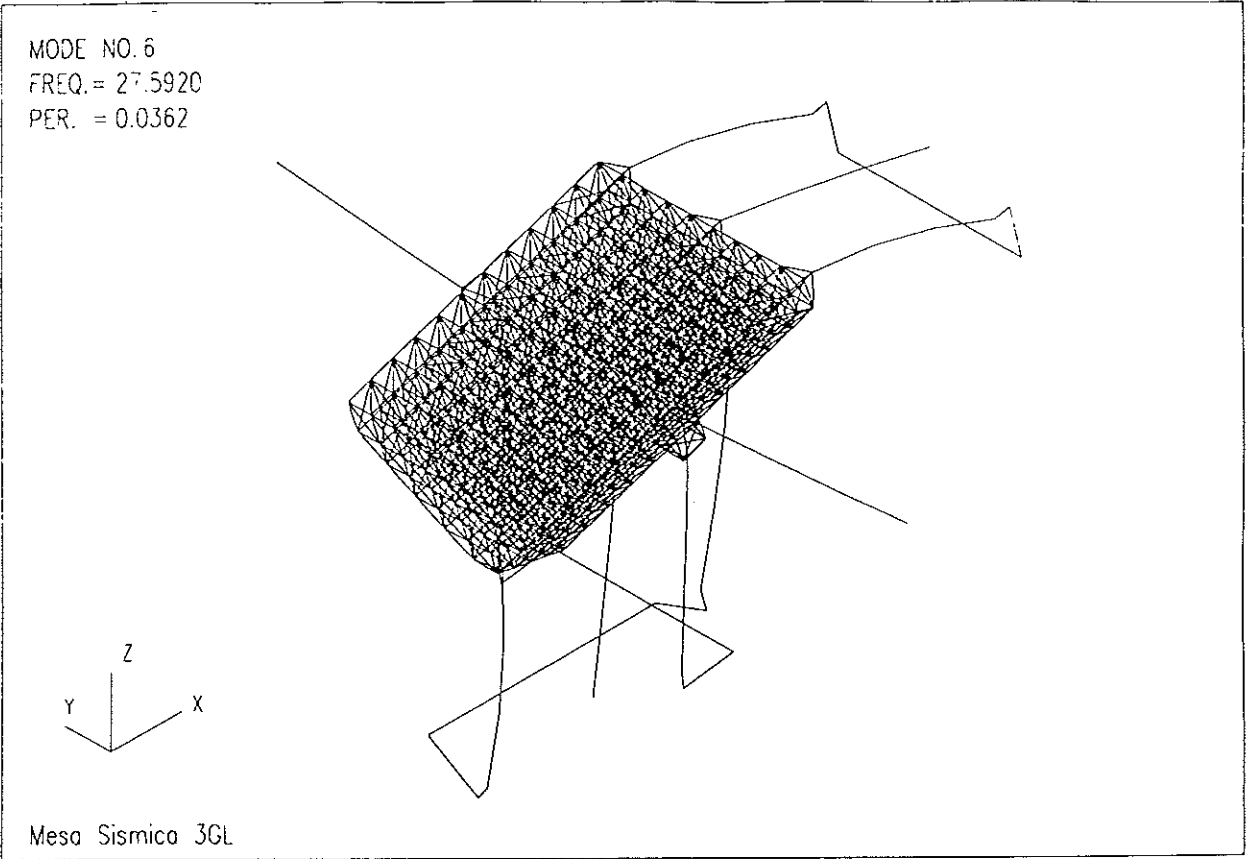
b) Plan view



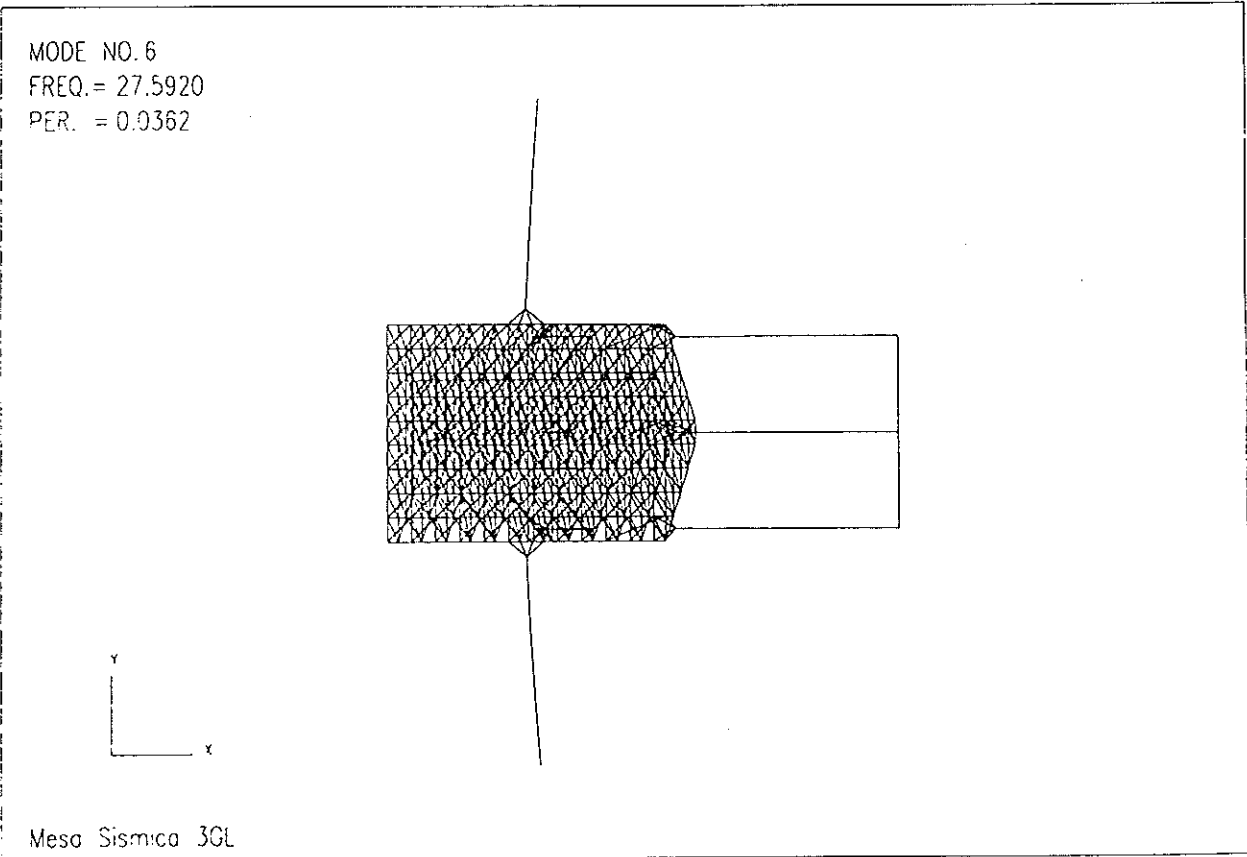
c) Transverse elevation



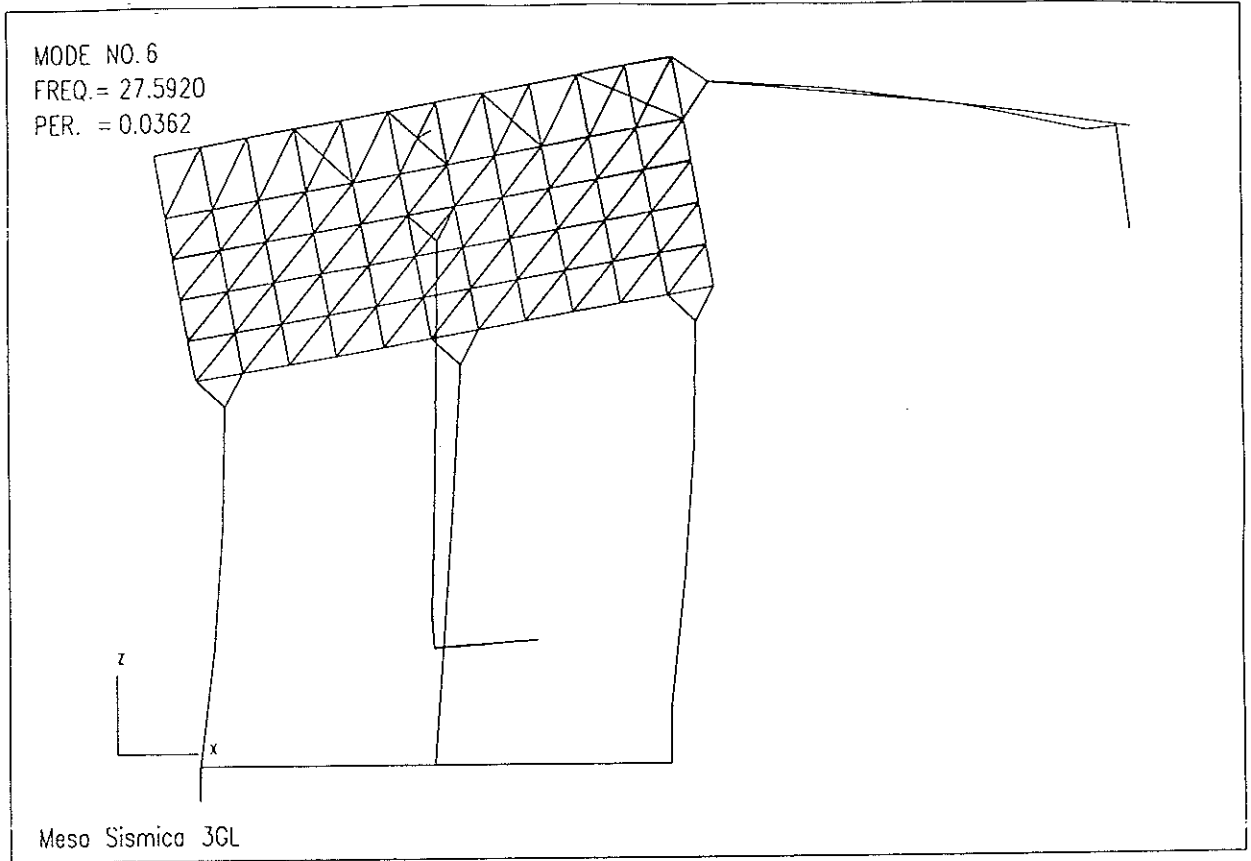
d) Longitudinal elevation



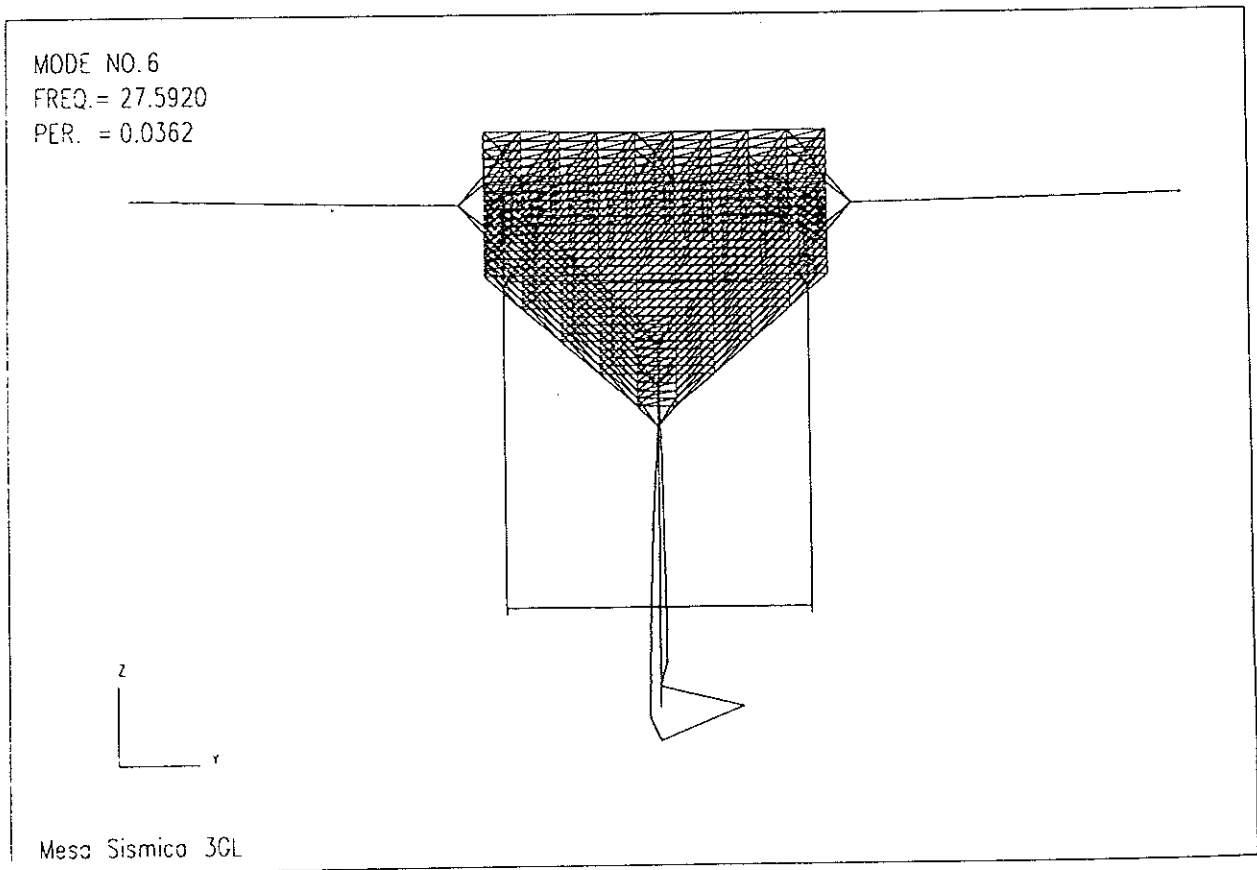
a) Isometric view



b) Plan view

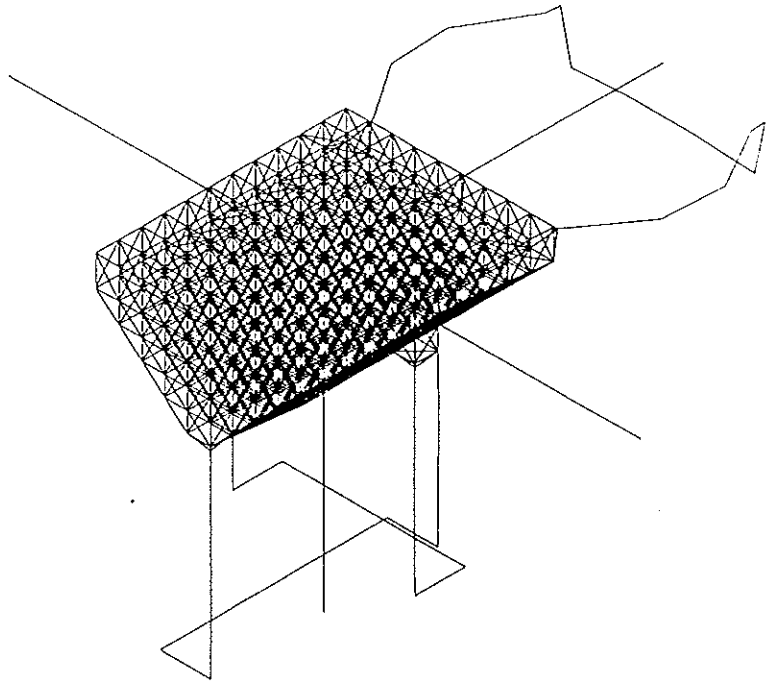
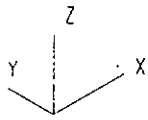


c) Transverse elevation



d) Longitudinal elevation

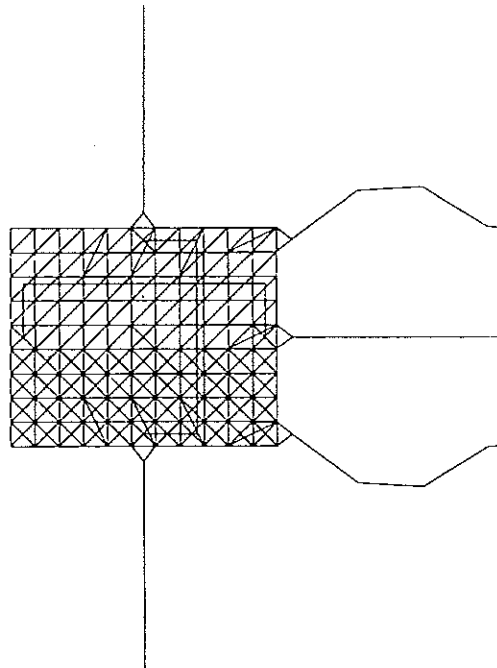
MODE NO. 7
FREQ. = 50.6020
PER. = 0.0198



Meso Sismica 3GL

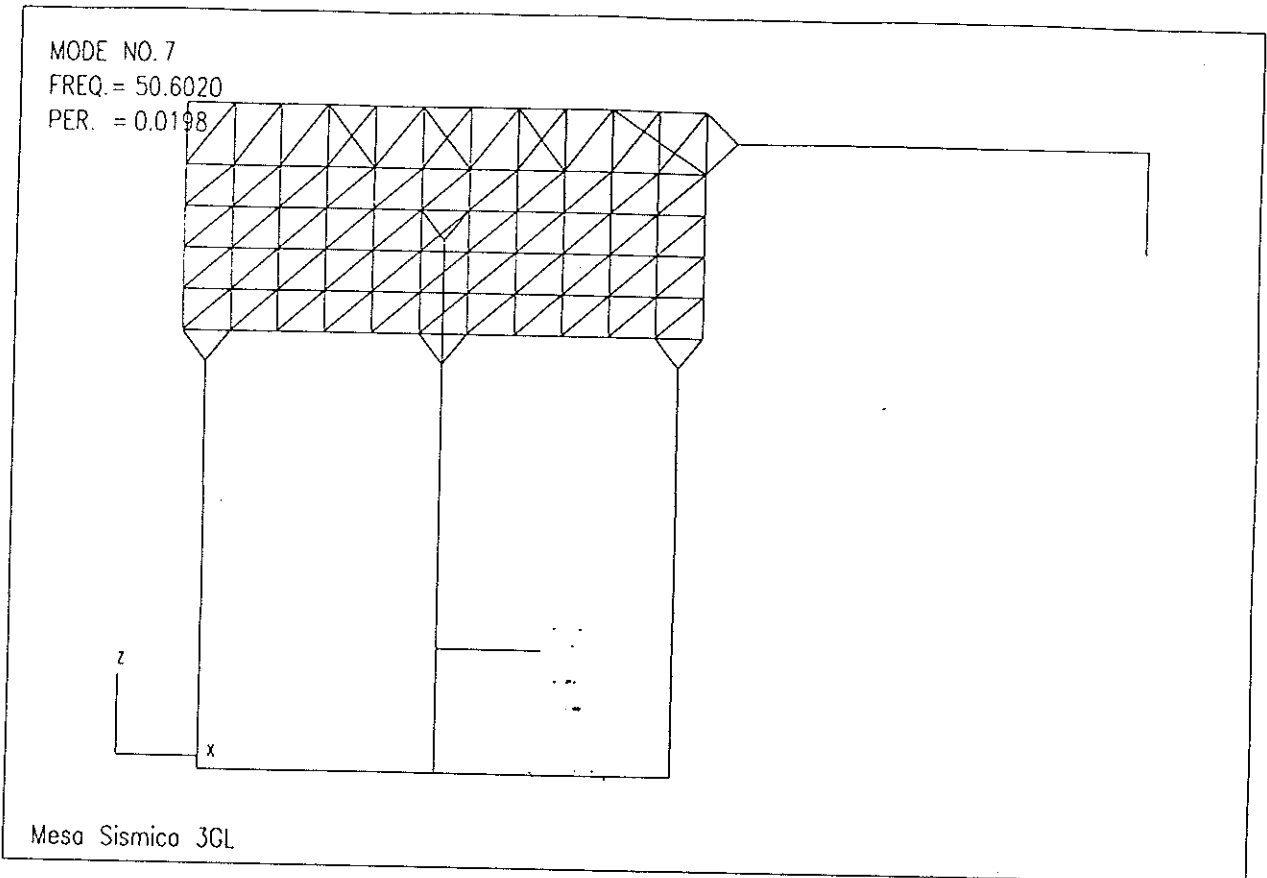
a) Isometric view

MODE NO. 7
FREQ. = 50.6020
PER. = 0.0198

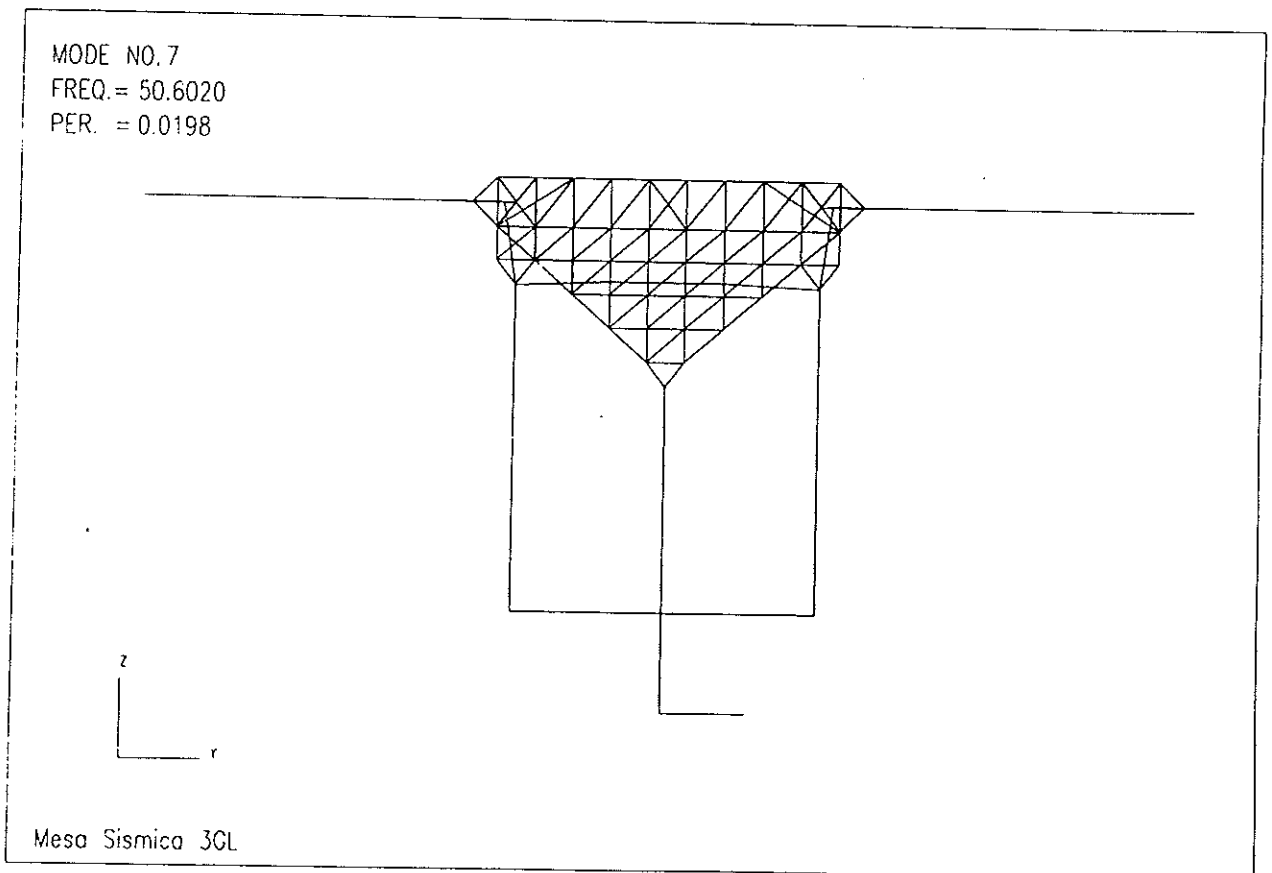


Meso Sismica 3GL

b) Plan view



c) Transverse elevation



d) Longitudinal elevation

Mode	Frequency [Hz]	Principal Components						Local Modes
		Translation			Rotation			
		longitudinal	transversal	vertical	roll	pitch	yaw	
1	7.0			F		P		
2	10.3		F				P	
3	12.1	F				P		
4	15.1						F	
5	27.2				F			
6	27.6					F		
7	50.6							Vertical Torsion Bar
8	51.7							Transversal Torsion Bar
9	51.9							Longitudinal Torsion Bar
10	52.1							All Torsion Bars
11	52.5							Torsion Bars (L & T)
12	52.6							All Torsion Bars
13	54.1							All Torsion Bars
14	54.4							All Torsion Bars
15	54.6							Torsion Bars (L & T)
16	54.9							Torsion Bars (L & T)
17	55.3							All Torsion Bars
18	55.4							All Torsion Bars
19	86.1							Actuator (L)
20	86.4							Actuator (L)
21	89.3							Longitudinal Torsion Bar
22	90.7							Deformation of the table

where: F = fundamental frequency
P = partial frequency

